HnRNP K mislocalisation and dysfunction in neurodegenerative disease and ageing

Alexander Bampton

Institute of Neurology

Primary supervisors:

Professor Tammaryn Lashley and Professor Pietro Fratta

A thesis submitted for the degree of

Doctor of Philosophy

University College London

April 2022

Declaration statement

I, Alexander Bampton, confirm that the work presented in this thesis is my own. Where information has been derived from other sources, I confirm that this has been indicated in the thesis

Acknowledgements

I dedicate this thesis to the memories of my dear grandparents, Nanny Mo, Grandad Bert, Nanny Sonia and Grandad Brian. The kindest, gentlest, most generous and loving grandparents I could ever have wished for. Thank you, I love you and will remember you always. (I told you I would do it Nan).

I owe a debt of gratitude to my two wonderful primary supervisors Tammaryn and Pietro. I could not have asked for two better mentors over the last 3-4 years and I feel so privileged to have worked alongside two such experienced, intelligent and creative scientists. Both have worked tirelessly to foster healthy and positive work environments and in doing so have nurtured successful lab groups full of happy and inspired scientists. Thank you for your kindness and thank you for having me.

A PhD is never a one-person journey and I have been lucky enough to have worked alongside many brilliant senior scientists that I have learnt so much from, not least my hnRNP K partner-in-crime Ariana Gatt. Ariana, thank you for your lab help and for all the fun we've had along the way exploring the wild and wacky world of hnRNP K biology

Indeed, I have been incredibly fortunate to have worked with so many amazing colleagues at the Queen Square Brain Bank and so to all of Team Tam, all of the technical staff, the admin team and the whole of the ground floor, thank you for making the last four years so enjoyable. I wish every one of you all the best for the future.

Thank you also to Matt Keuss and Benedikt Holbling whose iPSC expertise, teaching and patience was indispensable in helping me get an iPSC-derived neuron model off the ground from very little cell culture experience. Outside of UCL, I am extremely thankful for the invaluable input of our many brilliant external collaborators mentioned throughout this thesis and particularly to Dr

Jack Humphrey (Mount Sinai school of medicine, New York) for his excellence in RNA-seq analysis.

A big thank you also to my thesis committee: Professor Sonia Gandhi, Professor Adrian Isaacs and Dr Rina Bandhopadhyay. Their advice and counsel over the past 3 years, right from the PhD project's inception, has been instrumental in helping me navigate the inevitable challenges and obstacles that science has thrown at me along the way.

A thesis acknowledgement page would certainly not be complete without mentioning my family. My Mum and Dad have encouraged and supported me in everything I have ever done academically, sporting or otherwise from as long as I can remember. From a young age I was always made to feel like I could do anything or be anything I set my mind to. Despite not having the opportunity to attend university as school leavers themselves, both my parents worked hard to pursue education in later life with my dad obtaining a first class degree through the Open University and my mum who re-trained to become a fully qualified, professional counsellor. That being said, it is my brother Callum's work ethic that manages to blows us all out of the water. He worked incredibly hard in difficult circumstances to gain a first class degree from Oxford university and is now taking the wild world of investment banking by storm. Thank you Mum, Dad and Callum and know that I am as proud of you all, as you are of me.

Thank you to my beautiful and talented fiancée Zoe. Zoe if you read no further into this thesis (and I would not blame you in the least if you did not), know that you have been an unceasing source of love, emotional and gastronomical (!) support throughout my endeavour to prolong getting a job in the real word for as long as possible. I am grateful to you and your wonderful parents (and my soon to be in-laws Jerome and Karen) - thank you for all your support (Jerome in particular for proofing the introduction and Karen for many a dinner!) and for letting us live with you at sporadic periods throughout the last four years.

Thank you to Desmond Bates, the research programme manager of the Wolfson-Eisai programme and also to the former programme manager

Elizabeth Halton. The impact of Des and Elizabeth's hard work, doggedness and no doubt well-exercised patience over the years cannot be underestimated in their contribution to improving the lives and wellbeing of students under their wings. The Institute of Neurology and UCL as a whole are extremely lucky to have you.

Thank you to Eisai and the Wolfson foundation who, for many years have financially supported the Wolfson-Eisai 4-year PhD programme. I am sure if more PhD programmes followed their generous lead of providing well-funded studentships, I think we would have far more happier students in this country.

Finally, a thank you to all the donors and families, without whom the majority of the research described in this thesis would have been impossible. I am immensely humbled by all those who choose to donate their organs for transplantation or scientific research. Organ donation is a truly amazing, altruistic act and one that can often only be performed with the cooperation and assistance of surviving loved ones during upsetting and sometimes traumatic times.

We, as scientists, thank every single one of you.

Publication declaration forms

Form 1:

1. **For a research manuscript that has already been published** (if not yet published, please skip to section 2)**:**
    a. **Where was the work published?** Acta Neuropathologica
    b. **Who published the work?** Springer
    c. **When was the work published?** Aug 3rd, 2020
    d. **Was the work subject to academic peer review?** YES
    e. **Have you retained the copyright for the work?** YES [If no, please seek permission from the relevant publisher and check the box next to the below statement]:

        ☐ *I acknowledge permission of the publisher named under 1b to include in this thesis portions of the publication named as included in 1a.*

2. **For a research manuscript prepared for publication but that has not yet been published** (if already published, please skip to section 3)**:**
    a. **Where is the work intended to be published?** (e.g. journal name)
    b. **List the manuscript's authors in the intended authorship order:**
    c. **Stage of publication:**
        ☐ Not yet submitted
        ☐ Submitted
        ☐ Undergoing revision after peer review
        ☐ In press

3. **For multi-authored work, please give a statement of contribution covering all authors** (if single-author, please skip to section 4)**:**

    Alexander Bampton (AB), Lauren M. Gittings (LG), Pietro Fratta (PF), Tammaryn Lashley (TL), Ariana Gatt (AG).

    AG and TL conceptualised the idea for the article. **AB**, LG, AG and TL contributed to both the literature review and writing of the article with **AB** drafting the largest proportion of the manuscript. **AB** designed and created all figures / artwork. PF provided expertise on the RNA components of the review and all authors contributed to the critical revision and editing of the final script.

4. **In which chapter(s) of your thesis can this material be found?**

Chapter 1: Introduction

5. **Candidate's e-signature:** [redacted for purpose of publishing open access]
   Date: 28/03/2022

6. **Supervisor/senior author(s) e-signature:** [redacted for purpose of publishing open access]
   Date: 28/03/2022

Form 2:

1. **For a research manuscript that has already been published** (if not yet published, please skip to section 2)**:**
    a. **Where was the work published?** Acta Neuropathologica
    b. **Who published the work?** Springer
    c. **When was the work published?** Jul 18th, 2021
    d. **Was the work subject to academic peer review?** YES
    e. **Have you retained the copyright for the work?** YES [If no, please seek permission from the relevant publisher and check the box next to the below statement]:

        ☐ *I acknowledge permission of the publisher named under 1b to include in this thesis portions of the publication named as included in 1a.*

2. **For a research manuscript prepared for publication but that has not yet been published** (if already published, please skip to section 3)**:**
    a. **Where is the work intended to be published?** (e.g. journal name)
    b. **List the manuscript's authors in the intended authorship order:**
    c. **Stage of publication:**
        ☐ Not yet submitted
        ☐ Submitted
        ☐ Undergoing revision after peer review
        ☐ In press

3. **For multi-authored work, please give a statement of contribution covering all authors** (if single-author, please skip to section 4)**:**

    Alexander Bampton (AB), Ariana Gatt (AG), Jack Humphrey (JH), Sara Cappelli (SC), Dipanjan Bhattacharya (DB), Sandrine Foti (SF), Anna-Leigh Brown (ALB), Yasmine Asi (YA), Yi Hua Low (YHL), Marco Foiani (MF), Towfique Raj (TR), Emanuele Buratti (EB), Pietro Fratta (PF), Tammaryn Lashley (TL).

    TL and PF conceptualised the studies with guidance from EB. **AB**, AG and JH contributed equally. **AB** performed all the immunohistochemistry, immunofluorescence and analysis and drafted the majority of the manuscript. AG performed validation of cryptic exons in cell and patient brain. JH performed all the RNA-seq analysis with assistance from TR and ALB. SC generated the SH-SY5Y cell model of hnRNP K knockdown. YA and YHL performed earlier pathological investigations. DB assisted in the analysis of IHC staining. PF, TL, EB and MF all had input on the final manuscript.

4. **In which chapter(s) of your thesis can this material be found?**

Chapter 3: HnRNP K mislocalisation in pyramidal neurons of the frontal cortex.

5. **Candidate's e-signature:** [redacted for purpose of publishing open access]
   Date: 28/03/2022

6. **Supervisor/senior author(s) e-signature:** [redacted for purpose of publishing open access]
   Date: 28/03/2022

Form 3:

This form should be completed as many times as necessary. For instance, if a student had seven thesis chapters, two of which having material which had been published, they would complete this form twice.

1. **For a research manuscript that has already been published** (if not yet published, please skip to section 2)**:**
    a. **Where was the work published?** Neuropathology and applied Neurobiology
    b. **Who published the work?** Wiley
    c. **When was the work published?** Jan 22nd, 2022
    d. **Was the work subject to academic peer review?** YES
    e. **Have you retained the copyright for the work?** YES [If no, please seek permission from the relevant publisher and check the box next to the below statement]:

        ☐ *I acknowledge permission of the publisher named under 1b to include in this thesis portions of the publication named as included in 1a.*

2. **For a research manuscript prepared for publication but that has not yet been published** (if already published, please skip to section 3)**:**
    a. **Where is the work intended to be published?** (e.g. journal name)
    b. **List the manuscript's authors in the intended authorship order:**
    c. **Stage of publication:**
        ☐ Not yet submitted
        ☐ Submitted
        ☐ Undergoing revision after peer review
        ☐ In press

3. **For multi-authored work, please give a statement of contribution covering all authors** (if single-author, please skip to section 4)**:**

    Rahul Sidhu (RS), Ariana Gatt (AG), Pietro Fratta (PF), Tammaryn Lashley (TL) and **Alexander Bampton (AB)**

    AB and TL conceptualised the studies. **AB** and RS contributed equally to the pathological investigations and analysis. **AB** drafted the manuscript with input from TL, PF and AG.

4. **In which chapter(s) of your thesis can this material be found?**

Chapter 4: HnRNP K mislocalisation in neurons beyond the cortex.

5. **Candidate's e-signature:** [redacted for purpose of publishing open access]
   Date: 28/03/2022

6. **Supervisor/senior author(s) e-signature:** [redacted for purpose of publishing open access]
   Date: 28/03/2022

Form 4:

1. **For a research manuscript that has already been published** (if not yet published, please skip to section 2)**:**
    a. **Where was the work published?** Nature
    b. **Who published the work?** Springer Nature
    c. **When was the work published?** Feb 23rd, 2022
    d. **Was the work subject to academic peer review?** YES
    e. **Have you retained the copyright for the work?** YES [If no, please seek permission from the relevant publisher and check the box next to the below statement]:

        ☐ *I acknowledge permission of the publisher named under 1b to include in this thesis portions of the publication named as included in 1a.*

2. **For a research manuscript prepared for publication but that has not yet been published** (if already published, please skip to section 3)**:**
    a. **Where is the work intended to be published?** (e.g. journal name)
    b. **List the manuscript's authors in the intended authorship order:**
    c. **Stage of publication:**
        ☐ Not yet submitted
        ☐ Submitted
        ☐ Undergoing revision after peer review
        ☐ In press

3. **For multi-authored work, please give a statement of contribution covering all authors** (if single-author, please skip to section 4)**:**

    Anna-Leigh Brown (A.-L.B), Oscar G. Wilkins (O.G.W), Matthew J. Keuss (M.J.K), Sarah E. Hill (S.E.H), Matteo Zanovello (M.Z), Weaverly Colleen Lee (W.C.L), **Alexander Bampton** (A.B), Flora C. Y Lee (F.C.Y.L)., Laura Masino (L.M), Yue A. Qi (Y.A.Q), Sam Bryce-Smith (S.B.-S), Ariana Gatt (A.G), Martina Hallegger (M.G), Delphine Fagegaltier (D.F), Hemali Phatnani (H.P), NYGC ALS Consortium, Jia Newcombe (J.N), Emil K. Gustavsson (E.K.G), Sahba Seddighi (S.S), Joel F. Reyes (J.F.R), Steven L. Coon (S.L.C), Daniel Ramos (D.R), Giampietro Schiavo (G.S), Elizabeth M. C. Fisher (E.M.C.F), Towfique Raj (T.R), Maria Secrier (M.S), Tammaryn Lashley (T.L), Jernej Ule (J.U), Emanuele Buratti (E.B), Jack Humphrey (J.H), Michael E. Ward (M.E.W) & Pietro Fratta (P.F).

    Conceptualisation: A.-L.B., O.G.W., M.J.K., S.E.H., J.H., M.E.W. and P.F. Data curation: A.-L.B., O.G.W., M.Z., W.C.L. and S.B.-S. Formal analysis: A.-L.B., O.G.W., M.J.K., M.Z., W.C.L., S.B.-S., A.B., M.H., E.K.G., S.S.,

J.F.R., S.L.C. and D.R. Funding acquisition: P.F., M.E.W. and E.B. Investigation: A.-L.B., O.G.W., M.J.K., S.E.H., M.Z., W.C.L., F.C.Y.L., L.M., Y.A.Q., S.B.-S., **A.B** (BaseScope™ *in situ* hybridisation analysis on post-mortem brain)., A.G., M.H., E.K.G., S.S., J.F.R., S.L.C., D.R., E.K.G. and S.L.C. Methodology: A.-L.B., O.G.W., M.J.K., S.E.H., J.H., M.E.W. and P.F. Project administration: P.F. and M.E.W. Resources: H.P., T.L., E.B., D.F. and J.N. Software: A.-L.B., O.G.W., M.Z., S.B.-S., J.H. and M.J.K. Supervision: P.F., M.E.W., J.H., J.U., M.S., T.R., T.L., E.M.C.F., G.S. and T.F. Visualization: A.-L.B., O.G.W., M.J.K., W.C.L. and S.E.H. Writing, original draft: A.-L.B., O.G.W., M.J.K., M.E.W. and P.F. Writing, review and editing: S.E.H., W.C.L., E.B., J.U., J.H., M.E.W., P.F. A.-L.B., O.G.W. M.J.K. and S.E.H. contributed equally; therefore each may place their name first in author order when referencing this manuscript in personal communications.

4. **In which chapter(s) of your thesis can this material be found?**

Chapter 6: HnRNP K knockdown-induced splicing changes, cryptic exons and how to find them.

5. **Candidate's e-signature:** [redacted for purpose of publishing open access]
   Date: 28/03/2022

6. **Supervisor/senior author(s) e-signature:** [redacted for purpose of publishing open access]
   Date: 28/03/2022

Form 5:

1. **For a research manuscript that has already been published** (if not yet published, please skip to section 2)**:**
    a. **Where was the work published?** Neuropathology
    b. **Who published the work?** Wiley

    _____

    c. **When was the work published?** March 27th, 2022

    _____

    d. **Was the work subject to academic peer review?** YES
    e. **Have you retained the copyright for the work?** YES [If no, please seek permission from the relevant publisher and check the box next to the below statement]:

    ☐ *I acknowledge permission of the publisher named under 1b to include in this thesis portions of the publication named as included in 1a.*

2. **For a research manuscript prepared for publication but that has not yet been published** (if already published, please skip to section 3)**:**
    a. **Where is the work intended to be published?** (e.g. journal name)

    _____

    b. **List the manuscript's authors in the intended authorship order:**
    c. **Stage of publication:**
        ☐ Not yet submitted
        ☐ Submitted
        ☐ Undergoing revision after peer review
        ☐ In press

3. **For multi-authored work, please give a statement of contribution covering all authors** (if single-author, please skip to section 4)**:**

    Puja R. Mehta (PM), Tammaryn Lashley (TL), Pietro Fratta (PF), **Alexander Bampton (AB)**

    AB and PF conceptualised the article. **AB** and PM contributed equally to the manuscript with input from PF and TL. AB created the figure / artwork.

4. **In which chapter(s) of your thesis can this material be found?**

Chapter 6: HnRNP K knockdown-induced splicing changes, cryptic exons and how to find them.

5. **Candidate's e-signature:** [redacted for purpose of publishing open access]
   Date: 28/03/2022

6. **Supervisor/senior author(s) e-signature:** [redacted for purpose of publishing open access]
   Date: 28/03/2022

Abstract

Heterogeneous nuclear ribonucleoproteins (hnRNPs) are a diverse, multi-functional family of RNA-binding proteins. Many such proteins, including TDP-43 and FUS, have been strongly implicated in the pathogenesis of frontotemporal lobar degeneration (FTLD) and amyotrophic lateral sclerosis (ALS). By contrast hnRNP K, the focus of this thesis, has been underexplored in the context of neurodegenerative disease.

The first work to be described here involves a comprehensive pathological assessment of hnRNP K protein's neuronal localisation profile in FTLD, ALS and control brain tissue. Following pathological examination, hnRNP K mislocalisation from the nucleus to the cytoplasm within pyramidal neurons of the cortex was identified as a novel neuropathological feature that is associated with both neurodegenerative disease and ageing. Double immunofluorescence was used to confirm these neurons were anatomically distinct from those harbouring the classical TDP-43 or Tau proteinaceous inclusions used in the pathological diagnosis of FTLD. Nuclear loss and mislocalisation of hnRNP K to the cytoplasm was then identified to also occur in two further neuronal cell types within the dentate nucleus of the cerebellum and the CA4 region of the hippocampus. As with pyramidal neurons, similar associations were identified between disease, age and hnRNP K mislocalisation in neurons of the dentate nucleus. Hence, neuronal mislocalisation of hnRNP K across the brain has potentially broad relevance to dementia and the ageing process.

Almost all hnRNPs have been found to perform essential homeostatic functions in regulating appropriate target gene splicing activity. Recently, several hnRNPs have been found to have important roles in repressing the inclusion of non-conserved, so-called 'cryptic exons' within mature mRNA transcripts. Inclusion of cryptic exons following TDP-43 nuclear depletion and subsequent reductions in the functional levels of target transcripts and proteins is an emerging pathogenic theme of several neurodegenerative diseases

including FTLD and ALS. To recapitulate the functional implications of the hnRNP K nuclear depletion that is observed in brain tissue, a hnRNP K knockdown neuronal model was developed utilising an iPSC-derived CRISPR-interference based platform. RNA-seq analysis revealed that nuclear hnRNP K protein depletion within cortical neurons is associated with the robust activation of several cryptic exon events in mRNA targets of hnRNP K as well as the upregulation of other abnormal splicing events termed ‘skiptic exons’. Several of these novel splicing events were validated molecularly using three-primer PCRs.

Finally, an *in situ* hybridisation (ISH) based technology (BaseScope™) platform was optimised to visualise novel cryptic events in post-mortem brain tissue. The platform was used to detect a recently discovered cryptic exon within synaptic gene *UNC13A* and another in the insulin receptor (*INSR)* gene, two newly described targets of TDP-43. These events were found specifically in FTLD-TDP or ALS brains, validating it as a specific marker of TDP-43-proteinopathy. A methodological pipeline was also developed to delineate the spatial relationship between cryptic exons and associated TDP-43 pathology. Hence, providing a platform for the future detection, validation and analyses of novel cryptic exons associated with hnRNP K protein depletion in pyramidal neurons.

Impact statement

The vast majority of neurodegenerative diseases are incurable, unpreventable and progressively debilitating disorders which have a devastating impact on the quality of life of those affected. Advancing age is the biggest risk factor for these diseases and, in an ageing population, their threat to human health is increasing. Pathologically, neurodegenerative diseases converge on the progressive, irreversible dysfunction and eventual loss of neurons and synapses within the nervous system in a neuroanatomical pattern consistent with clinical symptomatology.

A better mechanistic understanding of the basic pathways that lead to neurodegeneration will be essential in order to unveil novel candidates with potential disease-modifying or biomarker utility. Perhaps the best known unifying feature of these diseases is the presence of proteinaceous inclusions within affected regions as a result of protein misfolding and subsequent aggregation of aberrant protein conformers. Biochemical identification of the primary protein component of these inclusions whether it be *β*-amyloid, tau, α-synuclein, TDP-43, FUS or other more rare examples has had major impacts on research efforts and therapeutic developments to date. Indeed, these protein hallmarks have acted as pathological guideposts which have directed the development of myriad cell and transgenic animal models aimed at faithfully recapitulating human disease. Many such models have yielded insightful discoveries that have led to a greater understanding of cellular and molecular pathways that underpin disease including a crucial role for perturbed RNA metabolism. However, preclinical models fail to completely phenocopy human disease and translatability remains a serious challenge. Therefore, there is an urgent need to investigate additional proteins and cell factors beyond those typically associated with protein inclusions, which may have broader relevance to the neurodegeneration phenotype.

Heterogeneous nuclear ribonucleoprotein K (hnRNP K) is an RNA-binding protein (RBP) which, until now, has been very underexplored in the context of

neurodegenerative disease. As with many RBPs, hnRNP K has crucial, widespread roles in the regulation of many, if not all RNA processes from transcription to translation. The research described in this thesis, much of which has been published in several peer review journals, introduces hnRNP K as a new protein player on the scene of neurodegeneration. The work to be presented includes the first pathological description of hnRNP K mislocalisation in neurons, an entirely novel neuropathological event found to be associated with several neurodegenerative diseases and ageing. Later and through the use of state-of-the-art CRISPR-interference (CRISPRi) iPSC technology, hnRNP K neuronal depletion was found to lead to widespread alterations in gene splicing including the inducement of non-conserved cryptic and skiptic exon events in some targets. Hence, this body of work also presents new, strong evidence for how hnRNP K nuclear depletion causes dysfunction in neurons and therefore also potentially in the human diseased brain. This of course also adds to the exponentially fast growing body of evidence for RNA misprocessing in neurodegeneration as a whole.

In summary, the work described has the possibility to inform and direct future research efforts aimed at gaining a better understanding of hnRNP K protein dysfunction in neurodegeneration as a potentially common theme of disruption across the neurodegenerative disease spectrum.

Table of Contents

List of Figures

List of Tables

Glossary of commonly used abbreviations

Aβ – Amyloid Beta

AD – Alzheimer's disease

ALS – Amyotrophic lateral sclerosis

CA1-4 – Cornu ammonis subfields 1-5

CAA – Cerebral amyloid angiopathy

CE – Cryptic exon

CRISPR – Clustered regularly interspaced short palindromic repeat

CRISPRi – CRISPR-interference

DAB – 3,3'-Diaminobenzidine

DEG – Differentially expressed gene

DPR – Dipeptide-repeat protein

FFPE – Formalin-fixed paraffin-embedded

FTLD – Frontotemporal lobar degeneration

GO – Gene ontology

GWAS – Genome-wide association study

HnRNP – Heterogeneous ribonucleoprotein

IHC – Immunohistochemistry

iPSC – Induced pluripotent stem cell

ISH – *in situ* hybridisation

LCD – Low complexity domain

LFC – Log_2 fold change

NLS – Nuclear localisation sequence

PCR – Polymerase chain reaction

PSI – Percentage spliced in (%)

PTC – Premature termination codon

RBP – RNA binding protein

RT-qPCR – Real-time (quantitative) PCR

SE – Skiptic exon

sgRNA – single guide RNA

TSS – Transcription start site

Publications and presentations produced during PhD

First author publications

Bampton, A., Gittings, L. M., Fratta, P., Lashley, T. and Gatt, A. (2020). "The role of hnRNPs in frontotemporal dementia and amyotrophic lateral sclerosis." *Acta Neuropathologica*, 140 (5), pp. 599–623. doi: 10.1007/s00401-020-02203-0.

Bampton, A., Gatt, A., Humphrey, J., Cappelli, S., Bhattacharya, D., Foti, S., Brown, A.-L., Asi, Y., Low, Y. H., Foiani, M., Raj, T., Buratti, E., Fratta, P. and Lashley, T. (2021). "HnRNP K mislocalisation is a novel protein pathology of frontotemporal lobar degeneration and ageing and leads to cryptic splicing." *Acta Neuropathologica*, 142 (4), pp. 609–627. doi: 10.1007/s00401-021-02340-0.

Last author publications

Sidhu, R., Gatt, A., Fratta, P., Lashley, T. and **Bampton, A**. (2022). "HnRNP K mislocalisation in neurons of the dentate nucleus is a novel neuropathological feature of neurodegenerative disease and ageing." *Neuropathology and Applied Neurobiology*. doi: 10.1111/nan.12793.

Mehta, P. R., Lashley, T., Fratta, P. and **Bampton, A**. (2022). "Markers of cognitive resilience and a framework for investigating clinical heterogeneity in ALS." *The Journal of Pathology*. doi: 10.1002/path.5897.

Co-author publications

Brown, A.-L., Wilkins, O. G., Keuss, M. J., Hill, S. E., Zanovello, M., Lee, W. C., **Bampton, A**., Lee, F. C. Y., Masino, L., Qi, Y. A., Bryce-Smith, S., Gatt, A., Hallegger, M., Fagegaltier, D., Phatnani, H., NYGC ALS Consortium, Newcombe, J., Gustavsson, E. K., Seddighi, S., Reyes, J. F. and Fratta, P. (2022). "TDP-43 loss and ALS-risk SNPs drive mis-splicing and depletion of UNC13A." *Nature*, 603 (7899), pp. 131–137. doi: 10.1038/s41586-022-04436-3.

Thompson, A. G., Gray, E., **Bampton, A**., Raciborska, D., Talbot, K. and Turner, M. R. (2019). "CSF chitinase proteins in amyotrophic lateral sclerosis." Journal of Neurology, Neurosurgery, and Psychiatry, 90 (11), pp. 1215–1220. doi: 10.1136/jnnp-2019-320442.

Essays

Bampton A. (2022). "HnRNP K: The new kid on the block in neurodegenerative disease and ageing."

- Winner of the 2021 Queen Square Essay prize.

First author oral presentations

Bampton, A et al. (2021). “Neuronal mislocalisation of hnRNP K in frontotemporal lobar degeneration and ageing”. In: AD/PD 2021 The 15th International Conference on Alzheimer’s & Parkinson’s Disease, (Online) 9-14 March 2021.

- Junior Faculty Award winner at AD/PD 2021.

First author poster presentations

Bampton, A et al. (2021). “HnRNP K mislocalisation in frontotemporal dementia.” In : 122nd Meeting of the British Neuropathological Society, London (online) 3-4 March 2021. Available from: https://app.oxfordabstracts.com/events/1992/program-app/submission/227573

- First Place Poster Prize at the 122nd meeting of the British Neuropathological Society (BNS) Conference.

Chapter 1 Introduction

1.1 Publication statement

The contents of this chapter in section **1.8** and **1.10** have been previously published open access within a review article (Bampton *et al.*, 2020) but have been substantially modified and updated for inclusion here. The work is reproduced as per the publisher's (Springer) reuse policy for 'scholarly and educational purposes.'

1.1.1 Statement of contribution

The author performed the entire literature review for this section and created all accompanying figures and artwork unless otherwise specified, including those previously published (Bampton *et al.*, 2020). Where required, copyright licences were obtained from individual publishers to reproduce figures as specified in the accompanying captions.

1.2 The growing burden of neurodegenerative disease

The term 'neurodegenerative disease' encapsulates a multitude of heterogeneous neurodegenerative disorders which, pathologically, converge on the progressive degeneration of the central or peripheral nervous system. Such diseases are highly diverse in their respective pathophysiologies and include conditions most associated with cognitive decline (dementias) and movement (neuromuscular) disorders.

Neurodegenerative disorders are exceptionally debilitating and have an enormous psychosocial impact on the lives of patients and their surrounding family and friends. Considering dementia alone, in 2016 the global number of individuals living with the condition was 43.8 million, an increase from 20.2 million in 1990, was the fifth leading cause of death globally (2.4 million) and accounted for 28.8 million disability-adjusted life years (DALYs) (GBD 2016

Dementia Collaborators, 2019). Indeed, the progressive functional loss experienced by patients and their resultant diminishing sense of independence has devastating and constantly evolving physical, emotional and financial consequences. The vast amount of these disorders, including all age-related neurodegenerative diseases, are incurable with no disease-modifying therapies available that are capable of halting or delaying the neurodegenerative process (Cummings *et al.*, 2017; Rezak and de Carvalho, 2020). In an ageing population, where age is the primary risk factor for most neurodegenerative diseases, how society responds to the challenges that accompany an increase in frequency of these diseases will be of global importance (GBD 2016 Neurology Collaborators, 2019).

The scientific community is dauntingly tasked with gaining a better understanding of the aetiological causes, pathomechanistic processes and potential molecular vulnerabilities of neurodegenerative disease. It is only via intensive broad-ranging research efforts, meticulous due process and appropriate deductive reasoning that light may be shed on clinically viable targets for therapeutic agents and novel treatment strategies.

The focus of the work in this thesis has been on frontotemporal lobar degeneration (FTLD) and to some extent the clinically, pathologically and genetically overlapping neuromuscular disorder amyotrophic lateral sclerosis (ALS) which are both discussed in the next sections. Alzheimer's disease, by far the most prevalent neurodegenerative disease is also discussed below and referred to throughout the body of work encompassing this thesis.

1.3 Frontotemporal lobar degeneration

1.3.1 Pathological overview

Frontotemporal lobar degeneration (FTLD) is an umbrella term for a heterogeneous group of neurological disorders that converge, pathologically, on the selective degeneration of the frontal and often anterior temporal lobes of the brain (Mackenzie and Neumann, 2016). The current pathological

classification system of FTLD recognises five major molecular sub-groups. Three of which: FTLD-TDP, FTLD-tau and FTLD-FUS are characterised by the presence of specific proteinaceous inclusions predominantly containing transactive response DNA-binding protein 43 (TDP-43), microtubule-associated protein tau or fused in sarcoma (FUS) protein respectively (Mackenzie *et al.*, 2009; Lashley *et al.*, 2015). FTLD-TDP is sub-classified into five sub-groups (type A-E) and FTLD-FUS into three sub-groups according to the histopathological deposition patterns of both proteins (Mackenzie *et al.*, 2009; Lashley *et al.*, 2015; Lee *et al.*, 2017). Example images of some of the histopathological characteristics of each FTLD-TDP subtype are shown in **Figure 1.1**.

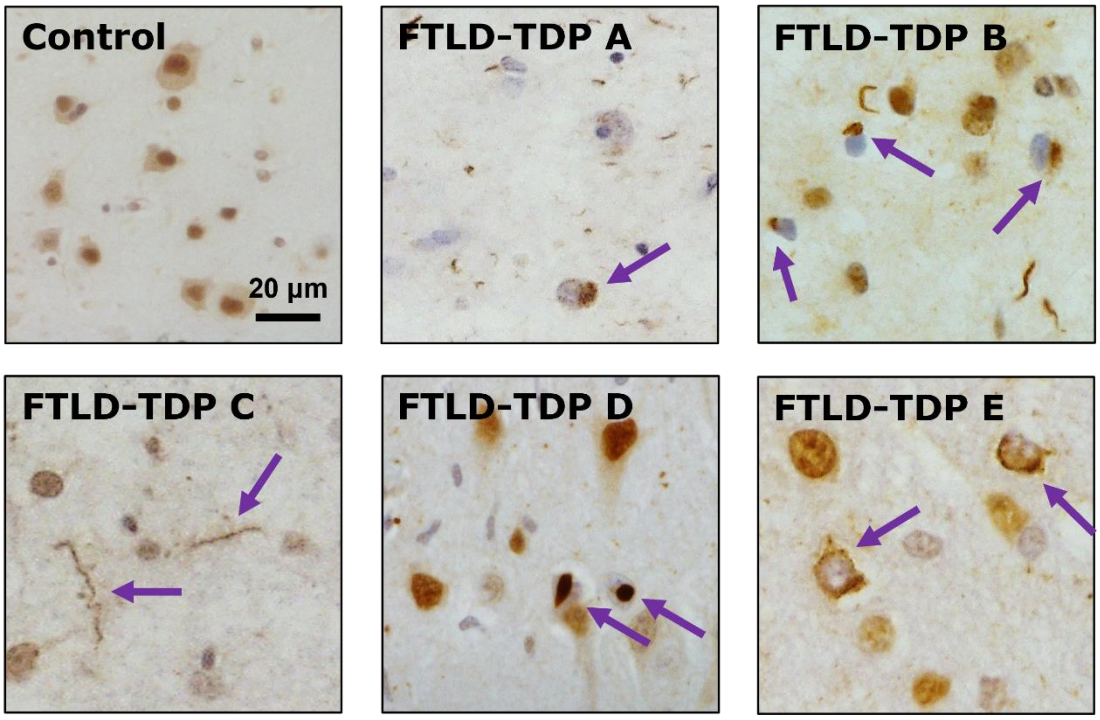

Figure 1.1. Histopathological characteristics of FTLD-TDP subtypes. Representative TDP-43 stained cortical sections showing normal nuclear neuronal staining in controls and the distinct, inclusion morphologies characteristic of FTLD-TDP A (dense cytoplasmic inclusions and short dystrophic neurites primarily within layer II), FTLD-TDP B (compact cytoplasmic inclusions with few neurites across cortical layers), FTLD-TDP C (long distinctive dystrophic neurites), FTLD-TDP D (intranuclear inclusions) and the recently defined FTLD-TDP E (granulofilamentous neuronal inclusions in frontal cortex. All cases were pathologically diagnosed and stained at the Queen Square Brain Bank.

Similarly, FTLD-tau is sub-classified into five diseases dependent on the biochemical composition of Tau (3- or 4-repeat) in addition to the morphology and sub-cellular locality of inclusions (Dickson *et al.*, 2011; Irwin *et al.*, 2015). There is a fourth rare sub-grouping of cases with, as yet, unclarified pathology. A major proportion of these cases contain ubiquitinated inclusions but that are tau, FUS and TDP-43 negative. These cases, re-classified as FTLD-UPS are commonly associated with a dominant mutation in charged multivesicular protein 2B (*CHMP2B*) (van der Zee *et al.*, 2008). An exceptionally rare subgroup of cases (FTLD-ni) meet diagnostic criteria for FTLD but are not currently associated with any inclusions (Mackenzie *et al.*, 2010) (**Figure 1.2**).

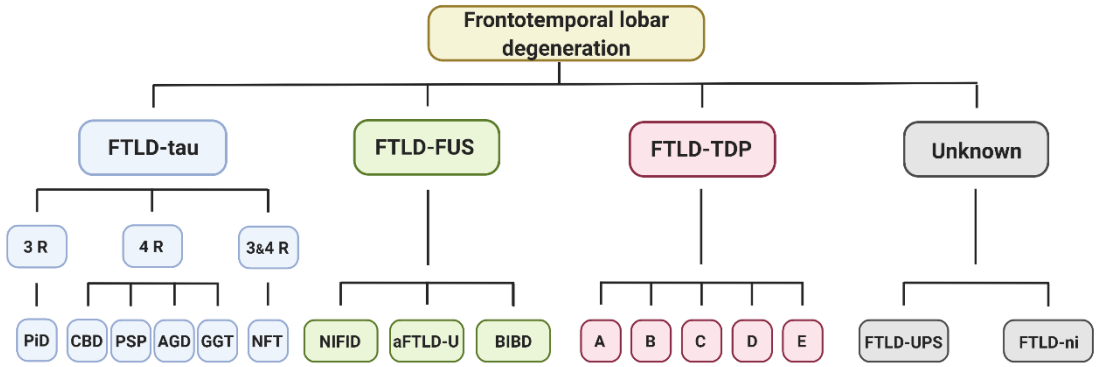

Figure 1.2. Pathological sub-classification of frontotemporal lobar degeneration subtypes. Recognised subtypes of FTLD-tau include 3 repeat (PiD, Pick's disease), 4-repeat (CBD, corticobasal degeneration; PSP, progressive supranuclear palsy; AGD, argyrophilic grain disease; GGT, globular glial tauopathy) and 3/4 R tau-repeat (NFT, neurofibrillary tangle predominant dementia) associated diseases. FTLD-FUS is subclassified into three subtypes (NIFID, neurofilament inclusion disease; aFTLD-U, atypical FTLD-FUS and BIBD, basophilic inclusion body disease). FTLD-TDP is subclassified A-E and as-yet uncharacterised FTLD cases are sub-grouped into either ubiquitin-positive (FTLD-UPS) or no known inclusion (FTLD-ni) subtypes.

1.3.2 Clinical presentation

The neurocognitive syndrome that results from the progressive dysfunction of these brain regions is broadly defined as frontotemporal dementia (FTD). Whilst FTD itself is a comparatively rare form of dementia, accounting for just under 5 % of all cases; it is the most common non-Alzheimer's type of young-onset dementia presenting in patients under 65 years of age (Rosso *et al.*, 2003). Clinically, there are three main FTD subtypes, the most frequently presenting behavioural variant (bvFTD) and two less common language

variants; semantic variant primary progressive aphasia (svPPA) and progressive nonfluent aphasia (PNFA) (Warren, Rohrer and Rossor, 2013).

In bvFTD, behavioural and psychiatric manifestations precede cognitive changes and include disinhibition, mood-changes, compulsive tendencies, apathy, reduced empathy and psychotic episodes as well as deficits in executive functioning (Lanata and Miller, 2016). Patients presenting with svPPA exhibit a progressive impairment of single-word comprehension and categorisation with an inability to ascribe words to their meanings within otherwise fluent speech (Gorno-Tempini *et al.*, 2011). By contrast, patients with initial PNFA presentation have relatively preserved comprehension and semantic memories but struggle with the formulation of speech leading to poor expressive language and fluency (Rosen *et al.*, 2006). Behavioural associated FTD symptoms may typically accompany a semantic dementia diagnosis, but rarely an PNFA one (Seelaar *et al.*, 2011).

Despite there being strong associations between certain clinical presentations and underlying genetics within each distinct FTLD pathology; clinicopathological correlations are very inconsistent (Irwin *et al.*, 2015; Kawakami, Arai and Hasegawa, 2019) although some relationships are illustrated later in **Figure 1.6**. This poses a challenge not only for differential diagnoses and clinical management but also for the development of novel therapeutics designed to target specific disease pathways.

1.3.3 Genetics

Approximately 40 % of FTLD cases are heritable and mutations within three genes: *C9orf72*, *MAPT* and *GRN* account for the majority of these autosomal dominant familial FTLD (fFTLD) cases (Rainero *et al.*, 2017). The most common genetic cause of fFTLD is a mutation within the non-coding hexanucleotide (G_6C_2) repeat expansion of the chromosome 9 open reading frame 72 (*C9orf72*) gene which accounts for around a quarter of fFTLD cases, mostly FTLD-TDP B, with an especially high prevalence in European and North American Caucasian populations (Balendra and Isaacs, 2018). The

pathological consequences underlying the pathogenicity of this mutation are described in detail later (**1.9.3**). Familial FTLD-tau is usually caused by mutations within microtubule associated protein tau (*MAPT*) and account for between 5–20 % of total fFTLD cases dependent on geographic distribution (Pottier *et al.*, 2016). Over 40 unique *MAPT* mutations have been identified and the vast majority of these exert there pathogenicity by altering the splicing regulation of *MAPT* exon 10 leading to an elevated 4-repeat/3-repeat region ratio (Strang, Golde and Giasson, 2019), discussed in more detail later in (**1.10.1**). Finally, mutations within the progranulin (*GRN*) gene represent the third major genetic cause of FTLD accounting for a further 5-25 % of fFTLD cases (Snowden *et al.*, 2006; Rademakers, Neumann and Mackenzie, 2012). Over 70 diverse mutations have been identified within *GRN* which all converge on a 50 % loss of function through the generation of nonsense-mediated decay (NMD)-sensitive mRNA isoforms (Baker et al. 2006). *GRN* mutations are strongly associated with FTLD-TDP A type pathology (Lee *et al.*, 2017).

A small number of rare, high-risk genes account for a further minority of fFTLD cases including those within charged multivesicular protein 2B (*CHMP2B*), valosin-containing protein (*VCP*), sequestosome 1 (*SQSTM1*), ubiquilin-2 (*UBQLN-2*), optineurin (*OPTN*), TANK binding kinase 1 (*TBK1*), and hnRNP A1/A2B1 among others, the former 4 of which are strongly implicated within the regulation of numerous proteostatic mechanisms (Pottier *et al.*, 2016). A small number of common risk variants including those in transmembrane protein 106B (*TMEM106B*) and *GRN* have also been identified from genome-wide association studies (GWASs) (Van Deerlin *et al.*, 2010) (**Figure 1.3**).

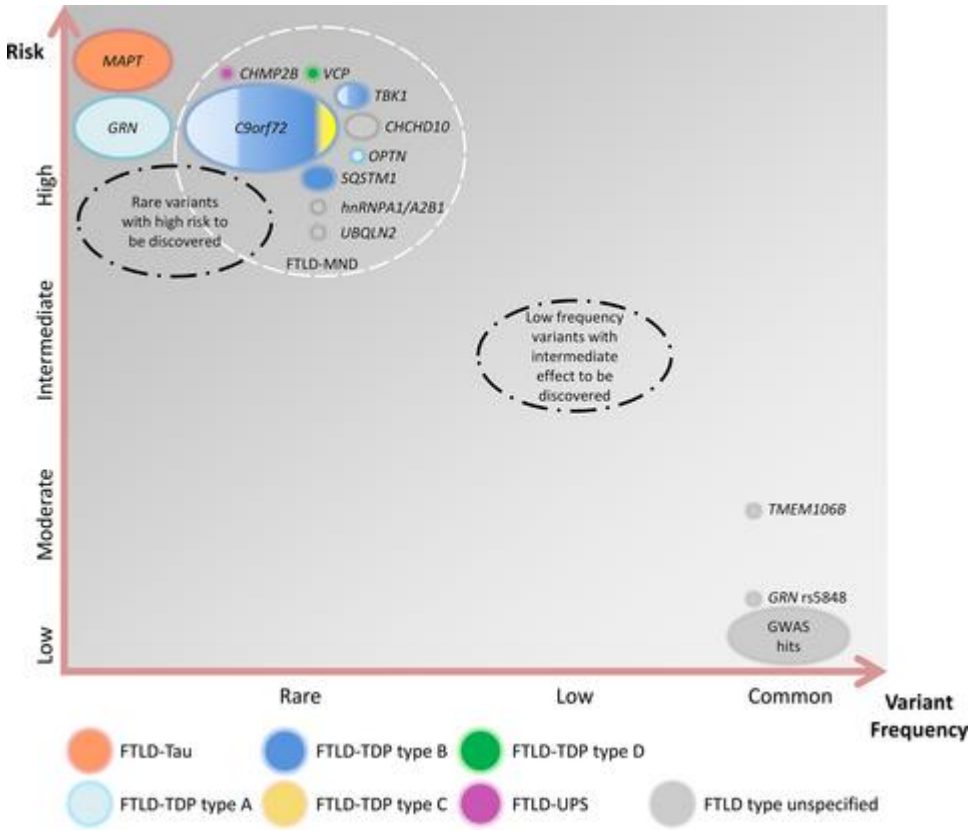

Figure 1.3. FTLD-associated gene variants. A graphical display of FTLD-associated gene variants along with their relative risk, general population frequency and associated pathological subtype (Pottier *et al.*, 2016, Wiley license: 5325381402298).

1.4 Amyotrophic lateral sclerosis

1.4.1 Pathological overview

Amyotrophic lateral sclerosis (ALS) is a devastating neuromuscular disease and the most common form of motor neuron disease (MND). It is characterised by the relentless neurodegeneration of both upper motor neurons (UMNs) of the pyramidal tracts and lower motor neurons (LMNs) within the brain stem and anterior horn of the spinal cord (Maekawa *et al.*, 2004). Microscopically, the hallmark pathological feature of ALS in 97 % of all cases is the presence of cytoplasmic TDP-43 inclusions in neurons and glial cells including astrocytes and oligodendrocytes (Suk and Rousseaux, 2020). Some examples of ALS neurons of the motor cortex and LMNs of the spinal cord (cervical) exhibiting TDP-43 pathology are shown in **Figure 1.4**. TDP-43

deposition is believed to begin within motor neurons of the cortex, the lower brain stem and spinal cord before spreading to frontal and parietal regions, the red nucleus, the substantia nigra and later still, the hippocampus (Braak *et al.*, 2013).

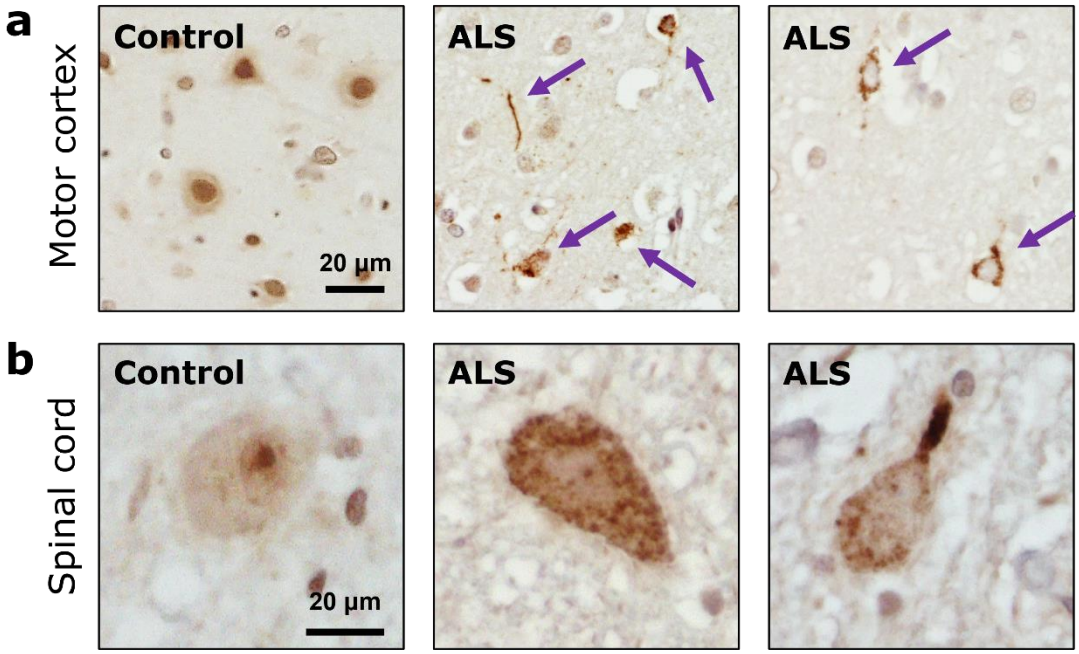

Figure 1.4. TDP-43 inclusions in ALS. (a) TDP-43 staining of control and ALS neurons of the motor cortex. Arrows indicate a variety of inclusion types including a dystrophic neurite and diffuse inclusions (centre panel) and neurons exhibiting robust nuclear depletion of TDP-43 and granular cytoplasmic accumulation (centre right). (b) TDP-43 staining of control and ALS LMNs of the cervical spinal cord. ALS motor neurons (anterior horn) exhibit TDP-43 nuclear depletion and accompanying granular deposition in the cytoplasm (bottom centre centre) and/or skein-like pathology (bottom right). ALS cases were pathologically diagnosed at Edinburgh Brain Bank and stained at the Queen Square Brain Bank.

In a minority of cases, the predominating pathological protein is not TDP-43 but immunoreactive inclusions of misfolded, mutant superoxide dismutase 1 (SOD1) and in an even small subset of cases an aggregation of the RNA-binding protein FUS (ALS-FUS) within motor neurons instead (Paré *et al.*, 2018; Marrone *et al.*, 2019) (**Figure 1.5**).

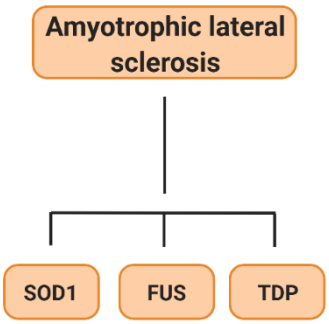

Figure 1.5. Pathological sub-classification of amyotrophic lateral sclerosis subtypes.

In addition to the presence of TDP-43, FUS or SOD1 immunoreactive inclusions which define distinct ALS pathological subtypes, other types of intraneuronal inclusions have also been identified as specific pathological hallmarks of sporadic and/or familial ALS. These include dense, oval-shaped and ubiquitin-negative eosinophilic inclusions called Bunina bodies (BBs), believed to be of lysosomal origin due to being immunoreactive for Cysteine C, an inhibitor of lysosomal cysteine proteases (Okamoto, Mizuno and Fujita, 2008). Upon pathological examination, the detection of intracellular BBs within surviving LMNs of the spinal cord and brain stem motor nuclei is almost diagnostic to ALS and is found within the vast majority of both sporadic and familial cases (Kimura *et al.*, 2014). Intensely ubiquitinated, filamentous skein-like inclusions (SLIs) and Lewy body-like hyaline inclusions (HIs), represent two further types of ALS-associated cytoplasmic inclusion most frequently found in anterior horn cells of the spinal cord (Blokhuis *et al.*, 2013). SLIs are commonly found in both sporadic and familial ALS cases whilst HIs are strongly associated with ALS-SOD1 pathology (Ince *et al.*, 1998). The biological significance of BBs, SLIs and HIs in ALS pathogenesis is poorly understood, but further advancements in ultrastructural analysis may shed further light on their exact compositional basis and functional impact.

1.4.2 Clinical presentation

Clinically, typical ALS manifests as a progressive weakening of voluntary skeletal muscles as motor units deteriorate with simultaneous UMN and LMN involvement at onset. Following a loss of inhibitory tone usually generated recurrently by upper motor neurons; patients also exhibit muscular fasciculations and chronic stiffness, termed spasticity (Ravits *et al.*, 2013). Indeed, the development of spasticity on top of muscle weakness significantly contributes to a patient's functional decline and represents a major clinical challenge for effective palliative care management (Meyer *et al.*, 2019). The majority of patients die from respiratory failure within 3-5 years from symptom onset (Niedermeyer, Murn and Choi, 2019).

Phenotypically, ALS can be classified into distinct clinical variants based on the level of anatomical involvement. Typical ALS (80 - 90 % of all cases) presents as weakness attributable to both UMN (e.g. hyperreflexia, spasticity, slowness of movement and poor balance) and LMN (e.g. muscular atrophy and fasciculations) characteristics (Ravits and La Spada, 2009; Yedavalli, Patil and Shah, 2018). More rarely, ALS presents as either of two extremes of UMN or LMN predominating syndromes warranting the need of two further clinical variants for diagnostic purposes (Grad *et al.*, 2017). Primary lateral sclerosis (PLS) is a purely UMN syndrome which presents with progressive weakness and spasticity of voluntary muscles most commonly beginning in the legs and ascending in a relatively symmetric fashion to the hands, arms and bulbar region (Turner *et al.*, 2020). Progression is slow (1-2 decade long mean disease duration) and insidious with none of the amyotrophy that eventually leads to the fatal complications associated with a typical ALS disease course (Tartaglia *et al.*, 2007; Floeter and Mills, 2009). At the other end of the spectrum, progressive muscular atrophy (PMA) is considered to be a LMN-predominating syndrome characterised by progressive flaccid weakness, amyotrophy, fasciculations and diminishing tendon reflexes. Like PLS, PMA is a diagnosis of exclusion and is often complicated by the later appearance of UMN signs (approximately 30 % develop within 18 months) with many more exhibiting subclinical evidence of UMN pathology at autopsy (Visser *et al.*,

2007; Turner and Talbot, 2013). Median survival duration post-symptom onset for patients with PMA is about 12 months longer than typical ALS cases and predominantly affects men under 50 years of age (Kim *et al.*, 2009). Clinical phenotypes of ALS may also be classified according to anatomical region of onset with an approximately two-third to one-third split between typical limb-onset and bulbar-onset (bulbar palsy) ALS cases, with the latter associated with a faster disease progression (Swinnen and Robberecht, 2014). Further phenotypical sub-classification can be made based on the more specific pattern of onset (e.g. pseudobulbar ALS, cervical/lumbar variants and flail limb variants), pattern of disease progression (e.g. Mill's hemiplegic variant or ascending / multifocal PLS) and/or comorbidity with FTD / cognitive impairment (Grad *et al.*, 2017). However, ALS is a very clinically and pathologically heterogeneous condition and over-classification into distinct clinical subtypes is controversial in the respect that such phenotypes cannot yet be reliably distinguished neuropathologically or genetically and may well just reflect different points on an ALS disease continuum (Ravits *et al.*, 2013).

Anti-glutamatergic drug Riluzole and free radical scavenger Edaravone are the only two licensed medications for ALS, however their expense is high and beneficial efficacies decidedly modest (Dharmadasa and Kiernan, 2018; Yoshino, 2019). Hence there is an urgent unmet clinical need for inexpensive and truly disease-modifying therapeutics for the treatment of ALS.

1.4.3 Genetics

The majority of ALS cases are sporadic (sALS) with no clear aetiological basis of disease. Between 5-10 % of cases are familial (fALS) caused by one or several genetic mutations that are most often inherited in an autosomal dominant pattern (Chen *et al.*, 2013). Interestingly, sALS and fALS variations of the disease appear virtually indistinguishable in a clinical setting. This observation has fuelled many lines of research using fALS mutant cell and animal disease models as well as mechanistic investigations into whether genes found to be mutated within fALS are involved within sporadic ALS (Van Damme, Robberecht and Van Den Bosch, 2017). The most common of these

is again the expansion mutation within *C9ORF72* accounting for approximately 40 % of fALS cases in Europe and North America, to be discussed in more detail later (Balendra and Isaacs, 2018). The remainder of known ALS-causing mutations are largely within three other genes: *SOD1*, *FUS* and TAR DNA binding protein TARDBP accounting for around 12 % (*SOD1*) and 2-3 % of fALS cases respectively (Renton, Chiò and Traynor, 2014). Both *SOD1* and *FUS* mutations are specific to ALS disease and are associated with corresponding SOD1 and FUS immunoreactive sub-type pathologies (Andersen, 2006; Vance *et al.*, 2009). Current evidence points to SOD1 mutations exerting a predominantly toxic gain of function potentially due to a diminished capacity of neurons to cope with oxidative stress whilst the pathogenicity of FUS mutations is even less clear (Berdyński *et al.*, 2022). *TARDBP* mutations have been linked to both loss of function effects including a dysregulation of TDP-43 regulated splicing and gain of function effects associated with the mutant TDP-43 protein (Kabashi *et al.*, 2008; Van Deerlin *et al.*, 2008). The TDP-43 pathology associated with *TARDBP* – linked fALS is similar to that observed in the vast majority of sALS cases. A number of other rare mutations, including *MATR3, NEK1, TIA1* and many of those aforementioned in FTLD including *UBQLN2*, *TBK1*, *OPTN*, *TBK1*, SQSTM1 and *HNRNPA1/A2* account for a small minority of other fALS cases (Nguyen, Van Broeckhoven and van der Zee, 2018; Goutman *et al.*, 2022).

In contrast to FTLD, a higher number of ALS-risk genes have been identified to confer a significant susceptibility or protective bias to sALS pathogenesis. The largest cross-ancestry GWAS to date (29,612 ALS patients, 122,656 controls), identified 15 risk loci. These included eight previously reported loci including polymorphisms within the aforementioned *C9ORF72*, *TBK1* and *SOD1* gene as well as within the synaptic protein-coding *UNC13A* and myelin-associated oligodendrocytic basic protein (*MOBP*) genes among others (van Rheenen *et al.*, 2021).

1.5 FTLD-ALS as a disease continuum

1.5.1 Clinical evidence

FTLD and ALS have long been thought to occupy two ends of a common disease continuum. From a clinical stand-point there is a striking overlap of symptomatology between the two conditions. An estimated 10-15 % of patients with FTD and especially bvFTD will develop concomitant MND (FTD-MND) (Woollacott and Rohrer, 2016). A much higher proportion of patients will develop sub-clinical motor symptoms such as occasional fasciculations and mild muscle wasting (Ferrari *et al.*, 2011). Conversely, FTD-MND can also manifest initially as a primarily MND syndrome. Indeed, cognitive, behavioural and psychiatric changes typical of the bvFTD syndrome including apathy, obsessive compulsivity and depression have been routinely reported within MND case studies since the early 20th century (Ziegler, 1930; Turner *et al.*, 2012). Frequently, the neuropsychological profile of concomitant FTD in initially diagnosed MND patients or the neuromuscular profile of concomitant MND in patients initially presenting with FTD is clinically indistinguishable from pure bvFTD and MND/ALS cases (Saxon *et al.*, 2017).

1.5.2 Pathological evidence

Pathologically, abnormal deposition of the RBP TDP-43 is the major neuropathological feature in 97 % of ALS cases and approximately 50 % of FTLD cases (FTLD-TDP) and are hence grouped together as TDP-43 proteinopathies (Irwin *et al.*, 2015; Suk and Rousseaux, 2020). In ALS, nuclear clearing of TDP-43 is accompanied by an accumulation of the protein into cytoplasmic inclusions (**Figure 1.4**). By contrast, the pattern of TDP-43 deposition across the FTLD-TDP pathological spectrum is far more heterogeneous with a variety of morphologically distinct cytoplasmic and intranuclear TDP-43 immunoreactive inclusions characterising each molecular sub-type (Lee *et al.*, 2017; Suk and Rousseaux, 2020) as shown previously (**Figure 1.1**).

FTD-MND is most commonly associated with FTLD-TDP type B and occasionally type A pathology (Kawakami, Arai and Hasegawa, 2019). In a smaller proportion of FTLD cases (~10 %), the major neuropathological feature is inclusions immunoreactive for FUS (FTLD-FUS) which also account for ~1 % of sporadic and 5 % of familial ALS cases (Lai *et al.*, 2011). Enigmatically though, in contrast to ALS-FUS there have been no FUS mutations in FTLD-FUS confirmed pathologically. The overlapping clinicopathological spectrum of FTLD and ALS is illustrated in **Figure 1.6**.

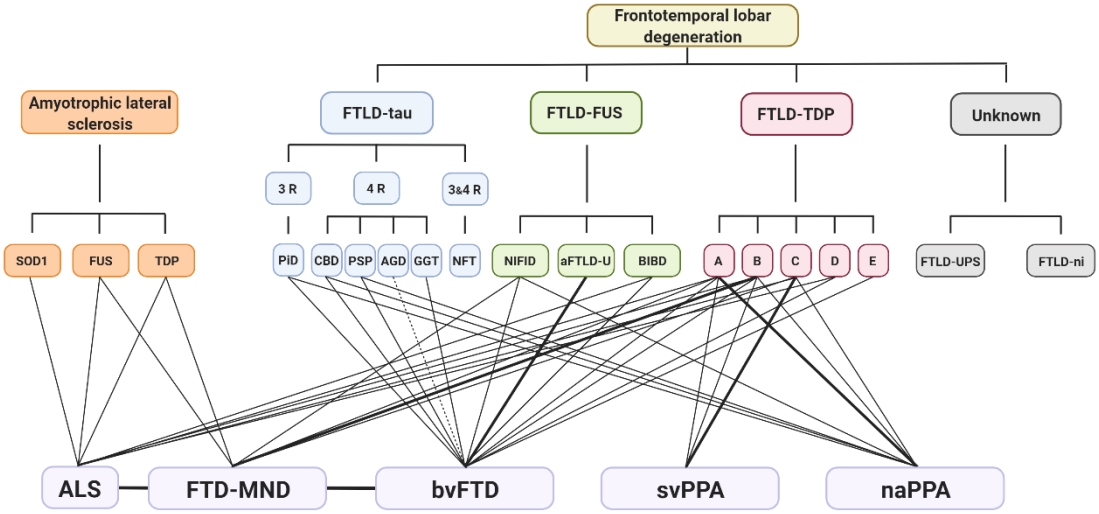

Figure 1.6. The clinicopathological spectrum of amyotrophic lateral sclerosis and frontotemporal lobar degeneration. Lines represent the presence of a correlation between an ALS/FTLD pathological subtype and each clinical subtype which themselves can overlap. Thicker lines indicate a stronger clinicopathological correlation whilst dotted lines indicate a less robust relationship.

1.5.3 Genetic evidence

Perhaps the most compelling evidence supporting the FTLD-ALS continuum comes from shared genetic aetiologies. Mutations in the TDP-43 encoding gene *TARDBP*, first linked to ALS in 2008, accounts for around 1 % of all ALS cases and an even smaller minority of FTLD cases (Van Deerlin *et al.*, 2008; Gendron, Rademakers and Petrucelli, 2013). Notably, rare mutations in several genes involved in protein clearance pathways have also been found to cause both FTLD and ALS individually or a phenotypic overlap between the two including *SQSTM1*, *VCP*, *TBK1* and *UBQLN-2* (Mejzini *et al.*, 2019).

However, the most common genetic cause of both FTLD and ALS is a hexanucleotide repeat expansion (G4C2)n mutation within the first intron of chromosome 9 open reading frame 72 (*C9orf72*) which accounts for around 40 % and 25 % of familial ALS and FTLD cases respectively (DeJesus-Hernandez *et al.*, 2011; Renton *et al.*, 2011). Alleles exceeding around 30 repeats is generally defined as pathogenic although an exact disease threshold remains unclear (van der Ende *et al.*, 2021). At post-mortem, patients with a *C9orf72* expansion mutation typically exhibit TDP-43 proteinopathy (FTLD-TDP type B in the majority of FTLD/FTLD-ALS cases) in addition to *C9orf72*–specific pathologies including intranuclear RNA foci and dipeptide protein repeat (DPR) inclusions from uncanonically translated transcripts (Balendra and Isaacs, 2018). Hence, there is evidence of both FTLD and ALS being on a genetic, as well as a clinicopathological disease spectrum.

1.6 Alzheimer's disease

1.6.1 Pathological overview

Alzheimer's disease (AD) is the most common form of progressive dementia in the world, affecting approximately 47 million people (Dos Santos Picanco *et al.*, 2018). At a gross level AD is characterised by generalised cortical atrophy with a predilection for the medial temporal lobe and a disproportionate degeneration of the hippocampus resulting in significantly reduced hippocampal volume (Perl, 2010). Pathologically though, AD is defined by the presence of two main neuropathological hallmarks or 'positive lesions', namely extracellular β-amyloid plaques and intracellular neurofibrillary tangles across cortical and limbic areas of the brain (Perl, 2010; Lane, Hardy and Schott, 2018) (**Figure 1.7**). Extracellular aggregation of β-amyloid protein is thought to arise from the erroneous cleavage and processing of amyloid precursor protein (APP) by β and γ-secretase enzymes leading to the over-production of insoluble Aβ fibrils with a high propensity towards oligomerisation and aggregation (Zhang *et al.*, 2012). Deposition of β-amyloid protein in and

around brain blood vessels, termed cerebral amyloid angiopathy (CAA) is another recognised major contributor to AD pathogenesis capable of compromising vascular integrity and proper functioning (Greenberg *et al.*, 2020).

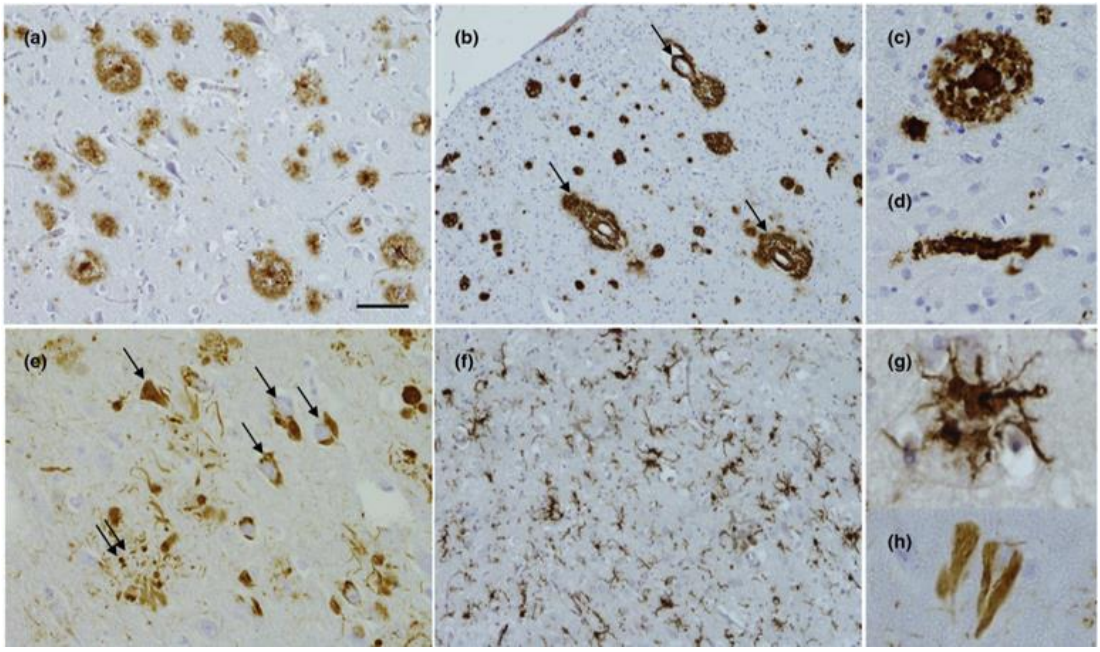

Figure 1.7. Pathological hallmarks of Alzheimer's disease. Top row - Aβ immunohistochemical staining of (a) amyloid plaques in the frontal cortex and at higher magnification (c). (b) deposition within blood vessels as indicated (cerebral angiopathy (CAA) and (d) higher magnification image of Aβ deposition within capillaries in severe CAA. (e) Tau immunohistochemistry of neurofibrillary tangles (arrows), neuritic plaques (double arrows) and a higher magnification neurofibrillary tangle (h). (f and g) reactive microglia. The bar represents 50 µm in a and f, 100 µm in b, 25 µm in c and e and 15 µm in d, g and h (Lane, Hardy and Schott, 2018, Wiley license: 5325250350249).

The second pathological hallmark, neurofibrillary tangles, arises from hyperphosphorylation of the microtubule-associated tau protein and subsequent oligomerisation of the protein into insoluble fibrils. The mechanisms underlying tau-mediated neural damage are incompletely elucidated, but are likely to implicate impaired nucleocytoplasmic transport due to a disrupted microtubule network between neurons (Eftekharzadeh *et al.*, 2018). The ‘Amyloid Cascade Hypothesis’ posits that β-amyloid protein build-up in the brain parenchyma is an essential trigger for tau hyperphosphorylation and thus progression of AD pathology (Hardy and Allsop, 1991; Hardy and Higgins, 1992). This is consistent with Aβ senile plaques predating

neurofibrillary tangle pathology and that tau positivey stains neurites within Aβ plaques (**Figure 1.7e**). However, this hypothesis has come under challenge in light of the failure of many Aβ-directed therapeutic approaches (Golde, Schneider and Koo, 2011; Gulisano *et al.*, 2018). Corticofibrillary pathology has been found to exhibit a predictable distribution pattern across the brain which has led to the development of a systematic six-point staging system of abnormal tau progression (Braak *et al.*, 2006). Early stage AD (I-II) necessitates the bulk of the pathological burden be confined to entorhinal and transentorhinal structures which then progresses to the temporal neocortex and limbic regions (III-IV) and eventually more widely into neocortical association areas (Braak *et al.*, 2006). Whilst both the accumulation of β-amyloid and tau pathologies have the potential to compromise neural functioning, clinical manifestations appear to be more closely correlated to tau-pathology and progression (Biel *et al.*, 2021).

Finally, whilst not a diagnostic pathological hallmark of AD, proliferation and activation of microglia is being increasingly recognised as an important neuropathological feature of AD. Reactive microgliosis or 'activated microglia' refers to an inflammatory response by microglial cells in response to insult or injury whereby microglia adopt an abnormal rod-like, unbranched morphology and accumulate at the site of damage (**Figure 1.7f**) (Hansen, Hanson and Sheng, 2018). Microglia transitioning to this morphology effectively transform into brain macrophages and perform a neuroprotective role in clearing cells and debris by phagocytosis (Hansen, Hanson and Sheng, 2018). However, the full extent of the roles, both beneficial and pathogenic, that microglia play in AD pathogenesis is far from clear. Some lines of research point towards a more deleterious role for microglia in AD, particularly when in a persistent reactive state, whereby they release harmful pro-inflammatory factors, mediate engulfment of neuronal synapses and even contribute to the propagation of tau pathology in the brain (Maphis *et al.*, 2015; Subhramanyam *et al.*, 2019).

1.6.2 Clinical presentation

AD pathogenesis is associated with progressive neurocognitive dysfunction. Early stage disease is commonly linked with mild impairments in cognitive impairment that begin to interfere with routine daily activities including short-term memory disturbances, concentration difficulties, disorientation, confusion and difficulties surrounding complex decision making (Arvanitakis, Shah and Bennett, 2019). Deficits in episodic memory become increasingly salient with progressive hippocampal degeneration and synaptic loss (Halliday, 2017). As the disease progresses from mild to moderate to severe, patients may experience a whole constellation of cognitive, psychiatric and behavioural changes which severely impedes even the simplest of daily activities. These include worsening memory, language impairments, symptoms of apathy and depression, hallucinations, disinhibited behaviour, agitation, aggression and disturbed sleep (Breijyeh and Karaman, 2020). Late stage AD is typically also accompanied by the development of more physical symptoms including mobility difficulties, falls, incontinence and difficulty eating. The clinical presentation of AD is however highly heterogeneous between individuals and is further complicated by the presence of other common comorbidities including other dementias (mixed dementia) and pre-existing age-related cognitive decline (Knopman and Petersen, 2014; Matej, Tesar and Rusina, 2019). There are four licensed medications for AD in the UK which are all targeted towards symptom management. Acetylcholinesterase inhibitors including Donepezil, Rivastigmine and Galantamine (mild-moderate AD) function to increase the bioavailability of acetylcholine neurotransmitter within cholinergic synapses (Hampel *et al.*, 2019). The fourth drug, memantine is used to treat moderate to severe dementia and acts pharmaceutically to dampen glutamatergic activity and associated excitotoxicity (Burns and Iliffe, 2009). The choice and prescribed dosage of these medications is dependent on the severity of symptoms and the patient-specific side effect profiles of each drug which may change throughout the course of disease.

1.6.3 Genetics

AD typically manifests as a late-onset (> 65 years) sporadic disorder (sAD) whilst familial forms of the disease (fAD) are exceedingly rare, accounting for fewer than 0.5 % of all cases. Mutations in three genes, amyloid precursor protein (*APP*), presenilin 1 (*PSEN1*) and presenilin 2 (*PSEN2*) are responsible for all known autosomal dominantly inherited fAD cases which are all associated with a younger onset of clinical symptoms (typically 30-50 years) (O'Brien and Wong, 2011). Mutations within all three genes are thought to convey their pathogenicity through the erroneous processing of the transmembrane APP protein. Indeed, within *APP* itself, mutations cluster around the γ-secretase or BACE1 cleavage sites (Tcw and Goate, 2017). However, *APP* gene locus duplication and triplication mutations have also been found to be causative of AD suggesting high Aβ load is sufficient to invoke pathological amyloidosis (Sleegers *et al.*, 2006). Indeed, early-onset AD in people with Down's syndrome is extremely common (> 50 %) due to their carrying of an extra copy of *APP*-containing chromosome (trisomy) 21 (Hof *et al.*, 1995). Mutations within presenilin proteins (179 *PSEN1* and 14 *PSEN2*), which are catalytic components of γ-secretase enzyme, are thought to exert their influence via a loss of function mechanism whereby reduced presenilin catalytic activity leads to the overproduction of the more insoluble and toxic Aβ42 protein isomer (Shen and Kelleher, 2007; O'Brien and Wong, 2011).

Genetic contributions are also believed to be extremely important in the aetiological underpinning of sAD. Over 20+ common, gene variants from high powered GWAS investigations have been identified to confer a significantly increased lifetime risk of developing sAD which increases considerably when considering a combination of variants (Sims, Hill and Williams, 2020). The most famous example being the three polymorphisms (ε2, ε3, and ε4) within Apolipoprotein E gene (*APOE*). *APOE* ε4 carriers confer the most significant risk with an odd's ratio of 3 and 12 for heterozygous and homozygous genotypes respectively, in contrast to the neuroprotective variant *APOE* ε2 (Verghese, Castellano and Holtzman, 2011; Goldberg, Huey and Devanand,

2020). The pathophysiological basis of these associations are likely to be at least in part related to APP processing fidelity, but Aβ-dependent roles have also been suggested (Verghese, Castellano and Holtzman, 2011). AD is a multifactorial disease and delineating the complex interplay of intrinsic (e.g. age), environmental (e.g. vascular risk factors) and genetic factors (e.g. *APOE* genotype) will be essential in order to better understand sAD aetiology.

1.7 Ageing as a risk factor for neurodegenerative disease

1.7.1 Hallmarks of ageing

Biologically, ageing may be defined as the physiological decline of an organism over time that leads to progressive functional loss. Such changes leave the organism increasingly vulnerable to disease and ultimately death. In 2013, López-Otin et al. described nine 'hallmarks of aging' in an attempt to characterise the (mammalian) ageing phenotype and provide a framework for future targeted research (López-Otín *et al.*, 2013). The authors drew clear inspiration from Hanahan & Weinbergs landmark review on the 'The Hallmarks of Cancer' (Hanahan and Weinberg, 2011).

These ageing hallmarks may be categorised into primary, antagonistic and integrative sub-categories. Primary hallmarks (genomic instability, telomere shortening, epigenetic changes and proteostasis dysfunction) cause direct damage to the cell and leaves the cell vulnerable to secondary or 'antagonistic' hallmarks of ageing (dysregulated nutrient sensing, mitochondrial dysfunction and cellular senescence) which further propagates cellular dysfunction. The distinction between the groupings being that primary hallmarks are immediately deleterious to the cell whilst the responsive antagonistic ones are beneficial at low levels in maintaining homeostasis but can also become toxic when sufficiently upregulated. Finally, so-called 'integrative hallmarks' of ageing (stem cell exhaustion and intercellular communication) are those which are most believed to contribute to the observed clinical manifestations of ageing as a combined consequence of other primary and antagonistic factors

(van der Rijt *et al.*, 2020). Whilst semantics and desire for a conceptual framework drive the inclination to study these hallmarks and groupings in isolation, the likelihood is they are intricately entwined with one another and indeed a major stream of ageing research is dedicated to understanding the interconnectedness of these elaborate networks.

The hallmarks described are largely applicable to the ‘ageing brain’ although notably, given the post-mitotic nature of neurons; cell senescence and telomere attrition may be considered less relevant (Mattson and Arumugam, 2018; Hou *et al.*, 2019). A more detailed evaluation of these hallmarks of ageing in the context of the ageing brain and neurodegenerative disease is presented in (**Table 1.1**).

Table 1.1. Hallmarks of ageing in the ageing brain and neurodegeneration.

Hallmark	Features and relevance to the brain and neurodegenerative disease
Primary hallmarks	
Genomic instability	Accumulated genetic damage throughout life from endogenous or exogenous agents, oxidative damage and deficiencies in DNA repair mechanisms is especially pertinent within neurons due to their post-mitotic nature. Genome and chromosomal instability are being increasingly recognised as key features in neurodegenerative disease pathogenesis (Jeppesen, Bohr and Stevnsner, 2011; Thanan *et al.*, 2014).
Telomere attrition	Telomere shortening, as observed within neuronal and glial cells with potential, as yet unclarified impacts on adult hippocampal neurogenesis in the ageing brain (Tan *et al.*, 2014; Palmos *et al.*, 2020).
Epigenetic alterations	Modifications to influence chromatin structure which affect transcriptional activity. Altered methylation and demethylation patterns in vulnerable brain regions are emerging as key mechanistic drivers of neurodegenerative disease pathogenesis, many of which involving dysregulation of restrictive element 1-silencing transcription factor (REST) (Hwang, Aromolaran and Zukin, 2017).
Loss of proteostasis	Interrupted balance between protein synthesis and degradation. Protein misfolding, aggregation and impaired lysosomes are key features of several neurodegenerative diseases with many Parkinson's disease (PD), FTLD and ALS-associated gene variants being implicated in lysosomal function (Wallings *et al.*, 2019).
Antagonistic hallmarks	
Dysregulated nutrient sensing	Ageing is associated with the dysregulation of key nutrient sensing cascades including glucose metabolic dysfunction which is intricately entwined with mitochondrial functioning. Diminished glucose metabolism and insulin resistance is observed in several models of neurodegenerative disease (Schubert *et al.*, 2004; Han, Liang and Zhou, 2021).
Mitochondrial dysfunction	Mitochondrial function declines with age which is associated with the upregulation of damaging reactive oxygen species (ROS). Neurons are subject to very high energetic and metabolic demands and are hence especially sensitive to mitochondrial dysfunction and oxidative stress. Defective mitophagy, the specialised autophagic process for appropriate turnover of mitochondria, has also been implicated in

	neurodegenerative disease and especially in PD and Huntington's disease (Khalil *et al.*, 2015; Malpartida *et al.*, 2021).
Cellular senescence	Stress-induced, stable cell cycle arrest defines the senescence-associated secretory phenotype employed to halt the functioning and/or proliferation of defective cells with high levels of DNA damage. Post-mitotic neurons are vulnerable to genotoxic stress which can lead to a persistently activated DNA-damage response pathways and/or erroneous re-entry into the cell cycle in neurodegenerative disease (Fielder, von Zglinicki and Jurk, 2017; Barrio-Alonso *et al.*, 2018).
Integrative hallmarks	
Stem cell exhaustion	Degenerative age-related changes in tissue-specific stem cells limit a tissue's homeostatic and regenerative capacity and therefore overall health. The extent to which neural stem cell depletion contributes to or protects against the neurodegeneration phenotype remains unclear but altered neurogenesis has been identified as an early critical event in some diseases and particularly AD (Mu and Gage, 2011).
Altered intercellular communication	Disrupted intercellular communication pathways, and particularly those pertaining to immune functioning, are key areas of interest within the ageing brain and neurodegeneration. Chronic inflammation and persistent activation of microglia (the brain's resident immune cells) is associated with a damaging pro-inflammatory phenotype in several age-related neurodegenerative disease (Hickman *et al.*, 2018; Subhramanyam *et al.*, 2019).

1.7.2 Age-related neuropathological changes

In recent years, it has become increasingly appreciated that several neuropathological changes and proteinopathies are common post-mortem findings within elderly adult brains donated by patients whom did not meet clinical diagnostic criteria for neurological disease in life. These neuropathologies may typically resemble neurodegenerative-disease associated proteinopathies but are nonetheless distinct.

Up to a third of healthy control adults exhibit significant deposition of the AD-associated protein, amyloid β (Aβ), most frequently across frontal, temporal and parietal cortical regions despite robust clinical histories of well-preserved cognitive and physical functioning (**Figure 1.8a**) (Gkanatsiou *et al.*, 2021; van

der Kall *et al.*, 2021). Cerebral amyloid angiopathy (CAA), caused by accumulation of amyloid within the tunica media and adventitia of arteries in the brain is a common age-related small vessel disease (SVD) (Biffi and Greenberg, 2011). Less than half of CAA cases are comorbid with AD despite the pathology being almost universally found in pathologically-diagnosed AD cases (Viswanathan and Greenberg, 2011).

To add further complexity to this apparent contradiction, a relatively new term 'primary age-related tauopathy' (PART) was introduced to describe brains with neurofibrillary tangles (the other pathological hallmark of AD) with no evidence of Aβ accumulation (Crary *et al.*, 2014). Tauopathy in these cases is most commonly found within structures of the medial temporal lobe but are also identified within the basal forebrain, brainstem and olfactory regions with very similar neurofibrillary tangle morphology as seen in AD (**Figure 1.8b**). The neocortex is relatively spared in contrast to AD where extensive p-tau staining is typically observed. These individuals (~25 %) again most typically presented with either normal cognitive functioning or mild cognitive impairment (MCI) and did not fulfil clinical criteria for AD diagnosis (Crary *et al.*, 2014).

Most recently a new term 'limbic-predominant age-related TDP-43 encephalopathy (LATE) was introduced to describe patients, most commonly past 80 years of age, with a stereotyped TDP-43 proteinopathy (Nelson *et al.*, 2019). These individuals (up to 50 % of > 80 years) exhibit regionally-restricted TDP-43 deposition pathologically distinct from FTLD-TDP cases though resembling FTLD-TDP type A morphology. LATE-associated TDP-43 deposition preferentially affects medial temporal lobe structures and is generally more anatomically restricted than FTLD-TDP (**Figure 1.8c**). However, unlike age-related amyloidosis and PART, LATE is commonly associated with a more substantial cognitive impairment that mimics AD-type symptomatology (Jo *et al.*, 2020). The diagnostic and pathological classification of LATE as a distinct clinicopathological entity is however, controversial. Some pathologists posit that the evidence for the disease being distinct from AD and/or FTLD-TDP pathology is inadequate and that the term 'limbic-predominant' is an over-simplification (Josephs *et al.*, 2019). LATE

neuropathological changes blur the lines between ageing and disease and perhaps represents an interface between normal ageing, pathological ageing and neurodegenerative disease development.

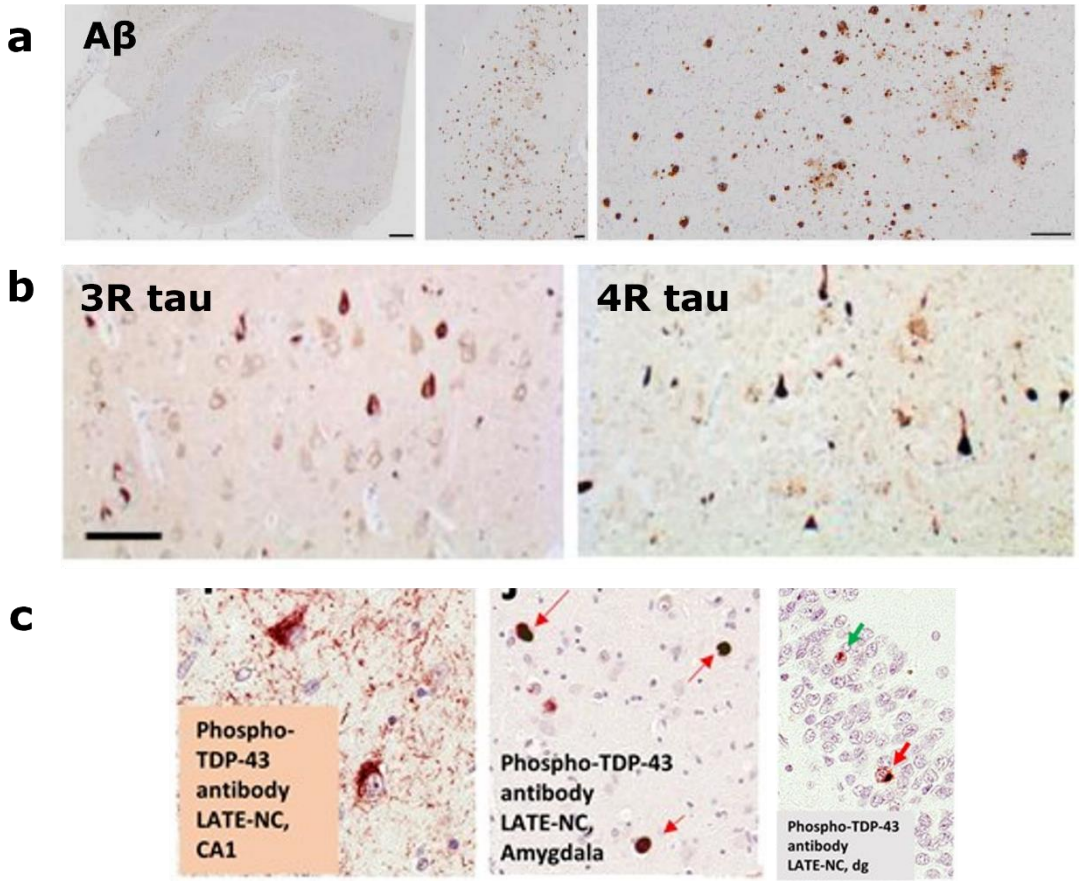

Figure 1.8. Age-related neuropathologies. (a) From left to right, Aβ burden in the frontal cortex, across the cortical layers and at higher (x4) magnification in a normal pathological ageing case. Scale bars at 2 mm, 200 µm and 200 µm respectively (Gkanatsiou *et al.*, 2021, Wiley license: 5325250540372). (b) 3R and 4R immunopositive neurofilament p-tau pathology within entorhinal cortex in PART resembles those observed in AD brain. Scale bars at 200 µm (Crary *et al.*, 2014, Springer license: 5325260146350). (c) From left to right, LATE associated phospho-TDP-43 (pTDP-43) neuropathological changes in the hippocampal CA1 region (including dystrophic neurites), amygdala (red arrows = tangle like inclusions) and dentate gyrus (green arrow = intranuclear inclusion, red arrow = cytoplasmic inclusion) demonstrating pTDP-43 positive inclusions similar to those observed in FTLD-TDP A proteinopathy (Nelson *et al.*, 2019, Oxford Academic license: 5325250992078).

Even more recent discoveries employing cryogenic electron-microscopy (cryo-EM) have identified that lysosomal protein TMEM106B also forms abundant amyloid filaments within brain in an age-dependent manner (Schweighauser *et al.*, 2022). It remains to be confirmed the extent to which this novel

proteinopathy is associated with neurodegeneration. However, *TMEM106B* risk variants have been previously linked with FTLD-TDP disease caused by *GRN* mutations (Van Deerlin *et al.*, 2010) and another recent cryo-EM investigation surprisingly identified that all examined amyloid fibrils within FTLD-TDP brain are composed of TMEM106B protein and not TDP-43, warranting further verification (Jiang *et al.*, 2022).

1.7.3 Cognitive decline

The normal ageing process is associated with the decline of several cognitive faculties including memory, conceptual reasoning, selective attention to tasks and executive functioning. This is in contrast to language domains and visuospatial abilities which are typically spared (Harada, Natelson Love and Triebel, 2013). There is even variability within individual cognitive domains. For example, the broad mental faculty of memory may be categorised into declarative memory (conscious recall) which is especially vulnerable to age-related decline and non-declarative memory (unconscious recall and procedural) which is relatively stable throughout life. However, there is significant heterogeneity in the cognitive profiles of ageing individuals with considerable variability in the relative rates of decline in different abilities (Wisdom, Mignogna and Collins, 2012).

The spectrum of cognitive decline ranges from normal age-related decline with no impairment of a person's ability to perform daily activities, all the way to diagnosable dementia (Harada, Natelson Love and Triebel, 2013). Mild cognitive impairment (MCI) or 'mild neurocognitive disorder' represents a transitional clinical diagnosis between these extrema used to identify individuals at risk of developing dementia in the future. MCI diagnosis is made upon patient or collateral history, clinical observation, neuroimaging, psychometric assessment and overall clinical judgement that a patient's cognitive impairment is beyond that expected of their age and education level, but not due to the presence of neurodegenerative disease (Bradfield, 2021).

The underlying pathological causes of age-related cognitive decline are incompletely understood, but imaging and electrophysiological investigations have identified several neural correlates including white and grey matter volume decreases. Positron emission tomograph (PET) scanning has identified β-amyloid (Aβ) load in the cortex and hippocampus to be associated with cognitive performance in non-demented elderly adults in several longitudinal cohorts (Kawas *et al.*, 2013; Rafii *et al.*, 2017; Timmers *et al.*, 2019). Accumulation of Aβ in the brain has been associated with both cortical and hippocampal grey matter volume loss which may underlie cognitive changes. Cerebrospinal fluid (CSF) Aβ42 inversely correlates with total Aβ load in the brain (Tapiola *et al.*, 2009). Unsurprisingly then, lower baseline CSF and plasma Aβ42 levels have also been found to be associated with a steeper rate of cognitive decline in non-demented individuals in multiple longitudinal analyses (Clark *et al.*, 2018; Verberk *et al.*, 2020). This is of course entirely consistent with Aβ deposition being an early, pre-clinical pathology in AD (Mormino and Papp, 2018) and the associations above can be reliably extended to AD staging. Higher rates of amyloid deposition in the brain of mild AD patients and lower baseline CSF/plasma levels of Aβ42 are prognostic biomarkers for a more rapid progression of dementia symptoms (Snider *et al.*, 2009).

Other structural changes associated with cognitive decline are white matter volume shrinkages as observed by diffuse tensor image investigations into white matter integrity. Age-related white matter reductions, particularly in the anterior corpus callosum and parahippocampal regions and other tracts have been correlated to deficits in cognitive performance including memory and executive functioning (Persson *et al.*, 2006; Rogalski *et al.*, 2012).

1.7.4 Ageing and neurodegeneration

Advancing age is the most significant risk factor attributed to the development of a vast number of human diseases including cancer, diabetes, osteoarthritis, age-related macular degeneration, respiratory and cardiovascular disease (Niccoli and Partridge, 2012). Neurodegenerative diseases are another group

of diseases unequivocally linked to the ageing process (Hou *et al.*, 2019). The prevalence of dementia especially appears to rise almost exponentially with age, doubling from around 20 % prevalence at age 80 to 40 % at 90 (Lobo *et al.*, 2000). Whilst rare familial forms of neurodegenerative disease can clinically manifest in middle aged and young adults (and extremely rarely, in juveniles), sporadic disorders are most commonly associated with the elderly.

Ageing is associated with significant reductions in brain weight (~150 g from an individual in their fifties to their nineties) (Elobeid *et al.*, 2016). Additionally, as discussed previously, several age-related pathologies are characterised by the deposition of proteins including β-amyloid, p-Tau and pTDP-43 and α-synuclein which resemble the defining pathological features of several neurodegenerative diseases (Wyss-Coray, 2016). However, the extent (severity) and neuroanatomical distribution of these age-related pathological burdens are generally distinct from those exhibited by diseased brains which typically display more extensive pathology and in several additional vulnerable brain regions. Moreover, the relationship between these pathologies and cognitive decline in non-demented individuals is far from clear cut with many cognitively unimpaired, aged individuals exhibiting abnormal accumulations of various protein deposits (Elobeid *et al.*, 2016). It would therefore be an over-simplification to consider neurodegenerative disease a simple extension of the ageing process and thus a pathological inevitability in elderly subjects. There is nevertheless clear pathological and clinical overlap and the extent to which these pathologies are either innocuous bystanders or precursors to neurodegeneration representing preclinical dementia, remains unelucidated (Wyss-Coray, 2016).

The aforementioned hallmarks of ageing as shared causes of brain ageing and neurodegeneration including dysregulated proteostasis, genomic instability, epigenetic changes and immune signalling dysfunction provides a framework for investigating intersecting processes between these phenomena that may shed light on key mechanistic differences between the two (Wyss-Coray, 2016). Additionally, phenotypic-focused neuroimaging, biomarker and transcriptomics research on clinically and pathologically stratified populations

of cognitively normal vs cognitively affected individuals with similar pathological profiles may illuminate potential compensatory/resilience pathways to neurodegeneration. A complex interplay of genetic, intrinsic and environmental factors are likely to underlie the significant pathological and clinical heterogeneity exhibited within elderly populations and future mechanistic investigations will need to account for these factors.

1.8 Heterogeneous nuclear ribonucleoproteins in FTLD and ALS

1.8.1 HnRNP structure and function

Heterogeneous nuclear ribonucleoproteins (hnRNPs) are a highly diverse family of RNA-binding proteins (RBPs) that form dynamic complexes with pre-mRNA (also known as hnRNA). Early nucleoplasm immunopurification studies first isolated and described three hnRNPs, named hnRNP A-C, to be highly abundant polypeptide components of mRNA-bound complexes within the nucleus (Dreyfuss *et al.*, 1993). The family has since expanded to include 20+ proteins, named alphabetically from hnRNP A1 to hnRNP U, although several of these proteins are often referred to by a more common alias (Table 1.2). Classification and nomenclature is further muddied by the more recent inclusion of several other RBPs into the family including TDP-43, TIA-1 and MATR3 which were not identified in early purification procedures (Geuens, Bouhy and Timmerman, 2016). Structurally, hnRNPs are best defined by their modular structure which includes one or more RNA-binding domains (**Figure 1.9**)**.** These domains bestow each protein member with a degree of binding specificity to RNA-targets in a sequence-specific manner. By contrast, a hnRNP's varying composition of less evolutionary conserved auxiliary domains affords them with the capacity to also bind a large number of non-specific RNA, DNA and protein targets within a vast interactome. Multiple hnRNPs also possess a nuclear localisation or import/export motif which enables them to shuttle between the nucleus and cytoplasm to perform functions within each (Michael, Eder and Dreyfuss, 1997).

Table 1.2 The hnRNP family and common aliases.

HnRNP protein	Alternative protein names
A1, A2/B1, A3, A/B	**hnRNP A1**; **hnRNP A2/B1**; **hnRNP A3**, HNRPA3; **hnRNP A/B**, ABBP-1
C	**hnRNP C**, hnRNP C1/C2
D (D0, DL)	**hnRNP D0**, AUF1; **hnRNP D-like**, laAUF1, JKT41-binding protein
E (E1, E2)	hnRNP E1, **PCBP1**, Alpha-CP1; hnRNP E2, **PCBP2**, Alpha-CP2
F	**hnRNP F**, nucleolin-like protein mcs94-1
G	hnRNP G, **RNA-binding motif protein, X chromosome (RBMX)**, Glycoprotein p43
H (H1, H2, H3)	**hnRNP H1**; **hnRNP H2**, FTP-3, hnRNP H'; hnRNP H3, hnRNP 2H9
I	hnRNP I, **PTB**, PPTB-1
K	**hnRNP K**, TUNP
L (L, LL)	**hnRNP L**; **hnRNP LL**, SRRF
M	**hnRNP M**
P	hnRNP P, **FUS**, 75 kDA DNA-pairing protein, oncogene TLS, POMp75
Q	**hnRNP Q**, SYNCRIP, GRY-RBP, NS1-associated protein
R	**hnRNP R**
U	**hnRNP U**, GRIP120, SAF-A, Nuclear p120 ribonucleoprotein

The most commonly used protein name for each hnRNP is highlighted in **bold text** (Bampton *et al.*, 2020).

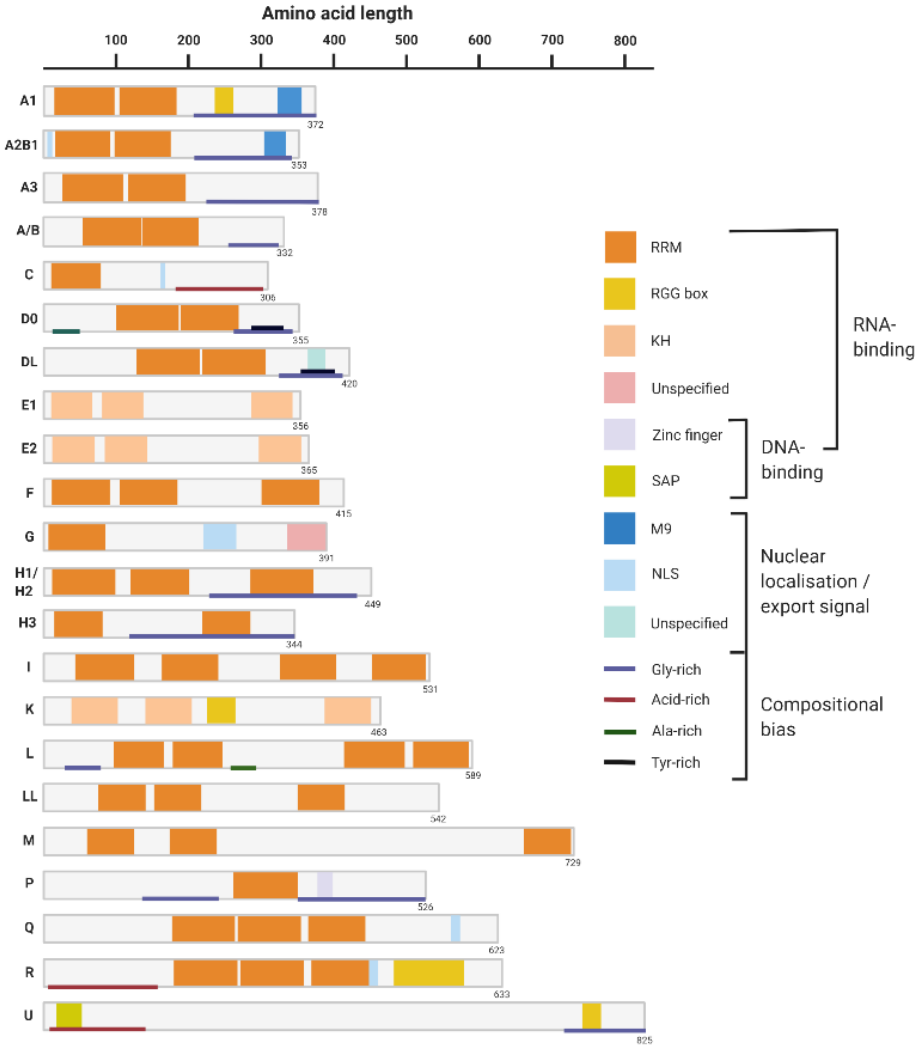

Figure 1.9. The hnRNP family: composition and structure. The hnRNP family are named alphabetically from A1 to U. The proteins exhibit a modular structure and all contain varying combinations of RNA-binding domains which facilitate their myriad functional roles in pre-mRNA processing. RNA-recognition motifs (RRMs) are the most commonly identified domain in this category. Several hnRNPs also possess a nuclear import/export signal to enable them to perform both nuclear and cytoplasmic functions. RRM, RNA recognition motif; KH, K-homology domain; RGG, Arg-Gly-Gly repeat domain; NLS, nuclear localisation signal. Number in the bottom right corner of each schematic indicates amino acid length (Bampton *et al.*, 2020).

There is considerable functional as well as structural divergence between different members of the hnRNP family. However, it is generally believed that through a constant remodelling of an mRNA-protein complexes' composition, including a changing constellation of hnRNPs and other RBPs, hnRNPs contribute to the regulation of all stages of an mRNAs life cycle, from transcription to translation. Indeed, hnRNPs have been functionally implicated in many aspects of nucleic acid metabolism including transcription initiation,

mRNA capping, splicing, polyadenylation, nucleocytoplasmic transport, stability and translational control (Krecic and Swanson, 1999; Bampton *et al.*, 2020).

1.9 HnRNPs and FTLD/ALS pathologies

There is an increasing body of evidence to suggest that hnRNPs have both direct and indirect functional roles in the pathogenesis of both FTLD and ALS (Purice and Taylor, 2018; Bampton *et al.*, 2020; Low *et al.*, 2021). At a superficial level, members of the hnRNP family have vast interactomes which overlap considerately with both each other and key FTLD/ALS pathological genes and proteins including TDP-43, *C9orf72*, FUS and Tau as demonstrated by ingenuity pathway analysis (IPA) (**Figure 1.10**).

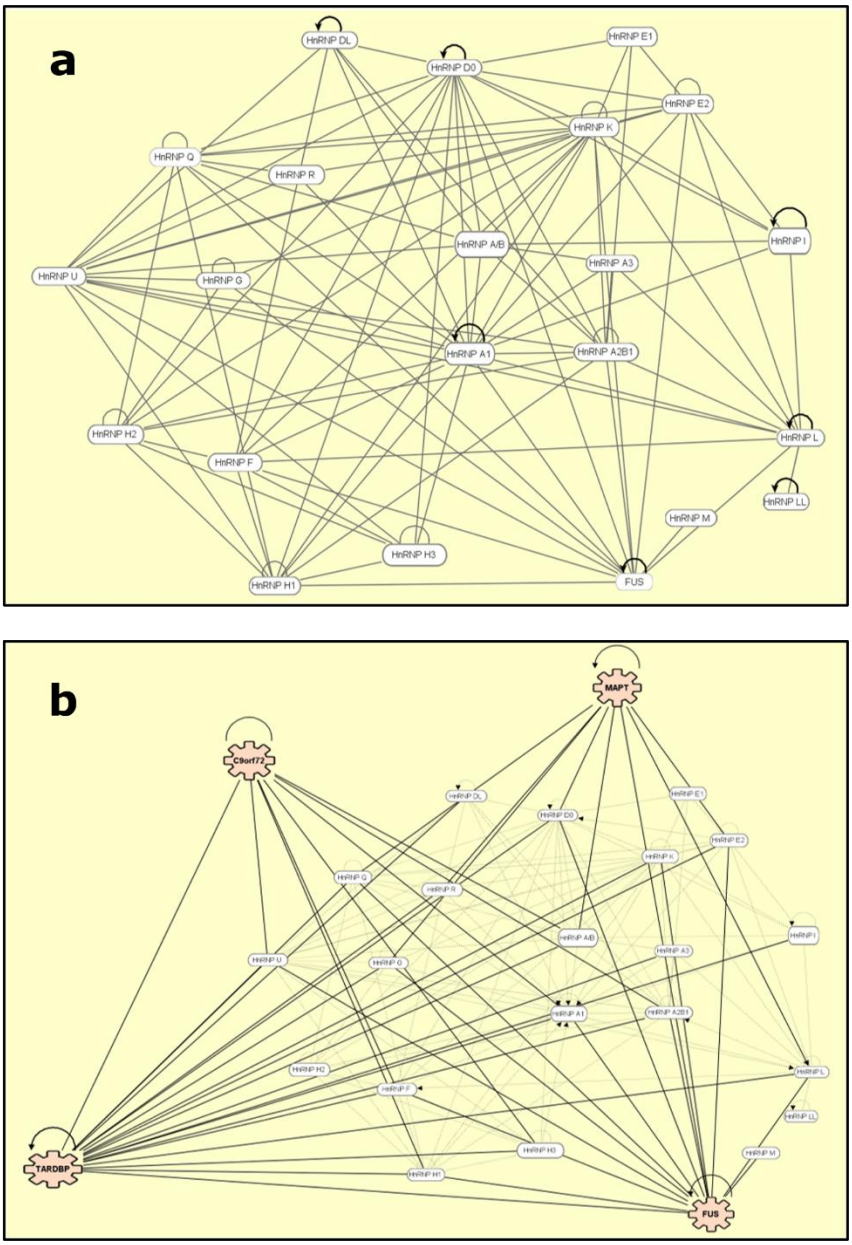

Figure 1.10. Ingenuity pathway analysis (IPA) of the hnRNP family. Network analyses obtained using IPA showing the direct, experimentally confirmed interactions of hnRNPs with both each other (a) and superimposed key FTLD/ALS genes and proteins (b): *TARDBP* (TDP-43), *C9orf72*, *FUS* and *MAPT* (Tau). Half-circle 'self' arrows indicate evidence of autoregulation whilst half-circle lines indicates evidence of self-binding only (Bampton *et al.*, 2020).

Perhaps the strongest link underpinning this relationship comes from an examination of each disorders' respective pathologies. Indeed, in some cases hnRNPs can be the principal component of proteinaceous inclusions as with TDP-43 and FUS-related diseases. Additionally, there is an increasing body of evidence to suggest that other hnRNPs are being recruited and potentially

functionally sequestered within FTLD and ALS-associated pathologies (**Figure 1.11**).

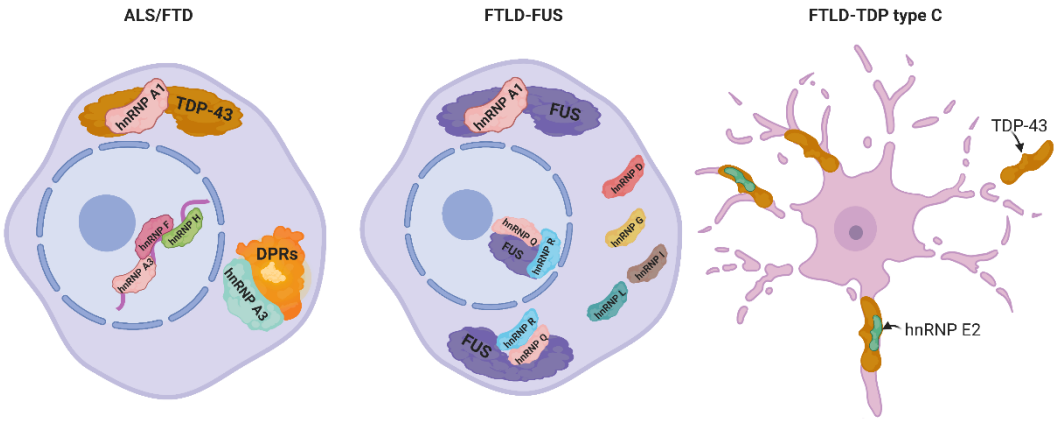

Figure 1.11. HnRNPs and FTLD inclusions. HnRNPs have been found to colocalise to repeat RNA nuclear foci and dipeptide repeat proteins in *C9orf72*-associated FTLD and ALS pathogenesis as well as TDP-43 in both C9 and sporadic FTLD/ALS (left panel). In FTLD-FUS, several hnRNPs have been found to co-deposit with intranuclear and cytoplasmic FUS inclusions and have also been found within FUS-negative inclusions (middle panel). Finally, hnRNP E2 has been found to colocalise to the distinctive twisted neurites that are characteristic of FTLD-TDP type C pathology (right panel) (Low *et al.*, 2021, reproduced under a Creative Commons license: http://creativecommons.org/licenses/by/4.0/).

1.9.1 TDP-43 pathologies

Abnormal deposition of the hnRNP TDP-43 is the major neuropathological hallmark in 97 % of ALS cases, 50 % of FTLD cases (FTLD-TDP) and is the defining pathology of the more recently described limbic-predominant age-related TDP-43 encephalopathy (LATE) (Nelson *et al.*, 2019; Wood *et al.*, 2021). As previously described, ALS and each known FTLD-TDP subtype (A-E) are characterised pathologically by both the morphology of the TDP-43 inclusions and their respective histopathological deposition profiles (Lee *et al.*, 2017). Pathological TDP-43 deposits are typically hyper-phosphorylated and ubiquitinated which are post-translational modifications known to substantially increase aggregation propensity (Neumann *et al.*, 2006). One such proposed gain of function mechanism linked to the accumulation of these aggregates is the subsequent sequestration of RNA and other RNA-binding proteins that could contribute to further ribostatic and proteostatic perturbations.

Polycytosine-binding protein 2 (*PCBP2*) or hnRNP E2 is one such RBP, identified via immunohistochemical analysis, to colocalise with both FTLD-TDP type A and type C pathologies in post-mortem brain (Davidson *et al.*, 2017; Kattuah *et al.*, 2019). Its supposed FTLD-TDP C subtype-specificity remains enigmatic however.

1.9.2 FUS pathologies

FUS, along with TDP-43 is another of the most intensively studied hnRNPs in neurodegeneration. In FTLD, FUS was identified as the major protein constituent within the pathological inclusions defining sporadic neuronal intermediate filament inclusion disease (NIFID), atypical FTLD with ubiquitin inclusions (aFTLD-U) and basophilic inclusion body disease (BIBD) (Munoz *et al.*, 2009; Neumann *et al.*, 2009). These diseases, collectively known as FTLD-FUS represent around 5 - 10 % of all ubiquitin-positive FTLDs (Lashley *et al.*, 2011). FUS is the predominating neuropathological feature in a far smaller proportion of ALS cases (FTLD-FUS) accounting for just 1 % of sporadic and 4 % of familial pathological diagnoses (Renton, Chiò and Traynor, 2014). As with FTLD-TDP, FTLD-FUS disorders are subclassified according to their distinctive histopathological features. Interestingly, the colocalisation of FET proteins TATA-binding protein-associated factor 15 (TAF15) and Ewing's sarcoma (EWS), selectively mark a proportion of FTLD-FUS inclusions, but not ALS-FUS aggregates indicating a more complex dysregulation of FET proteins (which also includes FUS) in FTLD-FUS pathobiology (Neumann *et al.*, 2011).

Several hnRNPs have been found to co-deposit with FUS-positive pathological inclusions including hnRNP R and Q (Gittings *et al.*, 2019) and hnRNP A1 in FTLD-FUS (Gami-Patel *et al.*, 2016). Intriguingly, several other hnRNPs including hnRNP D, L and I (PTB) were found within supposed FUS-negative inclusions within FTLD-FUS tissue, potentially supporting a more complex role of RBP dysregulation in FTLD-FUS (Gami-Patel *et al.*, 2016).

1.9.3 C9orf72 pathologies

Hexanucleotoide repeat expansion mutations in *C9orf72* give rise to 2 defining neuronal pathologies of C9-FTLD and C9-ALS in addition to TDP-43 inclusions. Firstly, the expansion repeats may be bidirectionally transcribed into both sense and antisense foci which can in-turn fold into intranuclear foci. Remarkably, these transcripts may also be uncanonically translated in every reading frame through a repeat-associated non-ATG (RAN) translation mechanism into five dipeptide-repeat proteins (DPRs) (Balendra and Isaacs, 2018).

Both RNA foci and DPRs have also been found to sequester RBPs and this is the leading theory behind how these pathologies exert their toxicity. HnRNP H1 and hnRNP H3 have been most consistently found to co-purify with HRE foci in cell and animal models (Haeusler *et al.*, 2014) as have hnRNP F, A1 and A3, all of which have been pathologically confirmed in C9-FTLD/ALS post-mortem brain tissue (Lee *et al.*, 2013; Cooper-Knock *et al.*, 2014; Rossi *et al.*, 2015; Conlon *et al.*, 2016). Additionally, several hnRNPs including hnRNP H1, F and M have been identified to specifically interact with DPR poly-PR (Suzuki *et al.*, 2019). HnRNP A3 on the other hand appears to bind to the DPRs more promiscuously (Mori *et al.*, 2013, 2016; Davidson *et al.*, 2017). Intriguingly, its nuclear depletion within C9-patient derived fibroblasts led to an accumulation of RNA foci suggesting a potentially bi-directional modulation of DPR and hnRNP/RBP-induced toxicity (Davidson *et al.*, 2017).

One unifying theory for explaining this aberrant (mis)localisation of hnRNPs, whether they be identified within FTLD-TDP, FTLD-FUS or *C9orf72*-associated pathological inclusions, is that it may reflect a broader dysfunction in nucleocytoplasmic transport within FTLD/ALS afflicted neurons (Jovičić, Paul and Gitler, 2016; Taylor, Brown and Cleveland, 2016).

1.10 HnRNP functional relevance to FTLD and ALS

Disrupted RNA and protein homeostasis have been identified as key emerging themes of neurotoxicity in both FTLD and ALS. By definition, RBPs which include hnRNPs are at the mechanistic interface of these processes and their dysfunction is of particular research interest in understanding pathways to disease. This section reviews hnRNP's involvement in several homeostatic processes that have been either directly or indirectly implicated in FTLD/ALS pathogenesis.

1.10.1 HnRNPs in alternative splicing

Alternative splicing is the post-transcriptional process during gene expression whereby non-coding 'intronic' sequences are removed from pre-mRNA and coding 'exon' sequences are differentially spliced together to form multiple mature mRNA isoforms. Alternative splice site selection and subsequent 'skipping over' of certain exons leads to several combinations of joined up exons. This is one such contributing mechanism that leads to extensive protein diversification from a limited genome (Baralle and Giudice, 2017).

Almost all hnRNPs and indeed many other RBPs can be considered splicing factors. That is, that they influence alternative 3' and 5' splice site selection on target genes by either direct RNA-binding or in concert with other components of the supraspliceosome complex (Dvinge *et al.*, 2019). HnRNPs are known to have capacity to inhibit splicing via several mechanisms including the 'looping out' of exons by dual-binding to flanking residues that bridge the exon to be repressed, competitive inhibition of RNA binding sites and direct displacement of other splicing factors (Okunola and Krainer, 2009; Preussner *et al.*, 2012; Erkelenz *et al.*, 2013). Conversely, hnRNPs can also operate within splicing activator complexes which can locate to exonic splicing enhancer (ESE) motifs to promote splice site selection (Caputi and Zahler, 2002). However, the vast majority of hnRNP-dependent splicing events are regulated by multiple hnRNPs and their directional effects are likely to be highly dependent on the

exact composition of the complexes they form with each other (Huelga *et al.*, 2012).

Splicing defects have been increasingly implicated in ALS and particularly C9-FTLD/ALS as a mechanism of neurotoxicity (Arnold *et al.*, 2013; Conlon *et al.*, 2016; Deshaies *et al.*, 2018). Conlon et al. conceptualise a model whereby RBPs exist in a state of solubility equilibrium. When this balance is tipped towards insolubility, perhaps as a result of TDP-43 aggregation or *C9orf72* mutation, widespread splicing defects follow in both sporadic and familial FTLD/ALS even in the absence of RBP-sequestering RNA foci (Conlon *et al.*, 2018; Gitler and Fryer, 2018).

The most intensively studied gene in the context of FTLD and splicing is microtubule-associated protein tau gene *MAPT* (Dickson *et al.*, 2011). FTLD with tau inclusions (FTLD-tau) accounts for nearly half of all FTLD cases and autosomal dominantly inherited mutations in *MAPT* represent up to 10 % of total FTLD cases. Interestingly, the majority of these mutations cluster around intron and exon 10 which is a key splicing region for this gene (Rohrer and Warren, 2011). The inclusion or exclusion of exon 10 dictates the relative translation of tau isoforms harbouring three (3R) or four (4R) microtubule-binding repeat regions. A disruption that results in an imbalance of these isoforms can lead to insoluble, hyperphosphorylated tau fibril assembly within filaments which pathologically defines FTLD-tau and perturbs normal axonal transport in the neurons they reside (Bowles *et al.*, 2022). Many of the aforementioned *MAPT* mutations exert their toxicity by destabilising a regulatory hairpin structure at the exon 10 5' splice site which promotes an increase in the 4R:3R splicing ratio (Grover *et al.*, 2002; Donahue *et al.*, 2006). Multiple hnRNPs have been implicated in the regulation of this key splicing event exerting opposite 'antagonistic' influences on splice site selection with hnRNP G (repressor) and hnRNP E2 (activator) being the best characterised examples (Hofmann and Wirth, 2002; Broderick, Wang and Andreadis, 2004) (**Figure 1.12**). It remains to be elucidated whether mutations directly influence splice site recognition or whether, indirectly, they do so by disrupting RBP/hnRNP binding. Gaining a better appreciation of the combinatorial nature

of slicing regulation and the spatial and temporal regulation of splicing factor activity levels will further hone therapeutic efforts in tauopathies.

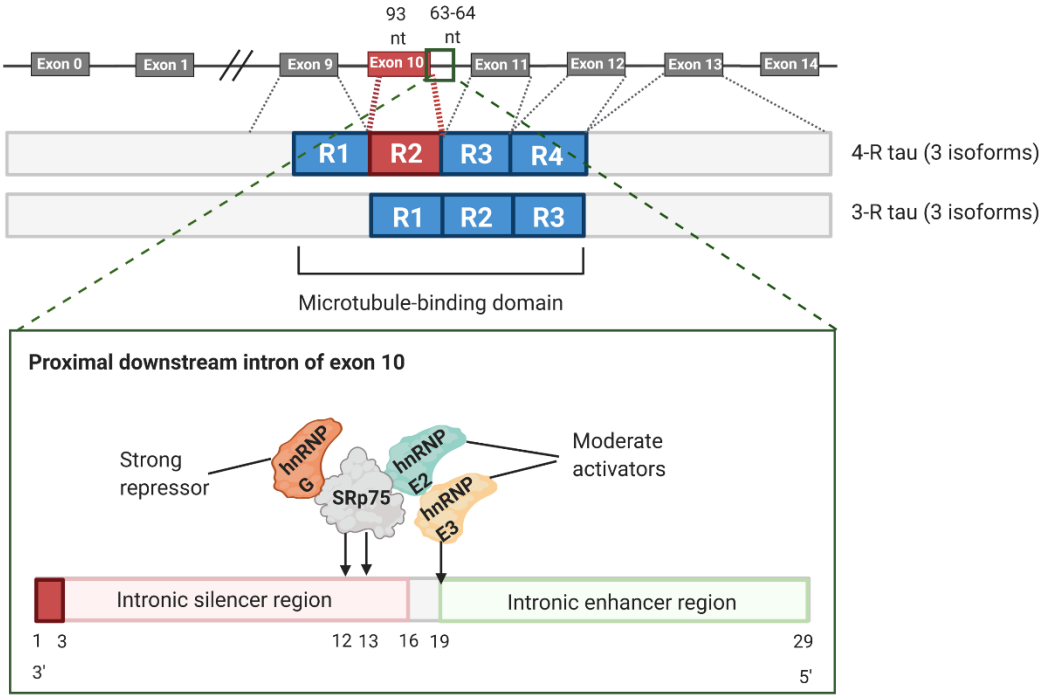

Figure 1.12. HnRNP involvement in the regulation of *MAPT* exon 10 alternative splicing. The rate of tau exon 10 inclusion determines the relative abundance of 3-repeat (3-R) and 4-repeat (4-R) tau isoforms. Three further isoforms of each type are generated from the additional alternative splicing of exons 2 and 3 (not shown). Multiple hnRNPs have been shown to participate in the regulation of tau exon 10 splicing by forming complexes at exon 10's proximal downstream intron. HnRNP G interacts with splicing factor SRp75 which directly binds to intron residues 12-13 within the intronic silencer region to interfere with spliceosome assembly. By contrast, hnRNP E3 and known interactor hnRNP E2 are moderate activators of exon 10 splicing through binding to residue 19 in the intronic enhancer region. Other non-hnRNP associated interactors are not shown here for clarity. Adapted model of tau exon 10 splicing from the work of (Broderick, Wang and Andreadis, 2004; Wang *et al.*, 2004, 2010).

1.10.2 HnRNPs in cryptic splicing

The role hnRNPs have in maintaining proper splicing fidelity extends beyond the regulation of alternative splicing events. In more recent times, many RBPs including several hnRNPs have also been identified as having key roles in the repression of non-conserved splicing events termed cryptic exons (CEs). CEs are a specific form of intron retention mis-splicing event that arises from the

aberrant inclusion of an intronic region (the so-named ‘cryptic exon’) following the erroneous selection of a sequence element by the spliceosome that only resembles a bona fide splice site (Calarco, 2013; Eom *et al.*, 2013). The resultant transcripts are then commonly targeted for NMD due to a shift in the open reading frame introducing a PTC. However, the possibility also exists whereby evolutionary untested mRNA isoforms could evade NMD and be translated into truncated or altogether different full-length protein isoforms (Humphrey *et al.*, 2017) (**Figure 1.13**).

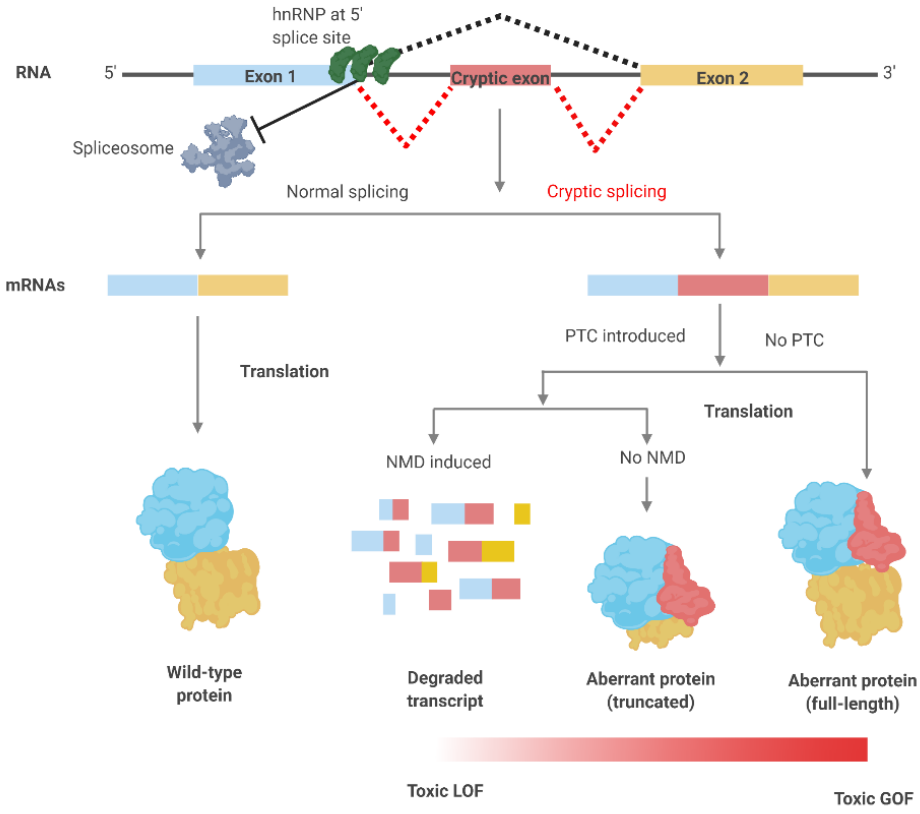

Figure 1.13. HnRNP involvement in cryptic exon repression. Several hnRNP proteins have been known to bind to exonic and intronic regions of pseudo/cryptic 5′ splice sites. Their presence sterically occludes appropriate assembly of the spliceosome, in-turn inhibiting cryptic exon inclusion. HnRNP dysfunction leads to elevated cryptic inclusion in the final mRNA transcript. If a premature termination codon (PTC) is introduced following a frameshift, non-sense mediated decay (NMD) may be activated to destroy the transcript. Alternatively, the transcript may be partially translated into a truncated, aberrant protein isoform. Indeed, if by chance no PTC is introduced upon cryptic splicing then the full-length transcript may be translated (Bampton *et al.*, 2020).

Several hnRNPs including hnRNP C, I (PTB), L and M have been shown to maintain splicing fidelity by repressing cryptic splicing (Zarnack *et al.*, 2013; Ling *et al.*, 2016; McClory, Lynch and Ling, 2018; West *et al.*, 2019). However, it wasn't until the identification that TDP-43 is a potent repressor of CEs within its molecular targets, that the notion of CE de-repression as a novel mechanism of neurotoxicity in diseased neurons came to prominence. Indeed, several TDP-43 cellular depletion paradigms have been shown to lead to widespread destabilisation of target transcripts through the incorporation of CEs and several of these events have been validated in FTLD/ALS and AD brain with TDP-43 proteinopathy (Ling *et al.*, 2015; Humphrey *et al.*, 2017; Sun *et al.*, 2017; Torres *et al.*, 2020). Most notably, two studies have identified a CE activated within the neuronal growth-associated factor stathmin-2 (*STMN2* gene) upon TDP-43 knockdown (Klim *et al.*, 2019; Melamed *et al.*, 2019). This cryptic event leads to an accumulation of truncated stathmin-2 and thus an overall reduction in functional transcript levels of the protein leading to reduced axonal outgrowth in neuronal cell models (Klim *et al.*, 2019; Prudencio *et al.*, 2020). This was the first example of a direct functional consequence of CE inclusion within a TDP-43 target that could have a detrimental impact on neuronal health. More recently, as will be discussed in this body of work, another TDP-43 associated CE in the synaptic gene *UNC13A* has been discovered which serves as another potential avenue of neuronal dysfunction in FTLD/ALS neurons (Brown *et al.*, 2022; Ma *et al.*, 2022).

The activation of CEs represent a loss of TDP-43 splicing function in nuclear-depleted neurons. Intriguingly, an ALS-causative mutation TDP-43 knock in mouse model used to investigate gain of function transcriptome alterations identified another novel splicing defect termed 'skiptic exons' (SEs) (Fratta *et al.*, 2018). So-called skiptic splicing is a splicing event whereby constitutively included exons are erroneously skipped over by the spliceosome. As with CEs, the overall expression of genes harbouring SEs was found to be downregulated.

It remains to be confirmed whether cryptic or skiptic exon repression by alternative hnRNPs to TDP-43 and FUS is in any way compromised in FTLD/ALS pathogenesis. Elevated levels of either event in other hnRNP targets may or may not result in any structural or functional changes to target proteins. However, a reduction in functional protein levels, as observed with stathmin-2, is potentially sufficient to induce neurotoxicity.

1.10.3 HnRNPs in the DNA-damage response

There is an increasing body of evidence to suggest that hnRNPs have active, pleiotropic roles within the DNA damage response (DDR) pathway. The DDR is a collective term for the elaborate network of mechanisms that survey, detect and respond to DNA damage resulting from genotoxic stressors (Jackson and Bartek, 2009). One well-characterised role of hnRNPs in responding to genotoxic stress is in the reconfiguration of alternative splicing programmes of key effector proteins (Cloutier *et al.*, 2018). Evidence for extensive, hnRNP-elicited transcriptional reprogramming of alternative splicing regulation has emerged from a number of molecular assays of DNA damage induction including double-stranded break (DSB)-inducing micro-irradiation leading to them being described as ‘gatekeepers of genome stability’ (Haley *et al.*, 2009; Naro *et al.*, 2015). Additionally and more directly, both hnRNP A1 and FUS have been implicated in telomere maintenance by enhancing telomerase activity (Zhang *et al.*, 2006; Takahama *et al.*, 2013) and in the activation of topoisomerase 1 activity that prevents potentially harmful R-loop formation during transcription (Czubaty *et al.*, 2005). Specifically within motor neurons, hnRNP R loss has been associated with impaired DDR due to reduced hnRNP R-dependent chromatin binding of Yb1 protein (Ghanawi *et al.*, 2021). HnRNPs may even have more direct, as yet unclarified roles in DNA-damage repair following evidence that hnRNP G and hnRNP L localises to DNA lesion sites (Adamson *et al.*, 2012; Hu *et al.*, 2019).

The role of DNA damage and compromised repair pathways in FTLD and ALS pathogenesis is a rapidly developing research area. This is in contrast to their more intensively studied roles in cancer biology where aberrant expression

and activity of splicing factors has been shown to be a contributing feature of oncogenesis (Naro *et al.*, 2015). DNA damage has been especially implicated in C9-FTLD/ALS pathobiology as a result of RNA foci and DPR-induced genotoxic stress (Lopez-Gonzalez *et al.*, 2016). However, recent evidence for TDP-43 being a key scaffolding component of the non-homologous end joining (NHEJ) pathway for DSB repair has also linked TDP-43 pathology to defective DNA repair in ALS (Mitra and Hegde, 2019; Mitra *et al.*, 2019). Finally, genome damage and defective repair are emerging phenotypic hallmarks of neurons with familial ALS *FUS* and *SOD1* mutations (Wang and Hegde, 2019; Kim *et al.*, 2020).This is unsurprising because the permanently post-mitotic state of neurons means these cells are especially vulnerable to compromised genome integrity. It remains to be elucidated whether a dysregulation of hnRNP-associated DDR roles contributes to FTLD/ALS pathology in an analogous fashion to oncogenesis.

1.10.4 HnRNPs and stress granule formation

Some hnRNPs are known to undergo liquid–liquid phase separation (LLPS) leading to the generation of membraneless organelles which include nuclear speckles, processing bodies, RNA transport granules and stress granules (Wolozin and Ivanov, 2019). These condensates define a transient cellular compartment enabling cells to concentrate biomolecular assemblies for functional-specific purposes in a highly dynamic fashion with high spatiotemporal control (Gomes and Shorter, 2019). The low complexity domain (LCD) is a key component driving the formation of these organelles which is characterised by regions rich in alanine, glycine, glutamine and proline residues (Molliex *et al.*, 2015; Wolozin and Ivanov, 2019). LCDs typically have a propensity to form low-affinity and highly dynamic protein complexes with rapidly fast binding and unbinding kinetics. LLPS refers to the reversible process by which extensive intermolecular binding between the LCDs of hnRNPs and other RBPs allows them to aggregate into droplet-like structures within an aqueous environment (Wolozin and Ivanov, 2019).

Stress granules are transient, membraneless organelles assembled in the cytoplasm through LLPS upon exposure to stressful stimuli. They function to stall mRNA translation by physically sequestering translation machinery to re-direct protein synthesis towards survival pathways (Molliex *et al.*, 2015). ALS and FTLD-associated mutations within the LCD regions of stress granule related RBPs, including hnRNPA1, hnRNPA2B1, FUS and TDP-43 function to lower the threshold for mutant RBPs to undergo LLPS and aggregate (Molliex *et al.*, 2015; Bowden and Dormann, 2016; Baradaran-Heravi, Van Broeckhoven and van der Zee, 2020). This leads to altered biophysical properties of stress granules and the subsequent accumulation of more stable, insoluble aggregates that persist within neurons (Purice and Taylor, 2018) (**Figure 1.14**). Additional complexity arises when considering the effects on LLPS of the many characterised post-translational modifications (PTMs) of RBPs. Indeed many such PTMs, and particularly those linked to TDP-43 and FUS, have been shown to either promote aberrant LLPS or reduce phase separation with potentially pathological or neuroprotective roles respectively (Gruijs da Silva *et al.*, 2022; Sternburg, Gruijs da Silva and Dormann, 2022).

Persisting stress granules are thought to act as ‘pathological seeding hubs’ for the further accumulation of other known aggregation-prone RBPs perpetuating further proteostatic and wider homeostatic dysfunction in the cell (Baradaran-Heravi, Van Broeckhoven and van der Zee, 2020). Prevention of pathological stress granule accumulation has been shown to confer neuroprotection in animal disease models of ALS and FTLD (Kim *et al.*, 2013; Wang *et al.*, 2020). However, further work is required to further clarify the relationship between chronic stress granules and neurodegenerative disease.

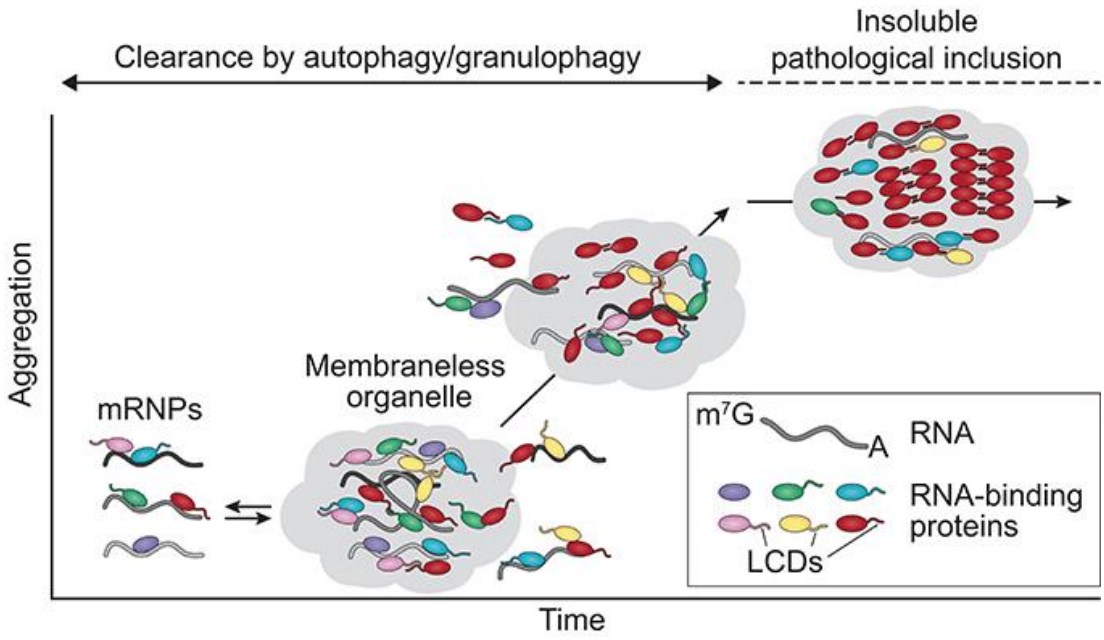

Figure 1.14. RNA-binding protein involvement in the generation of persistent stress granules. In response to noxious stimuli within the cell RBPs, including several hnRNPs, associate with mRNA transcripts to form messenger ribonucleoprotein particles (mRNPs). The LCD region of RBPs mediate phase separation and the formation of membraneless stress granule assemblies to inhibit mRNA translation. Upon stress signal cessation, stress granules are disassembled via the specialised autophagic process of granulophagy to release mRNA and RBPs back into the cytosol. However, ALS and FTLD-causing mutations in LCD regions of RBPs can lead to the generation of aggregation-prone RBPs (including TDP-43 and FUS) which promote the irreversible transition of stress granule assemblies into persistent stress granules which in-turn may further develop into pathological inclusions (Purice and Taylor, 2018, reproduced under a Creative Commons license: http://creativecommons.org/licenses/by/4.0/).

1.10.5 HnRNP autoregulation

Tightly regulated, concentration-dependent control of splicing factor expression is critical in order to maintain context-appropriate levels of splicing factors within the cell. Indeed, mRNA-autoregulatory pathways have been proposed to be a potentially unifying feature of the majority of, if not all, RNA binding proteins, although this remains to be experimentally confirmed (Buratti and Baralle, 2011).

To this end, a growing number of splicing factors have been found to autoregulate their own expression levels through alternative splicing-coupled NMD mechanisms. Perhaps the clearest example of this is the upregulation of

so-called ‘poison’ exons within transcripts. For example, the self-binding of hnRNP L protein to the intronic region immediately upstream of exon 6A of its own transcript serves to promote its ‘poisonous’ inclusion (Rossbach *et al.*, 2009). By contrast, elevated hnRNP I (PTB) protein levels leads to increased self-binding to intron 11 and subsequent promotion of exon 11 skipping, a so-called ‘essential exon’ (Wollerton *et al.*, 2004). In both instances, the resulting frameshift in the open reading frame causes a number of downstream PTCs which targets the transcript for NMD. Not all splicing-dependent mechanisms of autoregulation rely on NMD however. The FUS (hnRNP P)-induced upregulation of intron 6/7 was found to autoregulate FUS expression levels independently from NMD. Instead, intron 6/7-retaining transcripts are unable to undergo nuclear export, dramatically reducing their ability to be translated (Humphrey *et al.*, 2020). Indeed, increased nuclear retention is an additional mechanism of autoregulation employed by several other hnRNPs (**Figure 1.15a-c**).

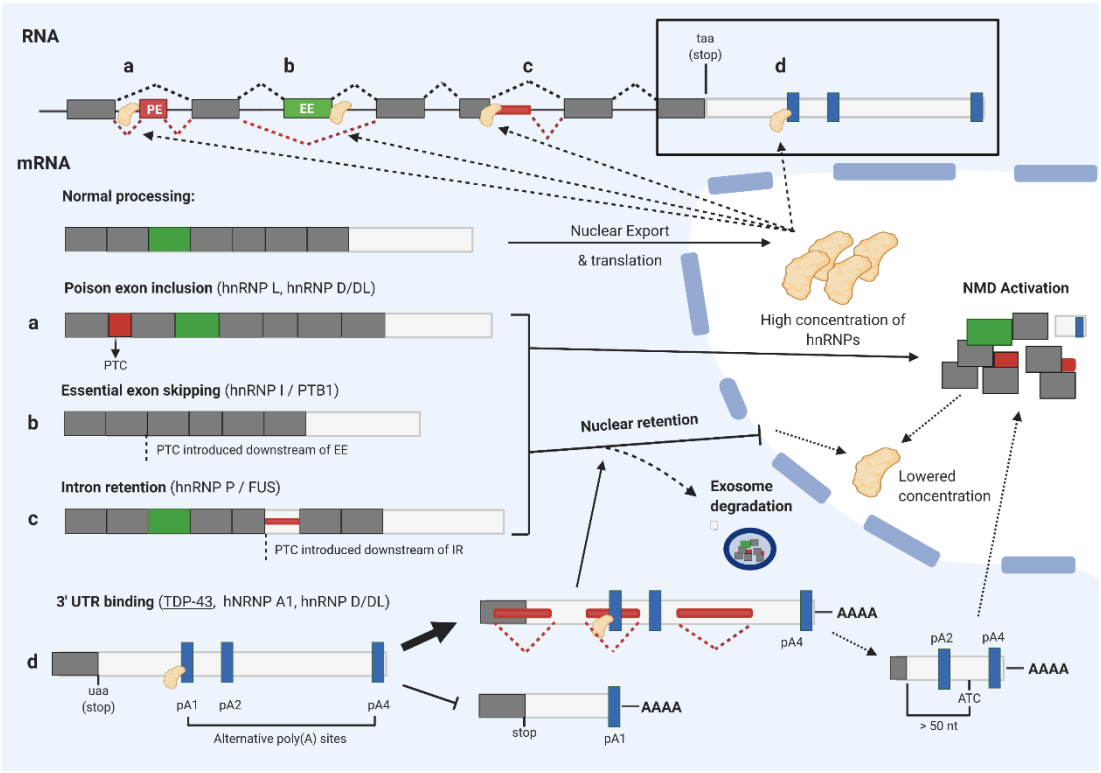

Figure 1.15. HnRNP autoregulation mechanisms. HnRNPs autoregulate their expression by several RNA processing mechanisms. HnRNP binding promotes specific splicing events that result in the production of NMD-sensitive mRNAs and/or transcripts confined to the nucleus (blue background). These include the activation of a normally skipped premature termination codon (PTC)-containing 'poison exon' (a), the skipping of a normally 'essential exon' (EE) (b) or retention of intronic RNA (IR) (c). TDP-43 binds to its 3′UTR *TARDBP* binding site within intron 7 and inhibits the selection of the proximal poly(A) site (pA1), up-regulating alternative polyadenylation at its more distal sites: pA4 and more rarely pA2 (isoform not shown) (d). The unstable isoform generated is detained in the nucleus and is subject to exosome-mediated degradation. TDP-43-binding and subsequent RNA Pol II stalling can also lead to alternative splicing of 3′ UTR intronic regions (red rectangles) which truncates the final exon, eliminates the true stop signal and exposes an alternative termination codon (ATC). The ATC being > 50 nt from the final exon-junction complex designates the transcript for NMD. This splicing event is not believed to significantly contribute to TDP-43 autoregulation, but is a crucial feature of hnRNP A1 and hnRNP D/DL autoregulatory mechanisms which activate 3′ UTR poison exon/intron events (Bampton *et al.*, 2020).

Additionally, 3′ UTR-dependent mechanisms of autoregulation have also been elucidated in several hnRNPs. Analogous to the RNA processing mechanisms described above, hnRNP A1 and hnRNP D/DL autoregulate their own expression levels by activating 3′ UTR poison exon and intron retention events in each of their transcripts, respectively (Chabot *et al.*, 1997; Kemmerer, Fischer and Weigand, 2018). Both splicing events designate the transcripts for

NMD by virtue of extending the gap between the last exon-junction complex and the termination codon beyond 50 nucleotides in length in keeping with the > 50 nt rule (Hug, Longman and Cáceres, 2016; Lindeboom, Supek and Lehner, 2016).

Finally, perhaps the most well-studied and mechanistically complex autoregulation loop belongs to TDP-43 (**Figure 1.15d**). Direct interactions between TDP-43 and its transcript at the 3′ UTR have been confirmed (Polymenidou *et al.*, 2011; Tollervey *et al.*, 2011). TDP-43 self-binding promotes nuclear detainment and transcript instability by the promotion of an alternative polyadenylation selection site. Retained transcripts were found to be at least partially vulnerable to exosome-mediated degradation (Ayala *et al.*, 2011). An additional layer of complexity arises from the observation that cellular levels of TDP-43 decrease dramatically throughout embryonic development and continue to decline in an age-dependent manner (Sephton *et al.*, 2010; Cragnaz *et al.*, 2015). Recent findings have discovered that age-related acceleration of DNA methylation within the autoregulatory region of *TARDBP* contributes to dysregulated TDP-43 autoregulation within the human motor cortex (Koike *et al.*, 2021). Hence, whilst TDP-43 autoregulates itself throughout life, it is very much an integrated mechanism that is highly synchronised with the aging process.

1.10.6 Tipping point model of hnRNP dysregulation

It is unclear whether hnRNP autoregulatory systems are being systematically overwhelmed or otherwise compromised in FTLD/ALS pathogenesis, however this will be an important question to answer given the potentially catastrophic consequences to neurons that may follow autoregulatory failure. A case in point is TDP-43 where nuclear depletion and cytoplasmic mislocalisation of the protein induces abnormal autoregulation within ALS motor neurons (White *et al.*, 2018). The balance of TDP-43 self-regulated *TARDBP* splicing variants is aberrantly shifted towards the production of translatable *TARDBP* transcripts which leads to further increases in *TARDBP* mRNA and protein in the cytoplasm (Koyama *et al.*, 2016). Similar conclusions have followed from both

toxic loss and gain of function, ALS-associated mutant *TARDBP* mouse models which both result in abnormally upregulated *TARDBP* mRNA levels (D'Alton, Altshuler and Lewis, 2015; White *et al.*, 2018). Similarly, NLS-disrupting, ALS-causing mutations in *FUS* also lead to perturbed splicing function and especially in intron retention events which FUS itself uses to regulate its own expression levels (Zhou *et al.*, 2013; Humphrey *et al.*, 2020). Hence, it is possible that hnRNPs which may be mislocalised or otherwise sequestered within FTLD/ALS-associated pathologies, may well be contributing towards a vicious cycle of neurotoxicity propagated by autoregulatory malfunction.

Owing to the many vital roles hnRNPs play in maintaining homeostasis within neurons, they are likely to be in high demand in order to counteract and neutralise potentially pathogenic events which characterise the early disease phases of FTLD/ALS, including many of those previously discussed. Hence, neurons may be especially sensitive to varying hnRNP levels even in the absence of significant functional depletion. Significant functional redundancy between hnRNPs / RBPs and their at-least partial ability to cross-regulate one another (e.g. TDP-43 co-regulation of FUS and hnRNPA1 expression levels) may provide some level of initial compensation (Huelga *et al.*, 2012; Deshaies *et al.*, 2018; Humphrey *et al.*, 2020). However, beyond a 'tipping point' of hnRNP functional inadequacy which may arise due to excessively high cellular demand, functional sequestration or more likely a combination of the two, the balance may tip from homeostatic control to whole network-level disarray at the RNA, DNA and protein levels (**Figure 1.16**). This, largely loss-of-function framework has the potential to exacerbate gain-of-function pathogenic events mediated by the primary pathology underlying FTLD/ALS disease (TDP-43, FUS, Tau, *C9orf72* etc.) and hence the most important molecular pathways affected by hnRNP dysregulation in each disease may reflect this pathological heterogeneity (Bampton *et al.*, 2020).

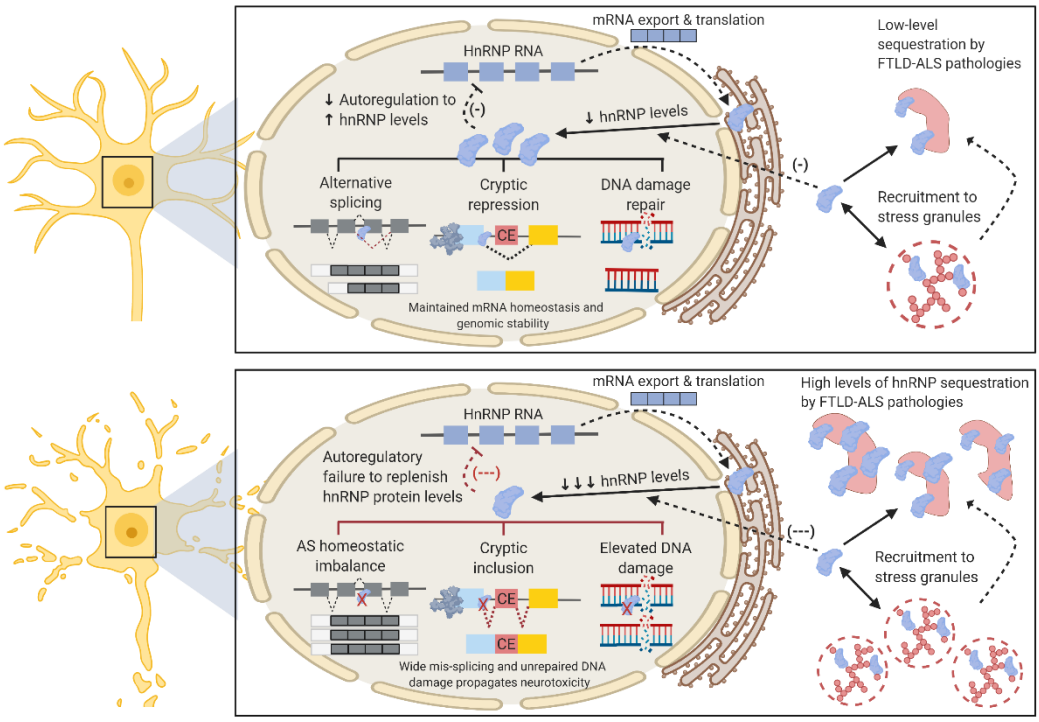

Figure 1.16. Proposed model of hnRNP dysfunction in FTLD-ALS. The upper panel illustrates hnRNPs continuing to perform their homeostatic functions under relatively low levels of stress e.g., at early stages of FTLD-ALS pathogenesis. HnRNP protein levels are reduced as a result of low-level sequestration within cytoplasmic pathological inclusions (nuclear inclusions not shown) and/or recruitment to stress granules. Indeed persistence of stress granules may be the root cause of some of these aggregates. However, autoregulation ensures adequate amounts of hnRNPs are replenished so they may perform their myriad nuclear functions including alternative splicing regulation, cryptic exon (CE) repression and DNA damage repair. By contrast, the lower panel illustrates a scenario whereby hnRNP depletion by pathological sequestration breaches a homeostatic 'tipping point' that is beyond compensation by autoregulatory means. At this stage, ensuing mRNA metabolic dysfunction from alternative splicing dysregulation and elevated CE activation in addition to unrepaired DNA damage may rapidly lead to neurotoxicity and accelerated neurodegeneration (Bampton *et al.*, 2020).

1.11 HnRNP K

1.11.1 HnRNP K structure and function

HnRNP K is one of the most abundantly expressed and best characterised proteins of the hnRNP family (Matunis, Michael and Dreyfuss, 1992). It contains three K homology (KH1-3) RNA-binding domains which have a high propensity to bind sequence-specific polycytosine tracts and share significant

sequence homology with hnRNP E1 and E2 (polycytosine-binding proteins 1/2) (Dejgaard and Leffers, 1996). Despite their name, KH domains are not structurally unique to hnRNP K and indeed polycytosine-binding proteins (PCBP) 1/2 (hnRNP E1/2) each also contain three such domains with high sequence homology to hnRNP K (Makeyev, Chkheidze and Liebhaber, 1999). By contrast, the K interactive (KI) region is unique to hnRNP K and contains several protein binding domains which enable it to serve as a docking platform for kinases and other proteins in numerous signal transduction pathways (Bomsztyk *et al.*, 1997). As with many other hnRNP proteins, hnRNP K contains an N-terminally located nuclear localisation (NLS) signal ensuring the protein is confined to the nucleus at steady state. It also contains a K-nuclear shuttling (KNS) domain, bestowing hnRNP K with the capacity for bi-directional transport across the nuclear envelope between the nucleoplasm and the cytoplasm for subcellular, region-specific functionality (Michael, Eder and Dreyfuss, 1997) (**Figure 1.17**).

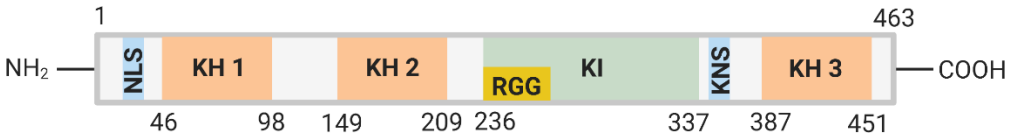

Figure 1.17. Schematic of hnRNP K structural domains. NLS, Nuclear localisation sequence; KH, K-homology domain; KI, K-interactive domain; RGG, Arg-Gly-Gly repeat domain; KNS, K-nuclear shuttling domain.

HnRNP K is widely and abundantly expressed across the brain (Trabzuni *et al.*, 2011). It has been found to interact antagonistically with fellow RBP ELAVL2 to induce cell cycle arrest and activate neuronal differentiating pathways in embryonic cells (Yano, Okano and Okano, 2005). Indeed, hnRNP K has been implicated as a key protein in the post-transcriptional regulation of several neurodevelopmental processes including axogenesis (Liu and Szaro, 2011), CNS myelination (Laursen, Chan and Ffrench-Constant, 2011) and in the mediation of synaptic plasticity in hippocampal neurons (Folci *et al.*, 2014; Leal *et al.*, 2017). HnRNP K exhibits an especially high expression in the hippocampus and other mesocorticolimbic structures during early development and has hence been associated with the regulation of several

neurotransmitter processes including acetylcholine and dopamine synthesis (Du, Melnikova and Gardner, 1998; Banerjee *et al.*, 2014; Folci *et al.*, 2014).

1.11.2 HnRNP K in disease

Unsurprisingly given the myriad roles hnRNP K performs in early neurodevelopmental pathways, *HNRNPK* genetic abnormalities are associated with severe phenotypic consequences. Complete, bi-allelic loss of *HNRNPK*(-null) leads to rapid embryonic lethality in mice by day 14 whilst *HNRNPK* haploinsufficiency results in neuronal developmental defects (Gallardo *et al.*, 2015). Rare, deleterious loss of function mutations within the human *HNRNPK* gene result in neurodevelopmental disorders including the autosomal dominantly inherited Au-Kline syndrome (Okamoto, 2019; Gillentine *et al.*, 2021) characterised by severe intellectual disability, craniofacial dysmorphism, cardiac defects and skeletal abnormalities.

HnRNP K has been most intensively researched, within the context of disease pathways, in oncology fields where an abundance of research has linked abnormal hnRNP K expression to enhanced malignancy in several cancers (Gallardo *et al.*, 2016). Transcriptional and immunohistochemical analysis of biopsied patient tissue have been instrumental in identifying that elevated *HNRNPK* expression levels and abnormal subcellular distribution patterns of the protein is a unifying pathological feature associated with enhanced malignancy in many different tumour types (**Figure 1.18**). Indeed, hnRNP K overexpression and mislocalisation from the nucleus to the cytoplasm has been observed in colorectal (Carpenter *et al.*, 2006), lung (Li *et al.*, 2019), kidney (Otoshi *et al.*, 2015), pancreatic (Zhou *et al.*, 2010) and blood cancers (Hornbaker *et al.*, 2016) among others and is consistently associated with higher tumour grade and poorer prognosis. However, hnRNP K has been proposed as both an oncogene and a tumour suppressor gene with one haploinsufficient mice model resulting in a myeloproliferative phenotype consistent with hnRNP K-containing chromosomal deletions being associated with acute myeloid leukemia cases (Dayyani *et al.*, 2008; Gallardo *et al.*, 2016). A mixture of both *HNRNPK* deficient and overexpression cell and

animal models will be important to disentangle the enigmatic roles of hnRNP K protein in the development and/or suppression of cancer in different cellular contexts.

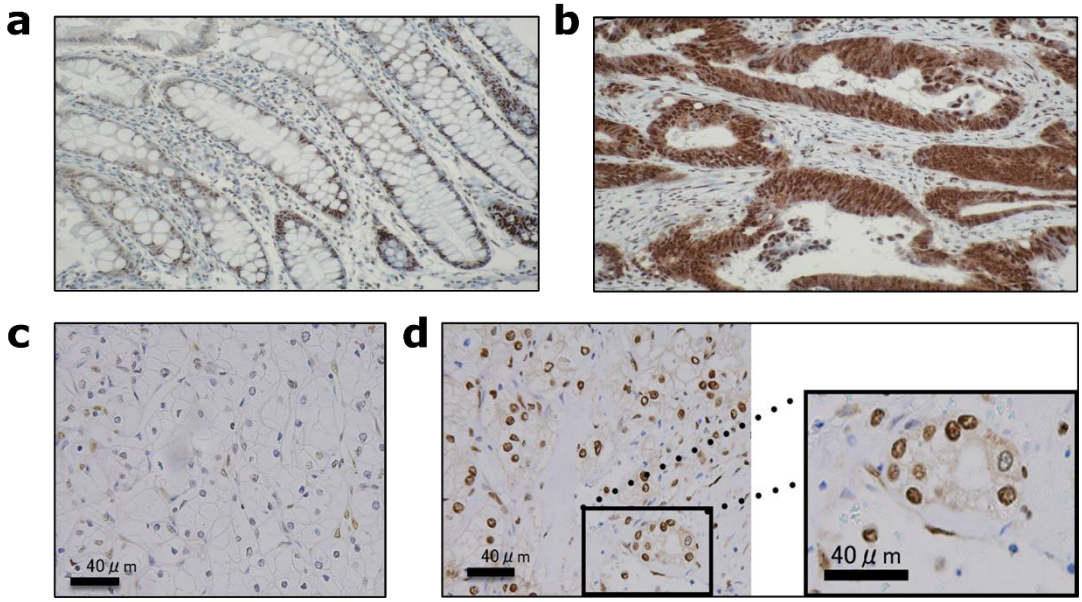

Figure 1.18. Examples of immunoreactivity for hnRNP K in normal and malignant tissue types. (a) Exclusively nuclear localisation of hnRNP K within crypt epithelial cells. (b) Elevated nuclear and cytoplasmic staining of hnRNP K within primary colorectal cancer (Carpenter *et al.*, 2006, reproduced under a Creative Commons license: http://creativecommons.org/licenses/by-nc-sa/3.0/). (c) Weakly positive neuronal staining of hnRNP K in low grade (Furhrman grade 1) clear cell type renal cell carcinoma (ccRCC). (d) Strong nuclear and cytoplasm-redistributed hnRNP K staining within an advanced ccRCC (Fuhrman grade 4) demonstrating a link to tumour aggressiveness (Otoshi *et al.*, 2015, reproduced under a Creative Commons license: http://creativecommons.org/licenses/by/4.0/).

1.11.3 HnRNP K and TDP-43

Although little is known about hnRNP K-regulated pathways in the context of neurodegenerative disease, hnRNP K has been found to be an important binding partner of TDP-43 in neuronal stress granule formation. Both RBPs have been found to colocalise within stress granules and indeed TDP-43 accumulation depends on prior phosphorylation of hnRNP K by cyclin-dependent kinase 2 (Moujalled *et al.*, 2015). Both RBPs have been found to be robustly nuclear depleted within iPSC-derived motor neurons subjected to osmotic stress, but hnRNP K did not translocate to the cytoplasm in response to other conventional stressors (Harley and Patani, 2020).

HnRNP K is also a key driver of the nuclear retention of long non-coding RNA (lncRNA) Malat1 through direct interactions between a short interspersed nuclear element (SINE) in Malat1 and hnRNP K–binding RBPs KHDRBS1 and TRA2A. When this interaction is disrupted, it leads to elevated Malat1-TDP-43 binding and a subsequent increased propensity for TDP-43 aggregation as observed in ALS patients (Nguyen *et al.*, 2020).

The extent to which dysregulated hnRNP K-TDP-43 perturbations contribute to the FTLD/ALS disease process is unclear but ALS-causing *TARDBP* mutations have been linked to impaired hnRNP K expression and associated failures in hnRNPK-regulated antioxidant pathways leading to elevated oxidative stress (Moujalled *et al.*, 2017). In further support of an interplay between these proteins, hnRNP K was identified as a modifier of TDP-43 in *Drosophila* and cell-based models of TDP-43 overexpression (Appocher *et al.*, 2017). To date, there is no evidence of an association between hnRNP K protein and TDP-43 in pathological inclusions. However, protein levels of hnRNP K as well as its subcellular localisation and phosphorylation status may be mechanistically important in maintaining normal stress granule assembly and TDP-43 proteostasis (Moujalled *et al.*, 2017; Nguyen *et al.*, 2020).

1.12 CRISPR-interference for gene knockdown

1.12.1 CRISPR

Clustered regularly interspaced palindromic repeats (CRISPR)-Cas9 is an RNA-based, adaptive immune system employed by prokaryotes to protect against viral infection (Jansen *et al.*, 2002; Barrangou *et al.*, 2007). The most well-characterised being the type II-A CRISPR-Cas9 system of Streptococcus pyogenes (Le Rhun *et al.*, 2019). The defence mechanism functions by capturing short segments of an invading virus's DNA, termed 'spacer sequences' and incorporating them into CRISPR loci. Upon re-infection by the same virus, the CRISPR arrays are used as a template to rapidly transcribe RNA segments termed CRISPR RNA (cRNA) that are specific to parts of the

viral genome (Brouns *et al.*, 2008). The transcribed cRNA, in-tandem with another RNA molecule: trans-activating crRNA (tracrRNA), then function to guide DNA endonuclease enzyme Cas9 to complementary regions of viral DNA (Deltcheva *et al.*, 2011). A 2-6 base pair protospacer adjacent motif (PAM) immediately upstream of the target sequence is also required for successful Cas9 binding (Deveau *et al.*, 2008). At the targeted location, Cas9 catalyses a site-specific double strand break to disable the virus (Barrangou *et al.*, 2007).

The CRISPR-Cas9 system has since been re-engineered for targeted genome engineering in human cells (Cho *et al.*, 2013; Cong *et al.*, 2013; Jinek *et al.*, 2013; Mali *et al.*, 2013). A vital part of the technologies' development was the production of a chimeric single guide RNA (sgRNA) generated by the fusion of both crRNA and tracRNA fusion transcripts (Jinek *et al.*, 2012). The sgRNA mimics the crRNA:tracRNA duplex formed *in vivo* and contains a customisable ~20 nucleotide sequence designed to target recombinant Cas9 protein to a specific gene of interest (Jinek *et al.*, 2012). Efficient cas9-induced cleavage of targeted DNA then up-regulates the high efficiency but low-fidelity process of NHEJ for DSB repair (Deriano and Roth, 2013). Frequently, NHEJ leads to small deletions and/or insertion (indel) mutations at the lesion site prior to re-ligation. Such coding errors are likely to induce a shift in the open reading frame leading to the generation of multiple downstream PTCs (Ran *et al.*, 2013). Transcripts harbouring PTCs are either degraded by NMD in the cytoplasm or are translated into non-functional truncated protein isoforms (Hug, Longman and Cáceres, 2016). Hence, CRISPR-Cas9 editing has evolved into a powerful method of gene knockout applicable to human cells.

1.12.2 CRISPR-interference

More recently the CRISPR system has been re-purposed for gene suppression or 'interference' studies. Cas9 is replaced by a nuclease-deactivated or catalytically 'dead' Cas9 (dCas9) enzyme (Gilbert *et al.*, 2013; Larson *et al.*, 2013; Qi *et al.*, 2013). Guide RNAs bind to targeted regions of DNA as before, except no DNA excision occurs. Instead, the bulky dCas9 protein functions to

sterically hinder transcription by physically occluding the recruitment of RNA Pol II and/or appropriate transcription factors, effectively silencing the gene of interest (Larson *et al.*, 2013) (**Figure 1.19**). Another proposed mechanism of dCas9-induced gene repression is through epigenetic alterations in chromatin structure that interfere with the initiation of transcription (Pulecio *et al.*, 2017). Often, dCas9 is fused with a transcriptional repressor domain such as a Krüppel associated box (KRAB) to promote an even stronger repression of gene expression at the transcriptional level (Gilbert *et al.*, 2013).

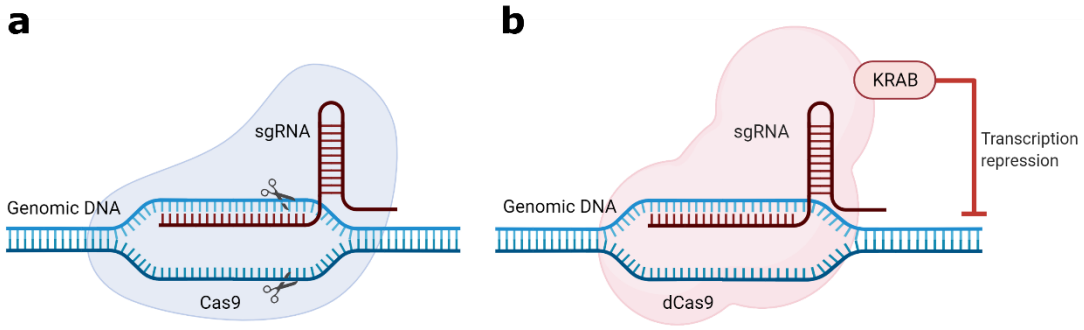

Figure 1.19. Comparing CRISPR and CRISPRi mechanisms of action. (a) CRISPR/Cas9-mediated gene knockout and (b) CRISPRi-mediated gene suppression.

1.12.3 Genome-wide CRISPRi screens

As with conventional CRISPR-Cas9, CRISPRi has recently been up-scaled for the creation of genome-wide phenotypic loss-of-function screens. Scalable gene perturbations throughout the whole genome have been made possible by the development of genome-wide sgRNA libraries (Gilbert *et al.*, 2014; Wang *et al.*, 2014; Horlbeck *et al.*, 2016). Machine learning algorithms have been built to design sgRNAs with high predicted activity. Importantly, sgRNAs must be targeted to sequences within a -25 and + 500 bp range from the primary or secondary transcription start site (TSS). Additionally, as with all CRISPR technologies, the target sequence must also be followed by an immediately downstream NGG PAM on the non-target strand (Horlbeck *et al.*, 2016). More recently, next-generation CRISPRi libraries that also incorporates chromatin accessibility into their predictive model have led to further improvements in the design of efficacious sgRNAs (Horlbeck *et al.*, 2016). This

followed evidence that nucleosome occupancy impedes both Cas9 and dCas9 access to target sites (Hinz, Laughery and Wyrick, 2015; Horlbeck *et al.*, 2016; Isaac *et al.*, 2016). Finally on the subject of sgRNA design, as sgRNA expression is usually under the control of a Pol III (U6) promoter, all sgRNA target sequences are prepended with a 5' G to facilitate robust transcription (Horlbeck *et al.*, 2016).

Genome-wide sgRNA libraries can be cloned onto a lentiviral vector system to facilitate efficient cellular delivery and integration of sgRNAs into a Cas9-expressing cell line (Kampmann, 2017). Indeed, Tian et al. have developed an iPSC-derived neuronal cell line constitutively expressing CRISPRi machinery integrated into the CLYBL safe harbour locus (Tian *et al.*, 2019). The CAG promoter-driven dCas9-BFP-KRAB construct elicited a robust knockdown of sgRNA-targeting genes for several weeks after neuronal differentiation (Tian *et al.*, 2019). The sgRNA lentiviral pool is transduced at a multiplicity of infection far below 1 to minimise the probability of multi-gene knockdown (Doench *et al.*, 2016). Alongside CRISPRi-mediated knockdown, next-generation RNA sequencing has recently emerged as a powerful complementary tool for high-throughput phenotypic screening (Adamson *et al.*, 2016; Jaitin *et al.*, 2016; Datlinger *et al.*, 2017; Xie *et al.*, 2017).
Sequencing the sgRNA-encoding locus at varying time points enables high-throughput quantification of cells expressing each sgRNA. How well represented a sgRNA is within a surviving cell population relative to a control sgRNA population at any one time can be compared to an un-engineered or untreated control sample. Whether or not an sgRNA is enriched or depleted serves as a proxy for interpreting how 'essential' a particular gene is within different genetic or environmental contexts (Xu and Qi, 2019).

1.12.4 Comparing gene knockdown technologies

Until recent times, RNA interference (RNAi)-based strategies have been the go-to platform for loss-of-function experiments and screens. Synthetically designed, double-stranded RNA molecules including small interfering RNAs (siRNAs) and short hairpin RNAs (shRNAs) have been used to post-

transcriptionally silence target gene expression via complementary binding to mRNA targets (Dana *et al.*, 2017). The introduced RNAi molecules are incorporated into the RNA-induced silencing complex (RISC) where they induce mRNA cleavage and subsequent degradation of the transcript (Hammond *et al.*, 2000). Experimentally, deployment of RNAi technology is arguably the most technically straightforward method of gene perturbation. Targeting RNA molecules are easy to generate and can be delivered to cells intracellularly by a simple lipid-mediated transfection. However, there is increasing concern that artificial RNAi molecules exhibit wide-spread off-target effects which potentially confound gene-level interpretation of data (Boettcher and McManus, 2015). Indeed, siRNAs are known to induce silencing of non-targeting mRNAs by binding to both 3'UTR and coding regions with limited sequence complementarity. A single siRNA molecule can potentially repress hundreds of transcripts in this way which can elicit an 'off-target phenotype' that predominates over the on-target one (Sigoillot and King, 2011; Franceschini *et al.*, 2014).

The emergence of gene-editing tools that rely on endonucleases for DNA cleavage including Cas9 in the CRISPR system and transcription activator-like effector nucleases (TALEN) have begun to overtake RNAi technology in functional genomic screens (Unniyampurath, Pilankatta and Krishnan, 2016). By virtue of CRISPR and TALEN being gene knockout techniques, CRISPRi and RNAi are the most functionally comparable tools with respect to gene knockdown. Both techniques are especially preferable to the former where either complete gene knockout is associated with cell lethality or incomplete knockdown better reflects the physiological conditions of the cell the experiment is attempting to recapitulate (Boettcher and McManus, 2015). Even when the importance of knockdown over knockout is not paramount, CRISPRi has further advantages over both genome editing and RNAi technologies. The most crucial being a striking lack of off-target effects, likely a reflection of both the high sensitivity of mismatches between sgRNA and target DNA sequence and the prerequisite condition that CRISPRi machinery must bind a narrow window centring around the TSS to be efficacious (Gilbert *et al.*, 2014; Evers *et al.*, 2016; Stojic *et al.*, 2018). This, in combination with

the absence of double-stranded breaks induced in conventional CRISPR screens, makes CRISPRi both a precise and non-toxic alternative technology for loss of function genomic screens. Further advantages and disadvantages of CRISPRi in comparison to CRISPR, TALEN and RNAi are summarised in **Table 1.3**.

Table 1.3. Comparing gene knockdown strategies

Feature	Genetic perturbation technology		
	CRISPR	**CRISPRi**	**RNAi**
Type of phenotype	Null (Complete knockout).	Hypomorphic (knockdown).	Hypomorphic (knockdown).
Phenotypic signal	Strong signal, but potentially rescuable if edited exon is skipped (Mou *et al.*, 2017).	Moderate signal depending on knockdown efficiency.	Moderate signal depending on knockdown efficiency.
Reversibility	Permanent.	Reversible.	Reversible.
Level of repression	Transcriptional.	Transcriptional.	Post-transcriptional.
Type of transcript	Both nuclear and cytoplasmic transcripts.	Both nuclear and cytoplasmic transcripts (Liu *et al.*, 2017).	Mature cytosolic transcripts only (Wilson and Doudna, 2013).
Known sequence	Requires only transcriptome to be known.	Requires genome with annotated TSS (Boettcher and McManus, 2015).	Requires only transcriptome to be known.
Off-target effects	High frequency of off-target mutations and chromosomal translocations associated with off-target DSBs (Fu *et al.*, 2013; Pattanayak *et al.*, 2013).	Very low, primarily due to small sgRNA targeting window around the TSS (Gilbert *et al.*, 2014).	Pervasive off-target effects on non-targeting genes with limited sequence complementarity (Semizarov *et al.*, 2003; Lin *et al.*, 2005) and can also displace endogenous microRNAs from the RISC (Khan *et al.*, 2009).
Toxicity	Potential high toxicity from DSB and off-target DNA editing but less than RNAi.	Minimal toxicity.	Off-targeting by siRNA can induce a toxic phenotype.
Cost	Low, sgRNAs are purchased at low cost.	Low, sgRNAs are purchased at low cost.	High, synthetic siRNA production is expensive. Not so using shRNAs.

Experimental difficulty	Medium, sgRNAs must be cloned into delivery constructs prior to delivery	Medium, sgRNAs must be cloned into delivery constructs prior to delivery	Easy, RNAi (siRNA) requires a single simple transfection, RNAi (shRNAs) requires pre-cloning
Time taken to phenotype	Several weeks, sgRNAs must be cloned and Cas9 functionality validated.	Several weeks, sgRNAs must be cloned and dCas9 / KRAB functionality validated	Days, RNAi (siRNA) is very fast

1.13 Aims of the thesis

The primary aims and sub-aims of the work described in this thesis, accompanying further research questions and each aim's accompanying chapter(s) are as follows:

1) **Identify brain regions and neuronal subpopulations that are vulnerable to hnRNP K mislocalisation (Chapters 3-4).**

a. Use immunohistochemistry to describe the morphological features of hnRNP K mislocalisation in afflicted neurons.

b. Develop a methodological pipeline (incorporating machine learning in the case of the frontal cortex) to detect, quantify and analyse hnRNP K localisation in identified regions of interest.

c. Determine the extent to which hnRNP K mislocalisation is associated with neurodegenerative disease and/or clinical and demographic covariates including age.

d. Utilise double immunofluorescence to characterise cytoplasmic puncta in neurons exhibiting hnRNP K mislocalisation and also to determine the spatial relationship with FTLD pathologies.

2) **Develop an iPSC-derived neuronal model of hnRNP K knockdown using CRISPR-interference technology (Chapter 5-6).**

a. Develop, optimise and validate a neuronal CRISPRi-i^3 methodological pipeline for knocking down hnRNP K protein.

b. Use RNA-sequencing analysis of neuronal derived RNA to determine differential expression in hnRNP K KD neurons.

c. Perform differential splicing analysis to determine hnRNP K-KD associated splicing changes including the presence of cryptic and/or skiptic exons and validate strong example hits molecularly.

3) **Use BaseScope™ *in situ* hybridisation to detect and validate cryptic exons in post-mortem brain tissue (Chapter 6)**

a. Optimise a BaseScope™ assay for the detection and validation of a novel TDP-43 depletion-associated cryptic exon (CE) in *UNC13A* in frozen FTLD brain.

b. Optimise a BaseScope™ assay for the detection and validation of *a* second CE in *INSR* within morphologically preserved FFPE ALS brain.

c. Establish a methodological pipeline for analysing the spatial relationship between TDP-43 neuronal inclusions and associated CE events in brain tissue by development of a dual ISH-IHC assay.

Chapter 2 General Methods

2.1 Pathological examinations

2.1.1 Results chapter relevance

Immunohistochemistry is the predominating pathological technique used in chapters 3 and 4, whilst the described immunofluorescence and brain homogenate derived western blotting and RT-qPCR techniques are featured in chapter 3 only. BaseScope™ *in situ* hybridisation is utilised in chapter 6.

2.1.2 Cases

Brain and spinal cord tissue was donated to the Queen Square Brain Bank (QSBB) for neurological disorders (UCL Queen Square Institute of Neurology) and the Medical Research Council (MRC) Edinburgh Brain & Tissue Bank. All tissue samples were donated with the full, informed consent of the donor, relative or nominated representative. All cases were diagnosed pathologically according to consensus criteria involving a thorough examination of each brain's macroscopic features and the batch deployment of routine immunohistochemical tests. Accompanying clinical and demographic data of all cases were stored electronically in compliance with the 1998 data protection act and are summarised in **Table 3.1** (Chapter 3) and **Table 4.1** (Chapter 4) each corresponding to distinct projects. Ethical approval for the study was obtained from the NHS research ethics committee (NEC) and in accordance with the human tissue authority's (HTA's) code of practice and standards under licence number 12198 (**Appendix 1**).

2.1.3 Tissue processing

Brains processed at QSBB were fixed in formalin and cut along the longitudinal fissure to separate the two cerebral hemispheres. In accordance with UK brain bank network standard operating procedures; the right hemisphere was snap

frozen at -80 °C for cryostat sectioning and the left hemisphere was dissected and embedded into anatomically-distinct paraffin blocks. Tissue was embedded by dehydration in a series of increasing grades of Ethanol (70-90 %), followed by clearing in chloroform and infiltration in paraffin wax. Blocks were sectioned at 8 µm using a Thermo Fisher™ HM.340E electronic rotary microtome. Sections were then floated on warm water, mounted onto glass microscope slides (Solmedia) and dried at 37 °C overnight.

2.1.4 Immunohistochemistry

Slides with 8 µm mounted tissue sections ready for immunohistochemical staining were incubated at 60 °C overnight. Sections were deparaffinised in three, 5-minute sequential washes of xylene and gradually rehydrated through three further washes in decreasing grades of alcohol (100, 90, 70 % IMS). Slides were then incubated in a hydrogen peroxide (0.3 %) solution of methanol for 10 minutes to block endogenous peroxidase activity. For heat-induced antigen retrieval, slides were then transferred to a boiling solution of 0.1 M citrate buffer (pH 6.0) and pressure cooked at maximum pressure for 10 minutes. Slides were then cooled under cold running water and incubated in 10 % non-fat milk (Marvel) for 30 minutes at room temperature to block non-specific binding. Tissue was outlined with a hydrophobic Pap pen (Sigma-Aldrich) and incubated in 200 µl (400 µl for large slides) of primary antibody for 1 hour at room temperature, at the predetermined concentrations. After three gentle 5-minute washes in tris-buffered saline with tween (TBS-T); slides were incubated for 45-minutes in 200 µl of species-specific biotinylated IgG secondary antibody (Vector Laboratories BA 9200, 1:200). Slides were washed as before and then incubated (30 minutes) in 200 µl of pre-conjugated Strept(avidin)-Biotin Complex (ABC; DAKO) for signal amplification. The slides were then washed for a final time and transferred to a 200 ml solution (TBS-T) containing 500 µg of hydrogen peroxide-activated (64 µl) 3,3'-Diaminobenzidine (DAB) chromogen. The slides were removed after adequate nuclear staining intensity was visually confirmed using a light microscope (3-5 minutes) and nuclear counter-stained for 40 seconds in Mayer's haematoxylin

(BDH). Finally, slides were dehydrated in increasing grades of alcohol (70, 90 and 100 % IMS) and cleared in three washes of xylene prior to coverslip mounting with DePeX mounting medium (Vector Laboratories). A schematic of the immunohistochemical staining process is detailed in **Figure 2.1**.

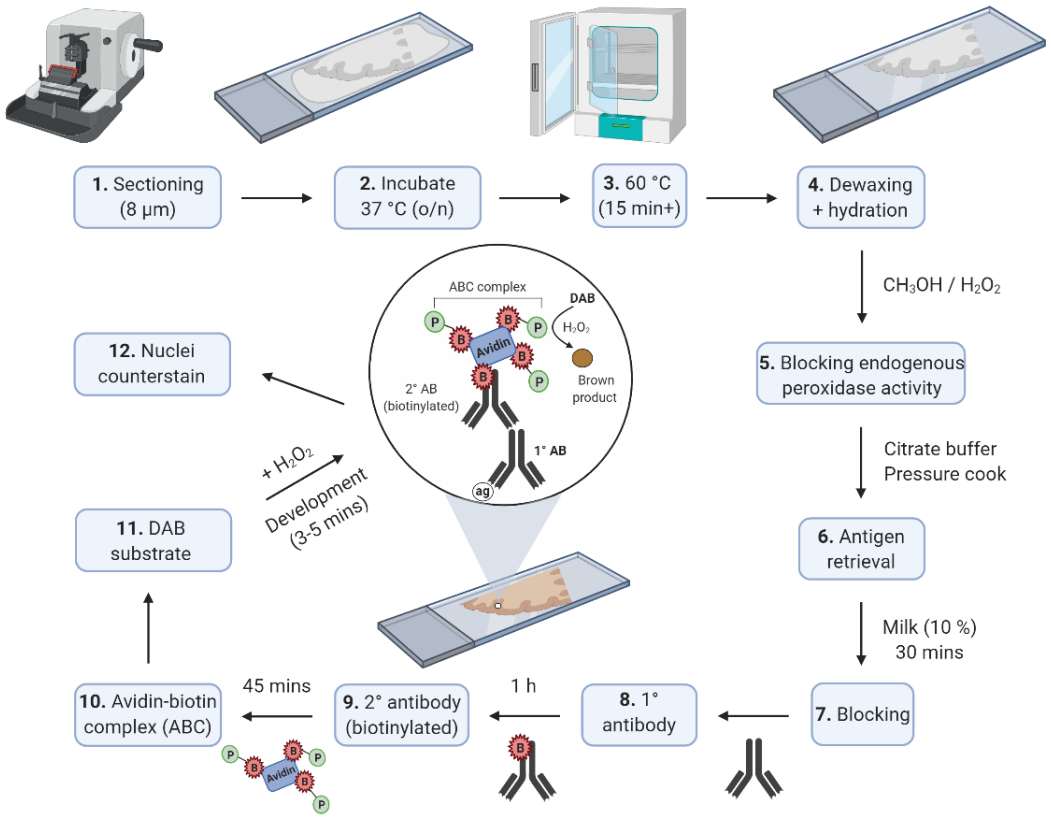

Figure 2.1. Immunohistochemistry workflow.

2.1.5 Double-label immunofluorescence

For double immunofluoresence, tissue sections were dewaxed, pre-treated and blocked as before (**2.1.5**). Sections were then either simultaneously or sequentially co-stained with mouse-derived anti-hnRNP K antibody (Abcam ab23644, 1:1000) and a second primary antibody requiring either a joint-single or double incubation period respectively. HnRNP K staining was amplified by incubation with a biotinylated IgG secondary antibody (DAKO / Vector laboratories, 1:200) prior to a 30 minute incubation with ABC at room temperature as previously described for IHC (**2.1.5**). Antibody binding was visualised using a TSA Cyanine 3 amplification kit (Perkin-Elmer) which was

applied to sections for 20 minutes at room temperature. After TBS-T washing, sections were incubated with species-appropriate Alexa Fluor 568 secondary antibodies (Invitrogen, 1:1000) for 2 hours at room temperature to visualise the second (non-hnRNP K) antibody. Sections were washed a final three times in TBS-T with the second wash incorporating a 10-minute incubation with 4',6-diamino-2-phenylindole (DAPI, Invitrogen, 1:1000) nuclei counterstain. Slides were mounted using Vectashield anti-fade mounting medium (Vector Laboratories) and sealed with nail varnish.

Cross-reactivity was controlled for by the addition of two control sections stained as above with the individual omission of each primary antibody. Representative fluorescent images were captured at 20x, 40x or 63x magnification using a Leica DM5500B fluorescence microscope and Z-stacks were subjected to a blind 3D deconvolution. Antibody staining was identified and imaged using the appropriate fluorescent channels, and colocalisation was confirmed or refuted on the combined, maximum-projected images.

A list of all primary and secondary antibodies used for both immunohistochemistry and double immunofluorescence labelling and their respective conditions of incubation with anti-hnRNP K antibody are detailed in **Table 2.1.**

Table 2.1. Antibodies used for immunohistochemistry and immunofluorescence.

Target	Host	Source	Dilution	Incubation	2° antibody
HnRNP K	Mouse	Abcam (Ab23644)	1:1000	1 h RT	Biotinylated goat-anti-mouse IgG (Vector Laboratories).
TDP-43	Mouse	Abnova (H00023435-MO1)	1:800	1 h RT	
pTDP43 (S409)	Rabbit	Cosmo Bio (TIP-PTD-P02)	1:10,000	Overnight (4 °C)	Alexa-fluor® 594-conjugated donkey anti-rabbit antibody (Invitrogen)
p-Tau (S202, T205)	Rabbit	Thermo Fisher (MN1020)	1:500	Overnight (4 °C)	
p62	Rabbit	Abcam (Ab155686)	1:500	Overnight (4 °C)	
LC3	Rabbit	Proteintech (14600-1-AP)	1:200	Overnight (4 °C)	
G3BP2	Rabbit	Sigma-Aldrich (HPA018304)	1:200	Overnight (4 °C)	
VDAC-1	Rabbit	Proteintech (10866-1-AP)	1:200	Overnight (4 °C)	

2.1.6 Brain tissue homogenisation

Tissue samples were prepared from frozen tissue chips of frontal cortex using a Precellys® Tissue homogenising CKMix kit. Briefly, chips were lysed in 1 ml of ice cold Lysis Buffer within tubes containing 1.4 mm and 2.8 mm-sized zirconium oxide beads. Samples were homogenised using the Precellys® volution tissue homogeniser which utilises vigorous 3-dimensional movement. Samples were then centrifuged at 1000 g (4 °C) for 10-minutes, the supernatant was then collected and the pellet was discarded.

2.1.7 Western blotting

An aliquot of the supernatant was prepared for protein concentration measurement by bicinchoninic acid (BCA) assay, performed according to manufacturer's instructions (Bio-rad).

Samples were then diluted to 1 µg / ml in equal volumes of NuPAGE reducing agent (10x), NuPAGE LDS sample buffer (4x) and an appropriate volume of deionised water. Samples were denatured at 90 °C for 10-minutes prior to loading. Denatured samples were resolved by electrophoresis on a NuPAGE TRIS-BIS gel (4–12 %) for 1.5 hours at 120 V prior to wet transfer (30 V, 1 h) to a 0.2 µM nitrocellulose membrane on ice. The blot was blocked in 10 % non-fat milk for one hour and then incubated with primary antibodies (HnRNP K, 1:1000) appropriately diluted in 5 % non-fat milk overnight at 4 °C. The membrane was washed three times in 0.1 % PBS-T for 5-minutes each and incubated with species-specific fluorescent secondary antibodies for one hour at room temperature (Li-cor). Blots were also incubated with β-actin antibody loading control for 30 minutes for normalisation purposes. Membranes were imaged using the Li-cor Odyssey® CLx image system and exported as Tiff files. Western blotting data was quantified, including densitometry analysis of selected bands, using ImageJ (v1.41) software.

2.1.8 RT-qPCR on brain tissue

RNA from human post-mortem brain tissue was isolated using a Qiagen miRNeasy Mini Kit according to manufacturer's instructions (Qiagen 217004). Briefly, 30 mg of brain tissue was lysed in 700 µl of Qiazol lysis buffer and homogenised using a TissueRuptor. Lysates were loaded into RNeasy Mini spin columns fitted with RNeasy silica membrane for RNA capture. Contaminants, including DNA, were efficiently removed through a series of sequential washes and a 15-minute treatment with DNaseI. RNA was eluted in 30 µl of RNAse free water. The concentration and quality of the eluted RNA was measured using a Nanodrop spectrophotometer. 2 µg of RNA were converted into cDNA by reverse transcription via the SuperScript IV VILO system (Thermo Fisher 11756050). A SYBR® Green real time quantitative polymerase chain reaction (RT-qPCR) was performed to analyse gene expression levels of *HNRNPK* in accordance with manufacturers instructions (Applied Biosystems). Primers used for qPCR and PCR cycling conditions are detailed in **Table 2.2** and **Table 2.3** respectively. Relative gene expression

levels were quantified in triplicate by the comparative threshold cycle (ΔΔCt) method using the housekeeping gene *RPL18A* as a reference for normalisation purposes.

Table 2.2. Primers used for measuring *HNRNPK* levels in brain tissue.

Primer	Primer sequence (5' to 3')
HNRNPK (Forward)	TTCAGTCCCAGACAGCAGTG
HNRNPK (Reverse)	TCCACAGCATCAGATTCGAG
RPL18A (Forward)	CCCACAACATGTACCGGGAA
RPL18A (Reverse)	TCTTGGAGTCGTGGAACTGC

Table 2.3 Thermal profile for RT-qPCR

Step	Temperature (°C)	Time	Cycles
Initial denaturation	95	10 mins	1
Annealing and extension	95	30 secs	40
	60	1 min	
	72	1 min	
	95	1 min	
Final extension	55	30 secs	1

2.1.9 BaseScope Assay

Cryptic exons (CEs) were detected in both frozen and formalin-fixed paraffin-embedded (FFPE) brain tissue using the BaseScope™ v2-RED assay (**Figure 2.2**). BaseScope probes were designed using the Bio-Techne bioinformatic pipeline to specifically target the CE-containing sequence. Custom and control probes used are listed in **Table 2.4**.

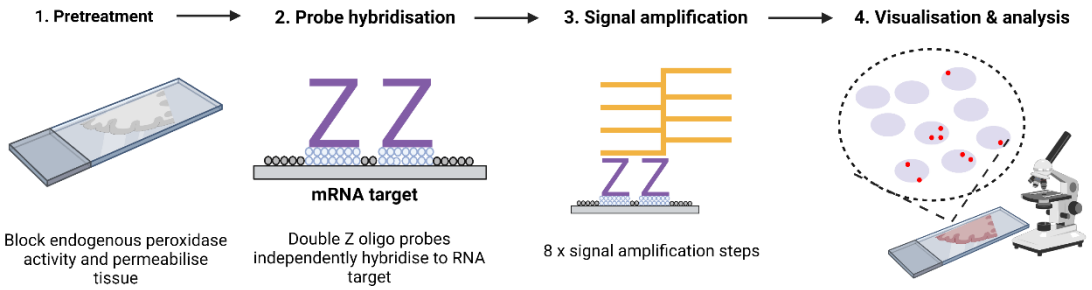

Figure 2.2. Workflow schematic of BaseScope™ assay from pre-treatment to analysis. The BaseScope™ assay utilises a single pair of signature 'double Z' probes which must both independently bind target RNA in tandem to be recognised by pre-amplifiers and amplifiers facilitating the specific and sensitive detection of splice variants.

Table 2.4 BaseScope™ probes used

Probe name	Probe type
HS-*PPIB*-1 ZZ	Positive control (human housekeeping gene)
DapB-1 ZZ	Negative control (bacterial gene)
BA-Hs-*UNC13A*-O1-1zz-st	Target probe (*UNC13A* CE)
BA-Hs-*INSR*-O1-2EJ-C1	Target probe (*INSR* CE)

Pre-treatment steps of frozen and FFPE sections respectively were performed according to sample-specific manufacturer's guidelines as out lined in **Table 2.5**. The BaseScope™ v2-RED assay was then performed using custom and control probes as instructed with no modifications (Advanced Cell Diagnostics, Newark, CA). In brief, after protease treatment, sections were incubated with applied target probe (3-4 drops) for 2 hours (40 °C) followed by incubation in 8 successive amplification buffers (AMP 1-8) for variable time periods at either 40 °C or room temperature (**Table 2.6**). Slides were also incubated with a positive control probe (Hs-*PPIB*-1 ZZ) targeting a common housekeeping gene and a bacterial gene-targeting negative control probe (*DapB*-1 ZZ) to assess background signal (< 1-2 foci per ~ 100 nuclei). All 40 °C incubations were performed within a humidified HybEZ™ II hybridisation oven. Sections were washed twice for 2 minutes in wash buffer between incubations. For signal detection, sections were then incubated in a 1:60 solution of BaseScope™ Fast Red-A : BaseScope™ Fast Red-B chromogen (120 µl per slide) for 10 minutes at room temperature and then rinsed in running tap water. Sections

were then nuclei counterstained in Mayer's haematoxylin (BDH) and mounted with DePeX mounting medium (Vector Laboratories).

Table 2.5 BaseScope assay pre-treatment steps for frozen and FFPE brain tissue

Step	Frozen specimens	FFPE specimens
Section preparation	Cryosectioned at 10 µm thickness onto Plus+Frost microslides (Solmedia).	Sectioned by microtome at 4 µm thickness.
Sample fixation	Fixed in pre-chilled (4 °C) 4 % paraformaldehyde (PFA).	Pre-fixed tissue in formalin at post-mortem (< 1 week).
Tissue dehydration	Slides incubated in increasing grades of ethanol, 50 %, 70 %, 2 x 100 % for 5 minutes each.	Deparaffinise in 2 x 5 minute xylene incubations followed by dehydration in 2 x 2 minute 100 % ethanol incubations.
Hydrogen peroxide	Create hydrophobic barrier with Immedge™ pen then add 3-4 drops of RNAscope® Hydrogen peroxide per slide for 10 minutes at room temperature.	Add 5-8 drops of RNAscope® Hydrogen peroxide to completely cover each slide for 10 minutes at room temperature.
Target retrieval	No target retrieval required.	Slides were transferred to a boiling solution of 0.1 M citrate buffer (pH 6.0) and pressure cooked at maximum pressure for 10 minutes.
Protease treatment	Add 3-4 drops of Protease IV to each section and incubate for 30 minutes at room temperature.	Add 3-4 drops of Protease IV to each section and incubate for 30 minutes at 40 °C.

Table 2.6 BaseScope™ amplification steps

Amplification	Conditions
AMP 1	30 minutes (40 °C)
AMP 2	30 minutes (40 °C)
AMP 3	15 minutes (40 °C)
AMP 4	30 minutes (40 °C)

AMP 5	30 minutes (40 °C)
AMP 6	15 minutes (40 °C)
AMP 7	45 minutes (room temperature)
AMP 8	15 minutes (room temperature)

2.1.10 BaseScope-Immunohistochemistry dual assay

BaseScope™ *in situ* hybridisation was performed on FFPE ALS tissue sections as previously described **2.1.9.** After sections were mounted (~1h), slides were scanned using an Olympus VS120 slide scanner at 20x magnification. Sections were then re-immersed in fresh xylene overnight to remove their coverslips in preparation for immunohistochemistry which was, again performed as previously described (**2.1.4)** using anti-TDP43 (mouse) antibody and inclusive of a second hydrogen peroxide and target retrieval steps. Washes with TBS-T were reduced to a minimum between steps in an attempt to preserve BaseScope™ signal.

2.1.11 Statistical analyses

All generated data plots and accompanying statistical analyses were conducted using Graphpad Prism software (v7.00 for Windows). In all cases, data sets were subjected to the D'Agostino-Pearson test for normal variance which in-turn guided the selection of further statistical tests for t-test comparisons and clinical data correlation purposes. In all statistical comparisons, a corresponding *p*-value of < 0.05 was considered statistically significant. The level of significance is demonstrated in figures as * for $p < 0.05$, ** for $p < 0.01$, *** for $p < 0.001$. Where appropriate, for all data-plots provided the corresponding statistical test, *n* value, *p* value and *r* value are detailed in the figure legend.

2.2 Molecular techniques

2.2.1 Results chapter relevance

The following molecular techniques were employed in the cloning steps required to generate the sgRNA-containing constructs that were used in the CRISPRi-mediated knockdown of hnRNP K in chapter 5.

2.2.2 Generation of sgRNA delivery constructs

HnRNP K and TDP-43 single guide RNA (sgRNA) delivery constructs were generated by subcloning the coding sequence for each sgRNA into the B3-CRISPRi-EF1a-BSD-T2A-mApple-NES (B3-CRISPRi) delivery vector. B3-CRISPRi was a gift from Dr Michael Ward, National Institute of Health generated as described in (Tian *et al.*, 2019). sgRNAs with the highest predicted target gene activity were selected from the latest hCRISPRi-v2 library (Horlbeck *et al.*, 2016).

B3-CRISPRi was digested with *BstXI and Blp1* in NEBuffer 2.1 overnight at 37°C to excise the 'control guide sequence'. Plasmid backbone fragments (2kb and 6.8kb) were isolated by gel extraction after agarose gel electrophoresis. Prior to ligation, complementary oligonucleotide sequences containing the sgRNA target sequences were diluted in DNase free water to a concentration of 300 ng / µl. Equal volumes of the equimolar oligonucleotides were mixed and incubated at 95 °C for 5 minutes prior to cooling to 25 °C over a 45 minute period. The annealed sgRNA inserts were then ligated into the linearised B3-CRISPRi construct in a 3-part ligation reaction of the short (2 kb) fragment : long (6.8 kb) fragment : sgRNA insert in a 1:2:7 ratio with T4 DNA ligase and T4 DNA Ligase Buffer at 16 °C overnight (**Figure 2.3**). To control for alternative ligation events, ligation mixtures of long fragment only (self-ligation) and long fragment + sgRNA insert (1:7) were also included. All enzymes and buffers were purchased from New England Biolabs.

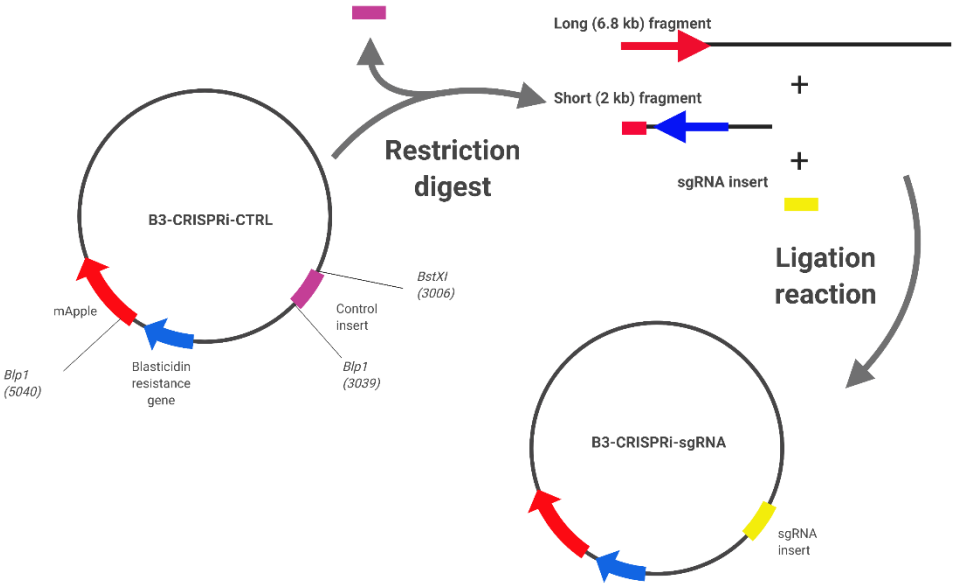

Figure 2.3. Schematic of sub-cloning a sgRNA insert into the CRISPRi-delivery vector.

2.2.3 Agarose gel electrophoresis

Gel electrophoresis was used to separate DNA fragments from resulting restriction enzyme digest reactions by size. A 1.0-1.5 % UltraPure™ Agarose solution was made in 100 ml of 1x tris-boric ethylenediaminetetraacetic acid (TBE) and microwaved (1-2 mins) until the agarose powder was completely dissolved. After a brief cooling period, the fluorescent nucleic acid dye GelRed® was added to a final concentration of 0.5 µg / ml. The agarose mixture was poured into a gel tray with a lane comb in place and allowed to set at room temperature for 30 minutes. Samples were diluted in 6x Gel Loading Dye, Purple (New England Biolabs). The gel was placed into the electrophoresis unit and fully immersed in 1X TBE. Samples were loaded into the agarose gel wells alongside a Quick-Load® Purple 1kb DNA ladder (New England) or HyperLadder™ IV (Bioline) for bands of interest up to 1 kb and > 1 kb respectively. The gels were run at 100-120 V for 1-1.5 hours until the dye-line was over half way down the gel. Bands were visualised with a Gel Dox XR™ system with integrated Quantity One® 1-D Analysis software (Bio-rad).

2.2.4 Gel extraction and purification

Desired DNA fragments were visualised using a UV transilluminator and excised with a sharp scalpel taking care to minimise inclusion of excess gel. Gel slices were placed into a labelled eppendorf tube and weighed. DNA was extracted using the QIAquick Gel extraction kit (Qiagen) according to manufacturer's instructions with the exception of an additional washing step. Briefly, gel slices were solubilised and transferred to a gravity-flow microcentrifuge QIAquick spin column with an integrated silica membrane to facilitate DNA adsorption. The membrane was washed with a series of ethanol-containing wash buffers and dried before a final elution of recovered DNA in 30 µl of warm (50 °C) double-distilled water (ddH_2O).

2.2.5 Preparation of LB agar plates

LB Agar was made by the addition of 1.5 g Agar powder (Sigma-Aldrich) to 100 ml of ddH_2O. The solution was sterilised by autoclaving (>121 °C, 20 psi) for 30 minutes ensuring the bottle was not airtight. After cooling to 40 °C, ampicillin antibiotic was added to the sterile mixture to a final concentration of 50 µg / ml under a flame. The agar was poured into plates (~ 20 ml / plate) and left at room temperature to solidify. Agar plates were stored at 4 °C until required.

2.2.6 Bacterial transformation

Aliquots of One Shot® TOP10 chemically competent *E.coli* (Thermo Fisher) were thawed on ice for 30 minutes. Approximately 100 ng of DNA from the overnight ligation mixtures was added to each *E.coli* aliquot which also included a positive (the original B3-CRISPRi plasmid) and negative (no DNA) control. Cells were incubated on ice for 30 minutes. Each transformation mixture underwent a heat shock (42 °C) for 30 seconds prior to being immediately returned to ice for 2 minutes. 250 µl of Super optimal broth with catabolite repression (SOC) medium was added to the transformation mixtures, which were then incubated at 37 °C, shaking (250 rpm) for 1 hour.

Under flame, each transformation mixture was poured into pre-warmed (37 °C) LB-Ampicillin plates and streaked evenly using an inoculation loop. The plates were dried in the near vicinity of the flame and then incubated overnight at 37 °C.

2.2.7 Preparation of LB broth

Luria-Broth (LB) was made by the addition of 2.5 g LB powder (Sigma-Aldrich) to 100 ml of ddH_2O and sterilised as before by autoclaving. The solution was sealed, left to cool and stored at room temperature until required. Ampicillin was added to LB immediately prior to use to a concentration of 50 µg / ml under flame.

2.2.8 Preparation of plasmid DNA from bacterial cultures

Single B3-CRISPRi-sgRNA transformed *E.coli* colonies were picked into 3 ml of LB-Amp under flame to generate liquid bacterial cultures and incubated (37 °C) whilst shaking for at least 6 hours until cloudy. Plasmid DNA was then isolated and purified using the QIAprep Spin Miniprep (Qiagen) according to manufacturer's instructions. Briefly, bacterial cells from 2 ml of the liquid cultures were lysed in an alkaline lysis solution and subsequently neutralised. After lysate clearing, the sample was transferred to a gravity-flow QIAquick microcentrifuge spin column with an integrated QIAprep silica membrane to facilitate DNA adsorption. The membrane was washed with a series of ethanol-containing wash buffers and dried before a final elution of plasmid DNA in 30 µl of warm (50 °C) ddH_2O.

Higher concentrations of plasmid stocks were prepared from remaining liquid bacterial cultures (1 ml) using an EndoFree Plasmid Maxi Kit (Qiagen) according to manufacturer's instructions. The process has an integrated bacterial endotoxin removal step during the cell lysis stage but is otherwise the same as the miniprep process with larger volumes of buffers. The silica membrane was washed with a series of ethanol-containing wash buffers and dried before a final elution of plasmid DNA in 200 µl of warm (50 °C) ddH_2O.

2.2.9 Bacterial glycerol stock preparation

Bacterial glycerol stocks were prepared for long-term storage of plasmid DNA. 1 ml stocks were made by resuspending 800 µl of bacterial liquid cultures in 200 µl of 100 % glycerol. Stocks were snap frozen and stored at - 80 °C until required.

2.2.10 DNA quantification

The concentration of DNA was measured at several different stages of the molecular cloning protocol including after agarose gel purification and bacterial plasmid isolation. The NanoDrop ND-1000 spectrophotometer (Thermo Fisher) was used to quantify DNA concentration by determining the absorbance at 260 nm. The purity was also indirectly determined using the 260 / 280 nm ratio. The spectrophotometer was calibrated with 1.5 µl of the eluent solution (ddH_2O) prior to sample measurements.

2.2.11 Colony screening by analytical digest

Liquid bacterial cultures of each picked colony were selected for plasmid Maxi-kit preparation if the intended ligation reaction was confirmed to have been successful. 3 µl of DNA from each mini-prep was enzymatically digested by *Blp1* in NEBuffer 2.1 at 37 °C for 1 hour and fragments were separated by gel electrophoresis as described previously. Plasmid DNA from samples which showed two distinctly separated bands at ~ 6.8 kb (long fragment) and 2 kb (short fragment) were considered to have successfully re-ligated with the intended sgRNA insert. Bands at these molecular weights are consistent with the predicted dual-site enzymatic activity of *Blp1.* Samples were run alongside a 100 ng / µl dilution of digested and undigested B3-CRISPRi as positive and negative control references (**Figure 2.4**).

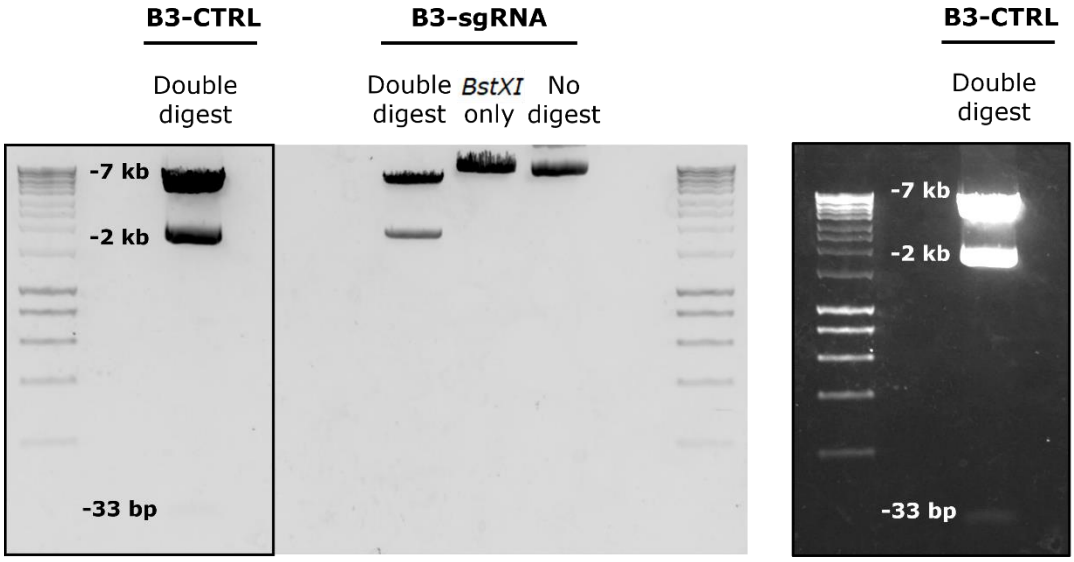

Figure 2.4. Analytical digest of B3-CRISPRi-sgRNA plasmid to confirm successful re-ligation. Electrophoretic gel of enzymatically digested plasmid samples. From left-to-right: Original B3-CTRL (positive) control sample + *Blp1* and *BstXI*, sub-cloned B3-sgRNA plasmid treated with *Blp1* and *BstXI*, *BstXI*-only or undigested respectively. On far right: cropped, inverted image of B3-CTRL double digest to highlight excised CTRL guide oligo at approximately 33 bp.

2.2.12 Plasmid sequencing

DNA Sanger sequencing of mini/maxi-preparations from selected colonies were performed by Source Bioscience for quality control purposes. Primers were designed for key regions of the plasmid sequence using Primer Basic local alignment search tool (Primer-Blast) software. Plasmid DNA and primers were diluted to 100 ng / µl and 3.2 pmol / µl respectively. Designed and stock (Source Bioscience) primers used for plasmid sequencing are listed in **Table 2.7**.

Table 2.7 Primers used for B3-CRISPRi-sgRNA construct sequencing

Primer	Primer sequence (5' to 3')
CMVF_pCDNA3	CAACGGGACTTTCCAAAATG
Insert_sequencing_fwd	CTCTCGGAGGGCGAAGAATC
Insert_sequencing_rev	TGCATGGCGGTAATACGGTT
mApple_up_rev	GGCCATGTTATTCTCCTCGC
mApple_down_fwd	TCGTGGAACAGTACGAACGC

2.3 iPSC cell culture, transduction and differentiation

2.3.1 Results chapter relevance

The iPSC methods described below are relevant to the CRISPRi-mediated knockdown of hnRNP K in neurons described in chapter 5.

2.3.2 Generation and characteristics of iPSC lines

CRISPRi-i^3 iPSCs were a kind gift of Dr Michael Ward (National Institute of Health) generated as previously described (Tian *et al.*, 2019). In brief, wild-type C11 (WTC11) iPSCs harbouring an AAVS1 safe harbour-integrated doxycycline-inducible mouse *NGN2* gene (termed i^3 iPSCs) was used as the parental iPSC line (Wang *et al.*, 2017; Fernandopulle *et al.*, 2018). iPSCs were co-transfected with the PC13N-dCas9-BFP-KRAB construct and TALENS for the robust expression of CRISPRi machinery from the CLYB1 safe harbour locus. BFP-positive cells were enriched by fluorescence-activated cell sorting (FACS) and individualised. Clones with successful, heterozygous integration of dCas9-BFP-KRAB was confirmed by PCR genotyping and cultured for further study.

2.3.3 Revival of cryopreserved iPSCs

Cryopreserved iPSCs were thawed rapidly in a 37 °C bead bath to limit exposure to Dimethyl sulfoxide (DMSO). Defrosted cells were then transferred to a centrifuge tube and resuspended in 1 ml DMEM / F12 prior to a 5-minute centrifugation step (300 g). The supernatant was removed and cells were resuspended in iPSC culture media (Essential 8™ Flex medium) supplemented with 10 µM Rho kinase (ROCK) inhibitor. Cells were transferred to one Geltrex™ coated well of a 6-well plate where they were grown and passaged for at least one week prior to lentiviral transduction.

2.3.4 Maintenance of iPSCs

CRISPRi-i^3 iPSCs were maintained on 6-well plates pre-coated with Geltrex™ reduced growth factor basement membrane matrix (Thermo Fisher) in Essential 8™ Flex medium (Thermo Fisher). Geltrex™ aliquots were thawed on ice at 4 °C overnight. Defrosted Geltrex™ was mixed by gentle pipetting and a half-culture volume was added to each well of a 6-well plate at a concentration of 150 µg / ml prior to overnight incubation at 37 °C. Revived cells were plated as previously described and incubated at 37 °C, 5 % CO_2 with daily exchange of Essential 8™ medium.

2.3.5 Passage of iPSC

iPSCs were passaged when cells reached approximately 70 % confluency, every 2-3 days. Culture medium was removed and cells were washed with PBS. Single cells were lifted by incubating with calcium-chelating agent ethylenediaminetetraacetic acid (EDTA, 0.5 mM in PBS) for 5 minutes at 37 °C. EDTA was removed taking care to avoid aspirating cell colonies. Remaining colonies were lightly resuspended in 1 ml Essential 8™ medium and sub-divided in fresh iPSC culture media between new Geltrex™ coated plates according to the desired splitting ratio (1:6 - 1:12 for 6-well plates).

2.3.6 Cryopreservation of iPSC

Serial vials of iPSCs were cryopreserved to minimise genetic drift associated with repeated passaging. iPSCs were prepared as for an accutase (0.5 mM) split (37 °C, 5 mins) and dissociated cells were resuspended in 1 ml of cryopreservation medium (90 % Essential 8™ medium, 10 % DMSO) supplemented with RevitaCell (Thermo Fisher A2644501) supplement (1:100). Cryopreservation cell solutions were transferred into a 1.5 ml cryovial which was then placed into a Mr. Frosty isopropanol caddy for gradual cooling (1 °C / minute) at -80 °C overnight. Frozen cryovials were transferred into liquid nitrogen for long-term storage.

2.3.7 Production of lentiviruses

Lenti-X™ 293T cells (Takara Bio) were revived and cultured in Dulbecco Modified Eagle Medium (DMEM) supplemented with 10 % fetal bovine serum (FBS, Labtech international) and 1:100 GlutaMAX (Thermo Fisher) at 37 °C, 5 % CO_2. Cells were passaged 1:2 and seeded into a T175 flask at ~50 % confluency.

Lenti-X™ 293T cells were co-transfected the following day with lentiviral transfer vector (14.1 µg), psPAX2 packaging vector (9.36 µg) and pVSV-G enveloping ratio (14.1 µg) in the ratio of 1.5: 1: 1.5 using Lipofectamine 3000 (60 µl, Thermo Fisher) and P3000TM enhancer reagent (75 µl, Thermo Fisher) in Opti-MEM™. Mixtures of plasmid-P3000TM and Lipofectamine 3000 were prepared in Opti-MEM separately and combined by drop-wise addition after a 15 minute incubation period at room temperature. Media was collected and stored at 4 °C at 48 h and 72 h post-transfection. All media was combined and centrifuged at 300 g for 10 minutes to remove cell debris.

2.3.8 iPSC lentiviral transduction

CRISPRi-i^3 iPSCs from each well of a 6-well plate were single-cell dissociated with 0.5 ml accutase (37 °C, 5 mins) and resuspended in 4.5 ml PBS, 1.5 ml Essential 8™ medium. The cell suspension was centrifuged at 300 g (5 mins) and the cell pellet was thoroughly resuspended in fresh Essential 8™ Flex medium with RevitaCell supplement (1:100). Dissociated cells were seeded at an approximate density of 250-300,000 iPSCs per Geltrex™ coated well of a 6-well plate. After 2 hours, half of the media from each well was replaced with viral supernatant and DEAE Dextran sulfate (final concentration 10 µg ml, Sigma Aldrich) to enhance transduction efficiency. The virus was removed at 24 h, replaced with fresh Essential 8™ Flex medium / RevitaCell and confirmation of mApple-expressing (CRISPRi-sgRNA construct) cells was performed by immunofluorescence in the red channel using the IncuCyte® live cell analysis system (Sartorius) at 48 hours post-transduction. Transduction efficiency was ~ 90 % for all constructs without further enrichment.

2.3.9 Induced neuronal differentiation

Neural induction was performed immediately upon removal of virus at 24-hours post-transduction. Cells were washed once with PBS and replaced with neuronal induction medium (**Table 2.8**) spiked with doxycycline (1:1000, 2 µg / ml) and RevitaCell (1:100). Full media changes were performed with fresh induction media and doxycycline at 24-hours (day 1) and 48-hours (day 2) post-induction. On day 3, in preparation for final plating cells were washed once more in PBS, detached with accutase (3 mins, 37 °C) and re-suspended in 8 ml PBS + 2 ml Essential 8™ medium. The cell suspension was centrifuged at 300 g (5 mins) and the cell pellet was re-suspended in cortical neuron culture medium (CNCM) (**Table 2.9**)**.** CNCM ~50 ml aliquots were made up and used within 2 weeks. Cells were seeded onto pre-Poly-L-Ornithine (100 µg / ml) and Laminin (1:1000 in DMEM) coated plates at a density of 1.5 – 2 x 10^6 per well of a 6-well plate.

Table 2.8 Composition of neuronal induction medium (500 ml)

Reagent	Volume (ml)
DMEM / F-12 GlutaMAX™ supplement (Gibco 10565018)	495
N-2 Supplement 100x (Gibxo 17502048)	2.5
MEM Non-Essential amino acids solution 100X (Gibco 11140050)	2.5

Table 2.9 Composition of cortical neuron culture medium (~50 ml)

Reagent	Volume
BrainPhys™ (StemCell Technologies)	50 ml
N2 supplement (Thermo 17502048)	0.5 ml
B-27 Supplement 50x, serum free (Thermo 17504044)	1 ml
BDNF 100 µg / ml (Peprotech 450-02)	1 µg in 10 µl

GDNF 100 µg / ml (Peprotech 450-10)	1 µg in 10 µl
Ascorbic Acid 1 mM (Sigma-Aldrich A0278)	10 µl
Dibutyrl cAMP 1M (Sigma-Aldrich D0627)	50 µl
Laminin 1 mg / ml (Thermo 23017015)	0.5 ml

2.3.10 Maintenance of CRISPRi-i^3 neurons

Half medium changes were performed on differentiating CRISPRi-i^3 neurons twice weekly with fresh CNCM until harvest at day 10. Phase contrast microscopy was used to demonstrate normal neuronal morphology including the presence of dendritic spines from day 7.

2.3.11 Immunocytochemistry

One day prior to staining, 5 x 10^4 cells were seeded onto each well of a Geltrex-coated chamber slide or coverslip. The following day, cells were washed once in PBS and fixed with 4 % paraformaldehyde (PFA) at room temperature. Blocking buffer was prepared using 4 % Bovine Serum Albumin (BSA) in PBS with 3 % Triton-X whilst washing buffer consisted of 0.3 % Triton-X in PBS. After a single PBS wash, cells were incubated in blocking buffer for one hour at room temperature. Cells were then incubated with primary hnRNP K antibody (Abcam, Ab23644) appropriately diluted (1:1000) in 4 % BSA in PBS overnight at 4 °C. After three washes with washing buffer, appropriately diluted secondary antibody (also within 4 % BSA-PBS) was applied to the cells for 1 hour at room temperature in darkness. Following a final three washes, cells were mounted with ProLong™ Gold Antifade Mountant with DAPI (Thermo Fisher Scientific) and imaged with a ZEISS LSM 880 confocal microscope.

2.3.12 Immunoblotting of CRISPRi- i^3 neurons

CRISPRi-i^3 iPSCs and neurons harvested from several different stages were pelleted for RNA and protein extraction. For protein extraction, cells were lysed in 200 µl lysis buffer (Pierce® RIPA buffer, 2 % SDS) supplemented with a PhosSTOP EASYpack phosphatase inhibitor cocktail tablet (Roche®) for 5 – 10 minutes. A cell scraper was used to collect lysed cells into an Eppendorf tube on ice. Samples were places onto an orbital shaker for 1 hour and centrifuged at 17,000 g (4 °C) for 20 minutes. The supernatant was transferred into a new, pre-chilled tube and stored at -20 °C until use. BCA analysis and western blotting was performed as before (**2.1.7**)**.**

Alternatively, protein lysates were also extracted from Qiazol-lysed cells by performing acetone precipitation from Buffer RLT lysates (Qiagen supplementary protocol). RLT cell lysate flow-through is collected from the RNeasy spin column, added to 4 volumes of ice-cold acetone and left on ice for 30 minutes. Samples were then centrifuged 17,000 g (4 °C) for 10 minutes and the supernatants were then carefully discarded. Pellets were briefly air dried, washed in 100 µl of ice-cold ethanol and allowed to dry again. The washed pellet was then resuspended in 200 µl lysis buffer.

2.3.13 RNA purification and RT-qPCR

For RNA extraction, cells were lysed in 700 µl of Qiazol lysis buffer. Lysate RNA was purified and quantified by RT-qPCR as in **2.1.8** with the same primers (**Table 2.2**) and thermal profile (**Table 2.3**). An aliquot was also taken for later RNA-seq analysis.

2.4 RNA-sequencing and analysis

2.4.1 Results chapter relevance

The RNA-sequencing analyses described later in this section are relevant to both chapter 5 (differential expression analysis) and chapter 6 (differential splicing analysis).

2.4.2 Statement of contribution

RNA-sequencing (**2.4.4**) was performed by UCL Genomics at the Zayed Centre for Research into Rare Disease in Children. The RNA-sequencing analyses to be described in this section (from **2.4.5** to **2.4.8**) were performed by collaborator Dr Jack Humphrey (Icahn School of Medicine at Mount Sinai, New York).

2.4.3 Sample preparation

As described previously, CRISPRi-i^3 neurons were harvested at day 10 (n = 4, control; n = 4 hnRNP K KD) and RNA was extracted and recovered in RNase-free water (50 µl) using a Qiagen miRNA Mini Kit (Qiagen 217004) following manufacturer's instructions as detailed in **2.3.13.** The concentration and purity (260/280nm absorbance) of the eluted RNA was preliminarily measured using a Nanodrop spectrophotometer. Samples were then sent to UCL genomics for RNA TapeStation quality control, library preparation and sequencing. Obtained RNA integrity numbers (RIN) ranged from 8.9-9.5 indicating sufficiently high RNA quality for sequencing.

2.4.4 RNA-sequencing

Library preparation was performed using a KAPA RNA HyperPrep kit with RiboErase (HMR) (Roche®). In brief, samples were first subjected to ribosomal RNA (rRNA) depletion by hybridisation of complementary DNA oligonucleotides. Any remaining rRNA-DNA duplexed rRNA was removed

using RNase H and DNase treatment. mRNA was then fragmented randomly using heat and magnesium to a mean length of 200 bp. First strand cDNA was synthesised using random hexamer priming. Subsequent second strand synthesis and A-tailing steps were performed concurrently to convert the cDNA:RNA hybrid to double stranded cDNA (dscDNA). During which, dUTP is incorporated into the second cDNA strand for stranded RNA sequencing and dAMP was added to the 3' end of resulting dscDNA. Specialised dsDNA adapters with 3' dTMP overhangs were then ligated to library insert fragments. Finally, the library was prepared by amplifying library fragments using high fidelity, low-bias PCR and purification of PCR products by KAPA Pure Beads for reaction cleanup. The dUTP-marked strand is not amplified, enabling strand-specific sequencing. Paired-end 150 bp reads were sequenced on an Illumina NextSeq 2000 P2 (300 cycles) machine.

2.4.5 Data pre-processing and alignment

150 bp paired-end reads were chosen to maximise the splicing information, but with small fragments lead to reading through into the sequencing adapters, which reduce the ability of the alignment algorithm to map the reads to the genome. Therefore, reads containing non-aligning adapter sequences were trimmed using Trimmomatic, which recognises the standard Illumina TruSeq adapter sequences and removes them from the reads (v0.40) (Bolger, Lohse and Usadel, 2014).

All samples were aligned to the GRCh38 genome built using STAR (v2.7.2) (Dobin *et al.*, 2013) with GENCODE v30 (Frankish *et al.*, 2019) as the transcript reference. The mean alignment rate of uniquely mapped reads was 89 % (~100 million uniquely mapped reads).

2.4.6 Differential gene expression analysis

Gene expression was quantified using RSEM (v1.3.1) (Li and Dewey, 2011) using gene models from GENCODE v30, which generated both total read counts per gene per sample as well as transcripts per million (TPM) values,

which account for gene length and per-sample library size. Lowly expressed genes, defined as those with a mean TPM < 1, were removed, leaving 20,347 genes for downstream analysis.

Principal component analysis (PCA) was then performed on the TPM values for the 20,347 genes. The first principal component, explaining 22.7 % of variance, separated hnRNPK KD samples from controls.

Differential expression was performed on all samples using the standard DESeq2 (Love, Huber and Anders, 2014) workflow. The model *expression ~ condition* was fitted to each gene to explore the effect of knockdown. The resulting $\log_2$ fold change effect size estimates were shrunk using apeglm fold-change shrinkage (Zhu, Ibrahim and Love, 2019). Gene counts were normalised using DESeq2's median of ratios which controls for sequencing depth and RNA composition. Genes were considered differentially expressed at a Benjamini-Hochberg false discovery rate (FDR) < 0.05. 209 genes were differentially expressed, with only 10 genes having an absolute log2FoldChange > 1, equivalent to a doubling or halving of expression.

Gene Ontology (GO) enrichment analysis was performed using the gprofiler2 package (Kolberg *et al.*, 2020) to identify significant pathways enriched within the differentially expressed gene populations, split into two groups of upregulated and downregulated in response to knockdown. A Bonferroni-adjusted $p < 0.05$ cut-off was employed as a threshold for significant enrichment. Only terms with at least 5 intersecting genes were kept.

2.4.7 Differential splicing analysis

Differential splicing was assessed using LeafCutter (Y. I. Li *et al.*, 2018), a tool used to identify and quantify novel and previously annotated alternative splicing events from short-read RNA-seq data by clustering overlapping splice junction reads and comparing their relative contributions between treatment groups. In brief, splice junction reads were extracted from each alignment file using Regtools (Feng *et al.*, 2018). Intron junctions were clustered together with the following imposed constraints: proportional contribution to cluster ≥ 0,

read contribution to cluster ≥ 60, intron length ≤ 200,000 bp. LeafCutter utilises a Dirichlet-multinomial generalised linear model to determine differences in intron usage across an entire cluster between control and hnRNP K KD derived RNA samples. A total of 1,090 (significant) clusters were found to be differentially spliced (FDR < 0.05).

A custom script (code availability at (Bampton *et al.*, 2021)) was used to specifically identify novel cassette exons. A cluster was annotated as a cassette exon if it met the parameters of containing three splice junctions in the correct orientation with two junctions flanking a central exon (inclusion junctions) and the third spanning the length of the cluster (exclusion or skipping junction). The exon length was capped at 250 bp.

The script also determined whether or not either junction(s) had been previously annotated in GENCODE (v30). A total of 364 differentially spliced clusters were subsequently classified as cassette exons.

The percent spliced in (PSI %) of each cassette exon in each sample was calculated by dividing the average read count of the two inclusion junctions by the read count of the skipping junction. The directionality (±) or delta PSI (dPSI) associated with each event was then calculated by subtracting the mean PSI of each cassette exon in the hnRNP K KD group from the corresponding mean PSI of the control group. Cassette exons were considered significantly spliced between groups if they exceeded a threshold of ± 10 % dPSI, which was met by 126 exons.

61 cassette exons had a dPSI > 10 % and 65 had a dPSI < -10 %. Cryptic exons (CEs) were defined both by annotation and by effect size, as unannotated (novel) junctions with PSI < 10 % in control samples and a dPSI > 10 % between groups. Conversely skiptic exons (SEs) were defined as previously unannotated (novel) junctions with PSI > 90 % in controls and a dPSI < - 10 %. Using these parameters, a total of 8 cassette exons met criteria for classification as CEs and 24 met criteria for classification as SEs. To identify genes that exhibited both differential expression and differential splicing, the two result tables were joined on a shared gene name. 14 splicing

events in 13 genes met both criteria of being differentially expressed (FDR < 0.05) and differentially spliced (FDR < 0.05). Of the 13 genes, 9 were upregulated and 4 were downregulated.

2.4.8 Figure and dataplot production

Data plots of RNA-seq data were generated in R v4.0.4 by Dr Jack Humphrey.

2.4.9 Three-primer PCR

Molecular validation of selected CRISPRi-i^3 neuron hnRNP K KD-associated cryptic and skiptic exons was performed using a three-primer (nested) PCR. As with RT-qPCR, cDNA was synthesised from CRISPRi-i^3 neuron-derived RNA using SuperScript IV VILO Master Mix with ezDNase enzyme step (Thermo Fisher). Cryptic and skiptic exons in predicted targets of hnRNP K were amplified using primer pairs that flank the cryptic/skiptic exon, as well as a third primer which spans the cryptic/skiptic exon. Primer sequences are presented in **Table 2.10**. PCR for all splicing events was conducted using 2x GoTaq PCR Master Mix (Promega) using the following touchdown thermal cycling conditions 95 °C for 5 min, (95 °C for 30 s, 75 °C for 45 s (− 1 °C per cycle), 72 °C for 1 min) × 15 cycles, (95 °C for 30 s, 60 °C for 45 s, 72 °C for 1 min) × 20 cycles, 72 °C for 5 min.

Table 2.10. Primers used in three-primer PCR validation of cryptic and skiptic exons.

Primer	Primer sequence (5' to 3')
Cryptic exons (CEs)	
HMBOX1 (Flank fwd)	CCCAGATGAAGCAAAGAGGG
HMBOX1 (Flank rev)	CTCCTGGACTCTGCACATCT
HMBOX1 (CE spanning)	AAAGCAGGTTTGTTAGGGCC
CACTIN (Flank fwd)	GTCCCGGATGCGGATCTT
CACTIN (Flank rev)	GTGGCTGATCCCCTTCTTCT
CACTIN (CE spanning)	AGGAGGAGGAGGAGGCATAA
TMEM132A (Flank fwd)	CTCACCGACACCACCCTC
TMEM132A (Flank rev)	GGATGGAGTCAGACAGTGGG
TMEM132A (CE spanning)	AGGGCCTGGAAGCTAGATTC
Skiptic exons (SEs)	
ABCB6 (Flank fwd)	CGTCTTCCTCAAGTTCCTCC
ABCB6 (Flank rev)	CCAATGATGATGTCGGCCAG
ABCB6 (SE spanning)	CTTCCTGTGGATCCGGGTG
WDR11 (Flank fwd)	ATGGAGCTGAAGTGTGGGAT
WDR11 (Flank rev)	GGAACAAGGAGATAGGGGCA
WDR11 (SE spanning)	TCTTGGCCTCAGATGATGGG

PCR products were electrophoresed and visualised on agarose gels with SybrSafe (Thermo Fisher) and then, using D1000 ScreenTape and reagents (Agilent), were also visualised on the 2200 Tapestation system (Agilent). 1 µl

of cDNA was mixed with 3 µl of D1000 (4x) sample buffer per reaction chamber.

Chapter 3 HnRNP K mislocalisation in pyramidal neurons of the frontal cortex

3.1 Introduction

3.1.1 Publication statement

The contents of this chapter have been previously published open access (Bampton *et al.*, 2021) and are included here in an adapted form as per the publisher's (Springer) policy on open access publication.

3.1.2 Statement of contribution

The author performed all the experimental work and analyses for this section except the development of the supervised machine learning algorithm for detection of normally stained hnRNP K neurons which was developed by collaborator Dr Dipanjan Bhattacharya (IFOM) as credited in-text.

3.1.3 Background

Abnormal expression and mislocalisation of hnRNP K to the cytoplasm has been observed and studied in the pathology of several malignancies (Barboro, Ferrari and Balbi, 2014; Gallardo *et al.*, 2016). However, prior to this body of work, hnRNP K was a protein not commonly associated with neurodegenerative disease. The first pathological observations of hnRNP K mislocalisation in the patient brain was observed during an unrelated project. An immunohistochemical screen of hnRNP proteins that may be potentially colocalising with FTLD inclusions was undertaken. Indeed, the lab had discovered several such hnRNPs that were found to co-deposit with FUS (hnRNP R and Q) and TDP-43 (hnRNP E2) immunoreactive inclusions (Gami-Patel *et al.*, 2016; Davidson *et al.*, 2017; Gittings *et al.*, 2019). By contrast, during a routine immunohistochemical staining of hnRNP K, it was noted that whilst there appeared to be no visible evidence for hnRNP K

accumulation in FTLD pathological inclusions, its staining profile in pyramidal neurons was strikingly abnormal. This prompted a pathological investigation into the neuronal localisation profile of hnRNP K in FTLD and control brain.

3.2 Methods

3.2.1 Cohort

All brains were donated to the Queen Square Brain Bank (QSBB) for neurological disorders (UCL Queen Square Institute of Neurology) and the Medical Research Council (MRC) Edinburgh Brain & Tissue Bank. All brains were processed, and tissue was sectioned as previously described (**2.1.3**). The cohort (n = 94) included pathologically diagnosed cases of FTLD-TDP A (n = 28), FTLD-TDP B (n = 3), FTLD-TDP C (n = 12), FTLD-TDP D (n = 2), FTLD-tau (n = 5), FTLD-ni (n = 2), ALS (n = 7) and neurologically normal controls (n = 35) (**Table 3.1**). This included 24 familial FTLD cases including individuals harbouring genetic mutations in *C9ORF72* (n = 14), *GRN* (n = 4), *MAPT* (n = 4), *TBK1* (n = 2) and *VCP* (n = 1) genes and 2 familial (*C9ORF72*) ALS cases.

Table 3.1 Cohort and clinical demographics

No.	Path. diagnosis	AAO	AAD	Sex	Brain weight (g)	Mutations	PM delay (h)
1	FTLD-TDP A	64	73	M	1252	*C9ORF72*	61.1
2	FTLD-TDP A	51	61	M	1065	-	35.3
3	FTLD-TDP A	59	65	M	1176	*C9ORF72*	30.0
4	FTLD-TDP A	66	72	M	1274	-	68.2
5	FTLD-TDP A	57	60	M	1673	-	40.4
6	FTLD-TDP A	58	66	F	850	*C9ORF72*	107.1
7	FTLD-TDP A	75	79	M	-	-	10.0
8	FTLD-TDP A	52	58	M	1303	*C9ORF72*	49.8
9	FTLD-TDP A	47	53	M	1390	-	33.7
10	FTLD-TDP A	53	63	M	955	*C9ORF72*	77.3
11	FTLD-TDP A	62	68	F	-	*GRN* (Q130fs)	99.8
12	FTLD-TDP A	67	69	M	1398	-	62.5
13	FTLD-TDP A	75	79	F	1119	-	36.3
14	FTLD-TDP A	83	87	F	1226	-	68.9
15	FTLD-TDP A	57	62	M	-	-	92.9
16	FTLD-TDP A	62	72	M	1320	*TBK1*	97.4
17	FTLD-TDP A	57	63	F	851	-	85.3
18	FTLD-TDP A	57	62	F	981	*C9ORF72*	63.1
19	FTLD-TDP A	53	61	M	994	*GRN* (C31fs)	72.6
20	FTLD-TDP A	58	67	F	1000	*GRN* + *C9ORF72*	115.0
21	FTLD-TDP A	62	68	M	1371	*C9ORF72*	99.0
22	FTLD-TDP A	43	45	M	1015	*C9ORF72*	25.9
23	FTLD-TDP A	56	67	F	789	*C9ORF72*	85.6
24	FTLD-TDP A	59	71	F	1014	*TBK1*	76.0
25	FTLD-TDP A	49	55	M	974	*GRN* (C31fs)	29.3
26	FTLD-TDP A	66	74	F	782	*C9ORF72*	85.8
27	FTLD-TDP A	54	60	M	1350	*C9ORF72*	32.3
28	FTLD-TDP A	66	71	M	1431	*C9ORF72*	51.9
FTLD-TDP A summary (*n* = 28)		59.6	66.1	18(M) :10(F)	1142	-	64.0
29	FTLD-TDP B	63	67	F	1232	-	45.5
30	FTLD-TDP B	67	69	M	1300	-	70.2
31	FTLD-TDP B	63	83	F	970	-	45.1
FTLD-TDP B summary (*n* = 3)		64.3	73.0	1(M): 2(F)	1167	-	53.6
32	FTLD-TDP C	52	65	F	899	-	27.7
33	FTLD-TDP C	64	66	F	1186	*C9ORF72*	94.1
34	FTLD-TDP C	73	83	M	1167	-	59.8

35	FTLD-TDP C	58	72	F	972	-	31.2
36	FTLD-TDP C	67	76	M	1086	-	39.5
37	FTLD-TDP C	58	73	F	976	-	37.9
38	FTLD-TDP C	59	73	F	936	-	83.7
39	FTLD-TDP C	64	78	M	1110	-	26.8
40	FTLD-TDP C	64	74	M	1230	-	19.0
41	FTLD-TDP C	50	65	M	1057	-	51.8
42	FTLD-TDP C	61	66	M	1117	-	70.8
43	FTLD-TDP C	77	80	F	1502	-	26.3
FTLD-TDP C summary (*n* = 12)		62.3	72.6	6(M): M6(F)	1103	-	47.4
44	FTLD-TDP D	-	48	F	1210	*VCP*	53.5
45	FTLD-TDP D	53	71	M	1363	-	54.1
FTLD-TDP D summary (*n* = 2)		53.0	59.5	1(M): 1(F)	1287	-	53.8
46	FTLD-tau	55	66	M	1208	*MAPT* (R406W)	60.8
47	FTLD-tau	54	58	M	1225	-	78.3
48	FTLD-tau	59	66	M	1399	*MAPT* (10+16)	58.2
49	FTLD-tau	68	74	M	1048	*MAPT* (K280del)	125.0
50	FTLD-tau	45	51	M	1046	*MAPT* (10+16)	52.6
FTLD-tau summary (*n* = 5)		56.2	63.0	5(M): 0(F	1185	-	75.0
51	FTLD-ni	48	54	F	1106	-	106.3
52	FTLD-ni	50	57	M	1444	-	44.0
FTLD-ni summary (*n* = 2)		49.0	55.5	1(M): 1(F)	1275	-	75.2
53	ALS	55	59	M	875	-	36.0
54	ALS	63	66	F	1316	-	66.0
55	ALS	58	63	F	1228	*C9ORF72*	66.5
56	ALS	40	53	F	1226	-	42.3
57	ALS	77	80	F	1086	-	5.0
58	ALS	80	84	M	1453	-	56.3
59	ALS	74	76	M	1138	*C9ORF72*	26.4
ALS summary (*n* = 7)		63.9	68.7	3(M): 4(F)	1189	-	42.6
60	Control	-	69	M	1435	-	171.0
61	Control	-	67	M	1350	-	2.5
62	Control	-	73	F	1214	-	24.0
63	Control	-	88	M	1077	-	16.3
64	Control	-	79	F	1288	-	88.8
65	Control	-	86	F	1234	-	120.0
66	Control	-	93	F	1128	-	29.7
67	Control	-	83	F	1263	-	99.0

68	Control	-	68	F	1330	-	45.1
69	Control	-	70	M	1544	-	53.5
70	Control	-	92	M	1213	-	46.3
71	Control	-	96	F	1032	-	60.0
72	Control	-	91	F	1130	-	71.8
73	Control	-	84	F	-	-	40.6
74	Control	-	80	M	-	-	11.5
75	Control	-	83	M	1244	-	105.5
76	Control	-	94	F	-	-	27.0
77	Control	-	29	M	1590	-	44.0
78	Control	-	25	M	1640	-	53.0
79	Control	-	30	M	1670	-	71.0
80	Control	-	25	M	1500	-	81.0
81	Control	-	28	M	1330	-	38.0
82	Control	-	34	M	1530	-	99.0
83	Control	-	39	M	1360	-	76.0
84	Control	-	37	F	1360	-	126.0
85	Control	-	39	M	1470	-	86.0
86	Control	-	46	M	1380	-	76.0
87	Control	-	46	F	1400	-	99.0
88	Control	-	48	M	1480	-	58.0
89	Control	-	50	M	1350	-	122.0
90	Control	-	57	M	1600	-	70.0
91	Control	-	58	M	1650	-	96.0
92	Control	-	53	F	1420	-	107.0
93	Control	-	57	F	1320	-	73.0
94	Control	-	51	M	1460	-	52.0
Control (*n* = 35)		-	61.4	21(M) :14(F)	1375		69.7

AAD, Age at death; AAO, Age at onset; ALS, Amyotrophic lateral sclerosis; FTLD, Frontotemporal lobar degeneration; PM, Post-mortem. Mutations: *C9ORF72* Chromosome 9 open reading frame 72, *GRN* Progranulin, *MAPT* microtubule-associated protein tau, *TBK1* TANK-binding kinase 1, *VCP* Valosin-containing protein. Adapted from (Bampton *et al.*, 2021).

3.2.2 Immunohistochemistry and quantitative pathological assessment with deep learning

Frontal cortex brain sections from all cases (*n* = 94) were immunohistochemically stained with anti-hnRNP K antibody (Bio-rad MCA2622 / Abcam Ab23644) as previously described (**2.1.4**). A quantitative immunohistochemical analysis of hnRNP K pathology in FTLD/ALS and

control frontal cortex was then performed on all cases. The sections were scanned using an Olympus VS120 slide scanner at 20x magnification. The region of interest (ROI) was digitally marked, cropped and extracted using the Olympus VS desktop software to minimise file size. Extractions were consistently performed in the upper, grey matter region of the second frontal gyrus. Extracted ROI images were launched in ImageJ (v1.41) and a macro was used to generate the maximum number of random, non-overlapping, 1000 x 1000 pixel of 0.345 mm^2 sized sample images (< 300) from each ROI. Across the cohort, the mean number of images analysed was 129 or 44.5 mm^2 of analysed tissue per ROI.

Neurons with normal hnRNP K staining, as defined by a predominantly nuclear localisation of the protein, were detected and quantified by a supervised machine learning algorithm as developed by Dr Dipanjan Bhattacharya (IFOM). A MATLAB-based program was used to generate the training datasets, which consisted of 250 images of frontal cortex neurons from different brain samples. AlexNet convolutional neural network with Adam optimizer (https://emcslabs.github.io/machinelearning/AdamOptimizer) was used for training of the datasets and which utilised a region-based convolutional neural network for identification of normally stained neurons. A manual estimation of the algorithm's accuracy found the detection rate to be consistently above 80 % with minimal false-positives. An equivalent algorithm for abnormal hnRNP K-stained neurons was not feasible due to both the heterogeneity of hnRNP K mislocalisation and the varied signal intensity between cases, neither of which are conducive to supervised machine learning training.

Neurons with abnormal hnRNP K pathology, as defined by nuclear clearance of hnRNP K and its subsequent mislocalisation to the cytoplasm, were counted manually within each randomly generated image in a blinded fashion. The total degree of hnRNP K mislocalisation in each case was given as the proportion (%) of all images with at least 1 abnormal neuron counted or the average number of abnormal neurons per mm^2 of tissue analysed. A schematic of the analytical pipeline is shown in **Figure 3.1**.

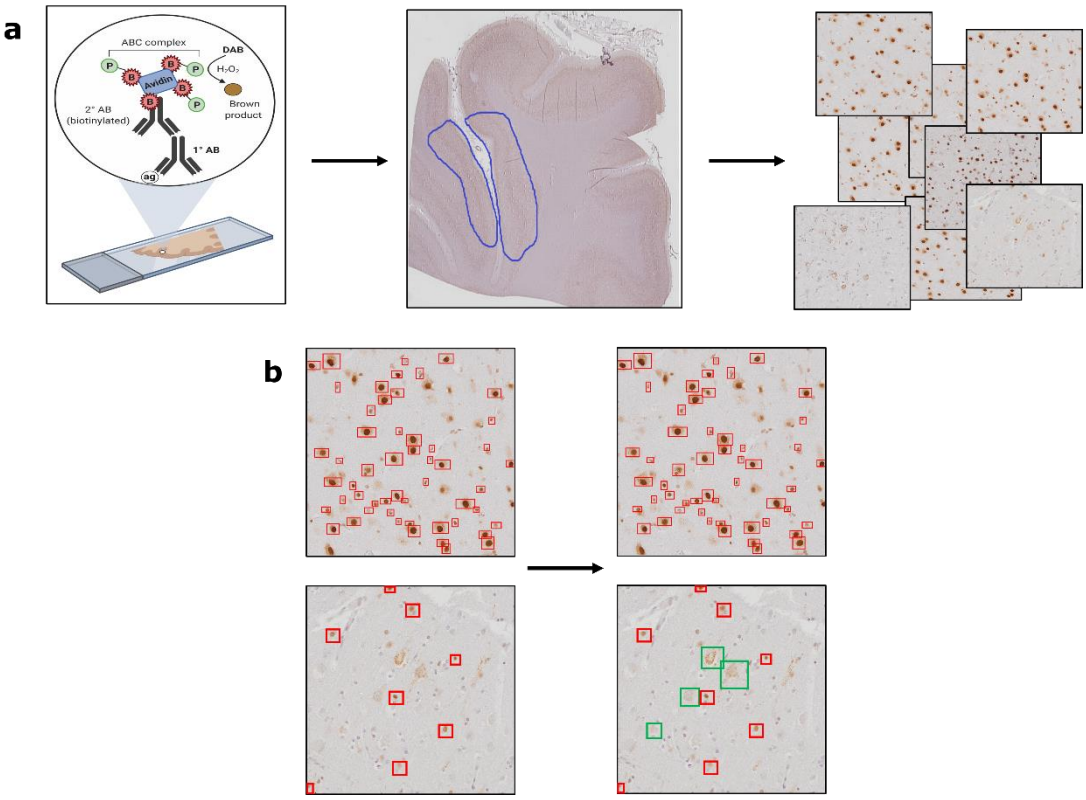

Figure 3.1 Workflow schematic of hnRNP K pathology quantitation in cortex. (a) Frontal sections are immunohistochemically stained with anti-hnRNP K antibodies and then scanned and digitised at 20x magnification. Randomly generated 1000 x 1000 px images (< 300) were sampled from an extracted region of interest (blue outline) within the grey matter region of the second frontal gyrus. (b) Matched sample images were then subjected to a two-step analysis procedure to detect and quantify normally stained neurons (in red boxes, automated algorithmic pipeline) and then abnormally stained neurons (green boxes).

3.2.3 Immunofluorescence

Double-label immunofluorescence was performed as described earlier in **2.1.5** to assess the spatial relationship between hnRNP K and FTLD inclusions as well as hnRNP K and other organelle markers as listed in **Table 2.1.**

3.2.4 Western blot and RT-qPCR on brain tissue

Frozen brain tissue samples from the frontal cortex of selected cases were homogenised using a Precellys® Tissue homogenising CKMix kit as described in **2.1.6**. Homogenised samples were then prepared for western blotting (**2.1.7**) or RT-qPCR (**2.1.8**) (**Table 2.2**, **Table 2.3**) to quantify protein and mRNA levels

of hnRNP K respectively within bulk brain tissue of cases pre-identified as exhibitong predominantly normal or mislocalised / abnormal hnRNP K staining profiles.

3.3 Results

3.3.1 HnRNP K mislocalisation in the frontal cortex

Immunohistochemical staining of hnRNP K in the frontal cortex revealed two strikingly different localisation profiles of the protein between neurons belonging to different cortical layers in some patient brains. Within the most superficial (layers I-II) cortical layers, neurons displayed a predominantly nuclear localisation of hnRNP K. Staining intensity was strongest in the nucleus in these neurons whilst perinuclear and cytoplasmic staining was much weaker. Since hnRNP K is a typically nuclear localised protein in normal (non-cancerous) tissues, this staining profile was classified as ‘normal’. Neurons within these layers exhibited almost exclusively ‘normal’ hnRNP K staining profiles irrespective of disease (FTLD) or control status (**Figure 3.2 a**). By contrast, the larger pyramidal neurons of layers III and V revealed a remarkedly different staining pattern in many FTLD cases compared to age-matched controls. In control brains, hnRNP K staining within pyramidal neurons resembled that of the more superficial layers – predominantly localised to the nucleus with only weak cytoplasmic staining. However, many FTLD brains exhibited vast regions of abnormal hnRNP K (mis)localisation typified by almost complete depletion of nuclear hnRNP K and a concurrent punctate accumulation of the protein in the surrounding cytoplasm that also extended into the neurites (**Figure 3.2b**). This abnormal staining pattern of hnRNP K was believed to be a novel neuropathological event.

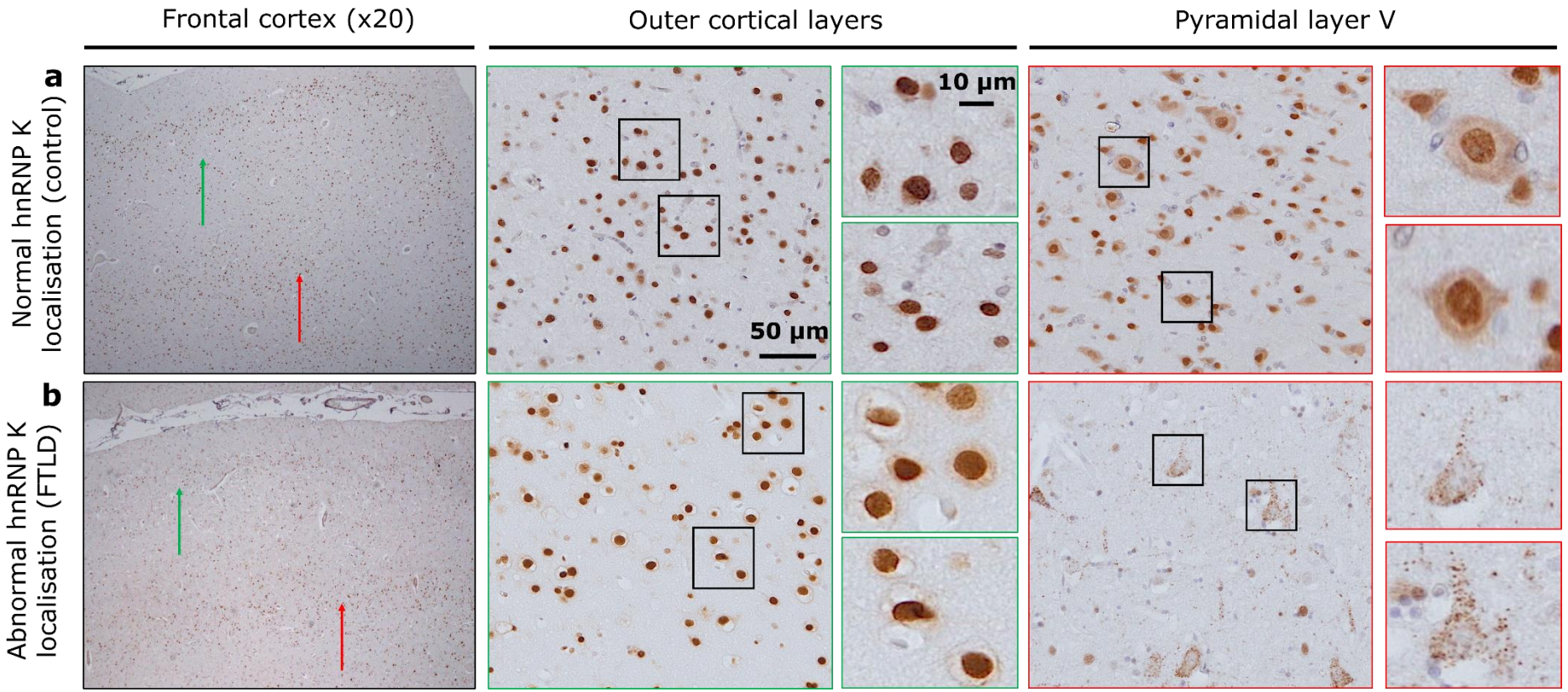

Figure 3.2. Immunohistochemical staining of hnRNP K neuronal pathology in FTLD and control subjects. (a) Normal nuclear localisation of hnRNP K localisation within neurons of outer and pyramidal cortical layers within a control subject (case 63). (b) FTLD-TDP A case (case 10) with normal neuronal staining within outer cortical layers and abnormal staining within pyramidal neurons as defined by hnRNP K nuclear depletion and accumulation of cytoplasmic puncta. Adapted from (Bampton *et al.*, 2021).

3.3.2 HnRNP K is frequently mislocalised within frontotemporal lobar degeneration subtypes

Upon closer examination, there were examples of hnRNP K mislocalisation within the pyramidal neurons of the frontal cortex across the FTLD-TDP and FTLD-tau pathological spectrum as well as in a rare FTLD-ni subject with no known pathological inclusions (**Figure 3.3**). The relatively selective degeneration of the frontal and temporal cortices is characteristic of all these disease subtypes.

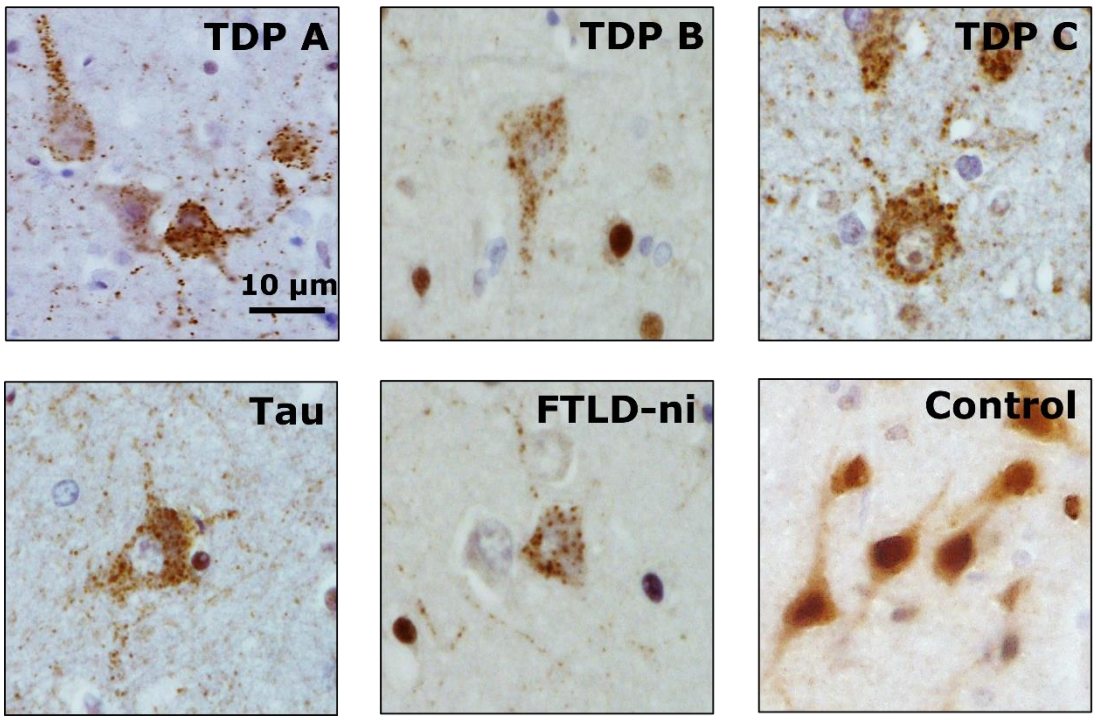

Figure 3.3. HnRNP K mislocalisation in pyramidal neurons of FTLD disease subtypes and a control subject. Representative images from (left to right) an FTLD-TDP A (case 10), FTLD-TDP B (case 30), FTLD-TDP C (case 43), FTLD-tau (case 46), FTLD-ni (case 51) cases and an age-matched control (case 68) case. Scale bars are as indicated in the first image. Adapted from (Bampton *et al.*, 2021).

The focus of this study was on FTLD-TDP A, FTLD-TDP C and FTLD-tau patient brains reflecting also the greater availability of these cases at Queen Square Brain Bank. Indeed, there were many examples of hnRNP K mislocalisation within these pathological subtypes (**Figure 3.4**).

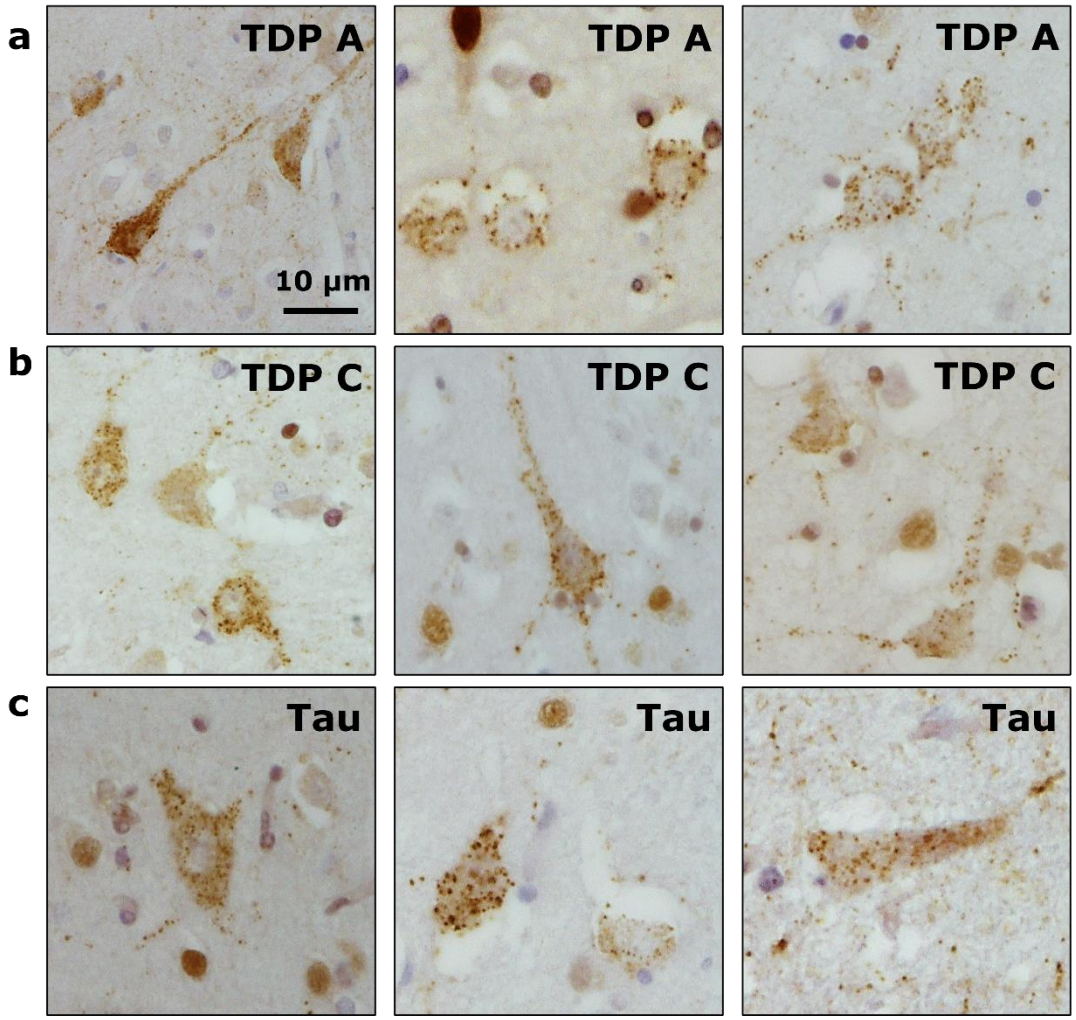

Figure 3.4. Further examples of hnRNP K mislocalisation in FTLD pyramidal neurons. Examples from three separate (a) FTLD-TDP A (left to right, cases 3, 4 and 16), (b) FTLD-TDP C (cases 34, 36 and 42) and (c) FTLD-tau (cases 47, 48 and 49) cases. Scale bars are as indicated in the first image. Adapted from (Bampton *et al.*, 2021).

To quantify this neuropathological event, large numbers of randomly generated images were sampled from the grey matter of immunohistochemically stained frontal cortex. An average of 129 images or 44.5 mm^2 of tissue were sampled from the region of interest for further analysis. Both normal (nuclear localisation) and abnormal (cytoplasmic mislocalisation) hnRNP K staining of neurons was quantified within each image as previously described (**Figure 3.1**). Neurons with normal staining were classified and quantified by an automated algorithm that utilised supervised machine learning (> 80 % specificity and sensitivity) developed by Dr Dipanjan Bhattacharya (IFOM). Quantitation of abnormally stained hnRNP

K neurons was conducted manually on matched sample images in a blinded fashion using robust morphological criterion. This was due to the morphologically heterogeneous nature of hnRNP K mislocalisation and variable staining intensity which prevented specific and sensitive detection of abnormal neurons using supervised machine learning.

Age-matched cases of FTLD-TDP A (n = 28), FTLD-TDP C (n = 12), FTLD-tau (n = 5) and control (n = 18) subjects were selected for comparative analysis (**Figure 3.5a**). A small ALS cohort (n = 7) was also included as a disease control due to the relative sparing of the frontal cortex in ALS pathology.

Disease categories were first compared according to their degree of normal hnRNP K staining by calculating each case's average number of normally stained neurons per mm^2 analysed. As expected, control cases had the greatest frequency of normal hnRNP K-stained neurons per image which was significant compared to the FTLD-TDP A disease subtype ($p = 0.013$) (**Figure 3.5b**). This reflected control frontal cortex, unsuprisingly having a greater number of surviving neurons than FTLD subjects.

The same groups were then compared on their degree of abnormal hnRNP K staining by calculating the proportion of all sampled images which contained at least one mislocalised neuron for each case. For example, a case with a mislocalisation score of 25 % would mean that 25 % of all the case's randomly sampled images contained at least one neuron with hnRNP K mislocalisation. By contrast to normal hnRNP K staining, FTLD-TDP A and FTLD-tau disease groups exhibited significantly more mislocalisation of hnRNP K protein relative to controls ($p = 0.004$, $p = 0.002$) (**Figure 3.5c**). There was no difference between controls and FTLD-TDP C subjects. Of interest, FTLD-tau cases also exhibited greater hnRNP K mislocalisation than ALS subjects – the disease control group ($p = 0.04$).

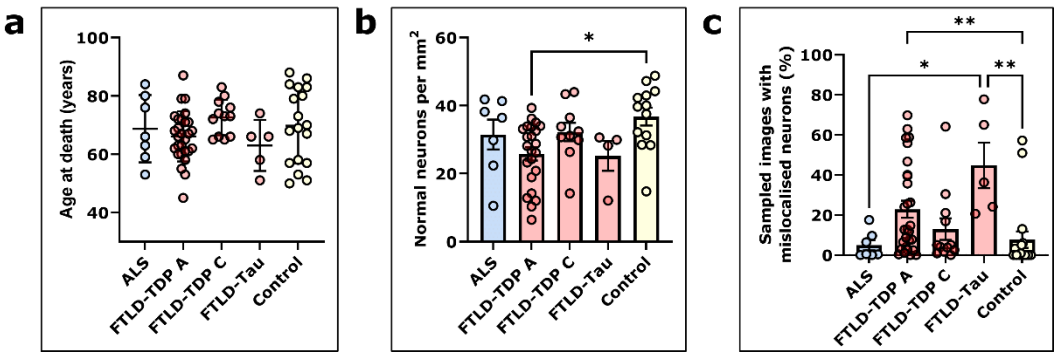

Figure 3.5. Quantitation of hnRNP K neuronal pathology in FTLD and control subjects. (a) ALS (*n* = 7), FTLD-TDP A (*n* = 28), FTLD-TDP C (*n* = 12), FTLD-tau (*n* = 5) and control (*n* = 18) cohorts were age-matched with no significant difference between mean age at death. (b) Age-matched controls showed significantly more normal hnRNP K-stained neurons per mm^2 region analysed ($p = 0.013$; Tukey's test). (c) FTLD-TDP A and FTLD-tau cases exhibited significantly more hnRNP K mislocalisation than controls expressed as proportion of sampled images with at least 1 (> 0) mislocalised neuron ($p = 0.004$, Kruskal-Wallis). FTLD-tau cases also exhibited significantly more mislocalised hnRNP K than ALS cases ($p = 0.002$). Error bars show mean ± SD (age at death) or SEM (mislocalisation scores). *$p < 0.05$, **$p < 0.01$, ***$p < 0.001$, ns = not significant. Adapted from (Bampton *et al.*, 2021).

3.3.3 HnRNP K mislocalisation is an age-related feature of neurodegenerative disease

Notably, hnRNP K mislocalisation was not found to be a specific pathological feature of any one FTLD subtype. Equally, not all individuals of any one subtype were vulnerable to hnRNP K mislocalisation. This prompted the exploration of the relationship between hnRNP K mislocalisation and other variables and in particular, age at death.

To investigate the effect of age in controls, a further 17 control subjects were recruited to the cohort (*n* = 35 total) with ages of death spanning 71 years from 25 to 96 years old. A combined FTLD disease group of FTLD-TDP and FTLD-tau groups (*n* = 50) was formed from the previously analysed FTLD-TDP A, FTLD-TDP C and FTLD-tau groups with the further addition of *n* = 3 and *n* = 2 FTLD-TDP B and FTLD-TDP D cases respectively. Analysing control individuals in isolation, age at death was found to strongly correlate with hnRNP K mislocalisation ($r = 0.552$, $p = 0.0006$) (**Figure 3.6a**). By contrast hnRNP K mislocalisation in the FTLD cohort was much more weakly

associated with age at death ($r = 0.201$, $p = 0.162$ ns). HnRNP K mislocalisation score did not correlate with any other known clinical covariate or demographic including Braak tau stage (data not shown).

To better visualise and compare the different relationships between increasing age and hnRNP K pathology in control and FTLD groups, a cumulative frequency plot was generated (**Figure 3.6b**). The rolling total of hnRNP K mislocalisation for each cohort was plotted against ascending age and normalised to the sum total of each group's total level of quantified mislocalisation. This illustrated the advanced nature of hnRNP K pathology onset in younger FTLD individuals relative to controls; with the median amount of mislocalisation in the FTLD's (reached at 68 years of age) being 18 years earlier than in controls (86 years) (**Figure 3.6b**).

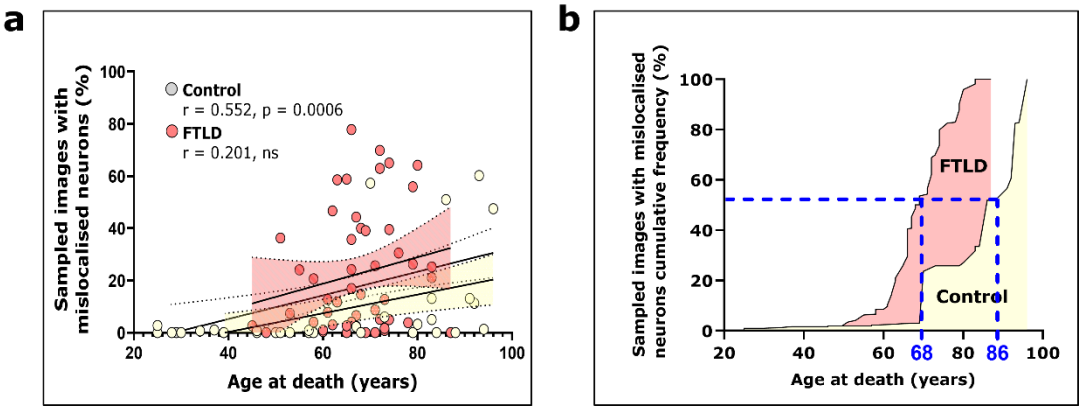

Figure 3.6. HnRNP K mislocalisation is an age-related pathology that is advanced in FTLD. (a) HnRNP K mislocalisation in controls (in yellow, $n = 35$) was found to positively correlate with age at death (Spearman's $r = 0.552$, $p = 0.0006$). Combined FTLD-TDP and FTLD-tau subjects (in red, $n = 50$) was found to be only weakly associated with age at death (Spearman's $r = 0.201$, ns). (b) A cumulative frequency plot of hnRNP K mislocalisation with ascending age normalised to total amount of quantified mislocalisation for each control/disease group. The intra-group median frequency of hnRNP K mislocalisation within the FTLD-TDP A group was 18-years in advance of the control cohort (dotted blue lines). Adapted from (Bampton *et al.*, 2021).

There was no significant difference in hnRNP K mislocalisation between FTLD cases subdivided into familial (fFTLD) ($n = 24$) and sporadic (sFTLD) cases ($n = 27$), despite the mean age at death of the sFTLD group being significantly older than the younger onset fFTLD group (**Figure 3.7**). This was again

consistent with age being a less important contributory factor to hnRNP K mislocalisation in neurodegenerative disease (FTLD) brain than in controls.

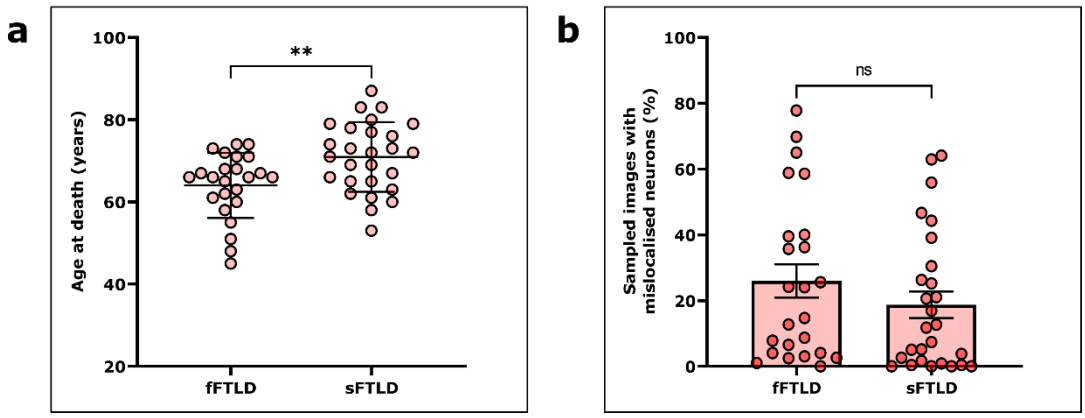

Figure 3.7. HnRNP K mislocalisation in familial and sporadic FTLD. The FTLD cohort split into familial (fFTLD) and sporadic (sFTLD) cases exhibit (a) significantly different mean age at death (64.0 ± 7.9 years vs 70.9 ± 8.5 years respectively, p = 0.004) but (b) no significant difference in hnRNP K mislocalisation score. Error bars show mean ± SD (age at death) or SEM (mislocalisation scores). Unpaired t-test; *$p < 0.05$, **$p < 0.01$, ***$p < 0.001$, ns = not significant.

3.3.4 Mislocalised hnRNP K is distinct from pTDP-43 and Tau inclusions

To confirm that neurons with hnRNP K pathology were distinct from those with pTDP-43 immunoreactive inclusions, double immunofluorescence was performed to determine the spatial relationship of these two pathologies in FTLD-TDP A.

Neurons with pTDP-43 inclusions that were predominantly found in cortical layer II displayed normal, nuclear-localised hnRNP K (**Figure 3.8a-b**). Conversely, cytoplasmic puncta of mislocalised hnRNP K in pyramidal neurons did not colocalise with pTDP-43 cytoplasmic inclusions in FTLD-TDP A (**Figure 3.8c**). Indeed, a similar double-negative result was obtained with antibodies against the classical inclusion marker SQSTM1/p62 (**Figure 3.8d**). Hence cytoplasmic hnRNP K puncta are unlikely to be components of ubiquitinated inclusions.

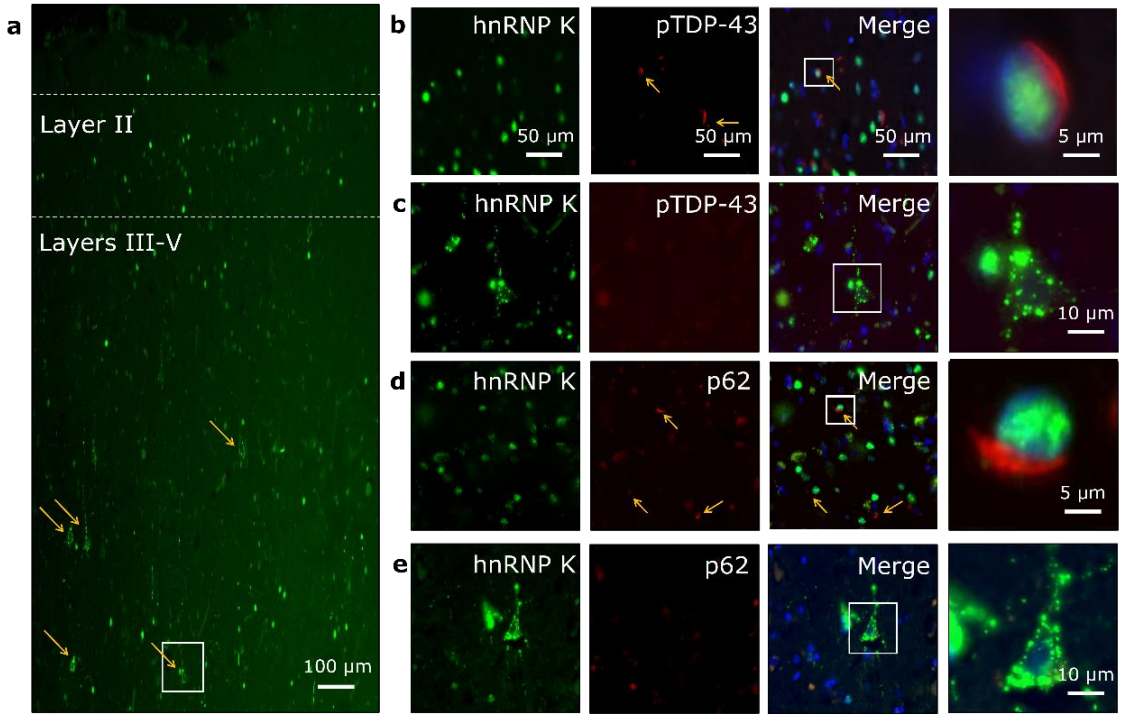

Figure 3.8. Neurons exhibiting hnRNP K mislocalisation are independent of those containing TDP-43 inclusions and hnRNP K pathology is p62-negative. (a) HnRNP K immunofluorescence of frontal cortex in FTLD-TDP A (case 5) showing the relative anatomical positioning of normal (layer II) and abnormal (pyramidal layers III & V) hnRNP K localisation. Arrows point to neurons with hnRNP K mislocalisation. (b and c) Representative images of double-label immunofluorescence in layer II exhibiting normal hnRNP K staining but with TDP-43 inclusions (b) and pyramidal layer V neurons with mislocalised hnRNP K (as boxed in a) but no TDP-43 pathology in the same case (c) demonstrating that hnRNP K mislocalisation and TDP-43 pathologies do not co-occur in the same neurons. (d and e) Double-label immunofluorescence of hnRNP K and p62 in FTLD-TDP A (case 4) cortical layers II and V showing neurons with p62-positive inclusions have normal nuclear localisation of hnRNP K (d) and that cytoplasmic puncta in pyramidal neurons with hnRNP K mislocalisation are p62-negative (e). Arrows point to TDP-43 / p62-positive inclusions and scale bars are as indicated in the first row unless otherwise stated. Adapted from (Bampton *et al.*, 2021).

Neurons with hnRNP K pathology were also found to be distinct from those with tau-positive inclusions within the frontal cortex of FTLD-tau cases. Tau inclusions were readily identifiable within the pyramidal cell layers, but again, were not found within neurons exhibiting hnRNP K mislocalisation (**Figure 3.9**). Hence neurons exhibiting hnRNP K mislocalisation are mutually exclusive from both pTDP-43 and tau proteinaceous inclusion that pathologically define FTLD-TDP and FTLD-tau disease.

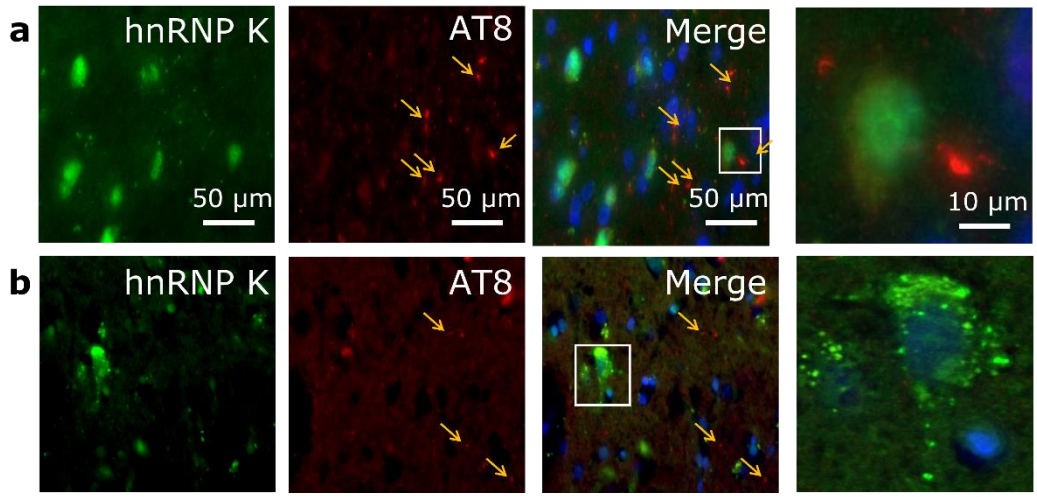

Figure 3.9. Neurons that exhibit hnRNP K mislocalisation are independent of those that exhibit tau-inclusions. Representative images of double-label immunofluorescence in pyramidal neurons with normal (a) and abnormal (b) hnRNP K localisation in FTLD-tau frontal cortex (case 46) with phospho-tau (AT8) marker demonstrating no clear colocalisation of cytoplasmic puncta. Orange arrows point to AT8-positive inclusions and scale bars are as indicated in the first row. Adapted from (Bampton *et al.*, 2021).

3.3.5 Mislocalised hnRNP K and other organelle markers

In further attempts to characterise the subcellular location of hnRNP K cytoplasmic puncta in mislocalised neurons, double fluorescence was also performed with mitochondrial marker voltage-dependent anion channel (VDAC-1), classical autophagosome marker LC3 and stress granule/RNA-binding protein GTPase-activating protein-binding protein 2 (G3BP2). VDAC-1, LC3 and G3BP2 staining was principally cytoplasmic but no marker was enriched at the site of hnRNP K puncta (**Figure 3.10**).

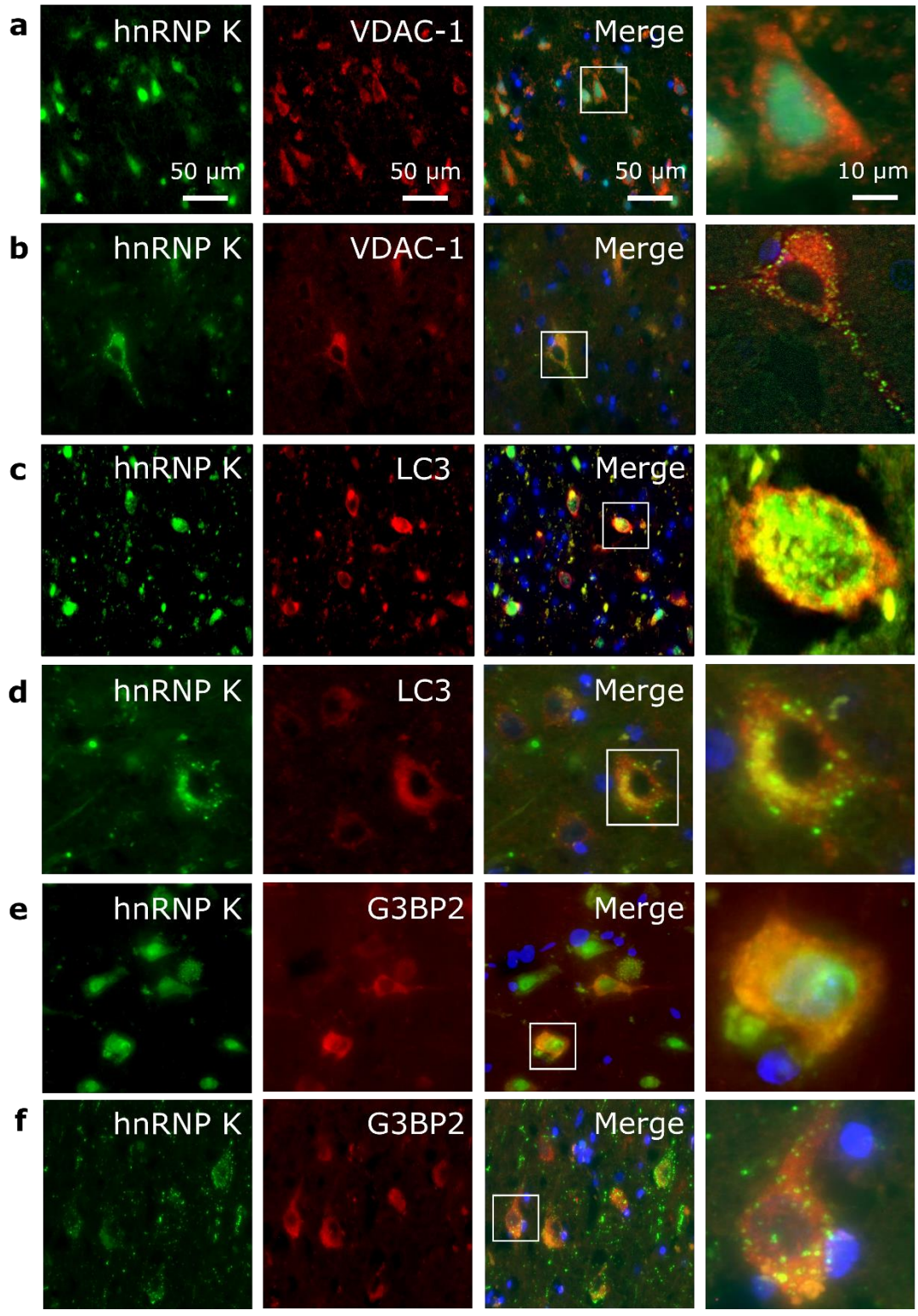

Figure 3.10. Mislocalised cytoplasmic hnRNP K does not colocalise with mitochondria, autophagy or stress granule markers. (a and b) Representative images of double-label immunofluorescence in pyramidal neurons with normal (a) and abnormal (b) hnRNP K localisation in control (case 63) and FTLD-TDP A (case 5) frontal cortex respectively with mitochondrial marker VDAC-1. (c and d) shows the spatial relationship between normal (c) and abnormally (d) localised hnRNP K with autophagy marker LC3 and (e and f) shows the same cases again with stress granule

/ RNA-binding protein marker G3BP2. In all cases no clear colocalisation was observed within cytoplasmic hnRNP K puncta. Scale bars are as indicated in the first row. Adapted from (Bampton *et al.*, 2021).

3.3.6 HnRNP K protein levels may be reduced in post-mortem brain tissue with mislocalised hnRNP K

HnRNP K protein levels were quantified by immunoblotting in bulk brain tissue from the frontal cortex. Cases were selected according to their hnRNP K localisation profile as being predominantly 'normal' or predominantly 'abnormal'. Normal cases were selected on the basis of having fewer than 5 % of sampled images with at least one mislocalised neuron. Abnormal cases were selected if over 30 % of images had at least one mislocalised neuron. Cases were selected blind to disease status although there was a bias to FTLD individuals due to exhibiting, on average, greater amounts of mislocalisation than controls.

Bulk levels of hnRNP K were found to be significantly higher in normal (n = 6) than abnormally categorised subjects (n = 6) relative to β-actin as quantified by immunoblotting (p = 0.0152) (**Figure 3.11a-b**). Although curiously, one 'normal' case was found to exhibit low hnRNP K protein, as shown below. However, at the transcriptional level there was no difference in bulk *HNRNPK* mRNA levels between the categories utilising a larger cohort for comparison (n = 35) (**Figure 3.11c**).

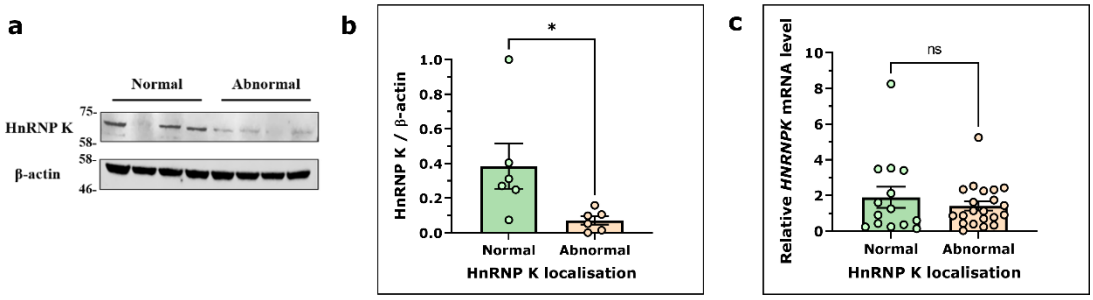

Figure 3.11. HnRNP K protein and mRNA levels in post-mortem brain tissue. Representative immunoblot of hnRNP K protein levels in brain tissue categorised as exhibiting predominantly normal or abnormal hnRNP K localisation. (b) Densitometry plot quantifying hnRNP K protein levels of immunoblots (n = 2) relative to β-actin loading control (p = 0.0152, unpaired t-test). (c) *HNRNPK* mRNA levels in brain tissue quantified by RT-qPCR and normalised to *RPL18A* housekeeping gene. Error bars show mean ± SD (age at death) or SEM (mislocalisation scores). Unpaired t-test; *p < 0.05, **p < 0.01, ***p < 0.001, ns = not significant.

3.4 Discussion

3.4.1 Summary of main findings

The pathological findings presented in this chapter identify a novel neuropathological event characterised by the mislocalisation of hnRNP K from the nucleus to the cytoplasm within pyramidal neurons of the frontal cortex in a highly punctate manner. HnRNP K mislocalisation was found to be more frequent in FTLD-TDP A and FTLD-tau patient brains than in age-matched, neurologically normal controls. However, mislocalisation also occurs in some elderly controls and indeed was found to correlate with age at death in control subjects. Hence it is possible that the higher rates of mislocalisation in the FTLD cohort may reflect an advanced-ageing phenotype.

3.4.2 HnRNP K mislocalisation in context

Neuronal hnRNP K mislocalisation as both a neurodegenerative disease and age-associated neuropathological event provides further evidence for both protein and in particular, RNA-binding protein (RBP) proteostatic dysregulation in the diseased and ageing brain. Indeed, hnRNP K joins the company of a long list of RBPs with strong genetic and/or pathological links to

neurodegeneration and especially to FTLD and ALS pathogenesis including TDP-43, FUS, EWS, TAF15, hnRNP A1, hnRNP A2/B1, TIA-1, FMRP, MATR3 and ATXN2 (Hanson, Kim and Tibbetts, 2012; Conlon and Manley, 2017). This, pending further mechanistic investigations, is in support of a wider and more complex network level dysregulation of RBP homeostasis which is not simply confined to the proteins that form hallmark pathological inclusions.

The concept of hnRNP K mislocalisation in neurodegeneration being an 'advanced-ageing' pathological phenomena would also not be unique to the hnRNP K protein. Several age-related pathologies including amyloidosis (Aβ), primary age-related tauopathy (PART, tau) and limbic-predominant age-related TDP-43 encephalopathy (LATE, TDP-43) are all characterised by the abnormal deposition and accumulation of the same proteins that pathologically define several neurodegenerative diseases (Coria, Castaño and Frangione, 1987; Crary *et al.*, 2014; Nelson *et al.*, 2019). The extent of the pathological burden and neuroanatomical distribution pattern of these pathologies generally distinguishes true disease from normal ageing. The difference in this study however, was that the hnRNP K mislocalisation observed in a subset of elderly control individuals was by all accounts indistinguishable from younger FTLD cases. The extent to which this overlap represents hnRNP K pathology being an accelerated ageing process in neurodegenerative disease and a potential precursor to disease remains unclear. Further pathological investigations into other neuroanatomical regions may shed light on potentially important differences that may help to differentiate normal ageing from the neurodegeneration phenotype.

Additionally, pyramidal neurons found to exhibit hnRNP K mislocalisation were confirmed to be mutually exclusive of those which harbour the proteinaceous TDP-43 and tau inclusions that pathologically define the major FTLD subtypes. This is a novel observation, compared to previous work on the pathological profile of other hnRNPs which has identified several other hnRNPs to be present within TDP-43 and FUS inclusions (Davidson *et al.*, 2017; Gittings *et al.*, 2019). In particular, the mutual exclusivity of neuronal hnRNP K mislocalisation and TDP-43 inclusions is perhaps surprising in light of hnRNP

Ks known inter-relationship with TDP-43 in mediating both appropriate stress granule assembly (White *et al.*, 2013; Moujalled *et al.*, 2015) and normal TDP-43 proteostasis (Nguyen *et al.*, 2020). There is an even greater abundance of research on the co-deposition of hnRNPs with *C9orf72*-FTLD/ALS associated pathologies including intranuclear RNA foci (Cooper-Knock *et al.*, 2014; Haeusler *et al.*, 2014) and dipeptide repeat proteins (Davidson *et al.*, 2017; Suzuki *et al.*, 2019). Further intriguingly, the cytoplasmic puncta of hnRNP K within afflicted neurons were found to be p62/ubiquitin negative which is comparatively rare for FTLD inclusions, although some FTLD-FUS inclusions have also been identified as ubiquitin-negative (Seelaar *et al.*, 2010).

Additionally, no colocalisation was found between hnRNP K puncta and markers of mitochondria, autophagosomes or stress granules despite an abundance of research linking hnRNP K to the functioning of these organelles (Dzwonek, Mikula and Ostrowski, 2006; White *et al.*, 2013; Z. Li *et al.*, 2018). Of these, hnRNP K has been most strongly implicated in the stress granular response where hnRNP K, along with binding partner TDP-43, has been shown to colocalise to stress granules in neurons during stress-induction protocols following hnRNP K phosphorylation by cyclin-dependent kinase 2 (White *et al.*, 2013; Moujalled *et al.*, 2015). HnRNP K protein has also been found to be robustly nuclear depleted within iPSC-derived motor neurons subjected to osmotic stress (Harley and Patani, 2020). Hence, protein levels of hnRNP K as well as its subcellular localisation and phosphorylation status may be mechanistically crucial in maintaining normal stress granule assembly and dissolution which may warrant further interrogation in cell models which exhibit clearer stress granule staining than in post-mortem tissue. Measuring hnRNP K protein levels from bulk brain tissue showed a trend towards reduction in cases known to exhibit cytoplasmic mislocalisation which may point towards a greater degree of cellular degeneration of hnRNP K in afflicted neurons. However, in the current absence of clear colocalisation with markers of proteostatic systems (e.g. autophagy), this remains unverified.

Pyramidal neurons are the most populous neuronal cell type in the mammalian cortex distributed throughout the cortex but particularly in layer III and even

more numerously in layer V (Harris and Shepherd, 2015). They are easily identifiable by their large somas and long single axons which project to both local (cortical) targets and distant structures including the striatum, midbrain and brainstem nuclei and even the spinal cord (Gerfen, Economo and Chandrashekar, 2018). There is however mounting morphological and genetic evidence for the existence of several distinct pyramidal neuron cell types with different patterns of connectivity (Molnár and Cheung, 2006; Nelson, Hempel and Sugino, 2006). It is unclear at this stage whether hnRNP K mislocalisation preferentially affects any one of these subtypes but the answer may prove very mechanistically insightful. Functionally, pyramidal neurons serve as information integration points which receive and processes information from a vast number of cortical neuron inputs via their extensive dendritic spines before transforming the integrated signal into a uniquely patterned action potential that is projected to distal targets (Bekkers, 2011). Unsurprisingly then, pyramidal neurons have been strongly implicated in the regulation of higher order cerebral processes including cognitive processing and neuroplasticity (Elston, 2003). Indeed, the cognitive changes that accompany neurodegenerative disease and in particular AD are believed to be in large part a result of the disproportionate loss of pyramidal neurons and dendritic spines in the cortex and subsequent deteriorations in network connectivity (Mann, 1996; Mijalkov *et al.*, 2021). Synapse dysfunction within pyramidal neurons has also been found to be a precursor to neurodegeneration within TDP-43 proteinopathies including FTLD and ALS (Handley *et al.*, 2017). Nevertheless, pyramidal neurons are not typically associated with pathological inclusions in neurodegenerative disease, particularly FTLD. Hence, the findings described here highlighting their predisposition to hnRNP K mislocalisation, is a salient reminder to not neglect the roles of other pathomechanistic phenomena, besides classical inclusion formation, within other neuronal subpopulations that may contribute to the neurodegeneration phenotype.

3.4.3 Future research avenues

From a pathological perspective, further investigations including additional double fluorescence, co-immunoprecipitation and biochemical fractionation studies will be vital in order to better characterise the observed cytoplasmic puncta in pyramidal neurons. It will also be important to clarify the potential roles of both intrinsic and extrinsic factors, in addition to age, that may be associated with hnRNP K mislocalisation propensity including post-translational modifications as well as other cellular and genetic factors. Additionally, further pathological examinations across the brain will be needed to identify whether other brain regions and/or specific neuronal cell types are vulnerable to hnRNP K mislocalisation.

More generally however, the aforementioned results raise the obvious question of what molecular consequences are likely to accompany a robust nuclear clearance of hnRNP K, a typically nuclear-confined protein at steady state, in neurons. Many hnRNPs have been identified as having important roles in splicing regulation within their molecular targets and hence this is one such cellular function that could well be compromised in neurons lacking appropriately localised hnRNP K protein (Bampton *et al.*, 2020). This prompted the development of a hnRNP K knockdown neuronal model to explore the functional consequences of hnRNP K nuclear depletion as detailed in later chapters.

Chapter 4 HnRNP K mislocalisation in neurons beyond the cortex

4.1 Introduction

4.1.1 Publication statement

The contents of this chapter relating to hnRNP K mislocalisation in the dentate nucleus have been previously published open access (Sidhu *et al.*, 2022) and are included here in an adapted form as per the publisher's (Wiley) policy on open access publication.

4.1.2 Statement of contribution

The experimental work and analyses presented in this chapter was conducted jointly between myself and MSc student Mr Rahul Sidhu whom was under my supervision. The project was led by myself and the resulting figures and manuscript were designed and written by me in full as senior (last) author.

4.1.3 Background

HnRNP K mislocalisation, characterised by nuclear depletion and accumulation of the protein into the cytoplasm, has been frequently identified within layer III and V pyramidal neurons of the frontal cortex in cases of neurodegenerative disease (FTLD) compared to age-matched controls. This novel neuropathological event was also found to positively correlate with age at death in an expanded control cohort (Bampton *et al.,* 2021).

Whilst the frontal cortex is a region of the brain selectively vulnerable to atrophy in FTLD pathogenesis, the pyramidal neurons residing within the deeper layers of the neocortex do not typically contain the classical, ubiquitinated pathological inclusions that define FTLD-associated pathology. Indeed, hnRNP K mislocalisation pathology within frontal cortex was confirmed to

occur in neurons distinct from those smaller cortical neurons harbouring pTDP-43 and tau-immunoreactive inclusions. This prompted the exploration of other disease-affected and unaffected brain regions. The hippocampus was selected as an area affected in all neurodegenerative diseases and the cerebellum an area that is relatively spared during the degenerative processes.

For this project an AD cohort was included along with a significant subset of the FTLD-TDP A disease and age-matched cohorts previously used in **Chapter 3**, to determine whether clinically and pathologically confirmed cases of AD also demonstrate hnRNP K mislocalisation. Previous findings showed that hnRNP K pathology was not confined to any particular FTLD subtype (although more evident in TDP A and tau subtypes) and so it was important to deduce whether hnRNP K mislocalisation has a broader relevance to the neurodegeneration field irrespective of the protein aggregates deposited.

4.2 Methods

4.2.1 Cohort

As before, all brains were donated to the Queen Square Brain Bank (QSBB) for neurological disorders (UCL Queen Square Institute of Neurology) and the Medical Research Council (MRC) Edinburgh Brain & Tissue Bank. All brains were processed and tissue was sectioned as previously described (**2.1.3**). The cohort (*n* = 58) included pathologically diagnosed cases of FTLD-TDP A (*n* = 18), Alzheimer's disease (*n* = 17) and neurologically normal controls (*n* = 32 including *n* = 21 age-matched) (**Table 4.1**).

Table 4.1 Cohort and clinical demographics

No.	Path. diagnosis	AAO	AAD	Sex	Brain weight (g)	Mutations	Braak stage	PM delay (h)
1	FTLD-TDP A	58	66	F	850	*C9ORF72*	1	107.1
2	FTLD-TDP A	75	79	M	-	-	3	10.0
3	FTLD-TDP A	47	53	M	1390	-	1	33.7
4	FTLD-TDP A	53	63	M	955	*C9ORF72*	0	77.3
5	FTLD-TDP A	66	72	M	1274	-	0	68.2
6	FTLD-TDP A	57	60	M	1673	-	2	40.4
7	FTLD-TDP A	67	69	M	1398	-	1	62.5
8	FTLD-TDP A	62	72	M	1320	*TBK1*	-	97.4
9	FTLD-TDP A	66	74	F	782	*C9ORF72*	1	85.8
10	FTLD-TDP A	62	68	M	1371	*C9ORF72*	1	99.0
11	FTLD-TDP A	66	71	M	1431	*C9ORF72*	2	51.9
12	FTLD-TDP A	57	63	F	851	-	2	85.3
13	FTLD-TDP A	49	55	M	974	*GRN* (C31fs)	1	29.3
14	FTLD-TDP A	53	61	M	994	*GRN* (C31fs)	1	72.6
15	FTLD-TDP A	51	61	M	1065	-	1	35.3
16	FTLD-TDP A	57	62	M	-	-	0	92.9
17	FTLD-TDP A	64	73	M	1252	*C9ORF72*	4	61.1
18	FTLD-TDP A	59	65	M	1176	*C9ORF72*	2	30.0
FTLD-TDP A summary (*n* = 18)		59.3	65.9	15 (M): 3 (F)	1172	-	1.4	63.3
19	AD	57	76	M	1303	-	6	57.8
20	AD	63	79	M	-	-	6	61.3
21	AD	55	64	M	1280	-	6	95.1
22	AD	52	71	M	1097	-	6	45.6
23	AD	49	69	F	986	-	6	40.2
24	AD	53	61	M	1144	-	6	78.3
25	AD	61	72	M	1024	-	6	27.4
26	AD	63	73	F	1005	-	6	89.6
27	AD	71	86	M	1203	-	5	95.2
28	AD	36	41	F	1108	*PSEN1* (Intron 4)	6	64.3
29	AD	31	37	F	1182	*PSEN1* (E120K)	6	24.3
30	AD	42	47	M	1225	*PSEN1* (A434T & T291A)	5	43.8

31	AD	44	52	M	1251	*PSEN1* (E280G)	6	34.4
32	AD	48	54	M	910	*PSEN1* (M146L)	6	115.6
33	AD	45	58	F	1024	*PSEN1* (E184D)	6	63.4
34	AD	46	65	F	762	*PSEN1* (R278I)	6	31.9
35	AD	59	70	M	-	*PSEN1* (S132A)	6	161.3
AD summary (*n* = 17)		51.5	63.2	11 (M): 6 (F)	1100	-	5.9	66.4
36	Control	-	29	M	1590	-	-	44.0
37	Control	-	25	M	1640	-	-	53.0
38	Control	-	30	M	1670	-	-	71.0
39	Control	-	25	M	1500	-	-	81.0
40	Control	-	28	M	1330	-	-	38.0
41	Control	-	34	M	1530	-	-	99.0
42	Control	-	40	M	1570	-	-	103.0
43	Control	-	39	M	1360	-	-	76.0
44	Control	-	37	F	1360	-	-	126.0
45	Control	-	39	M	1470	-	-	86.0
46	Control	-	50	M	1400	-	-	49.0
47	Control	-	46	M	1380	-	-	76.0
48	Control	-	46	F	1400	-	-	99.0
49	Control	-	48	M	1480	-	-	58.0
50	Control	-	50	M	1350	-	-	122.0
51	Control	-	57	M	1600	-	-	70.0
52	Control	-	58	M	1650	-	-	96.0
53	Control	-	53	F	1420	-	-	107.0
54	Control	-	57	F	1320	-	1	73.0
55	Control	-	51	M	1460	-	-	52
56	Control	-	34	M	-	-	0	14.0
57	Control	-	38	M	1581	-	0	80.6
58	Control	-	68	F	1330	-	0	45.1
59	Control	-	70	M	1544	-	-	53.5
60	Control	-	79	F	1288	-	0	88.8
61	Control	-	83	F	1263	-	0	99.0
62	Control	-	86	F	1234	-	0	120.0
63	Control	-	91	F	1130	-	1	71.8
64	Control	-	64	M	1695	-	0	80.0
65	Control	-	72	F	1257	-	1	36.0
66	Control	-	77	M	1327	-	2	40.2

67	Control	-	73	M	1291	-	-	47.0
Control summary (*n* = 32)		-	52.4	22 (M): 10 (F)	1432	-	0.5	73.6

AAD, Age at death; AAO, Age at onset; AD, Alzheimer's disease; Braak (Tau) stage (where available), FTLD, Frontotemporal lobar degeneration; PM, Post-mortem. Mutations: *C9ORF72* Chromosome 9 open reading frame 72, *GRN* Progranulin, *PSEN1* Presenilin-1, *TBK1* TANK-binding kinase 1. Adapted from (Sidhu *et al.*, 2022).

4.2.2 Immunohistochemistry and quantitative pathological assessment

Cerebellum (*n* = 67) and hippocampal brain sections (*n* = 62) from all cases were immunohistochemically stained with anti-hnRNP K antibody (Ab23644) as previously described (**2.1.4**). Once stained, eight random sample images (20x) of the dentate nucleus or five of the hippocampal CA4 region (regions of interest identified as being vulnerable to hnRNP K mislocalisation) were acquired per case. Two assessors counted neurons within each image field exhibiting either normal (nuclear) or mislocalised hnRNP K staining (nuclear loss and punctate cytoplasmic accumulation). All images were acquired and analysed blinded to disease status. Mislocalisation frequency was reported as two metrics, the proportion (%) of all counted neurons exhibiting hnRNP K mislocalisation and the number of mislocalised neurons counted per image. Agreement between assessors was high when comparing image-matched hnRNP K mislocalisation scores in a sample of 50 dentate nucleus images ($r = 0.838$, $p < 0.0001$) and hippocampal CA4 images ($r = 0.923$, $p < 0.0001$) (**Figure 4.1**). Images with a score discrepancy of greater than 20 % difference were either re-assessed together or analysed by a third counter.

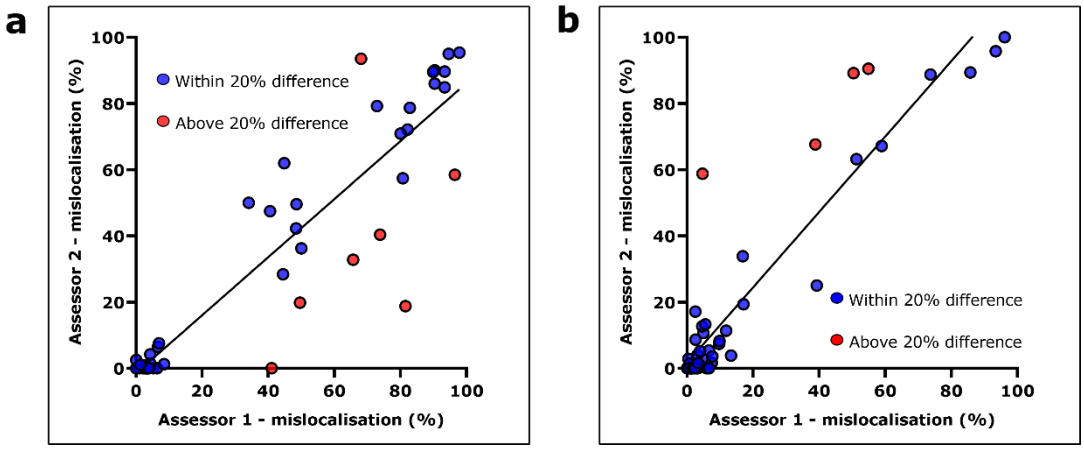

Figure 4.1. Scoring agreement between assessors. (a) Mislocalisation scores for sample-matched dentate nucleus between assessors strongly correlate (Pearson's r = 0.838, p < 0.0001) and (b) equivalent agreement for sample-matched CA4 cases (Pearson's r = 0.923, p < 0.0001). Red circles are those with a 20 % score discrepancy between scorers which would be either reassessed or re-counted by a third scorer.

4.3 Results

4.3.1 Normal hnRNP K localisation in neurons of the cerebellar cortex

Upon first examination of the cerebellar cortex, normal (nuclear) staining of hnRNP K was found across the three layers of the cortex irrespective of disease status. Neurons within the molecular and granular layers as well as Purkinje cell bodies all exhibited strong and predominantly nuclear staining patterns (**Figure 4.2**).

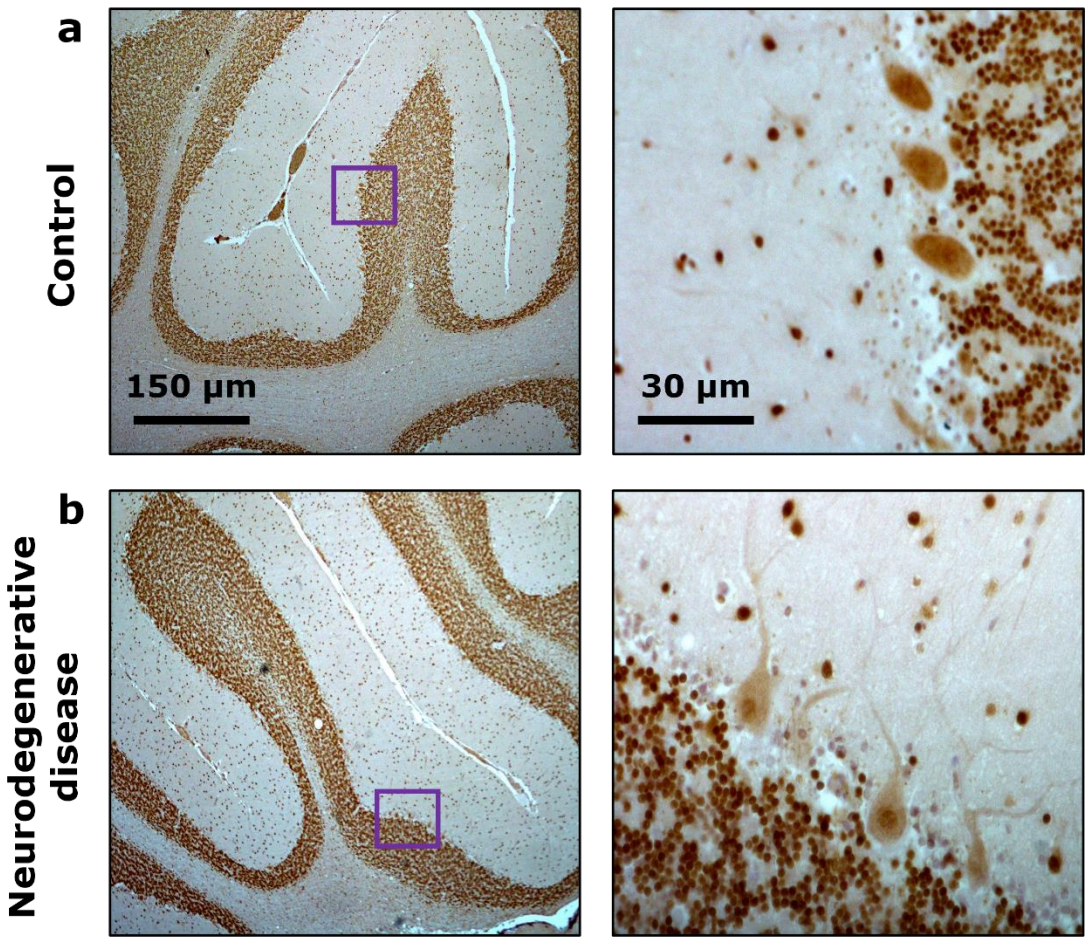

Figure 4.2. Normal hnRNP K localisation in the cerebellar cortex. Representative images of normal, predominantly nuclear hnRNP K staining in neurons of the cerebellum cortex in both (a) control (case 58) and (b) neurodegenerative disease (FTLD-TDP A, case 10) brain. Scale bars are as indicated in the first row ((Sidhu *et al.*, 2022)).

4.3.2 HnRNP K mislocalisation in the dentate nucleus

Attention was then turned to the dentate nucleus which could be visualised within the same section as the cerebellar cortex. Intriguingly, the dentate nucleus was identified as another region vulnerable to neuronal hnRNP K mislocalisation in many cases. In contrast to 'normal' nuclear staining within neurons of the dentate nucleus, in mislocalised cases, hnRNP K protein was again found to be depleted from the nucleus and deposited in the cytoplasm in a punctate fashion (**Figure 4.3**).

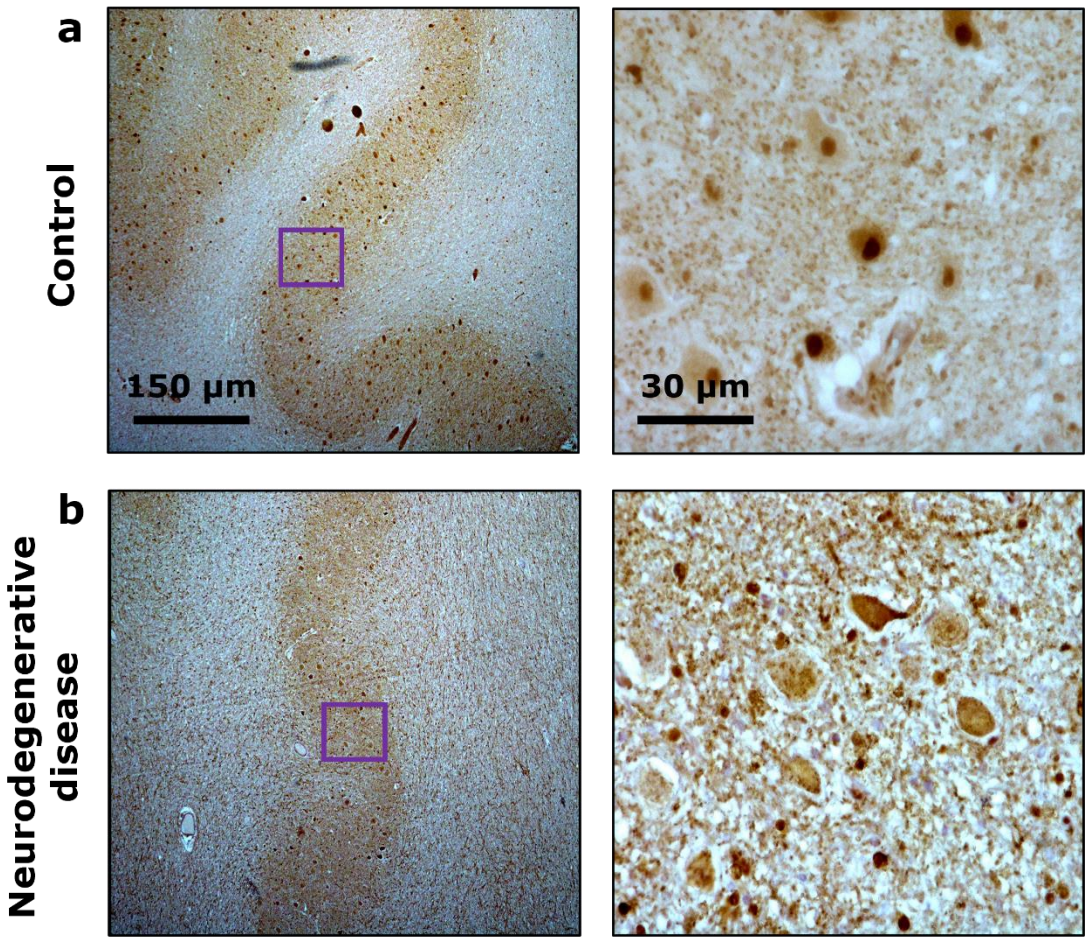

Figure 4.3 HnRNP K mislocalisation in the dentate nucleus. Representative images of (a) normal hnRNP K localisation within the dentate nucleus of a control subject (case 65) and (b) abnormal, mislocalisation of hnRNP K within a neurodegenerative disease (FTLD-TDP A, case 14) subject. Scale bars are as indicated in the first row.

4.3.3 Dentate nucleus hnRNP K mislocalisation in neurodegenerative disease

Neurons within the dentate nucleus were found to exhibit distinctly different hnRNP K localisation profiles across the cohorts. Typical control subjects exhibited normal hnRNP K localisation with strong nuclear staining intensity and weaker cytoplasmic staining (**Figure 4.4a**). By contrast FTLD-TDP A and AD subjects frequently exhibited a remarkably abnormal staining pattern within the same neuronal population. These neurons exhibited robust nuclear clearance of hnRNP K and granular cytoplasmic accumulation of the protein (**Figure 4.4b-c**).

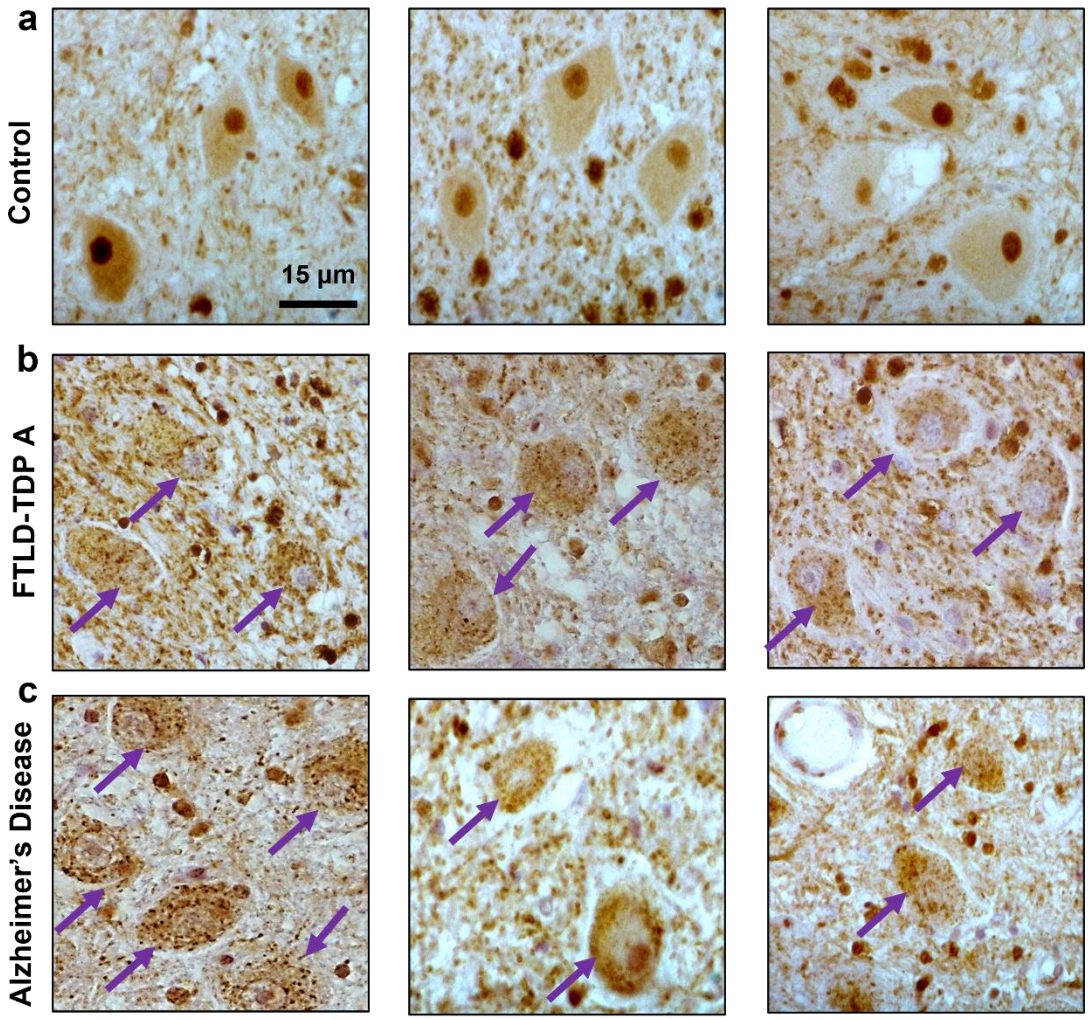

Figure 4.4. Dentate nucleus hnRNP K mislocalisation in neurodegenerative disease. (a) Representative images of normal, nuclear localisation of hnRNP K in neurons of the dentate nucleus within three control subjects (left to right, case 52, 58 and 60). (b) Representative images of abnormal, mislocalised neuronal staining of hnRNP K within three FTLD-TDP A (case 4, 10 and 16) cases exhibiting distinct nuclear depletion and cytoplasmic puncta accumulation. (c) Representative images of hnRNP K mislocalisation in three Alzheimer's disease (AD) (case 22, 24 and 26) cases. Purple arrows indicate neurons with clear hnRNP K nuclear depletion. Scale bars are as indicated in the first image ((Sidhu *et al.*, 2022)).

HnRNP K mislocalisation was quantified as described previously (**4.2.2**) on age-matched control, FTLD-TDP A and AD subjects (**Figure 4.5a**). The frequency (%) of neuronal mislocalisation of hnRNP K was significantly higher within FTLD-TDP A ($p = 0.0026$) and AD ($p = 0.0004$) groups versus age-matched control subjects (**Figure 4.5b**). The same result was observed when comparing the number of mislocalised neurons per image with both FTLD-TDP

A ($p = 0.0010$) and AD ($p = 0.0251$) exhibiting more frequent mislocalised neurons than controls (**Figure 4.5c**).

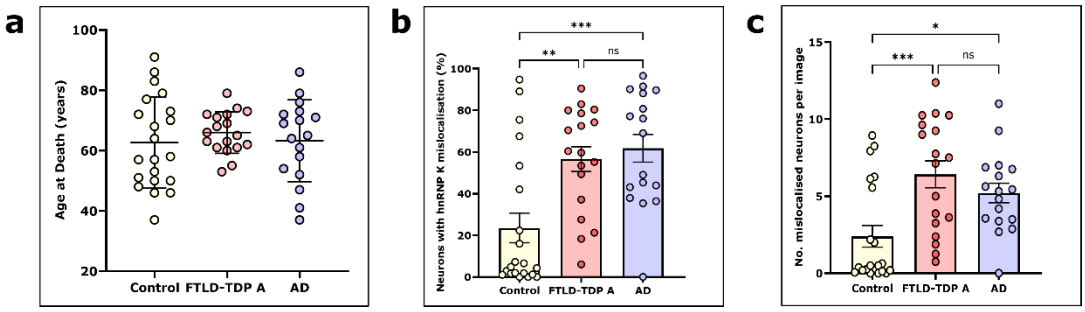

Figure 4.5 HnRNP K mislocalisation quantitation in the dentate nucleus. (a) Control (n = 21), FTLD-TDP A (n = 18) and Alzheimer's disease (AD) (n = 17) cohorts were age-matched with no significant difference between mean age at death. (b) Quantitation of hnRNP K mislocalisation expressed as proportion (%) of neurons with hnRNP K mislocalisation. (c) Equivalent quantitation and analysis expressing hnRNP K mislocalisation as number of neurons per image exhibiting mislocalisation. Individual data points indicate mean data from distinct cases. Error bars show mean ± SD (age at death) or SEM (mislocalisation scores). Ordinary one-way ANOVA with Tukey's post hoc test; *p < 0.05, **p < 0.01, ***p < 0.001, ns = not significant. Adapted from (Sidhu *et al.*, 2022).

4.3.4 Dentate nucleus hnRNP K mislocalisation and ageing

An additional set of controls (n = 31 total) were stained and analysed to investigate the relationship between hnRNP K mislocalisation in the dentate nucleus and age at death. Mislocalisation frequency (%) within control neurons significantly correlated with age at death (r = 0.433, p = 0.011) but this association was not reproduced in either the FTLD-TDP A or AD disease cohorts (**Figure 4.6**).

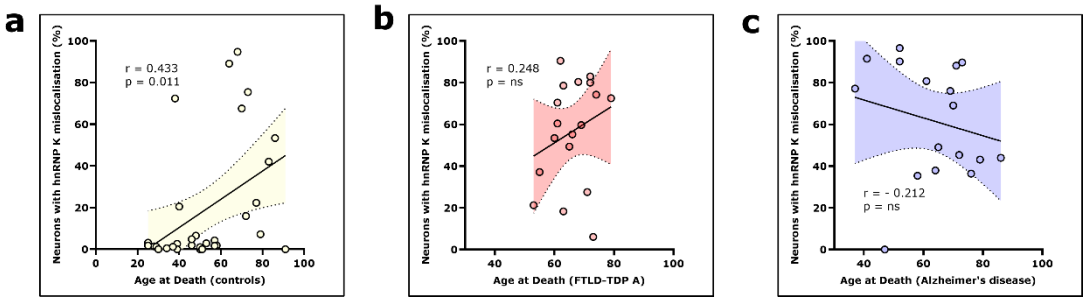

Figure 4.6 HnRNP K mislocalisation in the dentate nucleus and age at death. (a) HnRNP K mislocalisation in control subjects positively correlates with age at death (Pearson's $r = 0.433$, $p = 0.011$) but not in FTLD-TDP A (b) or AD (c) cohorts (ns). Adapted from (Sidhu *et al.*, 2022).

As with pyramidal neurons, there was no intra-group, significant differences in hnRNP K mislocalisation in the dentate nucleus between FTLD or AD cases subdivided into familial and sporadic disease. Notably, the mean age at death of the sAD group was significantly older than the younger onset fAD group but this difference was not found in the FTLD cohort (**Figure 4.7**).

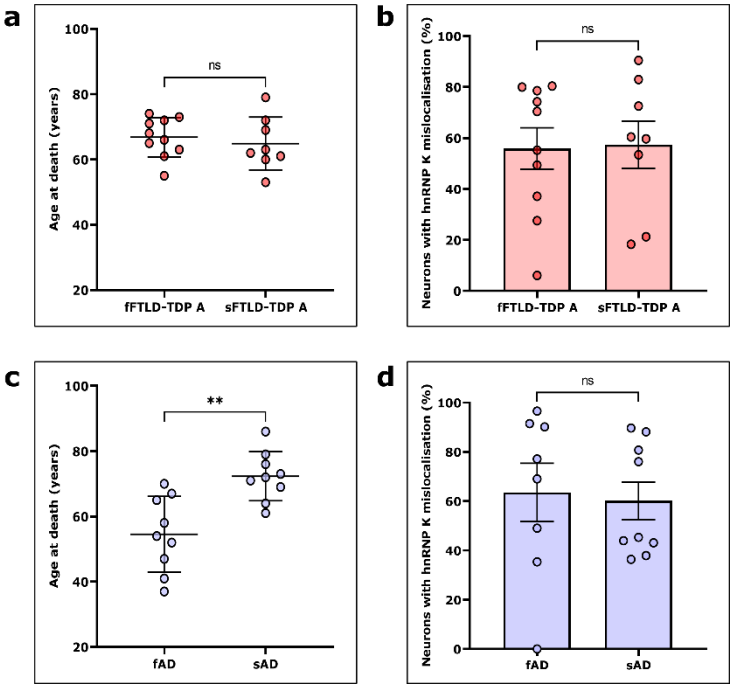

Figure 4.7. HnRNP K mislocalisation in familial and sporadic neurodegenerative disease. The FTLD-TDP A cohort split into familial (fFTLD-TDPA) and sporadic (sFTLD-TDP A) cases exhibited (a) no significant difference in either (a) mean age at death or (b) HnRNP K (dentate nucleus) mislocalisation score. (c) Sporadic (sAD) had a significantly older (72.3 ± 7.6 years) mean age at death than familial AD (fAD) (54.6 ± 11.6 years) cases ($p = 0.001$) but again, there was (d) no significant difference in hnRNP K mislocalisation between the sub-cohorts. Error bars show mean ± SD (age

at death) or SEM (mislocalisation scores). Unpaired t-test; *p < 0.05, **p < 0.01, ***p < 0.001, ns = not significant.

4.3.5 HnRNP K mislocalisation in the dentate nucleus correlates with equivalent mislocalisation in frontal cortex

Neurons within the dentate nucleus were the second studied neuronal subpopulation found to be vulnerable to hnRNP K mislocalisation after pyramidal neurons of the frontal cortex. To determine whether mislocalisation in the dentate nucleus was related to mislocalisation in the cortex, FTLD-TDP A mislocalisation scores from this cohort (**Figure 4.5b**) were correlated against case-matched frontal cortex mislocalisation cores from the previous dataset (**Figure 3.5c**). A significant association (r = 0.520, p = 0.027) was found between matched-case scores (n = 18) suggesting that cases vulnerable to hnRNP K mislocalisation in one brain region are also susceptible to mislocalisation in another (**Figure 4.8**).

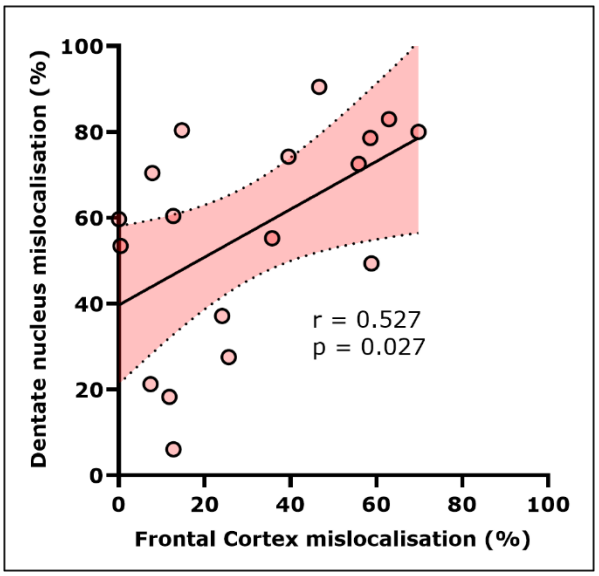

Figure 4.8. HnRNP K mislocalisation correlation between brain regions. HnRNP K mislocalisation in FTLD-TDP A neurons of the dentate nucleus significantly correlates with equivalent mislocalisation in the frontal cortex (Bampton *et al.*, 2021) within case-matched brains (Pearson's r = 0.527, p = 0.027). Adapted from (Sidhu *et al.*, 2022).

4.3.6 HnRNP K localisation and mislocalisation in the hippocampus

The hippocampus was then examined, a structure particularly vulnerable to neurodegeneration in both FTLD and AD disorders. By visual inspection, the dentate gyrus portion of the hippocampal formation stains strongly for nuclear hnRNP K protein in all cases. Neurons within the cornu ammonis (CA1-CA3) subfields also exhibited normal nuclear staining irrespective of control or disease status. Curiously however, in some cases neurons within the CA4 or 'hilar' region were identified as another subpopulation vulnerable to mislocalisation. Once again, afflicted neurons demonstrated robust hnRNP K nuclear depletion and accompanying granular cytoplasmic deposition (**Figure 4.9**).

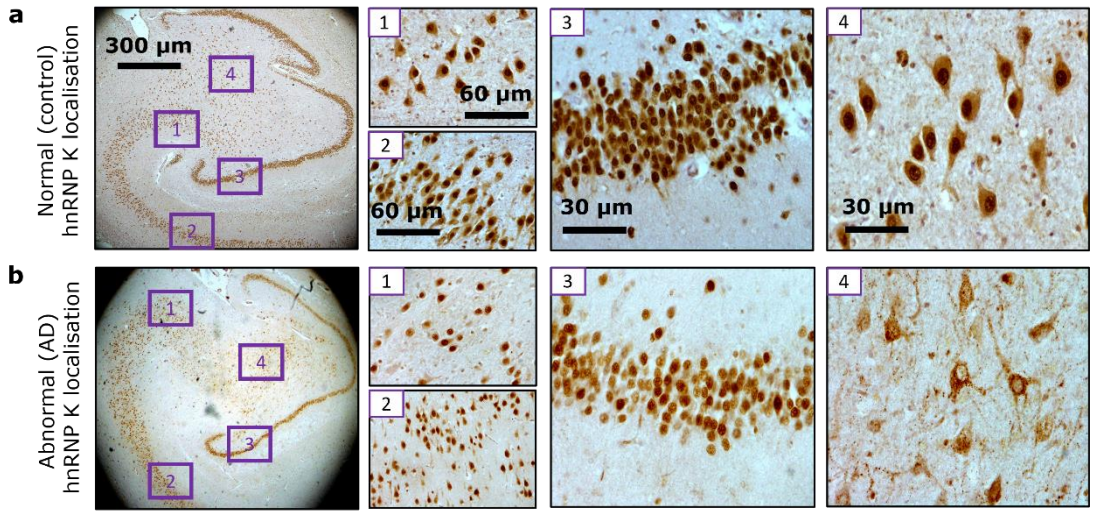

Figure 4.9. HnRNP K localisation in the hippocampus. (a) Normal nuclear localisation of hnRNP K within neurons of the CA3 (1), CA2 (2), dentate gyrus (DG) (3) and the CA4 (4) region of interest in a control (case 61) subject. (b) An AD (case 19) case with normal neuronal staining within CA3, CA2 and DG neurons and abnormal staining within neurons of the CA4 region as defined by hnRNP K nuclear depletion and accumulation of cytoplasmic puncta. Scale bars are as indicated in the first row.

4.3.7 CA4 hnRNP K mislocalisation in Alzheimer's disease and controls

Neurons within the CA4 region were examined more closely within control and neurodegenerative disease brains. There were many control and disease cases which exhibited normal staining. However, there was also a small subset

of cases in both the control and neurodegenerative disease groups which demonstrated the markedly abnormal but familiar cytoplasmic mislocalisation pattern. Within some neurons hnRNP K nuclear clearance was profound (**Figure 4.10**).

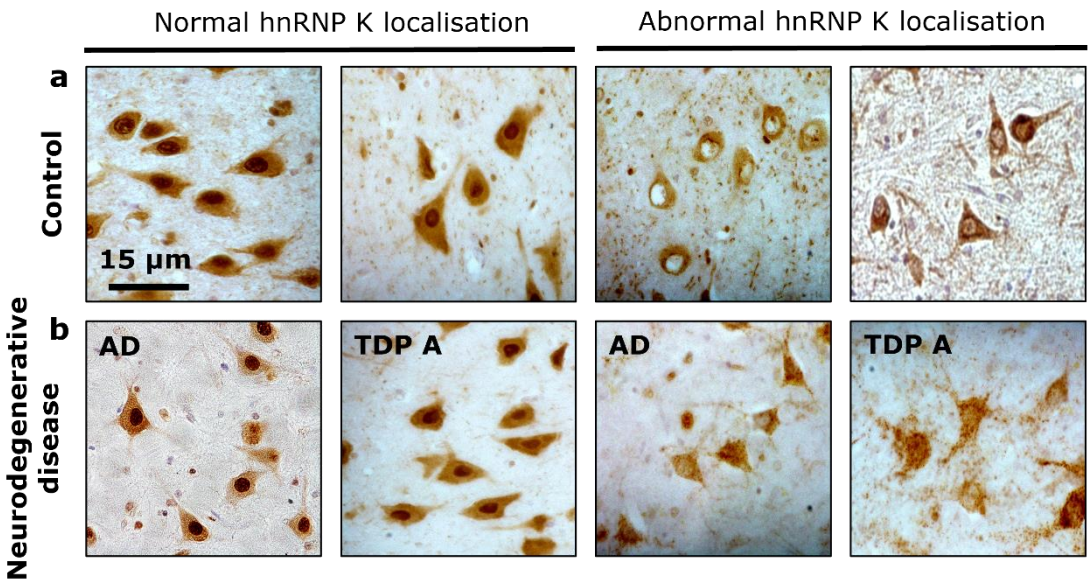

Figure 4.10. Examples of normal and abnormal hnRNP K localisation in the CA4 region of control and neurodegenerative disease cases. (a) Representative images of two normal, nuclear-localised hnRNP K control (left to right, cases 58 and 61) cases and two abnormally-localised control (cases 46 and 62) cases in CA4 hippocampal neurons of control subjects. (b) Equivalent representative images of two normal (left, cases 27 and 12) and two abnormal (right, cases 31 and 4) neurodegenerative disease cases (AD, Alzheimer's disease; TDP A, FTLD-TDP A). Scale bars are as indicated in the first image.

To determine whether there was any difference in mislocalisation frequency between control and disease cohorts, CA4 regions were sampled and analysed as previously described (**4.2.2**) on age-matched control, FTLD-TDP A and AD subjects (**Figure 4.11a**). Using both metrics of neuronal mislocalisation including mislocalisation frequency % and number of mislocalised neurons per image, there were no significant differences between groups (**Figure 4.11b-c**).

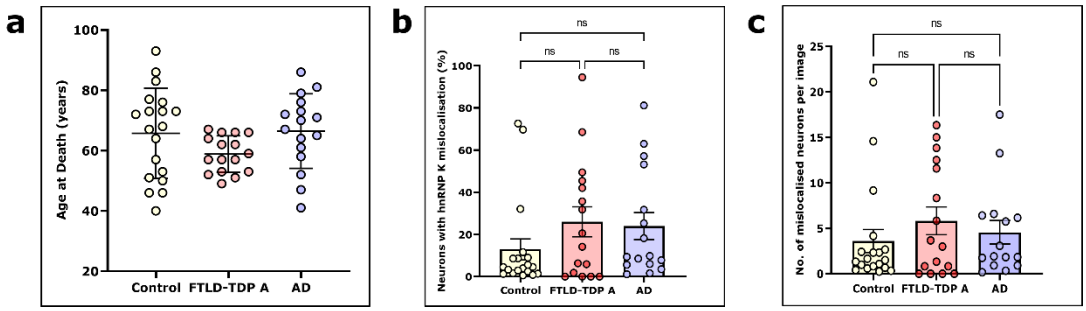

Figure 4.11. HnRNP K mislocalisation quantitation in the CA4 region. (a) Control (*n* = 19), FTLD-TDP A (*n* = 16) and Alzheimer's disease (AD) (*n* = 18) cohorts were age-matched with no significant difference between mean age at death. Quantitation of hnRNP K mislocalisation expressed as proportion (%) of neurons with hnRNP K mislocalisation. (c) Equivalent quantitation and analysis expressing hnRNP K mislocalisation as number of neurons per image exhibiting mislocalisation. Individual data points indicate mean data from distinct cases. Error bars show mean ± SD (age at death) or SEM (mislocalisation scores). Ordinary one-way ANOVA with Tukey's post hoc test; *p < 0.05, **p < 0.01, ***p < 0.001, ns = not significant.

4.3.8 CA4 hnRNP K mislocalisation does not correlate with age at death

Because hnRNP K mislocalisation has previously been found to be associated with age at death in the cortex and the dentate nucleus of control subjects, the same correlational analysis was conducted using CA4 mislocalisation data. However, no association was found between mislocalisation and age in any of the analysed cohorts (**Figure 4.12**).

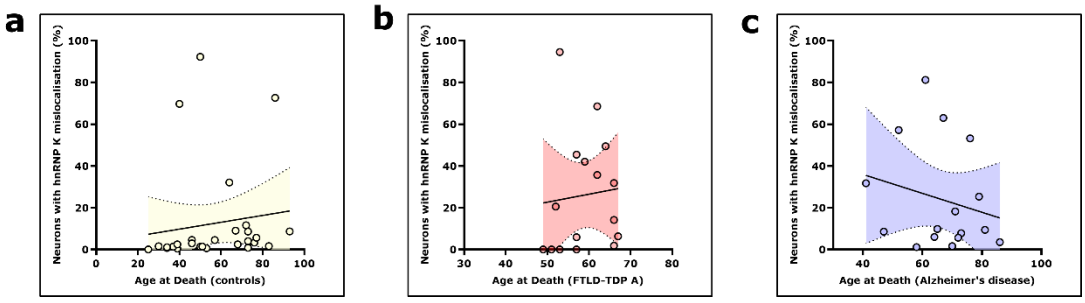

Figure 4.12. HnRNP K mislocalisation in the CA4 region and age at death. HnRNP K mislocalisation in the CA4 region does not correlate with age at death in control (a), FTLD-TDP A (b) or Alzheimer's disease (c) cohorts.

4.3.9 Total number of neurons in dentate nucleus and CA4

One potential reason for why hnRNP K mislocalisation frequency in the dentate nucleus is higher in neurodegenerative disease brains than in age-

matched control cases, but not the case for the CA4 region was thought to be differences in starting number of surviving neurons between cohorts. Therefore cohorts were also compared on the total number (normal + abnormal) of hnRNP K-stained neurons counted per image. As expected being a less pathologically affected region in both diseases, there was no significant difference between total number of neurons counted between control and either disease groups in the dentate nucleus (**Figure 4.13a**). Although unexpectedly there were significantly less neurons counted within AD subjects than in FTLD-TDP A subjects (p = 0.0142). This was in contrast to total neuron count within the CA4 region which was found to be much significantly lower than controls in both the FTLD-TDP A cohort (p = 0.0095) and the AD group (p < 0.0001) in keeping with the hippocampus being a region especially vulnerable to neurodegeneration and atrophy in these diseases (**Figure 4.13b**).

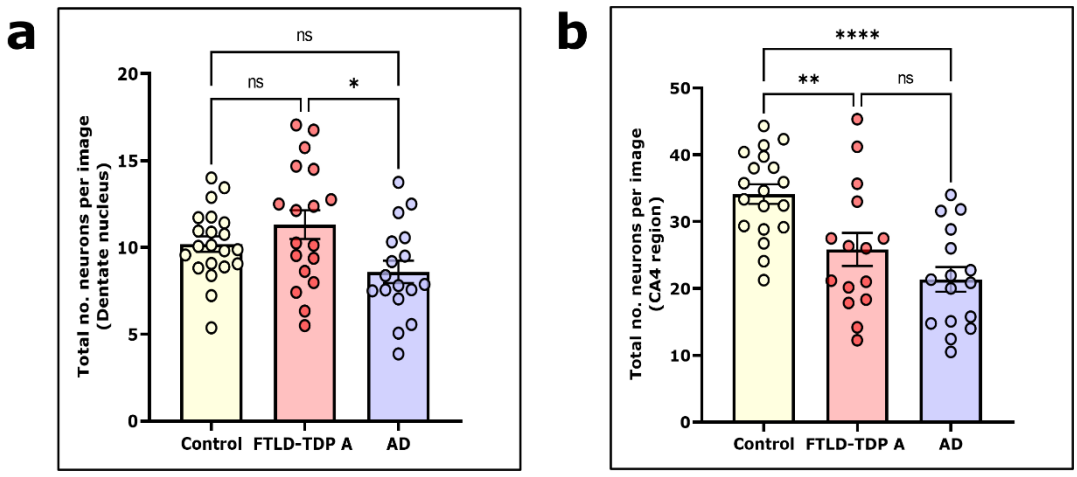

Figure 4.13. Comparing total neuron number in dentate nucleus and CA4 regions. Quantitation of total (normal + abnormal) hnRNP K-stained neurons within age-matched cohorts for both the (a) dentate nucleus and (b) CA4 regions of interest. Individual data points indicate mean data from distinct cases. Error bars show mean ± SEM. Ordinary one-way ANOVA with Tukey's post hoc test; *p < 0.05, **p < 0.01, ***p < 0.001, ns = not significant.

4.4 Discussion

4.4.1 Summary of main findings and relevance to dementia

The pathological findings of this chapter confirm that hnRNP K mislocalisation is not restricted to pyramidal neurons of the neocortex or even indeed to anatomical regions most susceptible to neurodegeneration. The identification of two further neuronal sub-populations vulnerable to hnRNP K mislocalisation, in the dentate nucleus of the cerebellum and the CA4 region of the hippocampus, provides further evidence for hnRNP K pathology being a more widespread phenomenon across the brain than previously thought.

As with earlier analyses within the cortex, hnRNP K mislocalisation in the dentate nucleus was found to be more frequent in neurodegenerative disease than in age-matched controls. This result was not limited to FTLD subjects as before, but also extends to AD cases and hence broadens the relevance of emerging hnRNP K pathobiology to the wider field of dementia.

The dentate nucleus is the largest of the four deep cerebellar nuclei (DCN), located within the deep white matter of each cerebellar hemisphere. It receives input from both cerebellar hemispheres and through projections from the corticopontocerebellar tract of the cerebral cortex. It predominantly outputs through the dentatothalamic tract via the red nucleus and contralateral thalamus prior to termination in the cortex (Bond *et al.*, 2017). Functionally, the dentate nucleus is best known for its well-characterised regulatory roles in the planning, execution and modification of fine motor movements. Indeed disruption of the dentate nucleus is associated with cerebellar ataxia syndrome characterised by impaired balance, gait and abnormal eye movements and also in the pathophysiological underpinning of ALS (Bharti *et al.*, 2020). However, the dentate nucleus and indeed the cerebellum as a whole has also been increasingly implicated in the regulation of non-motor faculties via its ventral domain which has substantial connectivity with several cortical association areas (Matano, 2001). Functional neuroimaging studies in humans have discovered that lesions of the posterior cerebellum in particular are

commonly associated with a ‘cerebellar cognitive affective syndrome’ characterised by impairments in several cognitive domains including executive functioning, verbal fluency, abstract reasoning and working memory as well concomitant language and visuospatial deficits (Schmahmann and Sherman, 1998; Hoche *et al.*, 2018). This syndrome has significant clinical overlap with several neurodegenerative disease presentations including AD and FTD (Chen *et al.*, 2010; Bocchetta *et al.*, 2021). In AD, Although amyloid plaque and neurofibrillary tangle pathology are largely spared within the dentate nucleus except in end-stage disease, damage to DCN and their associated pathways are believed to at least partially account for some of the cognitive manifestations of these diseases (Chen *et al.*, 2010; Olivito *et al.*, 2020). It remains to be clarified whether hnRNP K mislocalisation may serve as a potential pathological correlate of cerebellar-linked cognitive dysfunction in neurodegenerative diseases.

Again, reminiscent of earlier cortical findings, hnRNP K mislocalisation in neurologically normal control subjects is more commonly observed in older individuals (> 60 years), but this relationship with age was not observed in the disease cohorts. This is intriguing because although age-related loss of cerebellar Purkinje neurons and accompanying declines in cognitive and motor performance is well-established, there is no evidence for similar age-related neuronal loss within the dentate nucleus (Hall, Miller and Corsellis, 1975; de Leon and M Das, 2022). This raises the possibility that hnRNP K mislocalisation may be partially neuroprotective in these neurons, although this explanation is less applicable to pyramidal neurons of the cortex analysed previously which are preferentially killed in AD pathogenesis (Hof, Cox and Morrison, 1990; Bekkers, 2011). Interestingly, high or low hnRNP K mislocalisation frequency in the cortex correlated with mislocalisation within the dentate nucleus emphasising the importance of as-yet unclarified patient brain-specific vulnerability or resilience factors in these cases.

HnRNP K mislocalisation in the CA4 region of the hippocampus, which largely contains mossy cells and is actually considered to be an extension of the dentate gyrus, is more enigmatic (Amaral, 1978). Mislocalisation within this

region was found to be a far less common neuropathological event across the whole cohort compared to the dentate nucleus. Moreover and in contrast to previous regions, mislocalisation was not found to be any more frequent in age-matched disease subjects than controls and there was no clear relationship with age at death. One reason for this may be that in contrast to the dentate nucleus, the CA4 region (and the hippocampus more generally) was far more susceptible to cell death in the neurodegenerative process as verified by comparing total (surviving) neuron counts between regions. Indeed neurodegenerative changes (atrophy and misfolded protein deposition) in the hippocampus are observed even in the earliest stages of AD and are variably involved in other diseases including FTLD, dementia with Lewy bodies as well as in normal pathological ageing (Moodley and Chan, 2014). Hence, it could be argued that disease-specific differences in hnRNP K mislocalisation frequency are being strongly diluted by neuronal loss. Additionally, as with neurons of the cortex, it is possible that hnRNP K mislocalisation may not affect all neuronal subtypes equally within the CA4 area. This could mean the analytical approach of quantifying hnRNP K localisation scores across all neurons of the region in one stained section per case may lack the sensitivity required to detect real inter-cohort differences in signal.

4.4.2 Future research avenues

With neurons of the dentate nucleus and the CA4 region of the hippocampus joining pyramidal neurons of the cortex as subpopulations identified as being susceptible to hnRNP K mislocalisation, it will be of mechanistic interest to delineate structural and/or functional similarities between these cell types. Notably, all neurons examined are amongst the largest within their respective brain regions and it may follow that they all have similarly high energetic demands to sustain their metabolism which may increase their vulnerability to RNA-binding protein mislocalisation and dysregulation. Although, this would not explain the specific link to hnRNP K mislocalisation as opposed to, for example TDP-43 protein mislocalisation which typically affects other, smaller neuronal subtypes in neurodegenerative conditions. Indeed, none of the

neuronal subpopulations identified as being vulnerable to mislocalisation are typically associated with any other disease-associated proteinaceous inclusions which may be of mechanistic interest in itself. Characterisation studies aimed at identifying key links between neuronal subtypes that may include other morphological factors, neurotransmitter profiles or other shared histological features may shed light on why these neurons are especially associated with hnRNP K dysfunction.

With respect to the age-associated nature of hnRNP K mislocalisation within controls in the dentate nucleus, it will be of special interest to determine which factors determine the predisposition to hnRNP K mislocalisation in different individuals and disease statuses at varying ages. Clearly, hnRNP K pathology in different neuronal contexts is not a disease-specific or 'normal' ageing-specific neuropathological feature but rather one that is overrepresented in these demographics. The uncovering of other physiological or genetic correlates to differential hnRNP K localisation profiles will be crucial in demystifying this event. The former of which may require the deployment of neuronal cell models to assess phenotypic differences in neurons that mirror the *in vivo* observations of hnRNP K nuclear depletion or cytoplasmic localisation.

As discussed previously, the development of a hnRNP K neuronal knockdown model which encapsulates the pathological nuclear loss of hnRNP K protein in afflicted neurons is essential to more thoroughly interrogate the wider functional consequences of hnRNP K nuclear depletion in neurons. The next chapter invokes a model matching this brief which becomes a platform for assessing splicing function and dysfunction in hnRNP K-depleted neurons, a vital metabolic function performed by many if not all protein members of the hnRNP family.

Chapter 5 Developing a hnRNP K neuronal knockdown model

5.1 Introduction

5.1.1 Statement of contribution

The results from RNA-sequencing and associated data plots presented in this chapter (**5.3.5** - **5.3.6**) were performed and generated by collaborator Dr Jack Humphrey (Icahn School of Medicine at Mount Sinai, New York).

5.1.2 Background

Multiple immunohistochemical investigations have now confirmed that several neuronal sub-populations throughout the brain are vulnerable to hnRNP K mislocalisation. Brains afflicted with neurodegenerative disease and elderly control subjects are disproportionately affected. HnRNP K mislocalisation in all neuronal sub-populations examined including pyramidal neurons of the cortex and neurons within the dentate nucleus share a common neuropathological staining profile. Typically, afflicted neurons exhibit profound nuclear depletion of hnRNP K and granular deposition to the surrounding cytoplasm. Although hnRNP K continuously shuttles between the nucleus and the cytoplasm, it is known, as is the case with all hnRNPs, to predominantly reside in the nucleus at steady state (Michael, Choi and Dreyfuss, 1995). It therefore follows that neurons with mislocalised hnRNP K might be expected to elicit a nuclear hnRNP K loss of function phenotype. The goal of this section of work was to develop a neuronal cell model that recapitulates this nuclear depletion. We recently utilised an siRNA-mediated system of hnRNP K knockdown that strongly suppressed hnRNP K expression within human neuroblastoma SH-SY5Y cells (Bampton *et al.*, 2021). This model provided some preliminary evidence for hnRNP K having an important role in splicing regulation within RNA targets, but we now wanted to assess the role of hnRNP K-regulating

splicing within a more cell-type specific model of hnRNP K depletion in human-derived cortical neurons.

CRISPR-interference (CRISPRi) was selected for the purpose of this model as an inexpensive technique capable of robustly and specifically repressing gene expression at the transcriptional level with minimal associated toxicity (Tian *et al.*, 2019). The work described in this chapter utilises a CRISPRi-constitutively expressing i^3-iPSC line. i^3-iPSCs harbour an inducible neurogenin 2 (*NGN2*) transcription factor transgene integrated at the AAVS1 safe harbour loci which, when expressed, rapidly converts iPSCs into glutamatergic, cortical neurons with high reproducibility (Wang *et al.*, 2017; Fernandopulle *et al.*, 2018).

NGN2 is a master regulator of neurogenesis with several major roles in the commitment of progenitors to neurons including; the inhibition of glial fate (Sun *et al.*, 2001), promotion of cell cycle exit (Farah *et al.*, 2000), promotion of neuronal migration as well as the activation of many other neuronal genes (Ge *et al.*, 2006; Seo *et al.*, 2007). The biological relevance of neurons derived by forced *NGN2* overexpression has been questioned in contrast to those generated through more traditional, extrinsic factor-mediated differentiation protocols that attempt to recapitulate events in embryonic development (Hulme *et al.*, 2022). However, despite the skipping of multiple intermediate stages from pluripotency to neural precursor cells, this more direct differentiation model successfully yields electrophysiologically active neurons within 14 days (Zhang *et al.*, 2013; Busskamp *et al.*, 2014), albeit lacking the more complex spiking activity exhibited by neurons derived by dual-SMAD inhibition protocols (Rosa *et al.*, 2020). Furthermore, co-culture of inducible-neurons with astrocytes promoted the formation of more morphologically and electrophysiologically mature synapses (Fernandopulle *et al.*, 2018; Chen *et al.*, 2020). A recent study has challenged the proposed purity of cortical i^3-neurons. Indeed, considerable heterogeneity was identified (including the presence of neurons of the peripheral nervous system) within neuronal populations derived from multiple clones and cell lines using single-cell transcriptomics to dissect the molecular profiles of *NGN2*-induced neurons at numerous developmental stages (Lin *et al.*, 2021). Alternatively, these findings

may simply highlight the high sensitivity of neuronal fate acquisition in these neurons to extrinsic factors such as methodological rigour; emphasising the importance of meticulous cell culture technique and attention to detail in the maintenance of these cells. Nevertheless, the resulting i^3-iPSC-derived cortical neurons were favoured as a good model for the cortical pyramidal neurons (also excitatory) which have since been identified as a neuronal cell type particularly susceptible to hnRNP K mislocalisation in the human brain.

5.2 Methods

5.2.1 CRISPRi-induced knockdown protocol

HNRNPK and *TARDBP*-targeting sgRNAs (Horlbeck *et al.*, 2016) were cloned into CRISPRi-cassette containing (B3-CRISPRi) constructs (Tian *et al.*, 2019) as previously described in **2.2**. Then, sgRNA-containing (CRISPRi-sgRNA) constructs were packaged into lentiviral constructs (**2.3.7**) and delivered to CRISPRi-iPSCs via lentiviral transduction (**2.3.8**) which were then induced into cortical neurons (**2.3.9**). HnRNP K protein and mRNA levels were assessed at various developmental stages by immunocytochemistry (**2.3.11**), western blot (**2.3.12**) and RT-qPCR (**2.3.13**).

5.2.2 RNA-sequencing and analysis

RNA was purified from CRISPRi-i^3 hnRNP K knockdown neurons prior to sequencing (paired-ends, 150 bp) by UCL Genomics. All samples were aligned to the GRCh38 genome using STAR (v2.7.2) (Dobin *et al.*, 2013) with GENCODE v30 (Frankish *et al.*, 2019) as the transcript reference (**2.4.3**-**2.4.5**). Gene expression was quantified using RSEM (v1.3.1) (Li and Dewey, 2011) using gene models from GENCODE v30 and differential expression was performed on all samples using the standard DESeq2 workflow (Love, Huber and Anders, 2014) (**2.4.6**).

5.3 Results

5.3.1 Optimisation of a CRISPRi knockdown protocol

The Tian et al. protocol for CRISPRi knockdown was utilised to knockdown hnRNP K protein in CRISPRi-i^3 cortical neurons with substantial modifications and optimisations at all major stages from lentiviral production to neuronal differentiation and maintenance (Tian *et al.*, 2019) (**Figure 5.1**, **Table 5.1**).

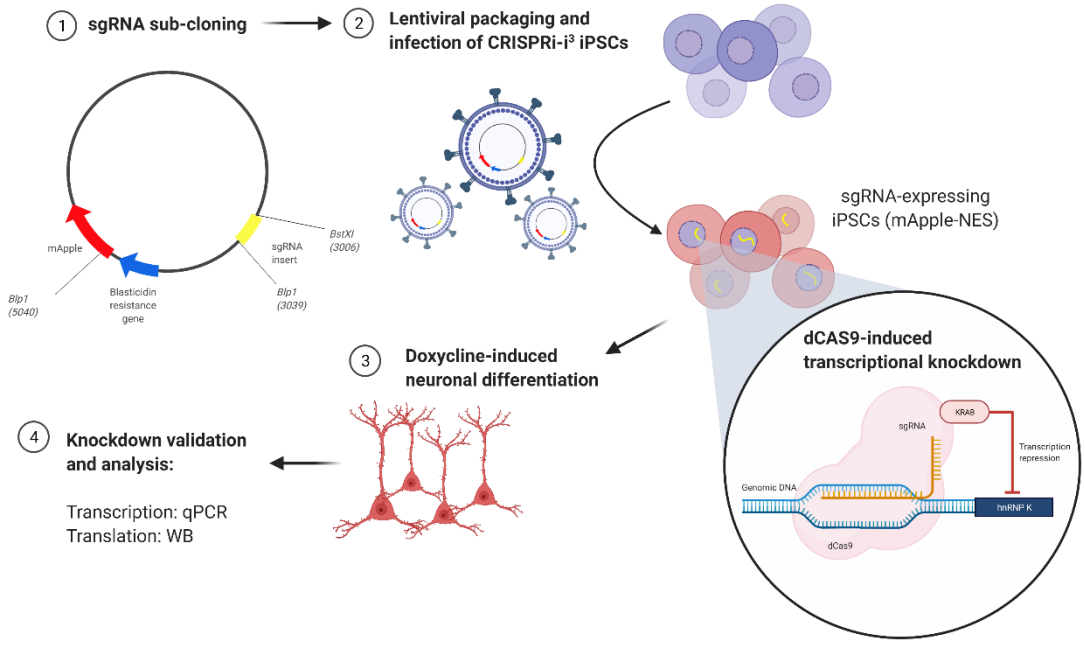

Figure 5.1. Overview of strategy for CRISPRi-induced gene knockdown in inducible i^3 neurons. A hnRNP K knockdown iPSC model was generated using the previously described CRISPR-interference (CRISPRi)-based platform (Tian *et al.*, 2019). Single guide RNAs (sgRNAs) with high predicted on gene (*HNRNPK*) target activity were sub-cloned into B3-CRISPRi constructs and packaged into high-titre lentiviral particles. CRISPRi-i^3 iPSCs were transduced and allowed to briefly recover. Neuronal differentiation of transduced iPSCs was doxycycline-induced to generate a polyclonal population of glutamatergic (cortical) neurons (Fernandopulle *et al.*, 2018). Transcriptional and translational confirmation of hnRNP K knockdown at both the iPSC stage and numerous passages of differentiated neurons was determined by qPCR and immunoblotting. A TDP-43 knockdown iPSC model was generated in parallel by Benedikt Holbling using a previously validated (Brown *et al.*, 2022) *TARDBP* sgRNA.

Table 5.1. Optimisation of CRISPRi knockdown protocol (Tian *et al.*, 2019). for hnRNP K knockdown in CRISPRi-i^3 neurons.

Protocol step	Feature modified or optimised	Rationale
Lentiviral production	Removed the viral concentration (Lenti-X concentrator) step. iPSCs transduced with standard virus-containing supernatant during a half media (1:1) change.	Lenti-X concentrated virus was found to be highly toxic to iPSCs at several dilutions.
	Selection of most efficient *HNRNPK*-targeting lentivirus.	Two *HNRNPK*-targeting sgRNA-containing constructs were successfully packaged into lentiviral constructs. However, one construct was associated with consistently higher transduction efficiency and was used from here on in. Only one (validated) *TARDBP*-targeting construct was employed.
Lentiviral transduction	CRISPRi cells transduced at the iPSC stage were plated at 250-300,000 per well of a 6-well plate.	Lentiviral transduction of early neurons (post-induction) resulted in poor transduction efficiency and high toxicity. iPSC density was found to be an important determinant of transduction efficiency with > 500,000 cells per well leading to poor transduction rate.
	Incorporated addition of DEAE-dextran sulfate (Sigma-Aldrich) at lentiviral transduction stage at a final concentration of 10 µg / ml plus RevitaCell supplement (1:100).	Dextran sulfate addition was found to boost transduction efficiency in iPSCs by as much as ~20-50 % and RevitaCell was found to promote cell survival post transduction.
Antibiotic selection	Removed blasticidin (50 - 100 µg / ml) selection step after lentiviral delivery.	Blasticidin enrichment was very weak even at the highest attempted dosage with accompanying elevated toxicity. For best results, high > 90 % initial transduction efficiency was ensured. Nb. Additional re-application of virus was associated with elevated cell death.
Neuronal differentiation	iPSC induction with doxycycline-spiked media changed from 2 days post-transduction to rapid (< 2 hours) post-transduction.	Delays associated with reduced transduction efficiency (and therefore knockdown) potentially due to a partial dilution effect of dividing (non-induced and non-transduced) cells.
Neuron maintenance	Cortical neuron culture medium switched from Neurobasal™	Neuronal cultures differentiated with BrainPhys™ media displayed more

	(Gibco 12348017) to BrainPhys™ (StemCell Technologies) media.	extensive neurite outgrowth relative to Neurobasal™ cultures. Neurobasal media was also found to impair electrophysiological maturation and synaptic functioning (Bardy *et al.*, 2015; Zabolocki *et al.*, 2020).

5.3.2 CRISPRi-induced hnRNP K knockdown in iPSCs and early neurons

Firstly, CRISPRi-i^3 iPSCs were transduced with *HNRNPK* or control (scramble) sgRNA-containing lentiviral constructs and immunocytochemistry was employed to compare protein distribution in transduced (mApple-expressing) and non-transduced iPSC cells (**Figure 5.2**). *HNRNPK*-sgRNA transduced cells demonstrated a clear reduction in nuclear hnRNP K relative to both uninfected neighbouring cells and those transduced with the non-targeting (control) sgRNA construct. Interestingly, *HNRNPK*-sgRNA cells appeared to exhibit, at least a partial redistribution of hnRNP K from the nucleus to the cytoplasm (**Figure 5.2b**).

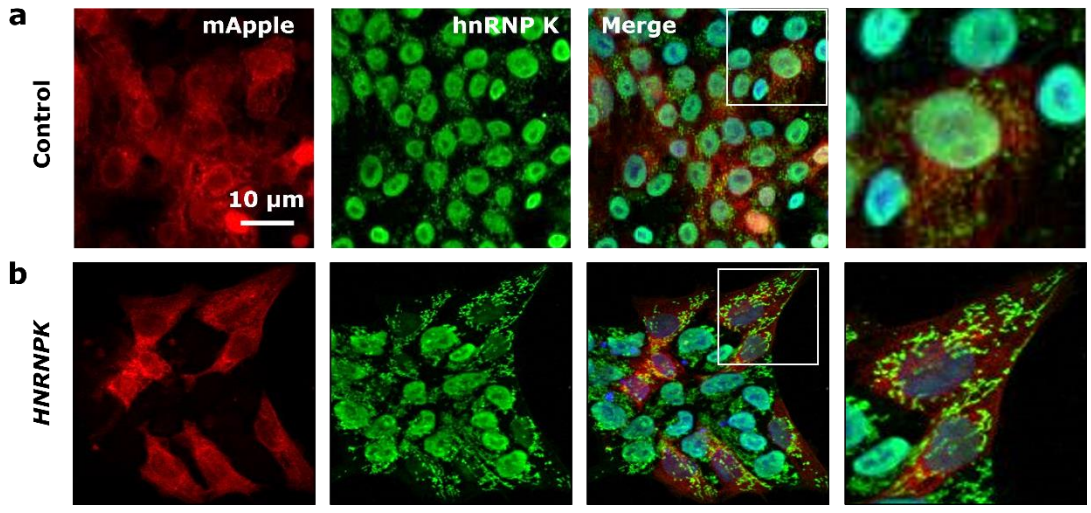

Figure 5.2. Transduction of sgRNA-carrying constructs into CRISPRi-i^3 iPSCs. Representative immunofluorescence images of CRISPRi-i^3 iPSCs demonstrating (a) stable hnRNP K protein (green) expression in both control-sgRNA transduced (mApple expressing) and un-transduced (non-mApple expressing) cells and in (b) marked nuclear depletion of hnRNP K in *HNRNPK*-sgRNA transduced cells compared to un-transduced cell neighbours consistent with hnRNP K protein knockdown.

Freshly plated CRISPRi-i^3 iPSCs were then transduced and rapidly induced into early neurons (neural precursor cells, NPCs) and one well per condition was kept for assessing protein hnRNP K levels by immunoblotting at 72 h post-induction. A *TARDBP*-sgRNA transduced well was also included to assess the specificity of the hnRNP K knockdown. Transduction efficiency was high for all guides (> 90 %) at the NPC stage (**Figure 5.3**). HnRNP K protein levels were dramatically and specifically reduced in *HNRNPK*-sgRNA NPCs compared to the control guide (93 % knockdown) and only very modestly reduced (11 %) in *TARDBP*-sgRNA expressing cells (**Figure 5.4a-b**). This knockdown was even more robust than the TDP-43 protein knockdown observed in NPCs transduced with the (validated) *TARDBP*-sgRNA construct (**Figure 5.4c**).

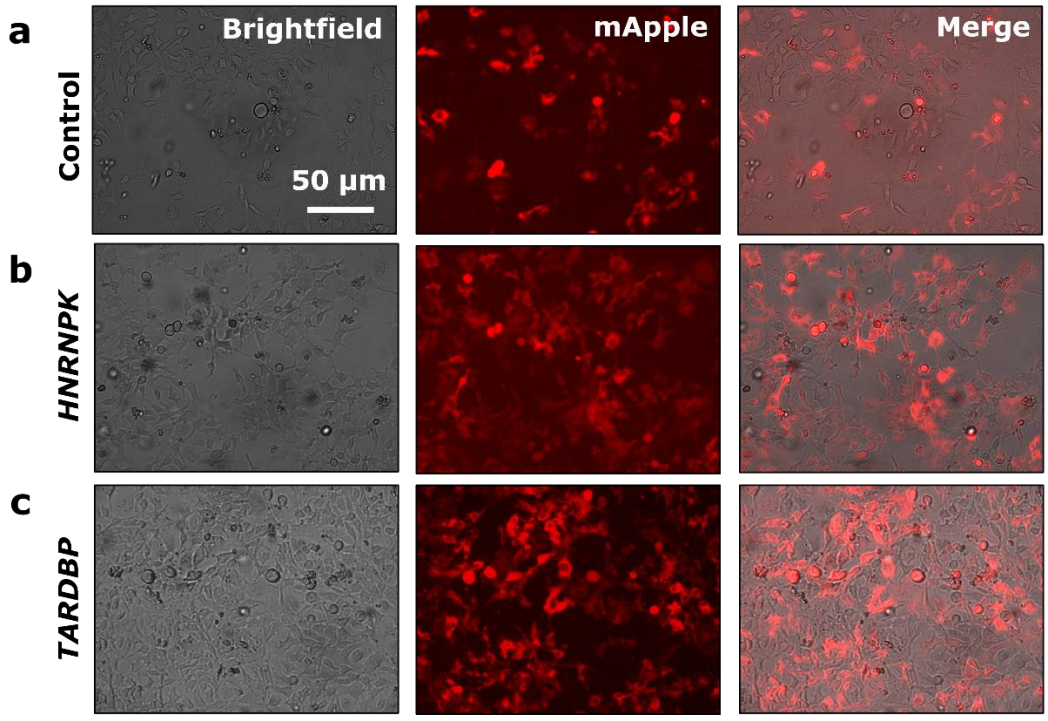

Figure 5.3. Transduction efficiency of sgRNA-carrying constructs in CRISPRi CRISPRi-i^3 NPCs. Representative images of high transduction efficiency of (a) control, (b) *HNRNPK* and (c) *TARDBP*-targeting sgRNA constructs in CRISPRi-i^3 neural precursor cells (NPCs) at 72h post-induction.

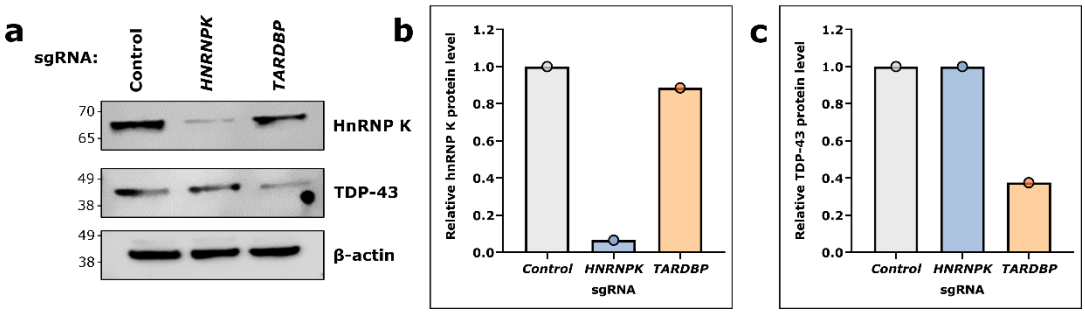

Figure 5.4. Robust and specific hnRNP K protein knockdown in NPCs. (a) Immunoblot of hnRNP K and TDP-43 protein levels in CRISPRi-i^3 NPCs shown in Figure 5.3 and densitometry plots quantifying (b) hnRNP K and (c) TDP-43 protein levels relative to β-actin loading control.

5.3.3 CRISPRi-induced hnRNP K knockdown in mature neurons

Following validation of hnRNP K protein knockdown in NPCs, fresh CRISPRi-i^{3}s iPSCs (*n* = 4 control, *n* = 4 *HNRNPK*) were plated, transduced and allowed to differentiate into mature (> day 7) cortical neurons prior to harvest (day 10) (**Figure 5.5a**). High transduction efficiency (> 80 %) was maintained across wells (**Figure 5.5b-c**). HnRNP K protein and RNA were collected for knockdown validation and RNA-sequencing. HnRNP K protein levels remained diminished in *HNRNPK*-sgRNA neurons (63 % mean knockdown) relative to control neurons at this time point (**Figure 5.6a-b**). Intriguingly however, *HNRNPK* mRNA levels only showed a trend towards knockdown (**Figure 5.6c**).

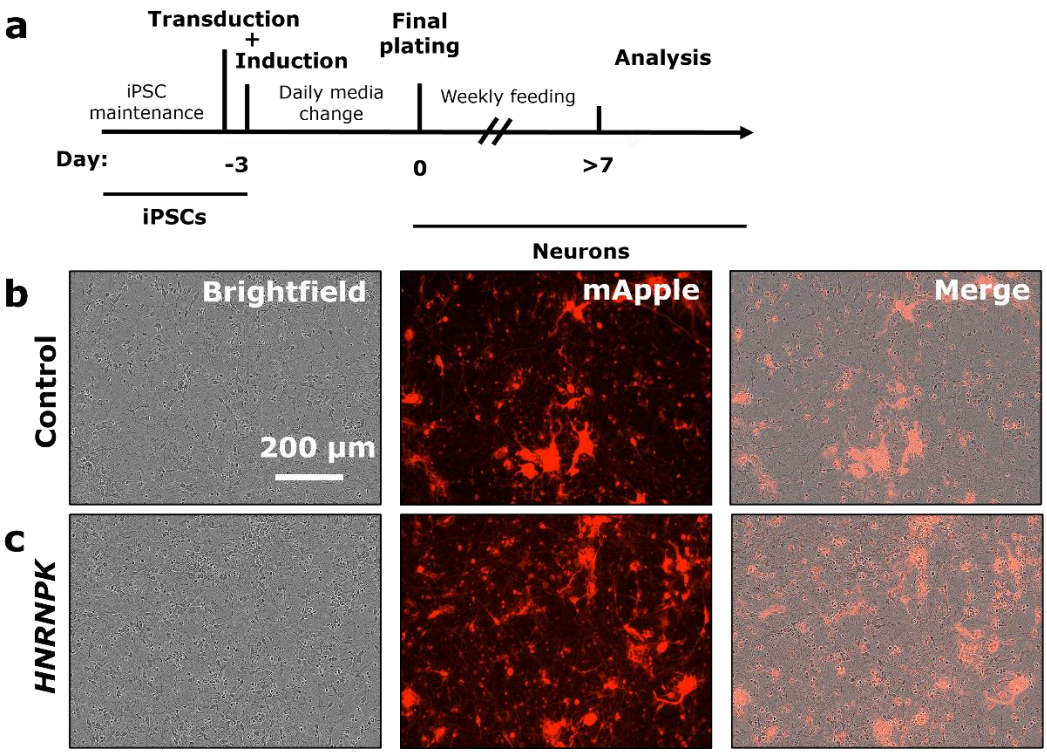

Figure 5.5. Transduction efficiency of sgRNA-carrying constructs in CRISPRi CRISPRi-i^3 neurons. (a) Timeline for sgRNA transduction, doxycycline-induced neuronal differentiation and analysis of CRISPRi-i^3 iPSCs and neurons. Representative images of high transduction efficiency of (a) control and (b) *HNRNPK*-targeting sgRNA constructs in CRISPRi-i^3 day 8 neurons.

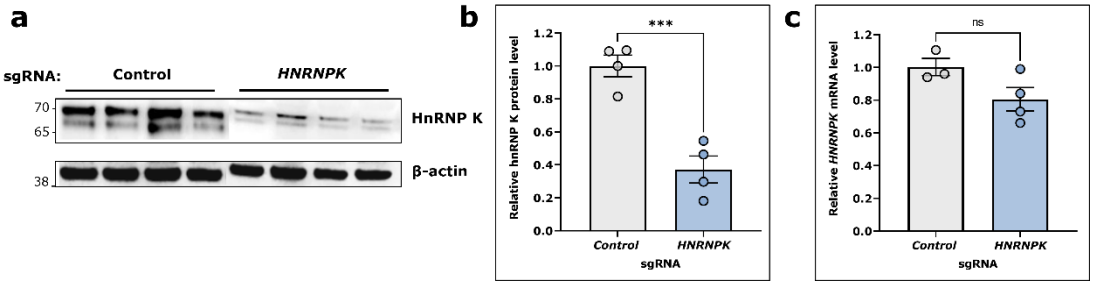

Figure 5.6. HnRNP K protein knockdown in mature (day 10) neurons. (a) Immunoblot of hnRNP K protein levels in day 10 CRISPRi-i^3 and (b) accompanying densitometry plot quantifying hnRNP K protein levels relative to β-actin loading control demonstrating strong hnRNP K knockdown (63 % mean knockdown, $p = 0.0010$). (c) By contrast, *HNRNPK* mRNA levels as quantified by RT-qPCR and normalised to *RPL18A* housekeeping gene, were not significantly reduced in neurons from the same experiment as shown in **Figure 5.5**. Error bars show mean ± SD (age at death) or SEM (mislocalisation scores). Unpaired t-test; *p < 0.05, **p < 0.01, ***p < 0.001, ns = not significant.

HNRNPK-sgRNA neurons are henceforth referred to as hnRNP K knockdown (KD) neurons. RNA-sequencing was then performed on RNA purified from hnRNP K KD (n = 4) and control (n = 4) neurons.

5.3.4 RNA quality control

All samples passed TapeStation quality control with a mean RNA integrity number (RIN) of 9.2 ± 0.2 (**Figure 5.7**).

a

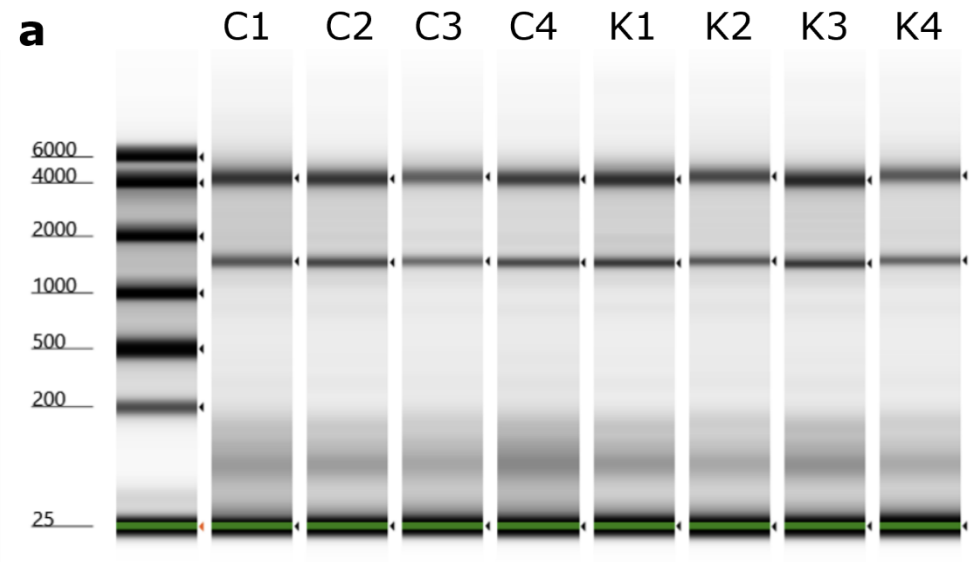

b

Sample	28S / 18S (Area)	RIN
Control 1	1.7	8.9
Control 2	1.7	9.2
Control 3	1.8	9.0
Control 4	1.7	9.2
HnRNP K KD 1	1.9	9.5
HnRNP K KD 2	1.7	9.0
HnRNP K KD 3	1.7	9.4
HnRNP K KD 4	1.6	9.0

Figure 5.7. TapeStation RNA quality control. (a) RNA quality of each sample (controls, C1-4; hnRNP K KD, K1-4) was assessed by calculating the relative abundance of 28S (higher band) and 18S (lower band) ribosomal (r)RNA from capillary electrophoresis peak area measurements as visualised by TapeStation. (b) Summary table of TapeStation quality control metrics for each sample as generated

from respective RNA electropherogram traces. A 28S/18S ratio of ~1.7 and computed RIN value of ~10 is associated with high RNA quality and minimal RNA degradation.

5.3.5 HnRNP K knockdown leads to widespread gene expression changes.

First, principal component analysis (PCA) of gene expression was conducted to visualise variation between control and hnRNP K KD samples. Principal component 1 (PC1) explained 22.7 % of gene expression variation and demonstrated a separation between treatment groups (**Figure 5.8**).

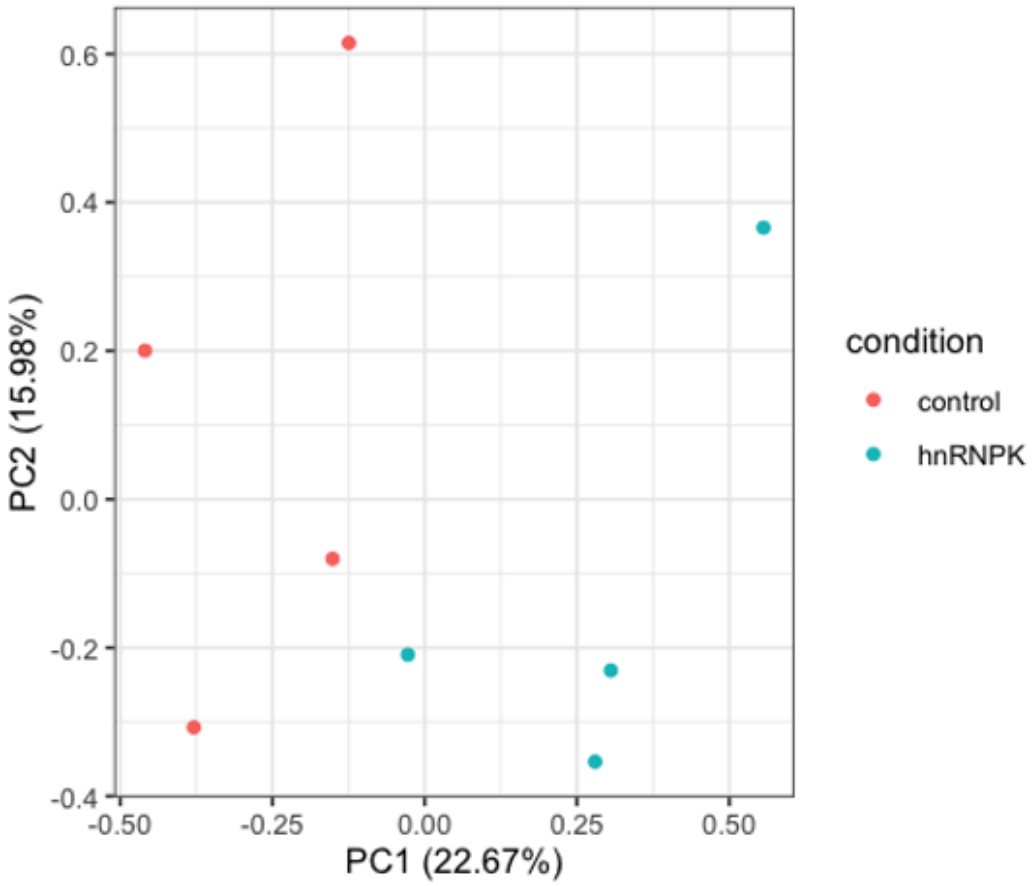

Figure 5.8 Principal component analysis. Samples show separation by treatment (control, red; hnRNP K KD, blue).

Differential expression analysis by DESeq2 demonstrated that hnRNP K protein knockdown was associated with reasonably widespread changes in the transcriptome including 209 differentially expressed genes (DEGs) with a Benjamini-Hochberg false discovery rate (FDR) < 0.05 (**Figure 5.9a)**. This

included 122 upregulated and 87 downregulated genes (**Appendix 2**). Although the magnitude of expression changes was comparably small with just 10 of these differentially expressed genes exhibiting a |log2FoldChange| > 1 (**Figure 5.9b**). Only a very modest reduction in *HNRNPK* expression itself (9 %) was detected, consistent with earlier RT-qPCR findings.

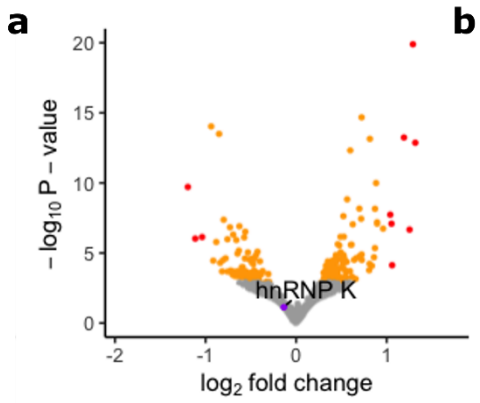

Differentially expressed genes	FDR < 0.05	FDR < 0.05, |LFC| > 1
Total	209	10
Up	122	7
Down	87	3

Figure 5.9. Differential gene expression results. (a) Volcano plot of gene expression changes associated with hnRNP K protein knockdown (FDR < 0.05, genes coloured orange/red; FDR < 0.05, |LFC| > 1, genes coloured red only). (b) Summary table of differentially expressed genes (DEGs) fulfilling each criterion.

DEGs from this dataset were then compared to DEGs from our previously validated hnRNP K KD SH-SY5Y model (Bampton *et al.*, 2021) to assess overlap. A total of 13,013 genes were tested in both models, and 79 genes were found to be differentially expressed (FDR < 0.05 in both) in both models. The direction of the $\log_2$ fold changes (LFCs) associated with each shared DEG were concordant for 54 out of the 79 genes (68 %) and the LFCs had some correlation between models (r = 0.26, p = 0.022) with a notably attenuated effect size (LFC) in the present CRISPRi-i^3 neuronal model (**Figure 5.10**).

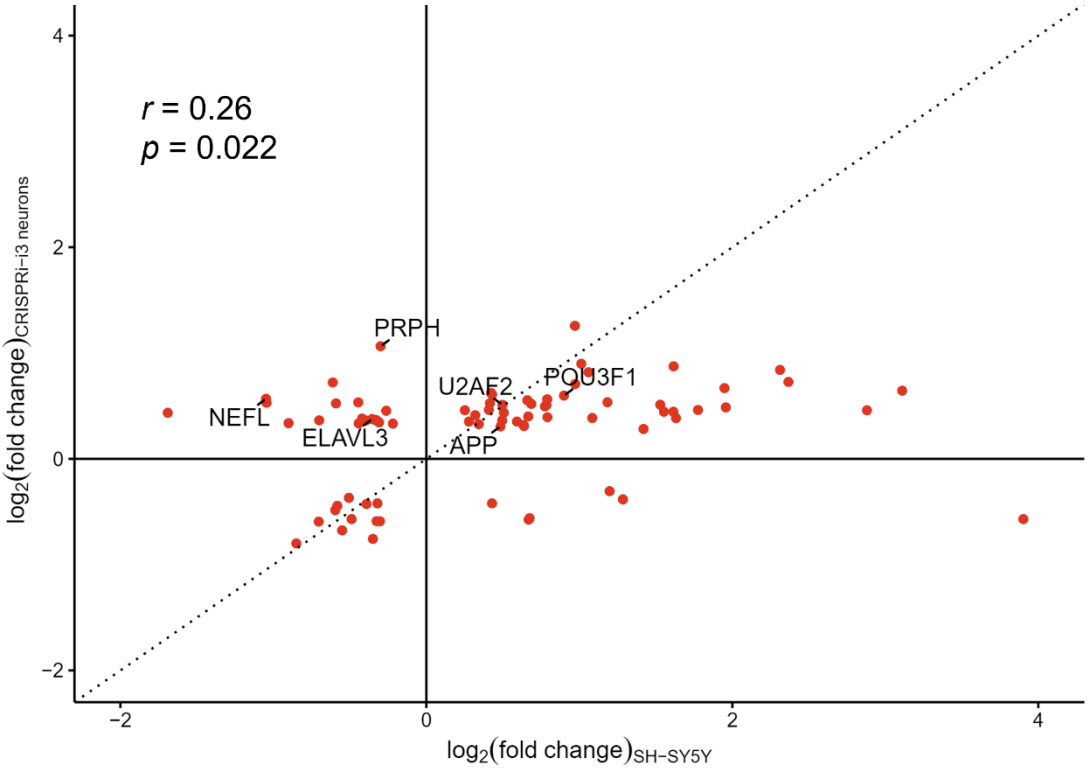

Figure 5.10. Concordance between differentially expressed genes (DEGs) in two hnRNP K knockdown models. 79 of the 209 DEGs identified in CRISPRi-i^3 neurons (the present study) were also differentially expressed in SH-SY5Y siRNA cells (Bampton *et al.*, 2021) with a positive correlation (r = 0.26, p = 0.022) between LFCs, albeit much attenuated in the present model. DEGs of interest from gene ontology (GO) analysis below are indicated.

5.3.6 Gene Ontology of DEGs

Next, Gene Ontology (GO) enrichment analysis was performed to determine whether the identified DEGs were associated with any particular molecular pathways and functions.

GO terms were only enriched within the upregulated gene population and the majority of these related to neuronal function and physiology (**Table 5.2**)**.** Of the 122 upregulated genes, 91 could be matched to genes within the GO Biological Process ontology and 89 to Cellular Component. Notably, several upregulated genes including Tubulin Beta 3 Class III (*TUBB3*), POU Class 3 Homebox 1 (*POU3F1*), Neurofilament light chain (*NEFL*) and ELAV-like protein 3 (*ELAVL3*) are specifically associated with neuronal cell architecture and neural development. Several others are known to be associated with one

or multiple neurodegenerative diseases including amyloid precursor protein (*APP*; Alzheimer's Disease), Peripherin (PRPH; ALS), U2 Small Nuclear RNA Auxillary Factor 2 (*U2AF2*; FTLD and Spinocerebellar Ataxia) as well as the aforementioned *POU3F1* (Charcot-Marie-Tooth disorder and a marker of Von Economo neurons, preferentially affected in bvFTD), *NEFL* (general marker of neurodegeneration) and *ELAVL3* (ALS) (Leung *et al.*, 2004; Gaetani *et al.*, 2019; Hodge *et al.*, 2020; Diaz-Garcia *et al.*, 2021).

Table 5.2. GO terms enriched in upregulated genes.

Go term	Query	*p*-value	Term size	Query size	Intersection size
Axon	UP	6.482×10^{-7}	661	91	18
Distal axon	UP	8.499×10^{-6}	307	91	12
Neuronal cell body	UP	6.089×10^{-5}	523	91	14
Growth cone	UP	8.368×10^{-5}	185	91	9
Site of polarized growth	UP	1.096×10^{-4}	191	91	9
Cell body	UP	2.866×10^{-4}	595	91	14
Cell junction	UP	3.725×10^{-4}	2107	91	27
Neuron projection	UP	5.827×10^{-4}	1384	91	21
Nervous system development	UP	2.645×10^{-3}	2484	89	30
Somatodendritic compartment	UP	5.394×10^{-3}	875	91	15
Neuron recognition	UP	7.701×10^{-3}	48	89	5
Cell projection	UP	8.235×10^{-3}	2337	91	26
Neurogenesis	UP	1.071×10^{-2}	1698	89	23
Plasma membrane bounded cell projection	UP	1.127×10^{-2}	2234	91	25

Perikaryon	UP	3.908×10^{-2}	160	91	6
Forebrain development	UP	4.629×10^{-2}	392	89	10
Axogenesis	UP	4.653×10^{-2}	479	89	11

Term size, number of genes in the term; Query size, number of genes used as input; Intersection size, number of genes in both the term and query.

5.4 Discussion

5.4.1 Summary of main findings

CRISPRi technology was utilised to successfully and strongly knockdown hnRNP K protein levels within inducible (i^3) cortical neurons. The generated CRISPRi-i^3 neurons thus serve as a suitable cell model for future exploration of the functional consequences following hnRNP K nuclear loss as observed pathologically in the human brain. Subsequent differential expression analysis of RNA-seq derived data from hnRNP K KD neurons revealed perturbed gene expression within a large number of genes despite only modest reductions in *HNRNPK* mRNA levels itself. GO analysis identified many neuronal terms enriched within the upregulated portion of hnRNP K KD-associated DEGs. Several such neuronal genes have been strongly implicated in neurodegeneration.

5.4.2 Suitability of the model and future directions

HnRNP K protein was successfully knocked down within mature cortical neurons. Hence, the neurons recapitulate the hnRNP K nuclear depletion observed within neurons identified as mislocalised in the human brain. To this end, the model was a success which opens the doors to a host of potential follow-up investigations including transcriptomics and phenotypic screens. However, it should also be noted that there are several caveats, biological and otherwise, to such a model which require some consideration for both interpretation of any future data arising from the model and/or the future use of CRISPRi-i^3 neurons as a reliable system for genetic perturbation in general.

Firstly, the optimised protocol necessitates that sgRNA-transduction occurs in advance of neuronal induction, i.e. whilst cells are still at the iPSC stage. Attempts to transduce early neurons (post-induction) resulted in low transduction efficiency and high lethality. Therefore, the gene of interest is already repressed in cells prior to them being forced through *NGN2*-induced differentiation. This has the potential to disrupt normal neuronal differentiation, which in-turn may skew resulting transcriptomic changes towards developmental pathways instead of reflecting those which would follow gene knockdown in normal, mature neurons. This caveat is especially pertinent to hnRNP K which has many known post-transcriptional roles in the regulation of neurodevelopmental processes (Laursen, Chan and Ffrench-Constant, 2011; Liu and Szaro, 2011) and indeed *HNRNPK* genetic abnormalities are linked to several neurodevelopmental disorders each characterised by severe developmental defects (Okamoto, 2019; Gillentine *et al.*, 2021). Hence the GO analysis of enriched terms within the differentially upregulated genes should be interpreted with some degree of caution. Many of these terms were related to neurodevelopmental processes, emphasising if nothing else the important functional roles hnRNP K plays in neuronal development. Tian et al. describe a modified CRISPRi-i^3 system which uses an inducible CRISPRi construct tagged with dihydrofolate reductase (DHFR) degrons to counteract this problem. In the absence of small molecule trimethoprim (TMP), the DHFR degron causes proteosomal degradation of fused proteins which leads to fragmentation and functional cessation of CRISPRi machinery (Tian *et al.*, 2019). However, addition of TMP, which could begin at the neuronal stage and not the iPSC stage, stabilises the CRISPRi construct and thus facilitates temporally-restricted CRISPRi-induced knockdown in neurons (Iwamoto *et al.*, 2010). This might represent one avenue for a future, non-developmentally affected neuronal hnRNP K knockdown which could be used to predict the true phenotypic consequences of hnRNP K neuronal depletion on neuronal viability and neurite outgrowth in mature neurons as well as providing a platform for identifying phenotypic modifiers. Notably though, DHFR-expressing CRISPRi activity was diminished compared to the conventional iPSC-stage strategy and may benefit from further optimisation before wider use (Tian *et al.*, 2019).

The second limitation of this model in particular is that, surprisingly and despite robust protein depletion, *HNRNPK* mRNA levels were only modestly reduced as measured by RT-qPCR and confirmed by RNA-seq. This discrepancy is especially mystifying because CRISPRi-induced repression of gene expression acts at the transcriptional level, as opposed to post-transcriptional mechanisms of gene repression such as siRNA (Adli, 2018). Whilst protein reduction represents the primary goal of gene knockdown strategies, it is worth considering potential explanations for a protein-mRNA disconnect. The sgRNA-*HNRNPK* targeting guide is predicted to bind several, but not all of the major alternative *HNRNPK* transcripts (ENSG00000165119), some of which use an alternative transcription start site (TSS). Therefore, CRISPRi-mediated gene suppression may, hypothetically, be evaded by compensatory upregulation of non-sgRNA targeting isoforms. However, these alternative isoforms are predicted to be protein-coding and are also predicted to be detected by the employed anti-hnRNP K, N-terminally-directed hnRNP K antibody. Nevertheless, multiple dual-acting sgRNAs targeting both major TSSs at once may confer a more robust knockdown in future studies (Horlbeck *et al.*, 2016). Another possible explanation underlying the difference is the potential for autoregulatory mechanisms being at play which may counteract the knockdown. To date, no known self-regulatory loops have been described for hnRNP K, but autoregulation has been proposed to be a potential unifying feature of many if not all splicing factors including hnRNPs (Buratti and Baralle, 2011). Splicing data may yield answers as to whether differential splicing pathways (e.g. upregulation of NMD-sensitive isoforms) are being deployed in hnRNP K KD neurons as in other hnRNP knockdown paradigms (e.g. (Humphrey *et al.*, 2017, 2020; Fratta *et al.*, 2018)). Although alternative, as yet undefined autoregulatory mechanisms at the RNA processing level could also be at play. Whatever the reasoning that underlies this unusual observation, it is important to remember protein and mRNA levels are measured at a single snapshot in time and it is difficult to disentangle a potentially complex and temporally-specific transcription-translational pathway from this individual data point. Indeed, the hnRNP K KD appeared to be much stronger at the NPC stage than in mature neurons. This may also reflect temporal shifts in the

relative expression levels of alternative, non-translatable *HNRNPK* isoforms (e.g. using an alternative TSS) during neuronal development that were not individually detected by the current RNA-seq protocol, but that are capable of masking *HNRNPK* mRNA decreases. Long-read sequencing of samples from longitudinal experiments, whilst also measuring both hnRNP K protein and mRNA levels (ideally from the same wells), from iPSCs to mature neurons may prove useful in elucidating this relationship. For this study though, hnRNP K protein loss was deemed to be sufficient to invoke hnRNP K dysfunction and indeed later splicing results are consistent with a specific, functional knockdown of hnRNP K in neurons as was planned.

Finally, it is worth mentioning that the model described here only partially encapsulates the pathological features of hnRNP K mislocalisation in the patient brain. HnRNP K protein is indeed depleted from the nucleus within mislocalised neurons, but it does not simply disappear, it instead appears to accumulate in the surrounding cytoplasm and neurites which begs the question of what is it doing there? CRISPRi platforms may well be best placed to emulate and investigate hnRNP K loss of function, but alternative cell and perhaps animal hnRNP K mutant models may be required to recapitulate potential toxic gain of function mechanisms. Neurons overexpressing cytoplasmic hnRNP K using an expression construct where the nuclear localisation sequence is deleted (HNRNPK ΔNLS) or otherwise disrupted may prove advantageous in this respect (Michael, Eder and Dreyfuss, 1997; Fallatah *et al.*, 2022).

The CRISPRi-i^3 based, cortical neuron hnRNP K knockdown model described in this section of work provides a suitable neuronal subtype (cortical)-specific platform for assessing specific transcriptomic changes that may accompany hnRNP K loss of function in the nucleus as is observed pathologically in brain. The next section of work focuses on splicing alterations and particularly the emergence of de-repressed cryptic and skiptic splicing events within hnRNP K KD neurons.

Chapter 6 HnRNP K knockdown-induced splicing changes, cryptic exons and how to find them.

6.1 Introduction

6.1.1 Publication statement

The contents of this chapter relating to validating a cryptic exon (CE) event in *UNC13A* within FTLD patient brain (Brown *et al.*, 2022) and in discussing the potential advantages of *in situ* hybridisation (ISH) as a validation technique in mechanistic investigations underlying ALS heterogeneity (Mehta *et al.*, 2022) are published open access and included here in adapted forms as per the publisher's (Springer & Wiley) policies on open access publication.

6.1.2 Statement of contribution

LeafCutter-derived differential splicing analysis and associated data plots presented in this chapter (**6.3.1**-**6.3.2**, **6.3.4**) were performed and generated by collaborator Dr Jack Humphrey (Icahn School of Medicine at Mount Sinai, New York). Dr Sarah Hill (National Institute of Neurological Disorders and Stroke, NIH, Bethesda) performed BaseScope™ on CRISPRi-i^3 TDP-43 knockdown neurons to detect *UNC13A* CE events *in vitro*.

6.1.3 Background

RNA splicing dysfunction as a pathomechanism of disease within neurons is a fast-evolving field of study within the neurodegeneration field. A whole spectrum of splicing defects have been associated with numerous neurodegenerative diseases including ALS, FTLD, AD, Spinal Muscular Atrophy and Huntington's disease which, to varying extents, are believed to contribute to disease pathogenesis (Daguenet, Dujardin and Valcárcel, 2015).

HnRNP K is known to play a major role in RNA processing within the nucleus and thus it was hypothesised that nuclear loss of hnRNP K within generated CRISPRi-i^3 KD neurons, would be predicted to impact the correct splicing of RNA targets. If true, this would have potential mechanistic relevance to both the neurodegenerative disease-afflicted and ageing brain where hnRNP K nuclear loss is common. This section of work therefore utilises differential splicing analysis to explore splicing changes that accompany hnRNP K depletion within the neuronal transcriptome. Particular attention is focused on the activation of two specific mis-splicing events called cryptic and skiptic exons.

Recently, the emergence of so-called 'cryptic splicing' as a molecular consequence of TDP-43 RBP depletion has manifested as a novel mechanism of neuronal neurotoxicity in TDP-43 proteinopathies (Polymenidou *et al.*, 2011; Tziortzouda, Van Den Bosch and Hirth, 2021). Under normal physiological conditions, TDP-43 constitutively represses the aberrant inclusion of non-conserved, intronic regions of RNA, termed cryptic exons (CEs) within mature mRNA targets (Ling *et al.*, 2015). However, TDP-43 depletion has been found to drive cryptic splicing in mRNAs which in-turn leads to nonsense-mediated decay (NMD) of destabilised, mis-spliced transcripts and overall loss of functional protein (Ling *et al.*, 2015; Jeong *et al.*, 2017; Sun *et al.*, 2017). Additionally and conversely, the promotion of skiptic exons (SEs), a gain-of-splicing event whereby constitutive exons are aberrantly excluded from mature transcripts, have also been identified within TDP-43 mutant models (Fratta *et al.*, 2018). Both mis-splicing events have the capacity to lead to diminished levels of functional target transcripts and resultant proteins.

Until recently, research into cryptic targets relevant to neurodegenerative disease has been dominated by the microtubule-associated protein stathmin-2 (*STMN2*). Reductions in TDP-43 binding to *STMN2* RNA have been shown to lead to the erroneous inclusion of a CE within its first intron leading to an alternative polyadenylation site and subsequent production of an alternative, truncated *STMN2* variant (Melamed *et al.*, 2019). This premature polyadenylation-mediated loss of full-length, functional stathmin-2 protein has

been validated in both ALS and FTLD-TDP brain tissue and has been demonstrated to exert detrimental consequences on neuronal health in neuronal cell depletion models (Klim *et al.*, 2019; Prudencio *et al.*, 2020; Krus *et al.*, 2022).

However, truncated *STMN2* is unlikely to be the only upregulated CE-containing transcript that has deleterious functional consequences within TDP-43 depleted neurons. Indeed, in this section of work two further CE events are validated in post-mortem brain tissue that have been found to be associated with TDP-43 loss of function. The first resides within the synaptic gene *UNC13A* as predicted by our in-house CE pipeline (https://github.com/frattalab/splicing) and is of especial mechanistic interest here due to its exceptionally close proximity to the well-established ALS/FTLD shared risk loci found in several genome-wide association studies (GWAS) (van Es *et al.*, 2009; Diekstra *et al.*, 2014; Nicolas *et al.*, 2018; Pottier *et al.*, 2019) (**Figure 6.1**). The second previously published event (Ling *et al.*, 2015) is within the insulin receptor gene (*INSR*) which is of interest because perturbed insulin signalling and insulin resistance has long been associated with several neurodegenerative diseases (Craft and Watson, 2004). BaseScope™ *in situ* hybridisation (ISH), as a spatial transcriptomics platform for the detection of specific splice variants (Baker *et al.*, 2017) in spatially resolved tissue, was employed here to validate these two novel events in FTLD-TDP/ALS human brain tissue. Thus, providing a proof-of-concept study for the future detection and validation of potential hnRNP K-associated CE/SEs (shown earlier in this chapter) in brains that are pre-stratified by hnRNP K (mis)localisation status.

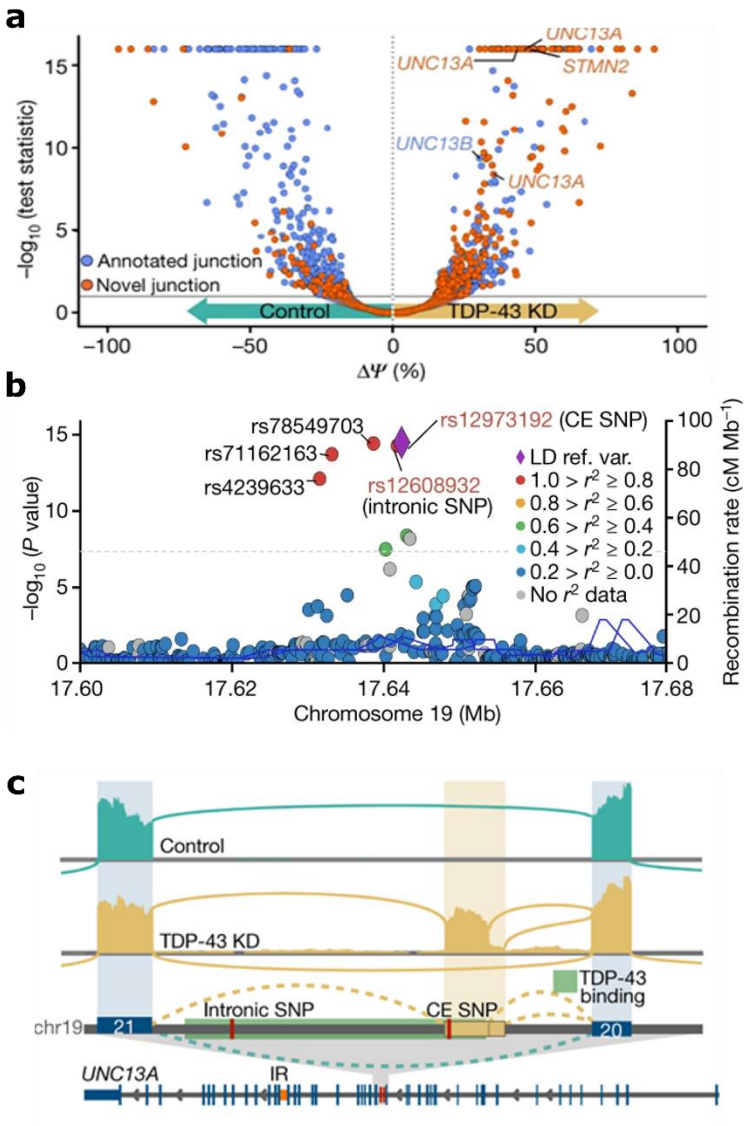

Figure 6.1. TDP-43 depletion driven cryptic splicing in *UNC13A* and GWAS relevance. (a) Differential splicing analysis by MAJIQ (Vaquero-Garcia *et al.*, 2016) following TDP-43 depletion in CRISPRi-i^3 TDP-43 KD neurons (n = 3) versus controls (n = 4). Each point denotes a splice junction. Significantly altered splice junctions in the validated *STMN2* gene is indicated for reference as are altered splice junctions within *UNC13A*. (b) LocusZoom plot of the *UNC13A* locus in the most recent ALS GWAS (Nicolas *et al.*, 2018). The dashed line indicates the risk threshold used in that study and the lead SNP *rs12973192* is represented as a purple diamond and designated the 'CE SNP' due to its close proximity to the CE. Other SNPs are coloured by linkage disequilibrium (LD). (c) Representative sashimi plot showing CE inclusion within exons 20 and 21 of *UNC13A* upon TDP-43 KD (yellow trace), as well as the relative positioning of the TDP-43 binding region (green) and two FTLD/ALS related SNPs (red) including the CE (adjacent) SNP. Adapted from (Brown *et al.*, 2022).

6.2 Methods

6.2.1 Differential splicing analysis

Differential splicing between CRISPRi-i^3 hnRNP K KD and control neurons was assessed using LeafCutter (Y. I. Li *et al.*, 2018) as previously described (**2.4.7**). A custom script (code available at (Bampton *et al.*, 2021)) was employed to specifically identify novel cassette exons and infer their annotation (GENCODE, V30) status. Percentage spliced in (PSI %) for each cassette exon was used as a proxy for effect size and was used to determine whether cassette exons were significantly spliced between groups (±10 % dPSI) and in the classification of both cryptic and skiptic exon events.

6.2.2 Three-primer PCR

A three-primer or 'nested' PCR (**2.4.9**) was employed to molecularly validate predicted hnRNP K depletion-associated cryptic and skiptic events using sets of primers as detailed earlier in **Table 2.10**.

6.2.3 BaseScope™ assays and analysis

BaseScope™ ISH was used to detect and validate the presence of two TDP-43 depletion-associated CEs in FTLD-TDP (*UNC13A* CE) and ALS (*INSR*) patient brain using sequence-specific custom probes (**2.1.9**) (**Table 2.4**). Frozen cryosections of frontal cortex from the QSBB were used in the validation of *UNC13A* CE and FFPE sections of motor cortex from the MRC Edinburgh Brain & Tissue Bank were used in the validation of the *INSR* CE. Specimen-specific pre-treatment steps were followed as previously detailed (**Table 2.5**) and amplification steps were performed the same for both experiments (**Table 2.6**).

All hybridised sections were scanned using an Olympus VS120 slide scanner. For quantitation of *UNC13A* CE on frozen tissue, equal-sized (34.5 mm^2) regions of interest were extracted from the centre of each section for each

individual case (FTLD-TDP, *n* = 9; FTLD (non-TDP / tau), *n* = 4 and neurologically normal controls, *n* = 5). All cases used were donated to the QSBB. The total number of red foci which should identify single transcripts harbouring the *UNC13A* CE event, were manually counted in ImageJ (v1.41). BaseScope™ *INSR* CE signal on FFPE ALS tissue was much stronger by comparison. CE foci frequency for this event was instead given per 1000 x 1000 px image (*n* = 30 per case; ALS, *n* = 11; controls, *n* = 6). The MRC Edinburgh Brain & Tissue Bank supplied the ALS and control FFPE sections for this study and all cases were required to have been in fixative for no longer than 14 days.

A dual ISH-IHC assay was then developed to investigate the spatial relationship between *UNC13A* CE and pTDP-43 pathology in FTLD-TDP neurons as well as *INSR* CE foci and TDP-43 protein within ALS neurons (**2.1.10**). Equivalent regions of *INSR* CE and TDP-43 stained motor cortex, identified with reference to neuroanatomical and neurovascular landmarks, were extracted on QuPath (v0.30.0) and co-visualised by overlaying both extractions in ImageJ (v1.41) with 50 % transparency. DAB signal intensity for each respective immunostaining profile was assessed in QuPath using a universally applied threshold on each respective region of interest.

6.3 Results

6.3.1 HnRNP K knockdown induces widespread differential splicing

Differential splicing analysis performed with LeafCutter found 364 cassette exons that exhibited significantly altered splicing (FDR < 0.05) following hnRNP K protein knockdown, of which 126 had an effect size change in splicing (PSI_{hnRNPK} - $PSI_{control}$ (dPSI)) > |10 %| (**Appendix 3**). This suggested hnRNP K has an important role in the regulation of appropriate splicing within the neural transcriptome.

Using GENCODE (v30) to annotate the introns used in each of the identified 126 cassette exon splicing events (dPSI > |10 %|), events were classified as

either novel inclusion (*n* = 61) or novel skipping (*n* = 65) junctions (or 151 included and 213 skipping junctions for all annotated, FDR < 0.05 events). These represent events which either make use of a normally constitutively repressed or 'unused' junction (novel inclusion) or skip over a normally constitutively included junction (novel skipping) respectively. However, this definition does not account for the degree to which these events are 'spliced in' (PSI) within control neurons which is important information used to determine whether or not these novel junctions are formally classified as cryptic or skiptic exons.

Because annotation of novel splicing events into gene and transcript models is constantly increasing, cryptic and skiptic exons were classified by their effect sizes, rather than their current annotation status. In line with other recent definitions and parameters, CEs were defined as altered cassette exons which were lowly included within control samples ($PSI_{control}$ < 10 %) but significantly more frequently included in hnRNP K knockdown samples (dPSI > 10 %). Skiptic exons were defined as altered cassette exons which were highly included within control samples ($PSI_{control}$ > 90 %) but significantly less frequently included in hnRNP K knockdown samples dPSI < - 10 %. A visual depiction of all cassette exons and their effect sizes including those classified as cryptic and skiptic exons are shown in **Figure 6.2**.

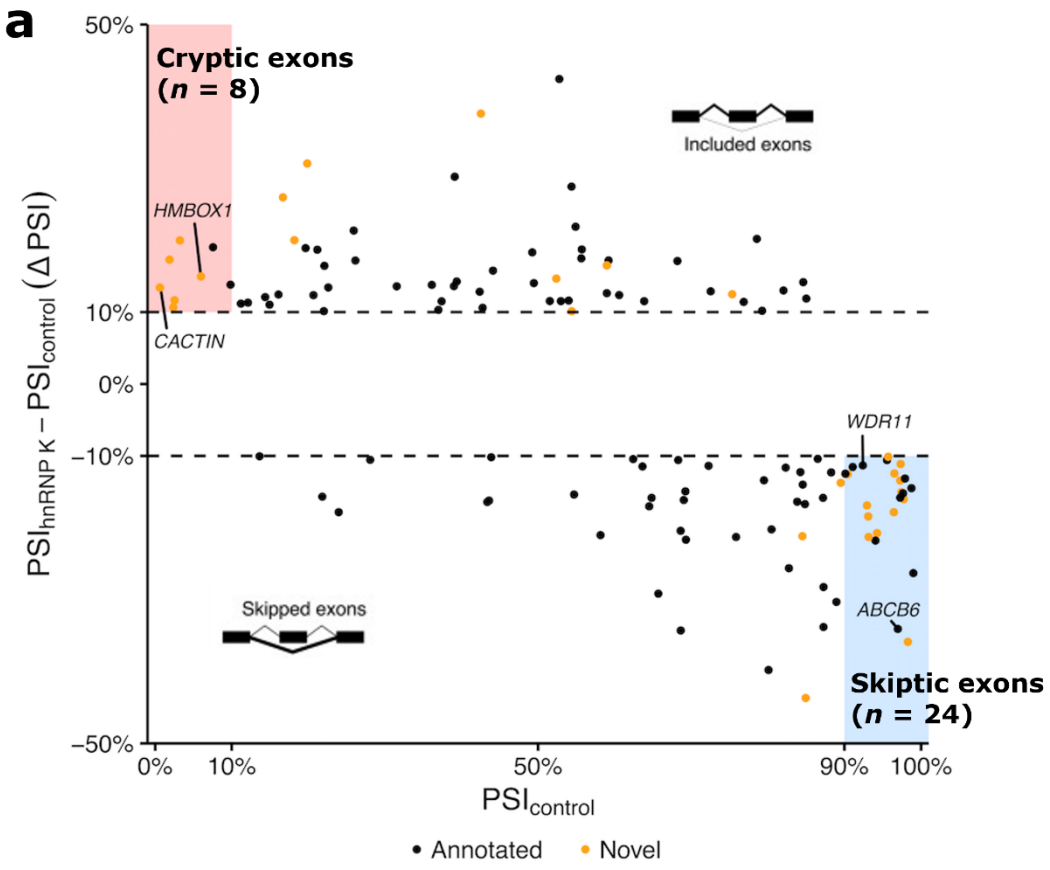

b

Significant clusters	Cassette exons	Novel exon inclusion	Novel exon skipping
Annotation	364	151	213
Effect size (dPSI) > 10 %	126	61	65
CE or SE classification	32	8	24

Figure 6.2. HnRNP K depletion leads to widespread splicing changes. (a) All cassette exons identified with corresponding effect sizes (percentage spliced in, deltaPSI) > 10 % (*n* = 126). Included exons have a positive deltaPSI and skipped exons have a negative deltaPSI. Cryptic exons (shaded red) were defined as lowly included in controls ($PSI_{control}$ < 10 %) and significantly more frequently included in KD samples (PSI_{hnRNPK} - $PSI_{control}$) > 10 %. Skiptic exons (shaded blue) were defined as highly included in controls ($PSI_{control}$ > 90 %) but significantly less frequently included in KD samples (PSI_{hnRNPK} - $PSI_{control}$ < - 10 %). Orange circles depict novel, previously unannotated events which are over-represented in the cryptic and skiptic exon sets (b) Summary table of cassette exons defined by annotation (data not shown above) and by effect size (dPSI) as illustrated above in a.

In the present dataset, just 8 cassette exons met criteria for classification as CEs (**Table 6.1**) and 24 met criteria for classification as SEs (**Table 6.2**). Of

the 8 CEs, 6 (75 %) were novel exons, compared to 6 out of the 53 (11 %) regular included exons which did not meet criteria for CE classification. 13 out of 24 SE events (54 %) were not annotated, compared to only 3 out of 41 (< 1 %) of the regular skipped exons which did not meet criteria for SE classification, indicating a bias towards novel annotation (**Figure 6.2**). The metadata associated with all identified cassette exon events can be found in **Appendix 3**.

Table 6.1. List of cryptic exons found in CRISPRi-i^3 hnRNP K KD neurons

Exon co-ordinates	Gene	PSI_{Con}	PSI_{KD}	dPSI	FDR	Novel?
chr1:32095659-32095762	*CNEP1R1*	0.075481	0.265712	0.190232	0.0217	No
chr8:22101975-22102062	*HMBOX1*	0.05982	0.209372	0.149553	0.00262	Yes
chr8:29046191-29046416	*TMEM39B*	0.098385	0.236431	0.138046	0.0246	No
chr11:111674323-111674384	*SIK2*	0.02529	0.141734	0.116444	0.0217	Yes
chr16:18342931-18342997	*LINC00665*	0.018683	0.191636	0.172953	0.023	Yes
chr16:50025650-50025701	*CACTIN*	0.006154	0.140287	0.134133	0.00261	Yes
chr19:3619349-3619546	*AC126755.1*	0.023693	0.130208	0.106515	1.82E-05	Yes
chr19:36313807-36313912	*FAM160B2*	0.032289	0.231958	0.199669	0.0178	Yes

PSI_{con}, mean percent spliced in within controls; PSI_{hnRNPK} mean percent spliced in within CRISPRi-i^3 hnRNP K KDs; dPSI, delta PSI (PSI_{hnRNPK} - PSI_{con}) which must be > 10 % for CE classification; FDR, False discovery rate applied by LeafCutter to each cluster; Novelty defined by prior annotation of junction in GENCODE (v30) (No) or not (Yes).

Table 6.2. List of skiptic exons found in CRISPRi-i^3 hnRNP K KD neurons

Exon co-ordinates	Gene	PSI_{Con}	PSI_{KD}	dPSI	FDR	Novel?
chr1:149977425-149977576	*OTUD7B*	0.957147	0.856045	-0.1011	0.0344	Yes
chr1:213000785-213000912	*ANGEL2*	0.9042	0.77879	-0.12541	0.0246	Yes
chr1:86868052-86868102	*SELENOF*	0.91078	0.795378	-0.1154	0.0011	No
chr10:120890715-120890887	*WDR11*	0.924023	0.810729	-0.11329	0.0486	No
chr10:73791323-73791499	*ZSWIM8*	0.972826	0.838528	-0.1343	0.0178	Yes
chr11:121570156-121570270	*SORL1*	0.977295	0.816937	-0.16036	0.0111	Yes
chr14:100540495-100540579	*BEGAIN*	0.931581	0.718786	-0.21279	0.0398	Yes
chr14:67557268-67557418	*PLEKHH1*	0.973375	0.862058	-0.11132	0.0241	Yes
chr16:655028-655147	*WDR90*	0.982798	0.62408	-0.35872	0.0253	Yes
chr17:44157832-44157941	*C17orf53*	0.989878	0.726793	-0.26309	0.00419	No
chr19:17327437-17327569	*ANO8*	0.931096	0.746943	-0.18415	0.0109	Yes
chr19:2191011-2191240	*DOT1L*	0.965229	0.840692	-0.12454	0.00325	Yes
chr19:29610408-29610632	*POP4*	0.97911	0.847557	-0.13155	0.0241	No
chr19:45616460-45616558	*EML2*	0.972747	0.814643	-0.1581	0.0151	No
chr19:57575803-57575930	*ZNF416*	0.94257	0.73511	-0.20746	0.00367	Yes
chr2:219215996-219216180	*ABCB6*	0.969734	0.628946	-0.34079	5.53E-04	No
chr4:139695196-139695267	*MGST2*	0.97652	0.824486	-0.15203	0.0297	No

chr4:2744696-2744945	*TNIP2*	0.987452	0.842538	-0.14491	0.0398	No
chr4:68332793-68332847	*YTHDC1*	0.901147	0.776285	-0.12486	0.039	No
chr5:141662042-141662255	*ARAP3*	0.940495	0.722696	-0.2178	0.0249	No
chr9:114269240-114269294	*COL27A1*	0.974174	0.823654	-0.15052	0.0125	Yes
chr9:36642996-36643083	*MELK*	0.929449	0.760488	-0.16896	0.0319	Yes
chrX:18951103-18951272	*PHKA2*	0.964461	0.786181	-0.17828	0.0408	Yes
chrX:47171027-47171258	*RBM10*	0.95553	0.849619	-0.10591	0.0304	No

PSI_{con}, mean percent spliced in within controls; PSI_{hnRNPK} mean percent spliced in within CRISPRi-i^3 hnRNP K KDs; dPSI, delta PSI (PSI_{hnRNPK} - PSI_{con}) which must be < - 10 % for SE classification; FDR, False discovery rate applied by LeafCutter to each cluster; Novelty defined by prior annotation of junction in GENCODE (v30) (No) or not (Yes).

As with DEGs analysed in the previous chapter, differentially spliced cassette exon genes from this dataset were then compared to equivalent events from the previously validated hnRNP K KD SH-SY5Y model (Bampton *et al.*, 2021) to assess overlap. Of the 364 cassette exons identified in this study, 200 (54.9 %) were also identified in the SH-SY5Y model. 143 splicing events (within 141 genes) shared the exact same exon coordinates, of which 131 (91.6 %) exhibited concordant directions in dPSI. When comparing dPSI of the shared splicing events between the two models, the CRISPRi-i^3 neurons demonstrated a consistently lower effect size compared to SH-SY5Y cells (r = 0.71, $p < 2.2 \times 10^{-16}$) (**Figure 6.3**).

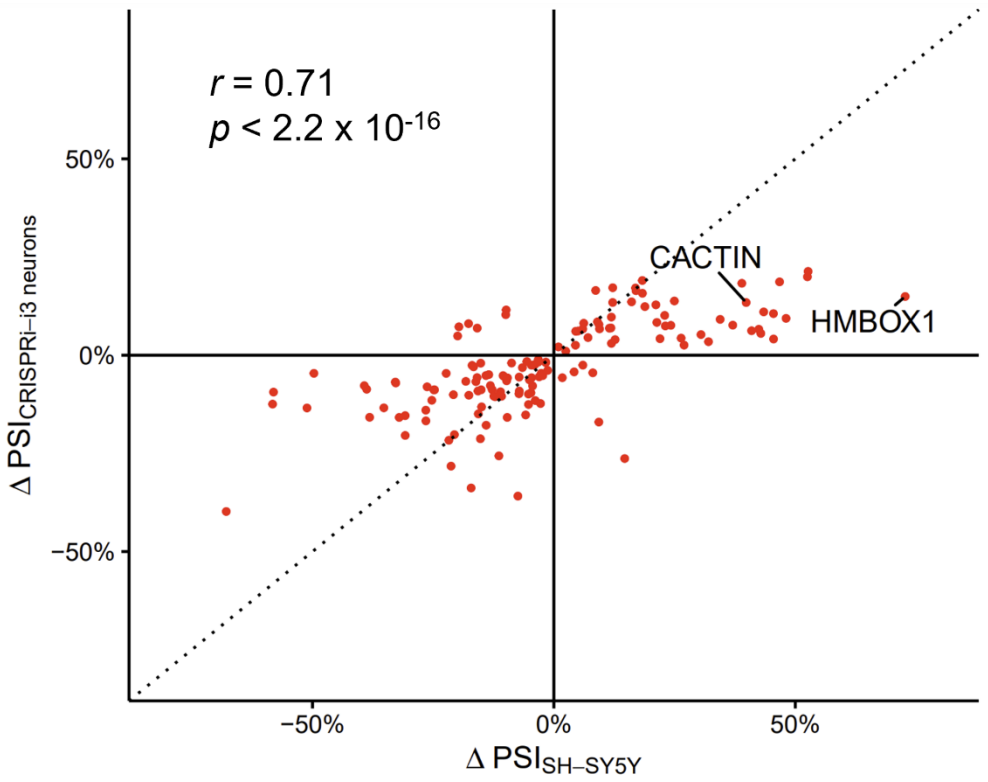

Figure 6.3. Concordance between cassette exons in CRISPRi-i³ neuron and SH-SY5Y models of hnRNP K knockdown. *CACTIN* and *HMBOX1* CEs indicated for reference as mutual (CE) splicing hits.

6.3.2 Splicing alterations within *HNRNPK* itself are subtle

Altered splicing within the *HNRNPK* transcript itself was also assessed because differential self-splicing may represent activation of a splicing-mediated autoregulatory loop of *HNRNPK* expression levels. However, no cassette exons were determined to be differentially spliced within the transcript. Interestingly, a significant splicing change was detected within the KD samples which made preferential usage (10-fold increase) of a cryptic junction between exon 2 and exon 3 (or 1a and 2 due to *HNRNPK* having two alternative start sites, 1/1a). However, this represents a decrease in using annotated junctions of just 8 % from 88 % in controls to 80 % in KD and hence is quite a subtle overall difference. There is also a shift in usage between the two annotated transcription start sites (TSS) between samples. HnRNP K KD samples made increased usage of the distal TSS (exon 1) over the proximal

(exon 2/1a) compared to controls which may represent a subtle autoregulatory response not previously observed in the SH-SY5Y model (**Figure 6.4**).

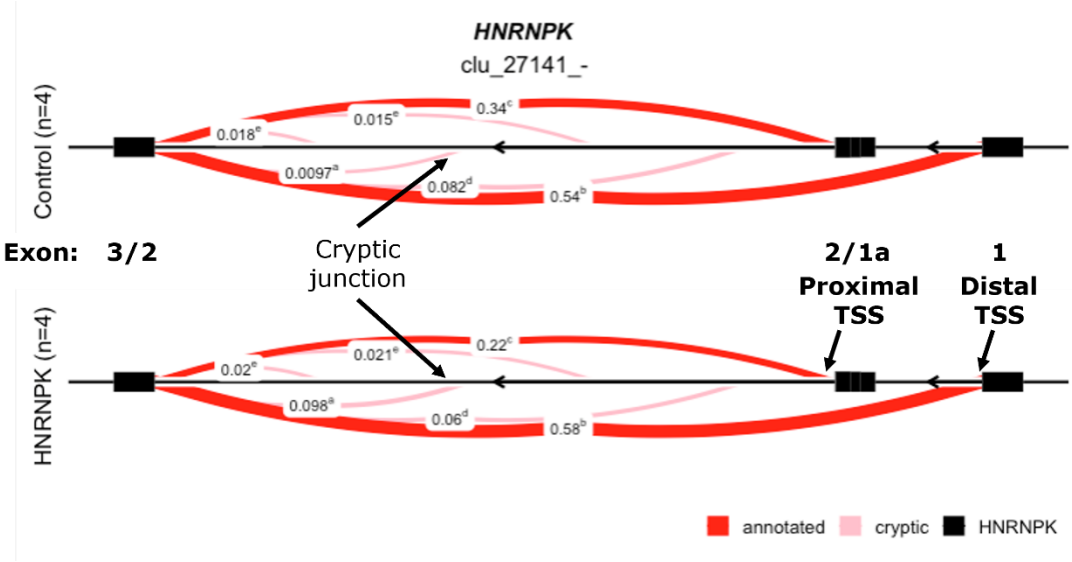

Figure 6.4. Altered splicing within *HNRNPK*. Leafviz plot showing elevated use of cryptic junction (indicated) from ~ 1 % in controls to ~ 10 % (~10-fold increase) in KD but equivalent to only an 8 % reduction in usage of annotated junctions overall. Additionally there was an increased use of distal TSS relative to proximal TSS in KD. Control samples use the distal TSS 1.59 times more frequently than the proximal TSS compared to 2.64 times in the KD.

6.3.3 Validation of cryptic and skiptic exon events

A three-primer PCR protocol was employed to molecularly validate the differential inclusion and exclusion of cryptic and skiptic exon events respectively, between control and hnRNP K knockdown samples. The assay was designed to generate amplicons both containing and excluding the cryptic or skiptic exon of interest that could be detected and quantified by electrophoresis (**Figure 6.5**).

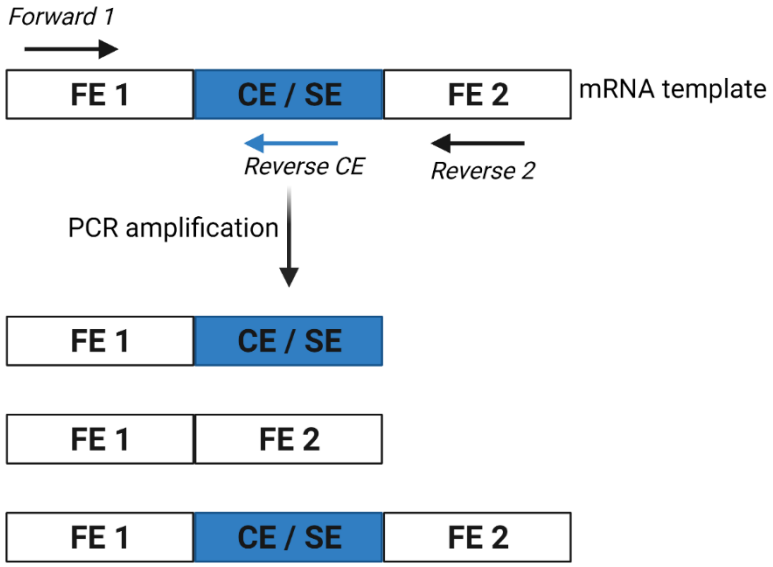

Figure 6.5. Schematic diagram of three-primer PCR method. A forward and reverse primer are designed on the flanking exons (FEs) and a third primer is designed to span the cryptic (CE) or skiptic exon (SE) of interest. Upon PCR amplification, three amplicons are generated, two of which contain the central cryptic or skiptic exon (blue) and one excluding it altogether. These PCR amplicons have different predicted product sizes and their relative abundances can be visualised and quantified by electrophoresis on the Agilent TapeStation system.

Two CEs within the *HMBOX1* and *CACTIN* genes were validated by three-primer PCR. CRISPRi-i^3 hnRNP K KD samples exhibited considerably greater CE inclusion relative to normal splicing than within control samples. CE incorporation within *HMBOX1* was 5.5 times higher in CRISPRi-i^3 KD relative to controls (p = 0.0009) and in *CACTIN* was 8.9 times higher (p = 0.0003) (**Figure 6.6a-b**). Both CEs within *HMBOX1* and *CACTIN* were also detected in the SH-SY5Y model of hnRNP K knockdown (**Figure 6.3**).

The same method was also applied to a CE event within *TMEM132A*, a weaker event that was identified within the SH-SY5Y model, but was not detected using the same LeafCutter pipeline within the present model at the RNA-seq level. Interestingly, CE incorporation was still significantly higher in the CRISPRi-i^3 samples relative to controls albeit to a lesser extent (2.0 times higher, p = 0.0038) (**Figure 6.6c**). This suggested that three-primer PCR is a more sensitive method of CE detection than the more stringent RNA-seq LeafCutter pipeline and that the pipeline may have detected the event if the knockdown had been stronger.

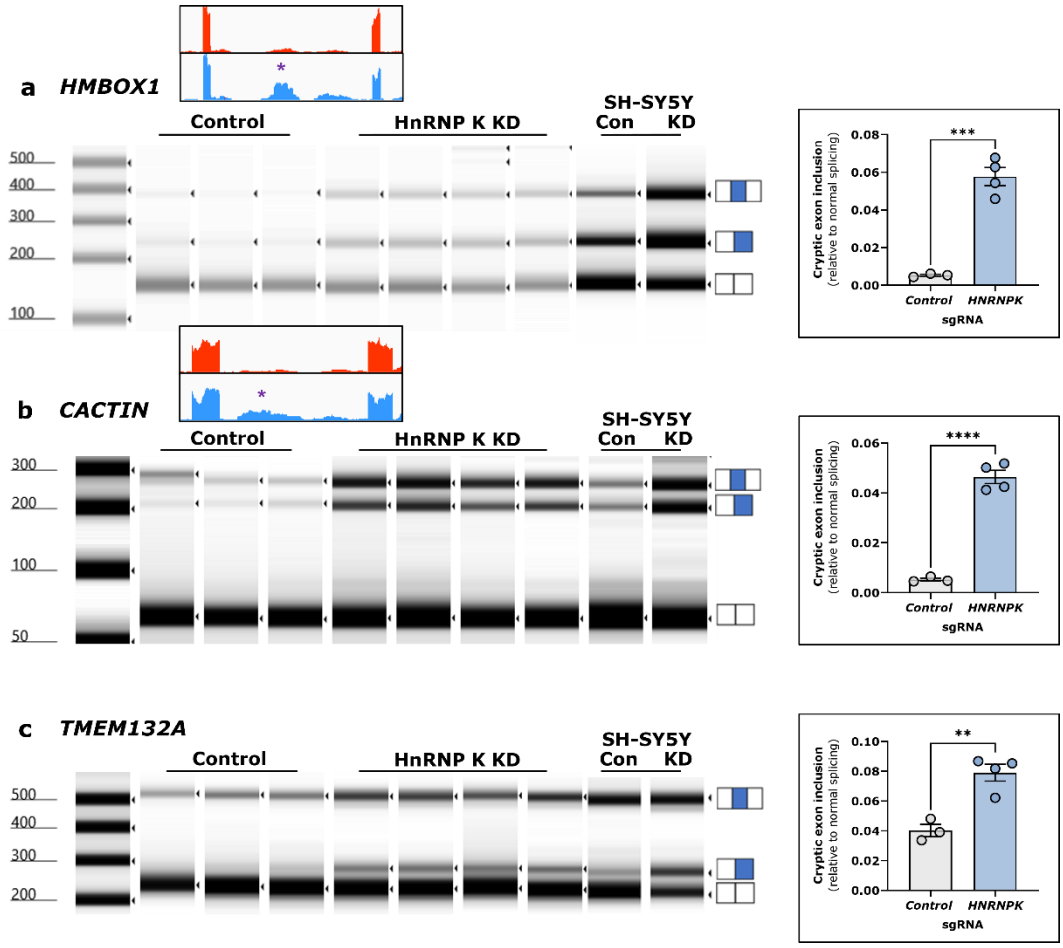

Figure 6.6. Molecular validation of hnRNP K-regulated cryptic exons in neurons. Two CE events (a) *HMBOX1* and (b) *CACTIN,* identified by differential splicing analyses in the current KD model and one CE event (c) *TMEM132A*, not identified in this model but previously identified within an SH-SY5Y model of hnRNP K KD (Bampton *et al.*, 2021), were validated in CRISPRi-i^3 neurons by three-primer PCR. The purple asterisk in each IGV (integrated genome viewer) trace indicates the CE (not shown for *TMEM132A*). The top trace (red) corresponds to the control reads, whilst the bottom (blue) trace corresponds to the hnRNP K KD. Three PCR products were generated, two of which containing the CE (blue) and one without which were separated by electrophoresis. cDNA from the validated SH-SY5Y KD and control (con) cells (Bampton *et al.*, 2021) were also included as a positive and negative control respectively. Quantification of CE inclusion for all events was calculated relative to normal (i.e. no CE) splicing and all were significantly more present in hnRNP K KD (n = 4) compared to controls (n = 3) (HMBOX1, p = 0.0009; *CACTIN*, p = 0.0003; TMEM132A, p = 0.0038). Error bars show mean ± SEM, unpaired t-test; *p < 0.05, **p < 0.01, ***p < 0.001, ns = not significant.

Two SE events in *ABCB6* and *WDR11* genes were validated by the same method, both of which were novel events that were not detected within the SH-SY5Y model and thus were unique to neurons. CRISPRi-i^3 hnRNP K KD samples exhibited significantly greater SE exclusion relative to normal splicing than within control samples. SE exclusion within *ABCB6* was 1.9 times higher

in CRISPRi-i^3 KD relative to controls (p = 0.021) and in *WDR11* was 1.6 times higher (p = 0.010) (**Figure 6.7**). Notably, the KD : Control ratio for these skiptic events was smaller than expected when considering their high dPSI % values (**Table 6.2**) compared to the CEs validated above (**Table 6.1**).

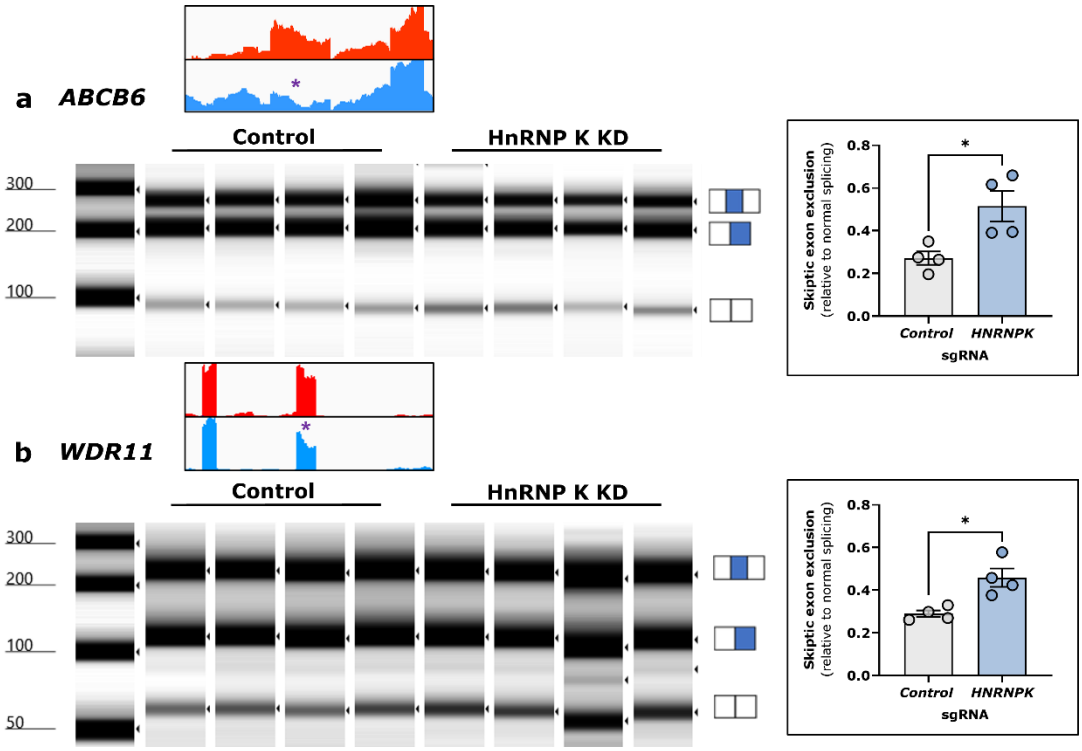

Figure 6.7. Molecular validation of hnRNP K-regulated skiptic exons in neurons. Two SE events (a) *ABCB6* and (b) *WDR11* were validated in CRISPRi-i^3 hnRNP K KD neurons by three-primer PCR. The purple asterisk in each IGV trace (red – control, blue – KD) indicates the SE. Three PCR products were generated, two of which containing the SE (blue) and one without ('skipped') which were separated by electrophoresis. Quantification of SE inclusion for both events was calculated relative to normal (i.e. no SE) splicing and both were significantly more present in hnRNP K KD (n = 4) compared to controls (n = 4) (*ABCB6*, p = 0.021; *WDR11*, p = 0.021). Error bars show mean ± SEM, unpaired t-test; *p < 0.05, **p < 0.01, ***p < 0.001, ns = not significant.

6.3.4 Few cassette exon events are associated with differential expression

The incorporation of CEs, the skipping over of SEs or indeed other novel splicing alterations can lead to frameshifts in resultant transcripts which can trigger NMD if PTCs are subsequently introduced. Hence mis-splicing events can result in a reduction of transcript levels in target genes. To investigate this,

genes were identified that exhibited both significant splicing alterations and significant alterations in gene expression. However, just 13 genes met both criteria and only 4 of these were significantly downregulated and none of these were classified as cryptic or skiptic exon events (**Figure 6.8a**). Within those splicing events classified as cassette exons (*n* = 7), there was no clear bias to exons being divisible by three which would be expected if splicing alteration-induced frameshifts were leading to upregulated protein degradation by NMD (**Figure 6.8b**).

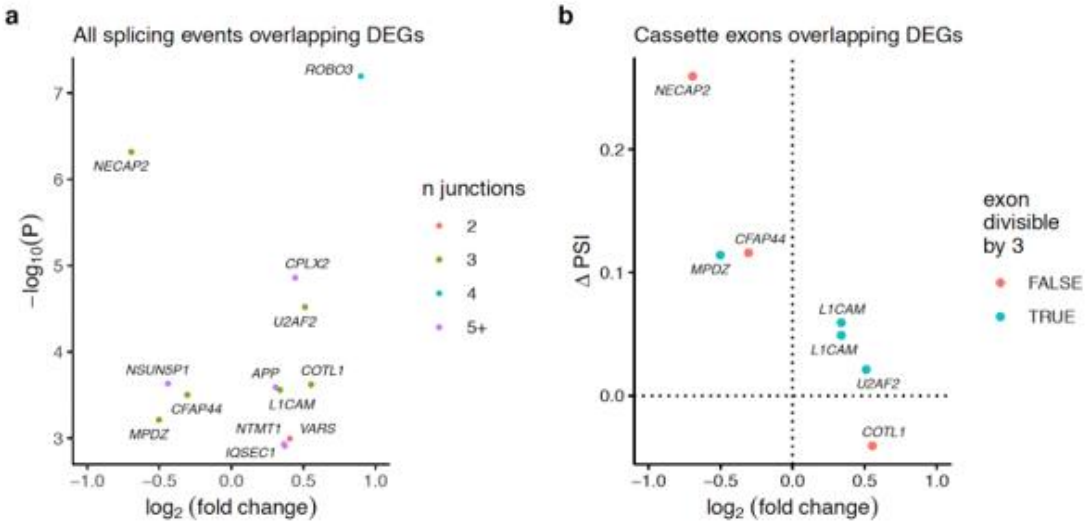

Figure 6.8. Genes with both gene expression and splicing changes. (a) Volcano plot for the 13 differentially expressed genes (DEGs) that also contain differential splicing events, coloured by number of junctions in cluster, i.e. red genes have only two junctions. More complex events capped at 5 or more junctions. (b) Comparing delta PSI (dPSI) for the 7 cassette exons (6 genes with 3 junctions in a, green) with the $\log_2$ fold change of differential expression of their host genes. Exon coloured by whether or not it is divisible by 3. Non-divisible exons (false) would lead to a shift of reading frame and be predicted to be sensitive to potential NMD.

The cassette exon associated with the greatest downregulation which met both differential splicing and gene expression criterion was in *NECAP2*. Elevated exon 2 splicing within *NECAP2* CRISPRi KD samples likely leads to premature termination of the transcript and subsequent downregulation of *NECAP2* as deduced from the event's corresponding Sashimi and Leafviz plots (**Figure 6.9**). However, clearly this was not a common finding within other differentially spliced genes.

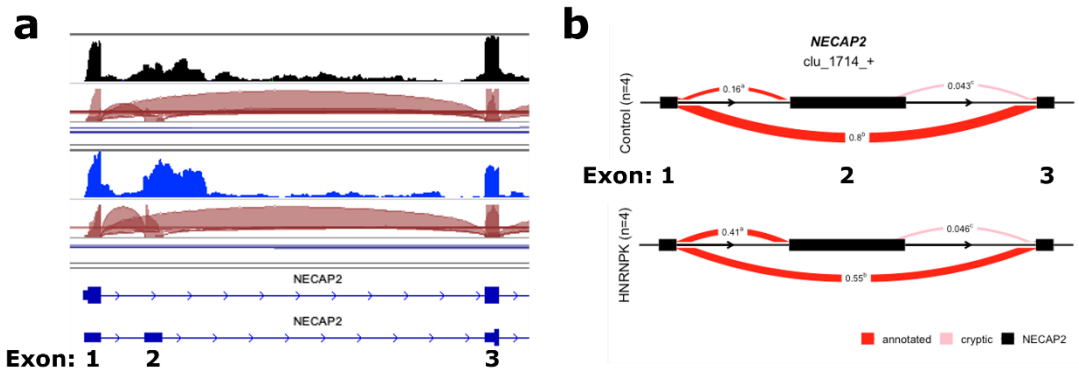

Figure 6.9. Increased *NECAP2* exon 2 splicing leads to premature truncation of the transcript and downregulation of *NECAP2* expression. (a) Sashimi plot with IGV trace of representative samples of a control and hnRNP K KD (lower panel) showing increased coverage of *NECAP2* exon 1 – exon 2 inclusion junction, with a much smaller increase in exon 2 – exon 3 junction, suggesting premature termination. (b) Leafviz plot showing average junction proportions in 4 control and 4 KD samples.

6.3.5 BaseScope™ validation of an *UNC13A* cryptic exon within FTLD-TDP brain

The next step was to utilise *in situ* hybridisation (ISH) to validate splicing alterations within cytoarchitecturally preserved post-mortem human brain tissue. Because, hnRNP K KD splicing events are novel and are not yet clearly linked to a particular pathological diagnosis, this platform was instead used to validate splicing events and in particular CE events associated with the more widely studied pathological event of TDP-43 depletion in TDP-43 proteinopathies as a proof-of-principle investigation. The first CE event to be validated was that within *UNC13A,* just downstream of the known FTLD/ALS SNP *rs12973192* (**Figure 6.1**).

BaseScope™ ISH was used for the purpose of detecting CEs in brain tissue because of its known capability for detecting splice variants. A custom probe was designed to target the CE containing sequence whilst simultaneously avoiding the SNP. The probe successfully detected CE foci in frozen frontal cortex tissue of FTLD-TDP brain at a significantly higher frequency relative to neurologically normal controls (p = 0.021) and non-TDP FTLD (FTLD-tau) disease controls (p = 0.010) (**Figure 6.10a-b**). Control and FTLD (non-TDP) signal was either below or equivalent to that exhibited by the negative control

probe. Collaborator Dr Sarah Hill (National Institute of Neurological Disorders and Stroke, NIH, Bethesda) then used the same probe to detect the presence of *UNC13A* specifically within CRISPRi-i^3 TDP-43 KD neurons and not in control neurons (**Figure 6.10c-d**) further confirming the CE's specificity to TDP-43 depletion.

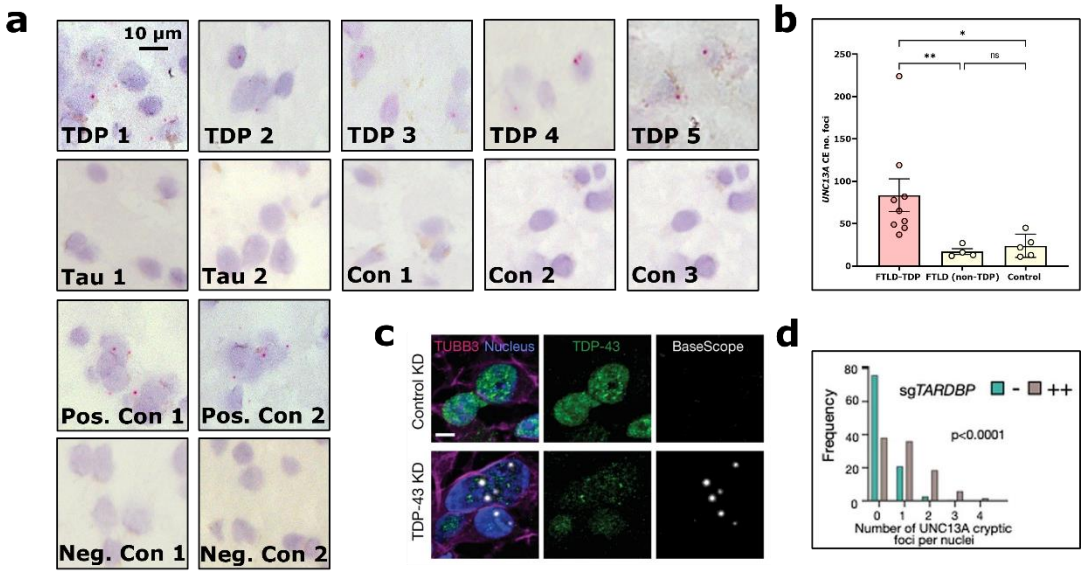

Figure 6.10. BaseScope™ detection of *UNC13A* CE in FTLD-TDP and TDP-43 KD neurons. (a) Representative images of *UNC13A* CE (red foci) BaseScope™ detection in cortical neurons of FTLD-TDP (TDP 1-5), FTLD-tau/non-TDP (Tau 1-2) and neurologically normal control (Con 1-3) subjects as well as positive (*PPIB*-targeting) and negative (*DapB*-targeting) probe signal. Scale bars are as indicated in the first image. (b) Quantitation of the total number of foci counted within the sampled region of each case. FTLD-TDP cases (n = 9) exhibited significantly higher frequency of foci relative to neurologically normal controls (n = 5, p = 0.021) and non-TDP FTLD (n = 4, FTLD-tau) disease controls (p = 0.010). Error bars show mean ± SEM, Kruskal-Wallis test with Dunn's multiple comparisons post hoc test; *p < 0.05, **p < 0.01, ***p < 0.001, ns = not significant. (c) BaseScope™ detection of *UNC13A* CE (white puncta) in control (top) and TDP-43 KD (bottom) CRISPRi-i^3 neurons. Neurons co-stained for TDP-43 (green), neuronal processes (TUBB3, pink) and nuclei (blue), scale bar 5 µm. (d) Histogram showing number of *UNC13A* CE foci per nuclei in control (blue) and TDP-43 KD (sg*TARDBP*, grey) (p < 0.0001, unpaired t-test). Adapted from (Brown *et al.*, 2022).

6.3.6 BaseScope™ validation of an *INSR* cryptic exon within ALS brain

A second probe was then designed for the detection of a CE within the insulin receptor (*INSR*). For this experiment, FFPE ALS and control tissue was used with the objective of achieving greater preservation of neuronal morphology to identify the upper motor neurons (Betz cells) most preferentially affected by

TDP-43 pathology. FFPE tissue was also used to better facilitate a dual ISH-IHC assay to later investigate the spatial relationship between CEs and TDP-43 pathology.

The probe detected the *INSR* CE in ALS motor cortex at a significantly higher frequency than in age-matched controls ($p = 0.032$), again demonstrating the specificity of the event to TDP-43 proteinopathy. Many of these CE foci were concentrated within the large, upper motor neurons (Betz cells) which were clearly identifiable within the deeper layers (predominantly cortical layer V) of the cortex (**Figure 6.11**).

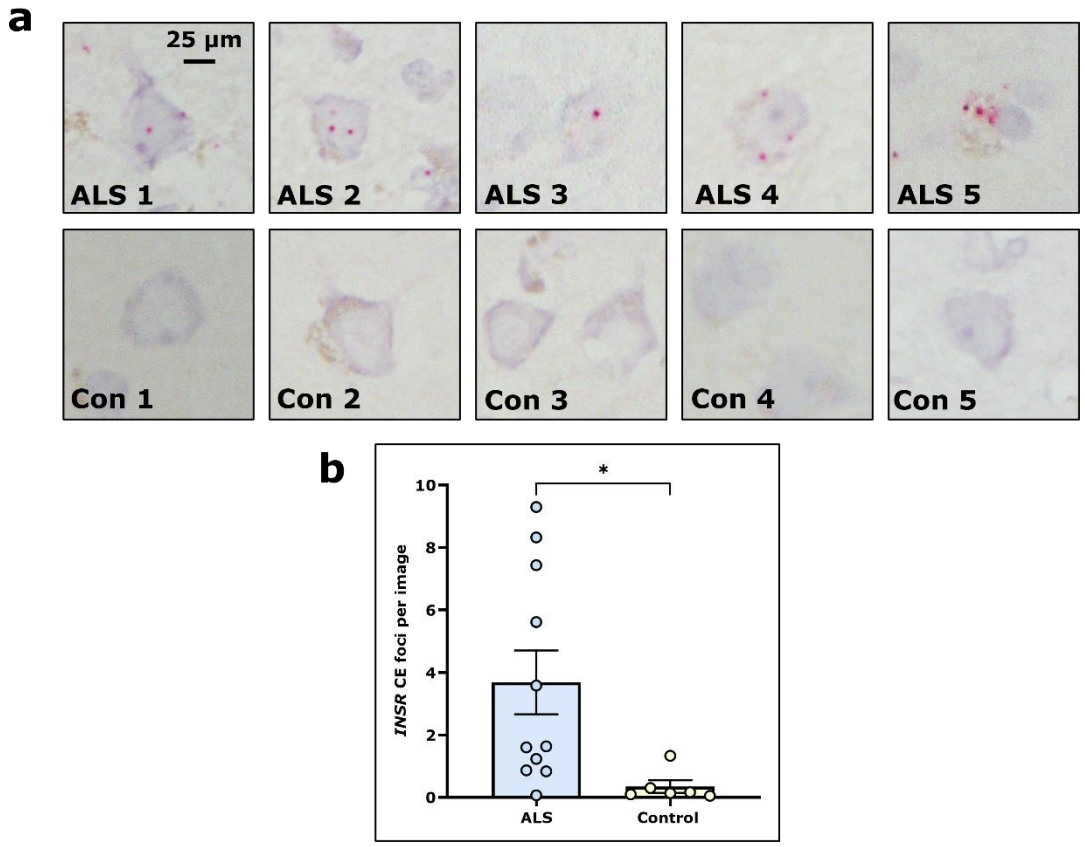

Figure 6.11. BaseScope™ detection of *INSR* CE in ALS motor neurons. (a) Representative images of *INSR* CE (red foci) BaseScope™ detection in upper motor neurons of ALS (ALS 1-5) and age-matched neurologically normal control (Con 1-3) subjects. (b) Quantitation of the number of foci counted per image ($n = 30$) within the sampled region of motor cortex in each case. ALS cases ($n = 11$) exhibited significantly higher frequency of foci relative to neurologically normal controls ($n = 6$, $p = 0.032$). Error bars show mean ± SEM, unpaired t-test; *p < 0.05, **p < 0.01, ***p < 0.001, ns = not significant.

6.3.7 Investigating the spatial relationship between cryptic exons and TDP-43 pathology

Within depletion cell models, CE incorporation within the neural transcriptome is believed to be a correlate for TDP-43 nuclear loss of function. Therefore the next step was to determine the extent to which these CEs, starting with *INSR* CE, is associated with TDP-43 protein load in ALS motor cortex. To do this, a dual BaseScope™ ISH-IHC assay was developed in order to overlay TDP-43 protein signal on to prior CE-probed brain sections. Notably, the alcohol-sensitive Fast Red chromogen used for CE visualisation was largely quenched during the immunostaining process, which is why sections were scanned before and after IHC to assess each stain individually and overlapped afterwards.

As a first analysis, TDP-43 DAB immunostaining in ALS motor cortex was equally thresholded on QuPath (v0.3.0) to determine the spatial extent (% DAB positive) of TDP-43 staining within the same annotated grey matter regions of interest analysed for BaseScope™-detected CE frequency earlier (**Figure 6.12a-b**). However, no clear association was found between *INSR* CE foci frequency and TDP-43 staining (**Figure 6.12c**), although the sample size was notably low (*n* = 9 xy pairs). This may more accurately reflect the fact that the percentage area of TDP-43 DAB positive staining is a poor correlate for TDP-43 dysfunction in ALS brain in the first place and indeed the same metric was unable to distinguish ALS from control motor cortex (**Figure 6.12d**).

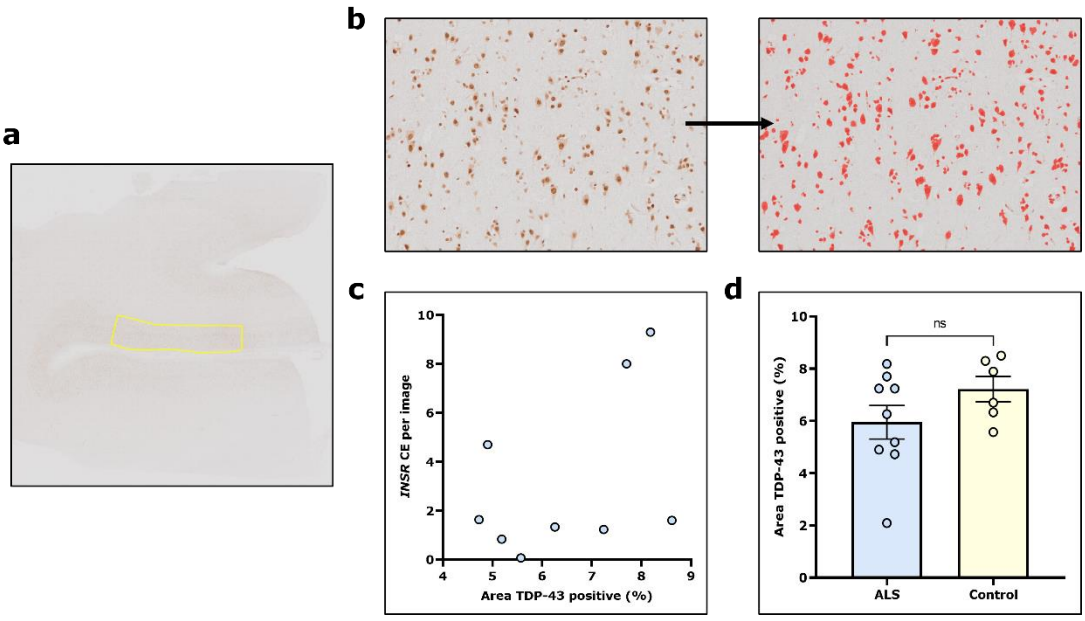

Figure 6.12. Relationship between TDP-43 immunostaining and *INSR* cryptic exon inclusion is unclear in ALS motor cortex. (a) TDP-43 IHC was performed on the same ALS motor cortex sections as BaseScope™ was performed and regions of interest (grey matter) were annotated on scanned sections. (b) Regions of interest were subjected to a DAB intensity threshold using QuPath (v0.3.0) to detect and quantify normal TDP-43 staining. (c) However, the spatial extent of TDP-43 staining, expressed as area analysed that was TDP-43 (DAB) positive (%), was not associated with BaseScope™-detected CE foci frequency (n = 9 xy pairs). (d) Indeed, there was no clear difference in TDP-43 staining between ALS (n = 9) and control (n = 6). Error bars show mean ± SEM, unpaired t-test; *p < 0.05, **p < 0.01, ***p < 0.001, ns = not significant.

Therefore, a similar analysis was conducted on pre-stained pTDP-43 FTLD-TDP frontal cortex sections at QSBB as a more direct pathological manifestation of TDP-43 dysfunction that had been previously BaseScope™-stained for *UNC13A* CE detection (**Figure 6.13a**). There was a large variation in the spatial extent of pTDP-43 pathological burden of pTDP-43 across the FTLD-TDP cohort analysed (n = 45) (**Figure 6.13b**). There was a trend towards higher pTDP-43 pathology within FTLD-TDP C vs FTLD-TDP A cases (**Figure 6.13c**), perhaps reflecting the more distributed nature of TDP-43 inclusions throughout the cortex in FTLD-TDP type C compared to type A pathology. A higher pTDP-43 pathological burden was also associated with a younger age of disease onset (**Figure 6.13d**). However, again there was no clear relationship with *UNC13A* CE inclusion measured by either CE PSI in

bulk-seq (**Figure 6.13e**) or BaseScope™ (**Figure 6.13f**) suggesting this method of regional analysis was not sufficiently sensitive.

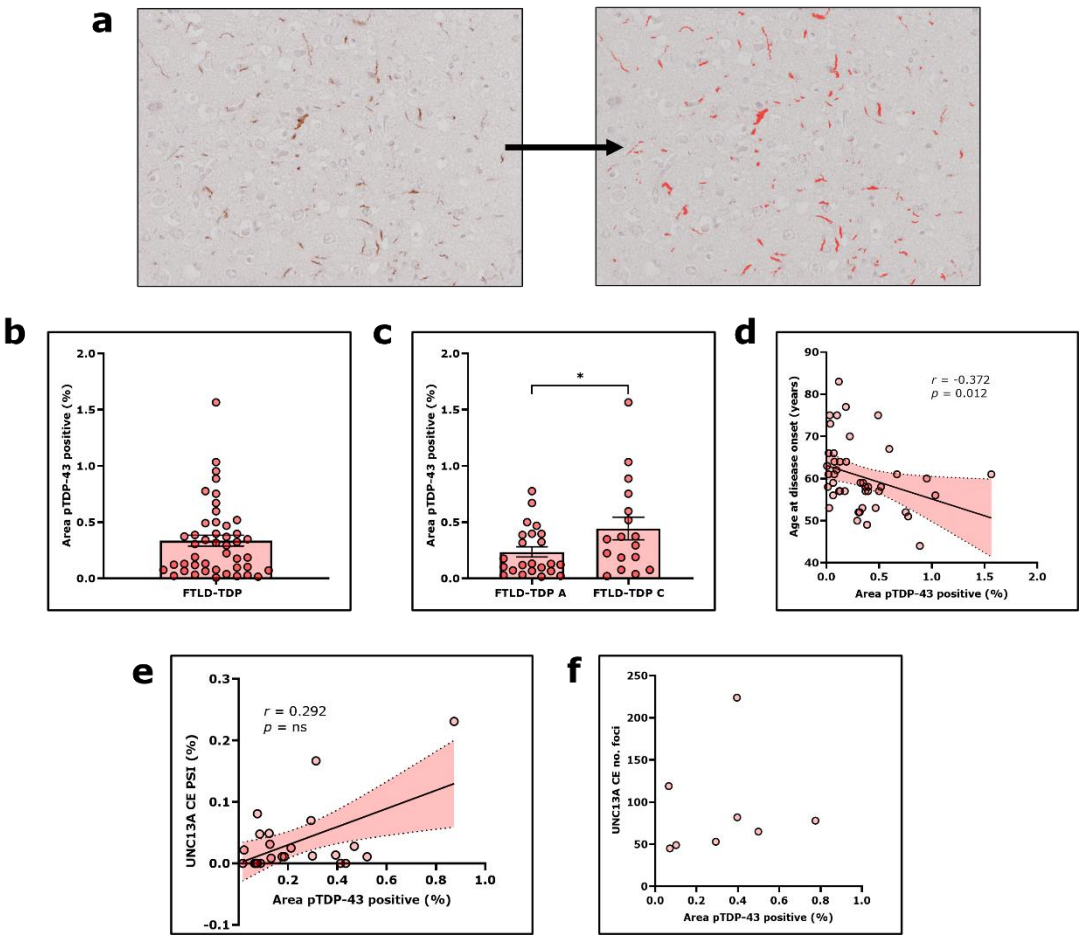

Figure 6.13. Relationship between pTDP-43 pathological burden and UNC13A cryptic exon inclusion is unclear in FTLD-TDP frontal cortex (a) Pre-pTDP43 immunostained frontal cortex scanned sections (left panel) were subjected to a DAB signal intensity threshold using QuPath (v0.3.0) to detect and quantify pTDP-43 pathological burden (right panel, red signal denotes DAB detection). (b) Complete FTLD-TDP cohort (n = 45) demonstrate wide variance in pTDP-43 pathological burden expressed as area analysed that was pTDP-43 (DAB) positive (%). (c) FTLD-TDP C (n = 17) exhibit significantly greater pTDP-43 signal positivity than FTLD-TDP A (n = 23) subjects. Error bars show mean ± SEM, unpaired t-test; *p < 0.05, **p < 0.01, ***p < 0.001, ns = not significant. (d) pTDP-43 pathological burden negatively correlates (n = 45 xy pairs, r = -0.372, p = 0.012) with age at disease onset in FTLD-TDP subjects. (e-f) pTDP-43 pathological burden does not significantly correlate with *UNC13A* CE inclusion in matched FTLD-TDP patient brain using either (e) CE PSI (%) (n = 23 xy pairs) or (f) BaseScope™-detected CE foci (n = 8).

A more sensitive method for exploring the spatial relationship between CE events and TDP-43 pathology would be to co-visualise ISH and IHC staining within the same neurons. Therefore, ISH (*INSR* CE) and IHC (TDP-43)

scanned images were aligned and overlaid using ImageJ (v1.41). Visual inspection of overlapped images yielded preliminary evidence for CE foci being present specifically within TDP-43 depleted nuclei (**Figure 6.14**). Hence, providing a platform for the future quantitation of relative CE frequency at single-cell resolution within neurons stratified by TDP-43 (or other disease-associated protein) localisation status.

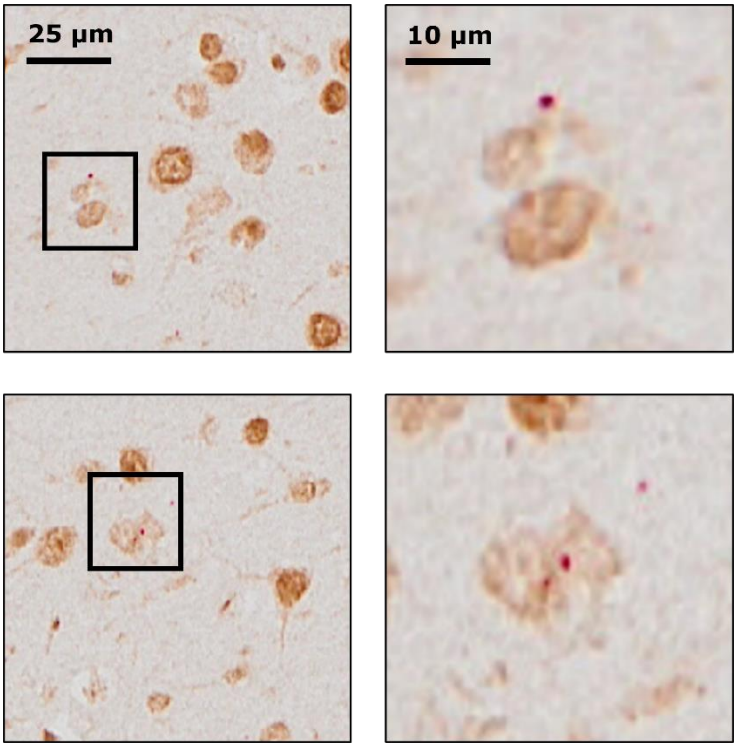

Figure 6.14. INSR CE inclusion in TDP-43 depleted neurons. Example images of overlaid BaseScope™ and IHC stained motor cortex showing *INSR* CE foci within TDP-43 depleted neurons and not in neighbouring neurons with normal TDP-43 staining.

6.4 Discussion

6.4.1 Summary of main findings

Using a CRISPRi-i^3 model of hnRNP K KD, hnRNP K has been identified as having an important regulatory role in maintaining splicing fidelity within cortical neurons. A large number of cassette exons (n = 364, FDR < 0.05; n = 126, dPSI > 10 %) were found to exhibit significantly altered splicing between control and KD groups. These included a subset of cryptic (n = 8) and skiptic

exon (*n = 24*) events which, under normal physiological conditions, hnRNP K constitutively represses. Several of these mis-splicing events were validated by three-primer PCR to demonstrate their robust activation within KD neuronal derived RNA compared to controls. Significant concordance was identified between differentially spliced cassette exons within this model and that of a previously validated SH-SY5Y siRNA model of hnRNPK KD (Bampton *et al.*, 2021) albeit with attenuated effect sizes in the present model. Interestingly, there was little evidence linking hnRNP K KD-induced splicing changes with any appreciable changes in gene expression despite NMD of non-canonically spliced variants being a well documented phenomena.

The second half of this work was concerned with the validation of TDP-43 depletion-associated CEs in post-mortem brain tissue using BaseScope™ ISH. The presence of two such CEs within the synaptic gene *UNC13A* (novel) and the insulin receptor gene *INSR* (Ling *et al.*, 2015) was detected specifically within FTLD-TDP and ALS brain respectively, relative to disease and neurologically normal control subjects. A dual ISH-IHC assay was also developed as a proof-of-principle project for the co-visualisation of CE events and associated protein staining. This not only validated the specificity of these CEs to TDP-43 proteinopathy in human brain for the first time, but also provides a platform for the future detection, quantitation and validation of aforementioned hnRNP K KD-associated splicing events.

6.4.2 HnRNP K-induced splicing and relevance to human brain

This body of work is the first to investigate and validate hnRNP K-regulated splicing events within human (cortical) neurons. The identification of many hnRNP K KD-attributed differential splicing events and particularly the upregulation of non-evolutionary conserved cryptic and skiptic events means hnRNP K joins the ranks of several other RBPs including TDP-43, hnRNP C, hnRNP L, PTBP1, SFPQ and MATR3 known to have important regulatory roles in CE and SE suppression (Zarnack *et al.*, 2013; Ling *et al.*, 2015, 2016; Tan *et al.*, 2016; Attig *et al.*, 2018; Fratta *et al.*, 2018; McClory, Lynch and Ling, 2018). Effectively, their inclusion provides a functional readout of

diminished hnRNP K protein levels and functioning within these neurons. Indeed, the relative rate of inclusion of several of these validated cryptic and skiptic hits not only provides further validation for the CRISPRi-i^3 KD model, which was previously only validated at the protein level, but may also serve as a proxy for hnRNP K functional inadequacy in other model systems of disease.

Structurally, hnRNP K mislocalisation has been observed across the neurodegenerative disease spectrum and frequently in ageing control brain but, pending validation in brain tissue, CE or SE inclusion within hnRNP K targets may offer an indirect metric for quantifying hnRNP K dysfunction in these cases. Looking much further afield, it could be envisioned that key splicing events may have pharmacodynamic biomarker capacity with the potential to monitor drug-efficacy aimed at restoring hnRNP K functioning. Longitudinal assays assessing stability and dose-response will be required to advance this line of thinking.

Notably, when comparing dPSI % values between shared 'hits' of the present model and a previous SH-SY5Y model of hnRNP K KD (Bampton *et al.*, 2021), splicing alterations were found to be frequently concordant in terms of directionality but typically attenuated in the present CRISPRi-i^3 system by comparison. This probably reflects the current model eliciting a less robust KD of hnRNP K. However, inadvertently this does confer the advantage of effectively filtering differentially spliced events by those that are most sensitive to smaller changes in hnRNP K protein levels within neurons. There were also many differentially spliced cassette exons (164 of 364) including 3 of 8 events classified as CEs and 18 of 24 events classified as SEs that were specific to the CRISPRi-i^3 neuronal model. These could represent splicing events which are particularly vulnerable to disruption within hnRNP K-depleted neurons and therefore most relevant to the neurodegeneration and/or ageing phenotype worthy of follow-up. Intriguingly, mild splicing differences within *HNRNPK* itself were identified upon KD which included a shift in propensity to use an alternative, more distal TSS. This could potentially represent an autoregulatory attempt to restore normal hnRNP K levels and functioning, or it may just be an

artefact of CRISPRi KD necessitating further study with more robust hnRNP K KD protocols.

The next steps will be to investigate the extent to which any of these identified hnRNP K-regulated splicing are disrupted in the human brain. Targeted RNA-seq on RNA derived from neurons that have undergone fluorescence activated cell sorting (FACS) and/or those isolated by laser capture microdissection (LCM) will shed light on transcriptomic changes between neuronal populations with and without hnRNP K mislocalisation (Fend and Raffeld, 2000; Liu *et al.*, 2019). Validation of any key molecular events within particular neuronal subtypes of interest e.g. pyramidal neurons of the cortex, will necessitate the employment of spatial transcriptomic techniques. With this in mind, a BaseScope™ ISH pipeline was optimised for the detection and visualisation of two CE events that had been strongly linked to TDP-43 nuclear depletion in neurons as a proof-of-concept study for validating novel hnRNP K-regulated CE/SE events in the future.

Thinking more broadly, it remains to be clarified the extent to which perturbation of hnRNP K-regulated splicing contributes to and potentially propagates, neurotoxicity within neurons. The central dogma for how de-repression of CE and SEs in target genes leads to loss of function in neurons is that their inclusion increases the likelihood of generating a PTC leading to transcript degradation by NMD, or a premature polyadenylation site leading to a truncated, non-functioning protein isoform (Ling *et al.*, 2015; Melamed *et al.*, 2019). However, in the present study there was no clear bias towards downregulation of expression within differentially spliced genes. The exception being within *NECAP2*, a gene known to have important roles within vesicle-mediated transport and clathrin-mediated endocytosis (Chamberland *et al.*, 2016). Within hnRNP K KD neurons, premature truncation of the *NECAP2* transcript, reminiscent of *STMN2* truncation in TDP-43 KD, was directly correlated with reduced *NECAP2* expression, highlighting the potential importance of this mis-splicing event in hnRNP K protein-depleted neurons. Ribosomal profiling (RP) as a transcriptome-wide measurement of translation, may provide a more precise indication of relative translation levels within other

differentially spliced genes (McGlincy and Ingolia, 2017). Even in the absence of clear NMD-mediated loss of function of hnRNP K-target genes though, it is difficult to imagine how all of these identified splicing alterations are biologically silent. Indeed, assessment of ribosomal occupancy via RP may even reveal that some CE, SE or other mis-spliced contained genes are indeed avoiding NMD and are instead being routinely translated into completely, evolutionary untested protein isoforms with potential gain of function consequences.

6.4.3 BaseScope™ as a platform for validating and interrogating disease-specific transcriptomic alterations

BaseScope™ was used to visualise and validate, for the first time, two TDP-43-regulated CE events in *UNC13A* and *INSR* within post-mortem human brain. Thus confirming the potential pathogenic relevance of these splicing defects in human neurons with TDP-43 depletion. Understanding the precise phenotypical consequences of CE incorporation within these targets will require further study. However, a loss of function may be firmly predicted for both proteins due to the fact that both CE-containing transcripts introduce a premature termination codon (PTC)-inducing frameshift which lead (strongly in the case of *UNC13A*) to NMD (Brown *et al.*, 2022). Phenotypic screens with appropriately depleted levels of both genes which assess synaptic functioning (*UNC13A* CE) and insulin-signalling pathways (*INSR* CE) may provide fresh insights as to the predicted biological consequences of these CEs. Although, the true disease phenotype is more likely to be the readout of a far more complex, cumulative model of dysfunction that takes into account all of the individual contributions of the many TDP-43 KD-associated splicing alterations.

In the case of the novel *UNC13A* CE, validating its presence in FTLD-TDP tissue (from BaseScope™ and bulk-seq investigations) was a vital piece of the puzzle which led to a mechanistic discovery that combined genetic associations (a well-established FTLD/ALS risk loci in *UNC13A*), pathological observation (neuronal TDP-43 depletion) and molecular insights (differential splicing analysis). Namely that TDP-43 loss leads to *UNC13A* CE de-

repression and subsequent reductions in *UNC13A* protein within neurons, which is an event potentiated by the presence of a neighbouring SNP (Brown *et al.*, 2022). These conclusions, also supported by BaseScope™ ISH investigations in the patient brain, were independently verified in a parallel study (Ma *et al.*, 2022).

The utility for using BaseScope™ to validate transcriptomic findings in the patient brain is clear, particularly in the case of detecting disease-specific signatures including TDP-43 regulated CEs. Dysregulated transcripts may be detected and visualised within brain or spinal-cord specific regions and potentially even within neuronal or glial subpopulations of interest with optimised dual-IHC co-staining. An advantage of BaseScope™ in future studies that is particularly pertinent to ALS pathogenesis, would be in the interrogation of key molecular signatures which may underpin specific disease phenotypes (Mehta *et al.*, 2022). A hypothetical methodological pipeline for investigating ALS heterogeneity which employs deeply clinically phenotyped cohorts, brain-region specific transcriptomics and spatially resolved BaseScope™ validation is outlined in **Figure 6.15**.

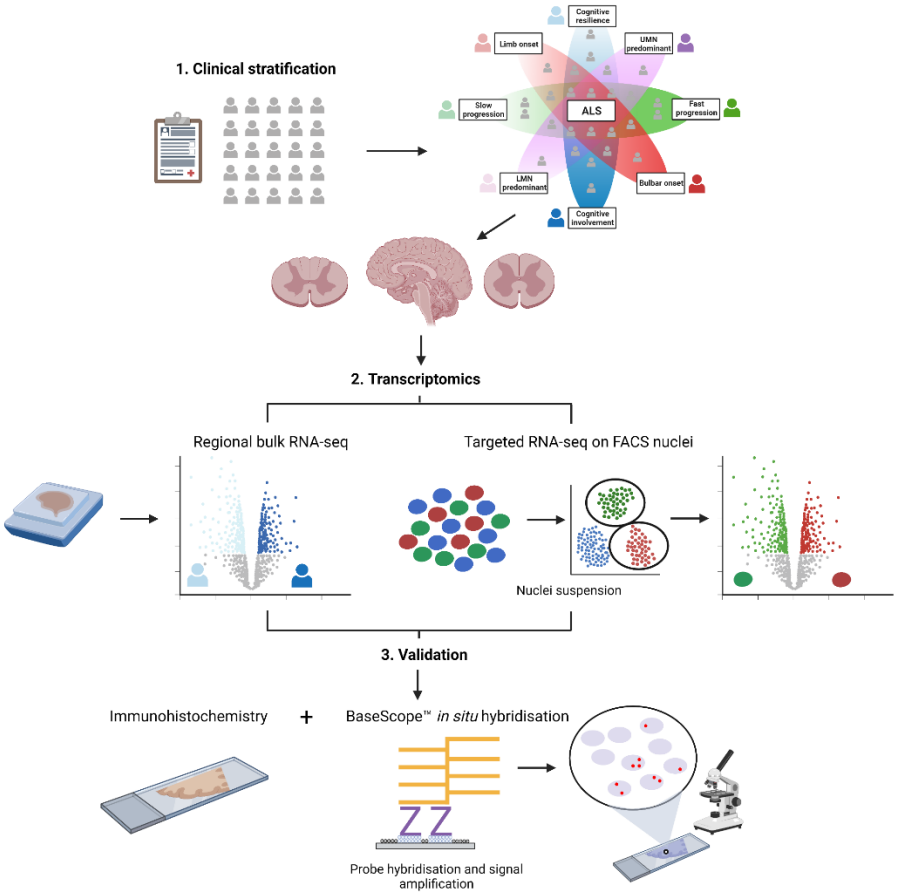

Figure 6.15. Methodological pipeline for delineating pathways underpinning ALS clinical heterogeneity. 1. ALS subjects are clinically stratified into distinct phenotypic subgroups according to their site of disease onset, rate of progression, upper (UMN) or lower motor neuron (LMN) predominance and cognitive status during life. 2. Clinico-anatomically relevant brain and spinal cord specimens from cohorts falling into two extremes of a selected phenotype (e.g. cognitive involvement vs cognitive resilience as in (Banerjee *et al.*, 2022)) can then be selected for region-specific bulk-sequencing or pathologically resolved transcriptomic analysis using fluorescence-activated sorting (FACS). 3. Finally, transcriptomic findings of interest can be further dissected using immunohistochemistry and BaseScope™ *in situ* hybridisation (Mehta *et al.*, 2022).

More challenging however, is the use of BaseScope™ to accurately quantify splicing events on a continuous scale as a reliable clinicopathological correlate. Indeed in this study, relative differences in CE frequency between ALS cases are more likely to be associated with brain tissue-specific factors affecting probe penetration and signal than they are to be linked with true biological variance. One potential solution to this may be to normalise all signal scores to a positive control probe applied to each serial section of the same-matched case, though financial implications are an important consideration

here. In the present study, this may be one reason for why TDP-43 protein was not found to be robustly associated with BaseScope™-detected *INSR* CE foci frequency. However, the dual ISH-IHC assay developed here to co-visualise CE and TDP-43 staining, which is of course feasibly applicable to other splicing event – protein pairings (e.g. those associated with hnRNP K mislocalisation), provides a platform for assessing the spatial relationships between RNA foci and related pathologies at single-cell level resolution. Thus, the platform opens up the future possibility for investigating hnRNP K KD-associated cryptic and skiptic splicing events of interest within cases pre-stratified by hnRNP K localisation status.

Chapter 7 Conclusions and future directions

7.1 Summary of main conclusions

The research described in this thesis puts hnRNP K firmly on the map alongside other hnRNPs known to be pathologically dysregulated in neurodegenerative disease including TDP-43, FUS and hnRNP A1. In chapter 3, neuronal hnRNP K nuclear depletion and mislocalisation to the cytoplasm was found to be a novel neuropathological feature in pyramidal neurons of the cortex. An event that was frequently observed in FTLD brains and also within elderly control subjects. This pathological redistribution of hnRNP K to the cytoplasm was found to occur in neurons which are mutually exclusive to those which harbour FTLD proteinaceous pathologies including pTDP-43 and pTau inclusions. In chapter 4, hnRNP K mislocalisation was shown to afflict additional neuronal sub-populations across the brain including neurons within the dentate nucleus of the cerebellum. As with pyramidal neurons of the cortex, this was a neuronal subtype not known to be typically associated with other disease-associated proteinaceous inclusions. Once again, hnRNP K mislocalisation within the dentate nucleus was frequently observed within neurodegenerative disease-afflicted brains (this time including FTLD and AD cohorts) and was also found to correlate with ageing in neurologically normal controls. Hence, hnRNP K neuronal pathology and potential dysfunction may be a neuroanatomically widespread phenomenon with a broader relevance to the wider dementia field and ageing process.

In an attempt to recapitulate nuclear, hnRNP K loss of function, a hnRNP K neuronal knockdown (KD) model was developed and optimised utilising CRISPR-interference (CRISPRi) technology in chapter 5. In chapter 6, hnRNP K nuclear depletion was found to be associated with widespread alterations in splicing within gene targets using differential splicing analysis. In particular, hnRNP K protein KD led to the de-repression of non-conserved cryptic (CE) and skiptic exon (SE) mis-splicing events which are an emerging pathomechanism of neurodegenerative disease. Finally, in order to validate an

in situ hybridisation (ISH) technique (BaseScope™) for the visualisation and quantitation of mis-splicing events in patient brain, an assay was established to detect TDP-43 depletion-associated CE events in the synaptic gene *UNC13A and* insulin receptor *INSR*. Indeed, both events were validated specifically within FTLD-TDP and ALS post-mortem brain tissue. A dual ISH-IHC strategy for the co-visualisation of RNA splice variants and associated protein immunostaining was developed to further interrogate the RNA-protein spatial relationship. Hence, providing a platform for the validation and exploration of hnRNP K-regulated splicing events in the future.

7.2 Future work

Future directions for hnRNP K mislocalisation in disease and ageing research will be targeted towards answering some of the most important questions raised throughout this thesis. From a pathological standpoint, what structural and/or functional features link neuronal subtypes most vulnerable to hnRNP K mislocalisation? Is hnRNP K mislocalisation in neurons a result of impaired nucleocytoplasmic transport, independent cytoplasmic demixing or related to other organelle-related disruption including stress granule assembly? Further attempts to characterise cytoplasmic hnRNP K puncta with the possible benefit of further immunofluorescence analyses, co-immunoprecipitation pull down assays and biochemical fractionation studies may well shed light on the biological origins of this novel neuropathology.

Investigating the functional consequences of hnRNP K nuclear depletion in CRISPRi-i^3 neurons has also led to as many questions as it has answers. To what extent are hnRNP K KD-associated mis-splicing events upregulated within human brain and to what relevance do these events have in disease pathogenesis? BaseScope™ may provide some answers to the former, but the employment of single-cell approaches including fluorescence-activated cell sorting (FACS)-seq and targeted sequencing of neurons isolated by laser capture microscopy (LCM) will likely have wider utility in identifying transcriptomic signatures distinct to those neurons exhibiting hnRNP K

mislocalisation. The selection of which particular splicing events to pursue for further study; cryptic, skiptic or otherwise may in part be determined by the extent to which they cause protein loss of function via (NMD)-mediated degradation and/or their relevance to the neuronal phenotype. Ribosomal profiling to determine non-translated (or aberrantly translated) transcripts as well as individual-nucleotide resolution crosslinking and immunoprecipitation (iCLIP) analyses to reveal those transcripts most closely associated with hnRNP K protein, may well prove fruitful in this capacity. It also remains to be ascertained whether, how and the extent to which, hnRNP K self-regulates its own expression in neurons. Additional cell KD protocols with varying degrees of robustness, accompanied by further accompanying differential splicing analyses may at least put to bed whether or not hnRNP K is negatively autoregulating itself via splicing-dependent means. Finally, and relevant to dysregulated splicing regulation more generally, it will need clarifying the degree to which cryptic, skiptic or other mis-splicing events correlate with related protein pathologies in brain tissue. For example in the case of TDP-43 proteinopathy, do CEs (including those validated in this study) appear only in neurons harbouring TDP-43 immunoreactive inclusions or are they also present in neurons exhibiting only mild TDP-43 depletion? Does sensitivity to TDP-43 protein levels differ between different CEs? The dual ISH-IHC assay developed towards the end of chapter 6 has the potential to provide new insights as to where CE incorporation comes in the TDP-43 inclusion-formation timeline. Dose-dependent RBP KD studies with CE-inclusion readout will also prove important here.

Finally and as discussed previously, the hnRNP K KD-induced splicing dysfunction explored in this thesis is, by definition, a loss of function phenotype. It is important to remember that hnRNP K mislocalisation involves granular accumulation within the cytoplasm in addition to nuclear depletion. The former of which may well be more associated with gain of function mechanisms of invoked-toxicity. Cell and animal hnRNP K overexpression paradigms and particularly those which disrupt hnRNP K’s nuclear localisation sequence, could facilitate gain of function phenotypic screens in the future.

7.3 Concluding remarks

Overall, the body of work described in this thesis introduces a new player, hnRNP K, in the neurodegeneration and ageing fields. Its mislocalisation in neuronal populations across the brain and its identified homeostatic roles in maintaining appropriate splicing fidelity within gene targets, together provides further evidence for RNA-binding protein (RBP) disruption and misprocessing being key drivers of neurodegeneration. The findings described here are an example for how pathology can direct mechanistic investigations aimed at elucidating structure and function interrelationships in disease.

References

Adamson, B., Norman, T. M., Jost, M., Cho, M. Y., Nuñez, J. K., Chen, Y., Villalta, J. E., Gilbert, L. A., Horlbeck, M. A., Hein, M. Y., Pak, R. A., Gray, A. N., Gross, C. A., Dixit, A., Parnas, O., Regev, A. and Weissman, J. S. (2016). "A Multiplexed Single-Cell CRISPR Screening Platform Enables Systematic Dissection of the Unfolded Protein Response." *Cell*, 167 (7), pp. 1867-1882.e21. doi: 10.1016/j.cell.2016.11.048.

Adamson, B., Smogorzewska, A., Sigoillot, F. D., King, R. W. and Elledge, S. J. (2012). "A genome-wide homologous recombination screen identifies the RNA-binding protein RBMX as a component of the DNA-damage response." *Nature Cell Biology*, 14 (3), pp. 318–328. doi: 10.1038/ncb2426.

Adli, M. (2018). "The CRISPR tool kit for genome editing and beyond." *Nature Communications*, 9 (1), p. 1911. doi: 10.1038/s41467-018-04252-2.

Amaral, D. G. (1978). "A Golgi study of cell types in the hilar region of the hippocampus in the rat." *The Journal of Comparative Neurology*, 182 (4 Pt 2), pp. 851–914. doi: 10.1002/cne.901820508.

Andersen, P. M. (2006). "Amyotrophic lateral sclerosis associated with mutations in the CuZn superoxide dismutase gene." *Current Neurology and Neuroscience Reports*, 6 (1), pp. 37–46. doi: 10.1007/s11910-996-0008-9.

Appocher, C., Mohagheghi, F., Cappelli, S., Stuani, C., Romano, M., Feiguin, F. and Buratti, E. (2017). "Major hnRNP proteins act as general TDP-43 functional modifiers both in Drosophila and human neuronal cells." *Nucleic Acids Research*, 45 (13), pp. 8026–8045. doi: 10.1093/nar/gkx477.

Arnold, E. S., Ling, S.-C., Huelga, S. C., Lagier-Tourenne, C., Polymenidou, M., Ditsworth, D., Kordasiewicz, H. B., McAlonis-Downes, M., Platoshyn, O., Parone, P. A., Da Cruz, S., Clutario, K. M., Swing, D., Tessarollo, L., Marsala, M., Shaw, C. E., Yeo, G. W. and Cleveland, D. W. (2013). "ALS-linked TDP-43 mutations produce aberrant RNA splicing and adult-onset motor neuron disease without aggregation or loss of nuclear TDP-43." *Proceedings of the National Academy of Sciences of the United States of America*, 110 (8), pp. E736-45. doi: 10.1073/pnas.1222809110.

Arvanitakis, Z., Shah, R. C. and Bennett, D. A. (2019). "Diagnosis and management of dementia: review." *The Journal of the American Medical Association*, 322 (16), pp. 1589–1599. doi: 10.1001/jama.2019.4782.

Attig, J., Agostini, F., Gooding, C., Chakrabarti, A. M., Singh, A., Haberman, N., Zagalak, J. A., Emmett, W., Smith, C. W. J., Luscombe, N. M. and Ule, J. (2018). "Heteromeric RNP Assembly at LINEs Controls Lineage-Specific RNA Processing." *Cell*, 174 (5), pp. 1067-1081.e17. doi: 10.1016/j.cell.2018.07.001.

Ayala, Y. M., De Conti, L., Avendaño-Vázquez, S. E., Dhir, A., Romano, M., D'Ambrogio, A., Tollervey, J., Ule, J., Baralle, M., Buratti, E. and Baralle, F. E. (2011). "TDP-43 regulates its mRNA levels through a negative feedback loop." *The EMBO Journal*, 30 (2), pp. 277–288. doi: 10.1038/emboj.2010.310.

Baker, A.-M., Huang, W., Wang, X.-M. M., Jansen, M., Ma, X.-J., Kim, J., Anderson, C. M., Wu, X., Pan, L., Su, N., Luo, Y., Domingo, E., Heide, T., Sottoriva, A., Lewis, A., Beggs, A. D., Wright, N. A., Rodriguez-Justo, M., Park, E., Tomlinson, I. and Graham, T. A. (2017). "Robust RNA-based in situ mutation detection delineates colorectal cancer subclonal evolution." *Nature Communications*, 8 (1), p. 1998. doi: 10.1038/s41467-017-02295-5.

Balendra, R. and Isaacs, A. M. (2018). "C9orf72-mediated ALS and FTD: multiple pathways to disease." *Nature Reviews. Neurology*, 14 (9), pp. 544–558. doi: 10.1038/s41582-018-0047-2.

Bampton, A., Gatt, A., Humphrey, J., Cappelli, S., Bhattacharya, D., Foti, S., Brown, A.-L., Asi, Y., Low, Y. H., Foiani, M., Raj, T., Buratti, E., Fratta, P. and Lashley, T. (2021). "HnRNP K mislocalisation is a novel protein pathology of frontotemporal lobar degeneration and ageing and leads to cryptic splicing." *Acta Neuropathologica*, 142 (4), pp. 609–627. doi: 10.1007/s00401-021-02340-0.

Bampton, A., Gittings, L. M., Fratta, P., Lashley, T. and Gatt, A. (2020). "The role of hnRNPs in frontotemporal dementia and amyotrophic lateral sclerosis." *Acta Neuropathologica*, 140 (5), pp. 599–623. doi: 10.1007/s00401-020-02203-0.

Banerjee, K., Wang, M., Cai, E., Fujiwara, N., Baker, H. and Cave, J. W. (2014). "Regulation of tyrosine hydroxylase transcription by hnRNP K and DNA secondary structure." *Nature Communications*, 5, p. 5769. doi: 10.1038/ncomms6769.

Banerjee, P., Elliott, E., Rifai, O. M., O'Shaughnessy, J., McDade, K., Abrahams, S., Chandran, S., Smith, C. and Gregory, J. M. (2022). "NLRP3 inflammasome as a key molecular target underlying cognitive resilience in amyotrophic lateral sclerosis." *The Journal of Pathology*, 256 (3), pp. 262–268. doi: 10.1002/path.5846.

Baradaran-Heravi, Y., Van Broeckhoven, C. and van der Zee, J. (2020). "Stress granule mediated protein aggregation and underlying gene defects in the FTD-ALS spectrum." *Neurobiology of Disease*, 134, p. 104639. doi: 10.1016/j.nbd.2019.104639.

Baralle, F. E. and Giudice, J. (2017). "Alternative splicing as a regulator of development and tissue identity." *Nature Reviews. Molecular Cell Biology*, 18 (7), pp. 437–451. doi: 10.1038/nrm.2017.27.

Barboro, P., Ferrari, N. and Balbi, C. (2014). “Emerging roles of heterogeneous nuclear ribonucleoprotein K (hnRNP K) in cancer progression.” *Cancer Letters*, 352 (2), pp. 152–159. doi: 10.1016/j.canlet.2014.06.019.

Bardy, C., van den Hurk, M., Eames, T., Marchand, C., Hernandez, R. V., Kellogg, M., Gorris, M., Galet, B., Palomares, V., Brown, J., Bang, A. G., Mertens, J., Böhnke, L., Boyer, L., Simon, S. and Gage, F. H. (2015). “Neuronal medium that supports basic synaptic functions and activity of human neurons in vitro.” *Proceedings of the National Academy of Sciences of the United States of America*, 112 (20), pp. E2725-34. doi: 10.1073/pnas.1504393112.

Barrangou, R., Fremaux, C., Deveau, H., Richards, M., Boyaval, P., Moineau, S., Romero, D. A. and Horvath, P. (2007). “CRISPR provides acquired resistance against viruses in prokaryotes.” *Science*, 315 (5819), pp. 1709–1712. doi: 10.1126/science.1138140.

Barrio-Alonso, E., Hernández-Vivanco, A., Walton, C. C., Perea, G. and Frade, J. M. (2018). “Cell cycle reentry triggers hyperploidization and synaptic dysfunction followed by delayed cell death in differentiated cortical neurons.” *Scientific Reports*, 8 (1), p. 14316. doi: 10.1038/s41598-018-32708-4.

Bekkers, J. M. (2011). “Pyramidal neurons.” *Current Biology*, 21 (24), p. R975. doi: 10.1016/j.cub.2011.10.037.

Berdyński, M., Miszta, P., Safranow, K., Andersen, P. M., Morita, M., Filipek, S., Żekanowski, C. and Kuźma-Kozakiewicz, M. (2022). “SOD1 mutations associated with amyotrophic lateral sclerosis analysis of variant severity.” *Scientific Reports*, 12 (1), p. 103. doi: 10.1038/s41598-021-03891-8.

Bharti, K., Khan, M., Beaulieu, C., Graham, S. J., Briemberg, H., Frayne, R., Genge, A., Korngut, L., Zinman, L., Kalra, S. and Canadian ALS Neuroimaging Consortium. (2020). “Involvement of the dentate nucleus in the pathophysiology of amyotrophic lateral sclerosis: A multi-center and multi-modal neuroimaging study.” *NeuroImage. Clinical*, 28, p. 102385. doi: 10.1016/j.nicl.2020.102385.

Biel, D., Brendel, M., Rubinski, A., Buerger, K., Janowitz, D., Dichgans, M., Franzmeier, N. and Alzheimer’s Disease Neuroimaging Initiative (ADNI). (2021). “Tau-PET and in vivo Braak-staging as prognostic markers of future cognitive decline in cognitively normal to demented individuals.” *Alzheimer’s research & therapy*, 13 (1), p. 137. doi: 10.1186/s13195-021-00880-x.

Biffi, A. and Greenberg, S. M. (2011). “Cerebral amyloid angiopathy: a systematic review.” *Journal of clinical neurology (Seoul, Korea)*, 7 (1), pp. 1–9. doi: 10.3988/jcn.2011.7.1.1.

Blokhuis, A. M., Groen, E. J. N., Koppers, M., van den Berg, L. H. and Pasterkamp, R. J. (2013). “Protein aggregation in amyotrophic lateral sclerosis.” *Acta Neuropathologica*, 125 (6), pp. 777–794. doi: 10.1007/s00401-013-1125-6.

Bocchetta, M., Malpetti, M., Todd, E. G., Rowe, J. B. and Rohrer, J. D. (2021). “Looking beneath the surface: the importance of subcortical structures in frontotemporal dementia.” *Brain Communications*, 3 (3), p. fcab158. doi: 10.1093/braincomms/fcab158.

Boettcher, M. and McManus, M. T. (2015). “Choosing the right tool for the job: rnai, TALEN, or CRISPR.” *Molecular Cell*, 58 (4), pp. 575–585. doi: 10.1016/j.molcel.2015.04.028.

Bolger, A. M., Lohse, M. and Usadel, B. (2014). “Trimmomatic: a flexible trimmer for Illumina sequence data.” *Bioinformatics*, 30 (15), pp. 2114–2120. doi: 10.1093/bioinformatics/btu170.

Bomsztyk, K., Van Seuningen, I., Suzuki, H., Denisenko, O. and Ostrowski, J. (1997). “Diverse molecular interactions of the hnRNP K protein.” *FEBS Letters*, 403 (2), pp. 113–115. doi: 10.1016/s0014-5793(97)00041-0.

Bond, K. M., Brinjikji, W., Eckel, L. J., Kallmes, D. F., McDonald, R. J. and Carr, C. M. (2017). “Dentate update: imaging features of entities that affect the dentate nucleus.” *American Journal of Neuroradiology*, 38 (8), pp. 1467–1474. doi: 10.3174/ajnr.A5138.

Bowden, H. A. and Dormann, D. (2016). “Altered mRNP granule dynamics in FTLD pathogenesis.” *Journal of Neurochemistry*, 138 Suppl 1, pp. 112–133. doi: 10.1111/jnc.13601.

Bowles, K. R., Pugh, D. A., Oja, L.-M., Jadow, B. M., Farrell, K., Whitney, K., Sharma, A., Cherry, J. D., Raj, T., Pereira, A. C., Crary, J. F. and Goate, A. M. (2022). “Dysregulated coordination of MAPT exon 2 and exon 10 splicing underlies different tau pathologies in PSP and AD.” *Acta Neuropathologica*, 143 (2), pp. 225–243. doi: 10.1007/s00401-021-02392-2.

Braak, H., Alafuzoff, I., Arzberger, T., Kretzschmar, H. and Del Tredici, K. (2006). “Staging of Alzheimer disease-associated neurofibrillary pathology using paraffin sections and immunocytochemistry.” *Acta Neuropathologica*, 112 (4), pp. 389–404. doi: 10.1007/s00401-006-0127-z.

Braak, H., Brettschneider, J., Ludolph, A. C., Lee, V. M., Trojanowski, J. Q. and Del Tredici, K. (2013). “Amyotrophic lateral sclerosis--a model of corticofugal axonal spread.” *Nature Reviews. Neurology*, 9 (12), pp. 708–714. doi: 10.1038/nrneurol.2013.221.

Bradfield, N. I. (2021). “Mild cognitive impairment: diagnosis and subtypes.” *Clinical EEG and neuroscience : official journal of the EEG and Clinical*

Neuroscience Society (ENCS), p. 15500594211042708. doi: 10.1177/15500594211042708.

Breijyeh, Z. and Karaman, R. (2020). “Comprehensive review on alzheimer’s disease: causes and treatment.” *Molecules (Basel, Switzerland)*, 25 (24). doi: 10.3390/molecules25245789.

Broderick, J., Wang, J. and Andreadis, A. (2004). “Heterogeneous nuclear ribonucleoprotein E2 binds to tau exon 10 and moderately activates its splicing.” *Gene*, 331, pp. 107–114. doi: 10.1016/j.gene.2004.02.005.

Brouns, S. J. J., Jore, M. M., Lundgren, M., Westra, E. R., Slijkhuis, R. J. H., Snijders, A. P. L., Dickman, M. J., Makarova, K. S., Koonin, E. V. and van der Oost, J. (2008). “Small CRISPR RNAs guide antiviral defense in prokaryotes.” *Science*, 321 (5891), pp. 960–964. doi: 10.1126/science.1159689.

Brown, A.-L., Wilkins, O. G., Keuss, M. J., Hill, S. E., Zanovello, M., Lee, W. C., Bampton, A., Lee, F. C. Y., Masino, L., Qi, Y. A., Bryce-Smith, S., Gatt, A., Hallegger, M., Fagegaltier, D., Phatnani, H., NYGC ALS Consortium, Newcombe, J., Gustavsson, E. K., Seddighi, S., Reyes, J. F. and Fratta, P. (2022). “TDP-43 loss and ALS-risk SNPs drive mis-splicing and depletion of UNC13A.” *Nature*, 603 (7899), pp. 131–137. doi: 10.1038/s41586-022-04436-3.

Buratti, E. and Baralle, F. E. (2011). “TDP-43: new aspects of autoregulation mechanisms in RNA binding proteins and their connection with human disease.” *The FEBS Journal*, 278 (19), pp. 3530–3538. doi: 10.1111/j.1742-4658.2011.08257.x.

Burns, A. and Iliffe, S. (2009). “Alzheimer’s disease.” *BMJ (Clinical Research Ed.)*, 338, p. b158. doi: 10.1136/bmj.b158.

Busskamp, V., Lewis, N. E., Guye, P., Ng, A. H. M., Shipman, S. L., Byrne, S. M., Sanjana, N. E., Murn, J., Li, Y., Li, S., Stadler, M., Weiss, R. and Church, G. M. (2014). “Rapid neurogenesis through transcriptional activation in human stem cells.” *Molecular Systems Biology*, 10, p. 760. doi: 10.15252/msb.20145508.

Calarco, J. A. (2013). “‘Cryptic’ exons reveal some of their secrets.” *eLife*, 2, p. e00476. doi: 10.7554/eLife.00476.

Caputi, M. and Zahler, A. M. (2002). “SR proteins and hnRNP H regulate the splicing of the HIV-1 tev-specific exon 6D.” *The EMBO Journal*, 21 (4), pp. 845–855. doi: 10.1093/emboj/21.4.845.

Carpenter, B., McKay, M., Dundas, S. R., Lawrie, L. C., Telfer, C. and Murray, G. I. (2006). “Heterogeneous nuclear ribonucleoprotein K is over expressed, aberrantly localised and is associated with poor prognosis in

colorectal cancer.” *British Journal of Cancer*, 95 (7), pp. 921–927. doi: 10.1038/sj.bjc.6603349.

Chabot, B., Blanchette, M., Lapierre, I. and La Branche, H. (1997). “An intron element modulating 5’ splice site selection in the hnRNP A1 pre-mRNA interacts with hnRNP A1.” *Molecular and Cellular Biology*, 17 (4), pp. 1776–1786. doi: 10.1128/MCB.17.4.1776.

Chamberland, J. P., Antonow, L. T., Dias Santos, M. and Ritter, B. (2016). “NECAP2 controls clathrin coat recruitment to early endosomes for fast endocytic recycling.” *Journal of Cell Science*, 129 (13), pp. 2625–2637. doi: 10.1242/jcs.173708.

Chen, J., Cohen, M. L., Lerner, A. J., Yang, Y. and Herrup, K. (2010). “DNA damage and cell cycle events implicate cerebellar dentate nucleus neurons as targets of Alzheimer’s disease.” *Molecular Neurodegeneration*, 5, p. 60. doi: 10.1186/1750-1326-5-60.

Chen, M., Maimaitili, M., Habekost, M., Gill, K. P., Mermet-Joret, N., Nabavi, S., Febbraro, F. and Denham, M. (2020). “Rapid generation of regionally specified CNS neurons by sequential patterning and conversion of human induced pluripotent stem cells.” *Stem Cell Research*, 48, p. 101945. doi: 10.1016/j.scr.2020.101945.

Chen, S., Sayana, P., Zhang, X. and Le, W. (2013). “Genetics of amyotrophic lateral sclerosis: an update.” *Molecular Neurodegeneration*, 8, p. 28. doi: 10.1186/1750-1326-8-28.

Cho, S. W., Kim, S., Kim, J. M. and Kim, J.-S. (2013). “Targeted genome engineering in human cells with the Cas9 RNA-guided endonuclease.” *Nature Biotechnology*, 31 (3), pp. 230–232. doi: 10.1038/nbt.2507.

Clark, L. R., Berman, S. E., Norton, D., Koscik, R. L., Jonaitis, E., Blennow, K., Bendlin, B. B., Asthana, S., Johnson, S. C., Zetterberg, H. and Carlsson, C. M. (2018). “Age-accelerated cognitive decline in asymptomatic adults with CSF β-amyloid.” *Neurology*, 90 (15), pp. e1306–e1315. doi: 10.1212/WNL.0000000000005291.

Cloutier, A., Shkreta, L., Toutant, J., Durand, M., Thibault, P. and Chabot, B. (2018). “hnRNP A1/A2 and Sam68 collaborate with SRSF10 to control the alternative splicing response to oxaliplatin-mediated DNA damage.” *Scientific Reports*, 8 (1), p. 2206. doi: 10.1038/s41598-018-20360-x.

Cong, L., Ran, F. A., Cox, D., Lin, S., Barretto, R., Habib, N., Hsu, P. D., Wu, X., Jiang, W., Marraffini, L. A. and Zhang, F. (2013). “Multiplex genome engineering using CRISPR/Cas systems.” *Science*, 339 (6121), pp. 819–823. doi: 10.1126/science.1231143.

Conlon, E. G., Fagegaltier, D., Agius, P., Davis-Porada, J., Gregory, J., Hubbard, I., Kang, K., Kim, D., New York Genome Center ALS Consortium, Phatnani, H., Shneider, N. A. and Manley, J. L. (2018). “Unexpected similarities between C9ORF72 and sporadic forms of ALS/FTD suggest a common disease mechanism.” *eLife*, 7. doi: 10.7554/eLife.37754.

Conlon, E. G., Lu, L., Sharma, A., Yamazaki, T., Tang, T., Shneider, N. A. and Manley, J. L. (2016). “The C9ORF72 GGGGCC expansion forms RNA G-quadruplex inclusions and sequesters hnRNP H to disrupt splicing in ALS brains.” *eLife*, 5. doi: 10.7554/eLife.17820.

Conlon, E. G. and Manley, J. L. (2017). “RNA-binding proteins in neurodegeneration: mechanisms in aggregate.” *Genes & Development*, 31 (15), pp. 1509–1528. doi: 10.1101/gad.304055.117.

Cooper-Knock, J., Walsh, M. J., Higginbottom, A., Robin Highley, J., Dickman, M. J., Edbauer, D., Ince, P. G., Wharton, S. B., Wilson, S. A., Kirby, J., Hautbergue, G. M. and Shaw, P. J. (2014). “Sequestration of multiple RNA recognition motif-containing proteins by C9orf72 repeat expansions.” *Brain: A Journal of Neurology*, 137 (Pt 7), pp. 2040–2051. doi: 10.1093/brain/awu120.

Coria, F., Castaño, E. M. and Frangione, B. (1987). “Brain amyloid in normal aging and cerebral amyloid angiopathy is antigenically related to Alzheimer’s disease beta-protein.” *The American Journal of Pathology*, 129 (3), pp. 422–428.

Craft, S. and Watson, G. S. (2004). “Insulin and neurodegenerative disease: shared and specific mechanisms.” *Lancet Neurology*, 3 (3), pp. 169–178. doi: 10.1016/S1474-4422(04)00681-7.

Cragnaz, L., Klima, R., De Conti, L., Romano, G., Feiguin, F., Buratti, E., Baralle, M. and Baralle, F. E. (2015). “An age-related reduction of brain TBPH/TDP-43 levels precedes the onset of locomotion defects in a Drosophila ALS model.” *Neuroscience*, 311, pp. 415–421. doi: 10.1016/j.neuroscience.2015.10.037.

Crary, J. F., Trojanowski, J. Q., Schneider, J. A., Abisambra, J. F., Abner, E. L., Alafuzoff, I., Arnold, S. E., Attems, J., Beach, T. G., Bigio, E. H., Cairns, N. J., Dickson, D. W., Gearing, M., Grinberg, L. T., Hof, P. R., Hyman, B. T., Jellinger, K., Jicha, G. A., Kovacs, G. G., Knopman, D. S. and Nelson, P. T. (2014). “Primary age-related tauopathy (PART): a common pathology associated with human aging.” *Acta Neuropathologica*, 128 (6), pp. 755–766. doi: 10.1007/s00401-014-1349-0.

Cummings, J., Lee, G., Mortsdorf, T., Ritter, A. and Zhong, K. (2017). “Alzheimer’s disease drug development pipeline: 2017.” *Alzheimer’s & Dementia : Translational Research & Clinical Interventions*, 3 (3), pp. 367–384. doi: 10.1016/j.trci.2017.05.002.

Czubaty, A., Girstun, A., Kowalska-Loth, B., Trzcińska, A. M., Purta, E., Winczura, A., Grajkowski, W. and Staroń, K. (2005). “Proteomic analysis of complexes formed by human topoisomerase I.” *Biochimica et Biophysica Acta*, 1749 (1), pp. 133–141. doi: 10.1016/j.bbapap.2005.03.007.

D’Alton, S., Altshuler, M. and Lewis, J. (2015). “Studies of alternative isoforms provide insight into TDP-43 autoregulation and pathogenesis.” *RNA (New York)*, 21 (8), pp. 1419–1432. doi: 10.1261/rna.047647.114.

Daguenet, E., Dujardin, G. and Valcárcel, J. (2015). “The pathogenicity of splicing defects: mechanistic insights into pre-mRNA processing inform novel therapeutic approaches.” *EMBO Reports*, 16 (12), pp. 1640–1655. doi: 10.15252/embr.201541116.

Dana, H., Chalbatani, G. M., Mahmoodzadeh, H., Karimloo, R., Rezaiean, O., Moradzadeh, A., Mehmandoost, N., Moazzen, F., Mazraeh, A., Marmari, V., Ebrahimi, M., Rashno, M. M., Abadi, S. J. and Gharagouzlo, E. (2017). “Molecular Mechanisms and Biological Functions of siRNA.” *International journal of biomedical science : IJBS*, 13 (2), pp. 48–57.

Datlinger, P., Rendeiro, A. F., Schmidl, C., Krausgruber, T., Traxler, P., Klughammer, J., Schuster, L. C., Kuchler, A., Alpar, D. and Bock, C. (2017). “Pooled CRISPR screening with single-cell transcriptome readout.” *Nature Methods*, 14 (3), pp. 297–301. doi: 10.1038/nmeth.4177.

Davidson, Y. S., Flood, L., Robinson, A. C., Nihei, Y., Mori, K., Rollinson, S., Richardson, A., Benson, B. C., Jones, M., Snowden, J. S., Pickering-Brown, S., Haass, C., Lashley, T. and Mann, D. M. A. (2017). “Heterogeneous ribonuclear protein A3 (hnRNP A3) is present in dipeptide repeat protein containing inclusions in Frontotemporal Lobar Degeneration and Motor Neurone disease associated with expansions in C9orf72 gene.” *Acta neuropathologica communications*, 5 (1), p. 31. doi: 10.1186/s40478-017-0437-5.

Dayyani, F., Wang, J., Yeh, J.-R. J., Ahn, E.-Y., Tobey, E., Zhang, D.-E., Bernstein, I. D., Peterson, R. T. and Sweetser, D. A. (2008). “Loss of TLE1 and TLE4 from the del(9q) commonly deleted region in AML cooperates with AML1-ETO to affect myeloid cell proliferation and survival.” *Blood*, 111 (8), pp. 4338–4347. doi: 10.1182/blood-2007-07-103291.

DeJesus-Hernandez, M., Mackenzie, I. R., Boeve, B. F., Boxer, A. L., Baker, M., Rutherford, N. J., Nicholson, A. M., Finch, N. A., Flynn, H., Adamson, J., Kouri, N., Wojtas, A., Sengdy, P., Hsiung, G.-Y. R., Karydas, A., Seeley, W. W., Josephs, K. A., Coppola, G., Geschwind, D. H., Wszolek, Z. K. and Rademakers, R. (2011). “Expanded GGGGCC hexanucleotide repeat in noncoding region of C9ORF72 causes chromosome 9p-linked FTD and ALS.” *Neuron*, 72 (2), pp. 245–256. doi: 10.1016/j.neuron.2011.09.011.

Dejgaard, K. and Leffers, H. (1996). “Characterisation of the nucleic-acid-binding activity of KH domains. Different properties of different domains.” *European Journal of Biochemistry / FEBS*, 241 (2), pp. 425–431. doi: 10.1111/j.1432-1033.1996.00425.x.

Deltcheva, E., Chylinski, K., Sharma, C. M., Gonzales, K., Chao, Y., Pirzada, Z. A., Eckert, M. R., Vogel, J. and Charpentier, E. (2011). “CRISPR RNA maturation by trans-encoded small RNA and host factor RNase III.” *Nature*, 471 (7340), pp. 602–607. doi: 10.1038/nature09886.

Deriano, L. and Roth, D. B. (2013). “Modernizing the nonhomologous end-joining repertoire: alternative and classical NHEJ share the stage.” *Annual Review of Genetics*, 47, pp. 433–455. doi: 10.1146/annurev-genet-110711-155540.

Deshaies, J.-E., Shkreta, L., Moszczynski, A. J., Sidibé, H., Semmler, S., Fouillen, A., Bennett, E. R., Bekenstein, U., Destroismaisons, L., Toutant, J., Delmotte, Q., Volkening, K., Stabile, S., Aulas, A., Khalfallah, Y., Soreq, H., Nanci, A., Strong, M. J., Chabot, B. and Vande Velde, C. (2018). “TDP-43 regulates the alternative splicing of hnRNP A1 to yield an aggregation-prone variant in amyotrophic lateral sclerosis.” *Brain: A Journal of Neurology*, 141 (5), pp. 1320–1333. doi: 10.1093/brain/awy062.

Deveau, H., Barrangou, R., Garneau, J. E., Labonté, J., Fremaux, C., Boyaval, P., Romero, D. A., Horvath, P. and Moineau, S. (2008). “Phage response to CRISPR-encoded resistance in Streptococcus thermophilus.” *Journal of Bacteriology*, 190 (4), pp. 1390–1400. doi: 10.1128/JB.01412-07.

Dharmadasa, T. and Kiernan, M. C. (2018). “Riluzole, disease stage and survival in ALS.” *Lancet Neurology*, 17 (5), pp. 385–386. doi: 10.1016/S1474-4422(18)30091-7.

Diaz-Garcia, S., Ko, V. I., Vazquez-Sanchez, S., Chia, R., Arogundade, O. A., Rodriguez, M. J., Traynor, B. J., Cleveland, D. and Ravits, J. (2021). “Nuclear depletion of RNA-binding protein ELAVL3 (HuC) in sporadic and familial amyotrophic lateral sclerosis.” *Acta Neuropathologica*, 142 (6), pp. 985–1001. doi: 10.1007/s00401-021-02374-4.

Dickson, D. W., Kouri, N., Murray, M. E. and Josephs, K. A. (2011). “Neuropathology of frontotemporal lobar degeneration-tau (FTLD-tau).” *Journal of Molecular Neuroscience*, 45 (3), pp. 384–389. doi: 10.1007/s12031-011-9589-0.

Diekstra, F. P., Van Deerlin, V. M., van Swieten, J. C., Al-Chalabi, A., Ludolph, A. C., Weishaupt, J. H., Hardiman, O., Landers, J. E., Brown, R. H., van Es, M. A., Pasterkamp, R. J., Koppers, M., Andersen, P. M., Estrada, K., Rivadeneira, F., Hofman, A., Uitterlinden, A. G., van Damme, P., Melki, J., Meininger, V. and Veldink, J. H. (2014). “C9orf72 and UNC13A are shared risk loci for amyotrophic lateral sclerosis and frontotemporal dementia: a

genome-wide meta-analysis.” *Annals of Neurology*, 76 (1), pp. 120–133. doi: 10.1002/ana.24198.

Dobin, A., Davis, C. A., Schlesinger, F., Drenkow, J., Zaleski, C., Jha, S., Batut, P., Chaisson, M. and Gingeras, T. R. (2013). “STAR: ultrafast universal RNA-seq aligner.” *Bioinformatics*, 29 (1), pp. 15–21. doi: 10.1093/bioinformatics/bts635.

Doench, J. G., Fusi, N., Sullender, M., Hegde, M., Vaimberg, E. W., Donovan, K. F., Smith, I., Tothova, Z., Wilen, C., Orchard, R., Virgin, H. W., Listgarten, J. and Root, D. E. (2016). “Optimized sgRNA design to maximize activity and minimize off-target effects of CRISPR-Cas9.” *Nature Biotechnology*, 34 (2), pp. 184–191. doi: 10.1038/nbt.3437.

Donahue, C. P., Muratore, C., Wu, J. Y., Kosik, K. S. and Wolfe, M. S. (2006). “Stabilization of the tau exon 10 stem loop alters pre-mRNA splicing.” *The Journal of Biological Chemistry*, 281 (33), pp. 23302–23306. doi: 10.1074/jbc.C600143200.

Dos Santos Picanco, L. C., Ozela, P. F., de Fatima de Brito Brito, M., Pinheiro, A. A., Padilha, E. C., Braga, F. S., de Paula da Silva, C. H. T., Dos Santos, C. B. R., Rosa, J. M. C. and da Silva Hage-Melim, L. I. (2018). “Alzheimer’s Disease: A Review from the Pathophysiology to Diagnosis, New Perspectives for Pharmacological Treatment.” *Current Medicinal Chemistry*, 25 (26), pp. 3141–3159. doi: 10.2174/0929867323666161213101126.

Dreyfuss, G., Matunis, M. J., Piñol-Roma, S. and Burd, C. G. (1993). “hnRNP proteins and the biogenesis of mRNA.” *Annual Review of Biochemistry*, 62, pp. 289–321. doi: 10.1146/annurev.bi.62.070193.001445.

Du, Q., Melnikova, I. N. and Gardner, P. D. (1998). “Differential effects of heterogeneous nuclear ribonucleoprotein K on Sp1- and Sp3-mediated transcriptional activation of a neuronal nicotinic acetylcholine receptor promoter.” *The Journal of Biological Chemistry*, 273 (31), pp. 19877–19883. doi: 10.1074/jbc.273.31.19877.

Dvinge, H., Guenthoer, J., Porter, P. L. and Bradley, R. K. (2019). “RNA components of the spliceosome regulate tissue- and cancer-specific alternative splicing.” *Genome Research*, 29 (10), pp. 1591–1604. doi: 10.1101/gr.246678.118.

Dzwonek, A., Mikula, M. and Ostrowski, J. (2006). “The diverse involvement of heterogeneous nuclear ribonucleoprotein K in mitochondrial response to insulin.” *FEBS Letters*, 580 (7), pp. 1839–1845. doi: 10.1016/j.febslet.2006.02.043.

Eftekharzadeh, B., Daigle, J. G., Kapinos, L. E., Coyne, A., Schiantarelli, J., Carlomagno, Y., Cook, C., Miller, S. J., Dujardin, S., Amaral, A. S., Grima, J. C., Bennett, R. E., Tepper, K., DeTure, M., Vanderburg, C. R., Corjuc, B. T.,

DeVos, S. L., Gonzalez, J. A., Chew, J., Vidensky, S. and Hyman, B. T. (2018). “Tau protein disrupts nucleocytoplasmic transport in alzheimer’s disease.” *Neuron*, 99 (5), pp. 925-940.e7. doi: 10.1016/j.neuron.2018.07.039.

Elobeid, A., Libard, S., Leino, M., Popova, S. N. and Alafuzoff, I. (2016). “Altered proteins in the aging brain.” *Journal of Neuropathology and Experimental Neurology*, 75 (4), pp. 316–325. doi: 10.1093/jnen/nlw002.

Elston, G. N. (2003). “Cortex, cognition and the cell: new insights into the pyramidal neuron and prefrontal function.” *Cerebral Cortex*, 13 (11), pp. 1124–1138. doi: 10.1093/cercor/bhg093.

van der Ende, E. L., Jackson, J. L., White, A., Seelaar, H., van Blitterswijk, M. and Van Swieten, J. C. (2021). “Unravelling the clinical spectrum and the role of repeat length in C9ORF72 repeat expansions.” *Journal of Neurology, Neurosurgery, and Psychiatry*, 92 (5), pp. 502–509. doi: 10.1136/jnnp-2020-325377.

Eom, T., Zhang, C., Wang, H., Lay, K., Fak, J., Noebels, J. L. and Darnell, R. B. (2013). “NOVA-dependent regulation of cryptic NMD exons controls synaptic protein levels after seizure.” *eLife*, 2, p. e00178. doi: 10.7554/eLife.00178.

Erkelenz, S., Mueller, W. F., Evans, M. S., Busch, A., Schöneweis, K., Hertel, K. J. and Schaal, H. (2013). “Position-dependent splicing activation and repression by SR and hnRNP proteins rely on common mechanisms.” *RNA (New York)*, 19 (1), pp. 96–102. doi: 10.1261/rna.037044.112.

van Es, M. A., Veldink, J. H., Saris, C. G. J., Blauw, H. M., van Vught, P. W. J., Birve, A., Lemmens, R., Schelhaas, H. J., Groen, E. J. N., Huisman, M. H. B., van der Kooi, A. J., de Visser, M., Dahlberg, C., Estrada, K., Rivadeneira, F., Hofman, A., Zwarts, M. J., van Doormaal, P. T. C., Rujescu, D., Strengman, E. and van den Berg, L. H. (2009). “Genome-wide association study identifies 19p13.3 (UNC13A) and 9p21.2 as susceptibility loci for sporadic amyotrophic lateral sclerosis.” *Nature Genetics*, 41 (10), pp. 1083–1087. doi: 10.1038/ng.442.

Evers, B., Jastrzebski, K., Heijmans, J. P. M., Grernrum, W., Beijersbergen, R. L. and Bernards, R. (2016). “CRISPR knockout screening outperforms shRNA and CRISPRi in identifying essential genes.” *Nature Biotechnology*, 34 (6), pp. 631–633. doi: 10.1038/nbt.3536.

Fallatah, A., Anastasakis, D. G., Manzourolajdad, A., Sharma, P., Wang, X., Jacob, A., Alsharif, S., Elgerbi, A., Coulombe, P. A., Hafner, M. and Chung, B. M. (2022). “HNRNPK is retained in the cytoplasm by Keratin 19 to stabilize target mRNAs.” *BioRxiv*. doi: 10.1101/2022.01.24.477557.

Farah, M. H., Olson, J. M., Sucic, H. B., Hume, R. I., Tapscott, S. J. and Turner, D. L. (2000). “Generation of neurons by transient expression of

neural bHLH proteins in mammalian cells." *Development*, 127 (4), pp. 693–702. doi: 10.1242/dev.127.4.693.

Fend, F. and Raffeld, M. (2000). "Laser capture microdissection in pathology." *Journal of Clinical Pathology*, 53 (9), pp. 666–672. doi: 10.1136/jcp.53.9.666.

Feng, Y.-Y., Ramu, A., Cotto, K. C., Skidmore, Z. L., Kunisaki, J., Conrad, D. F., Lin, Y., Chapman, W., Uppaulri, R., Govindan, R., Griffith, O. L. and Griffith, M. (2018). "RegTools: Integrated analysis of genomic and transcriptomic data for discovery of splicing variants in cancer." *BioRxiv*. doi: 10.1101/436634.

Fernandopulle, M. S., Prestil, R., Grunseich, C., Wang, C., Gan, L. and Ward, M. E. (2018). "Transcription Factor-Mediated Differentiation of Human iPSCs into Neurons." *Current protocols in cell biology / editorial board, Juan S. Bonifacino ... [et al.]*, 79 (1), p. e51. doi: 10.1002/cpcb.51.

Ferrari, R., Kapogiannis, D., Huey, E. D. and Momeni, P. (2011). "FTD and ALS: a tale of two diseases." *Current Alzheimer research*, 8 (3), pp. 273–294. doi: 10.2174/156720511795563700.

Fielder, E., von Zglinicki, T. and Jurk, D. (2017). "The DNA Damage Response in Neurons: Die by Apoptosis or Survive in a Senescence-Like State?" *Journal of Alzheimer's Disease*, 60 (s1), pp. S107–S131. doi: 10.3233/JAD-161221.

Floeter, M. K. and Mills, R. (2009). "Progression in primary lateral sclerosis: a prospective analysis." *Amyotrophic Lateral Sclerosis*, 10 (5–6), pp. 339–346. doi: 10.3109/17482960903171136.

Folci, A., Mapelli, L., Sassone, J., Prestori, F., D'Angelo, E., Bassani, S. and Passafaro, M. (2014). "Loss of hnRNP K impairs synaptic plasticity in hippocampal neurons." *The Journal of Neuroscience*, 34 (27), pp. 9088–9095. doi: 10.1523/JNEUROSCI.0303-14.2014.

Franceschini, A., Meier, R., Casanova, A., Kreibich, S., Daga, N., Andritschke, D., Dilling, S., Rämö, P., Emmenlauer, M., Kaufmann, A., Conde-Álvarez, R., Low, S. H., Pelkmans, L., Helenius, A., Hardt, W.-D., Dehio, C. and von Mering, C. (2014). "Specific inhibition of diverse pathogens in human cells by synthetic microRNA-like oligonucleotides inferred from RNAi screens." *Proceedings of the National Academy of Sciences of the United States of America*, 111 (12), pp. 4548–4553. doi: 10.1073/pnas.1402353111.

Frankish, A., Diekhans, M., Ferreira, A.-M., Johnson, R., Jungreis, I., Loveland, J., Mudge, J. M., Sisu, C., Wright, J., Armstrong, J., Barnes, I., Berry, A., Bignell, A., Carbonell Sala, S., Chrast, J., Cunningham, F., Di Domenico, T., Donaldson, S., Fiddes, I. T., García Girón, C. and Flicek, P.

(2019). “GENCODE reference annotation for the human and mouse genomes.” *Nucleic Acids Research*, 47 (D1), pp. D766–D773. doi: 10.1093/nar/gky955.

Fratta, P., Sivakumar, P., Humphrey, J., Lo, K., Ricketts, T., Oliveira, H., Brito-Armas, J. M., Kalmar, B., Ule, A., Yu, Y., Birsa, N., Bodo, C., Collins, T., Conicella, A. E., Mejia Maza, A., Marrero-Gagliardi, A., Stewart, M., Mianne, J., Corrochano, S., Emmett, W. and Acevedo-Arozena, A. (2018). “Mice with endogenous TDP-43 mutations exhibit gain of splicing function and characteristics of amyotrophic lateral sclerosis.” *The EMBO Journal*, 37 (11). doi: 10.15252/embj.201798684.

Fu, Y., Foden, J. A., Khayter, C., Maeder, M. L., Reyon, D., Joung, J. K. and Sander, J. D. (2013). “High-frequency off-target mutagenesis induced by CRISPR-Cas nucleases in human cells.” *Nature Biotechnology*, 31 (9), pp. 822–826. doi: 10.1038/nbt.2623.

Gaetani, L., Blennow, K., Calabresi, P., Di Filippo, M., Parnetti, L. and Zetterberg, H. (2019). “Neurofilament light chain as a biomarker in neurological disorders.” *Journal of Neurology, Neurosurgery, and Psychiatry*, 90 (8), pp. 870–881. doi: 10.1136/jnnp-2018-320106.

Gallardo, M., Hornbaker, M. J., Zhang, X., Hu, P., Bueso-Ramos, C. and Post, S. M. (2016). “Aberrant hnRNP K expression: All roads lead to cancer.” *Cell Cycle*, 15 (12), pp. 1552–1557. doi: 10.1080/15384101.2016.1164372.

Gallardo, M., Lee, H. J., Zhang, X., Bueso-Ramos, C., Pageon, L. R., McArthur, M., Multani, A., Nazha, A., Manshouri, T., Parker-Thornburg, J., Rapado, I., Quintas-Cardama, A., Kornblau, S. M., Martinez-Lopez, J. and Post, S. M. (2015). “hnRNP K Is a Haploinsufficient Tumor Suppressor that Regulates Proliferation and Differentiation Programs in Hematologic Malignancies.” *Cancer Cell*, 28 (4), pp. 486–499. doi: 10.1016/j.ccell.2015.09.001.

Gami-Patel, P., Bandopadhyay, R., Brelstaff, J., Revesz, T. and Lashley, T. (2016). “The presence of heterogeneous nuclear ribonucleoproteins in frontotemporal lobar degeneration with FUS-positive inclusions.” *Neurobiology of Aging*, 46, pp. 192–203. doi: 10.1016/j.neurobiolaging.2016.07.004.

GBD 2016 Dementia Collaborators. (2019). “Global, regional, and national burden of Alzheimer’s disease and other dementias, 1990-2016: a systematic analysis for the Global Burden of Disease Study 2016.” *Lancet Neurology*, 18 (1), pp. 88–106. doi: 10.1016/S1474-4422(18)30403-4.

GBD 2016 Neurology Collaborators. (2019). “Global, regional, and national burden of neurological disorders, 1990-2016: a systematic analysis for the Global Burden of Disease Study 2016.” *Lancet Neurology*, 18 (5), pp. 459–480. doi: 10.1016/S1474-4422(18)30499-X.

Gendron, T. F., Rademakers, R. and Petrucelli, L. (2013). “TARDBP mutation analysis in TDP-43 proteinopathies and deciphering the toxicity of mutant TDP-43.” *Journal of Alzheimer’s Disease*, 33 Suppl 1, pp. S35-45. doi: 10.3233/JAD-2012-129036.

Gerfen, C. R., Economo, M. N. and Chandrashekar, J. (2018). “Long distance projections of cortical pyramidal neurons.” *Journal of Neuroscience Research*, 96 (9), pp. 1467–1475. doi: 10.1002/jnr.23978.

Geuens, T., Bouhy, D. and Timmerman, V. (2016). “The hnRNP family: insights into their role in health and disease.” *Human Genetics*, 135 (8), pp. 851–867. doi: 10.1007/s00439-016-1683-5.

Ge, W., He, F., Kim, K. J., Blanchi, B., Coskun, V., Nguyen, L., Wu, X., Zhao, J., Heng, J. I.-T., Martinowich, K., Tao, J., Wu, H., Castro, D., Sobeih, M. M., Corfas, G., Gleeson, J. G., Greenberg, M. E., Guillemot, F. and Sun, Y. E. (2006). “Coupling of cell migration with neurogenesis by proneural bHLH factors.” *Proceedings of the National Academy of Sciences of the United States of America*, 103 (5), pp. 1319–1324. doi: 10.1073/pnas.0510419103.

Ghanawi, H., Hennlein, L., Zare, A., Bader, J., Salehi, S., Hornburg, D., Ji, C., Sivadasan, R., Drepper, C., Meissner, F., Mann, M., Jablonka, S., Briese, M. and Sendtner, M. (2021). “Loss of full-length hnRNP R isoform impairs DNA damage response in motoneurons by inhibiting Yb1 recruitment to chromatin.” *Nucleic Acids Research*, 49 (21), pp. 12284–12305. doi: 10.1093/nar/gkab1120.

Gilbert, L. A., Horlbeck, M. A., Adamson, B., Villalta, J. E., Chen, Y., Whitehead, E. H., Guimaraes, C., Panning, B., Ploegh, H. L., Bassik, M. C., Qi, L. S., Kampmann, M. and Weissman, J. S. (2014). “Genome-scale CRISPR-mediated control of gene repression and activation.” *Cell*, 159 (3), pp. 647–661. doi: 10.1016/j.cell.2014.09.029.

Gilbert, L. A., Larson, M. H., Morsut, L., Liu, Z., Brar, G. A., Torres, S. E., Stern-Ginossar, N., Brandman, O., Whitehead, E. H., Doudna, J. A., Lim, W. A., Weissman, J. S. and Qi, L. S. (2013). “CRISPR-mediated modular RNA-guided regulation of transcription in eukaryotes.” *Cell*, 154 (2), pp. 442–451. doi: 10.1016/j.cell.2013.06.044.

Gillentine, M. A., Wang, T., Hoekzema, K., Rosenfeld, J., Liu, P., Guo, H., Kim, C. N., De Vries, B. B. A., Vissers, L. E. L. M., Nordenskjold, M., Kvarnung, M., Lindstrand, A., Nordgren, A., Gecz, J., Iascone, M., Cereda, A., Scatigno, A., Maitz, S., Zanni, G., Bertini, E. and Eichler, E. E. (2021). “Rare deleterious mutations of HNRNP genes result in shared neurodevelopmental disorders.” *Genome Medicine*, 13 (1), p. 63. doi: 10.1186/s13073-021-00870-6.

Gitler, A. D. and Fryer, J. D. (2018). “A matter of balance.” *eLife*, 7. doi: 10.7554/eLife.40034.

Gittings, L. M., Foti, S. C., Benson, B. C., Gami-Patel, P., Isaacs, A. M. and Lashley, T. (2019). “Heterogeneous nuclear ribonucleoproteins R and Q accumulate in pathological inclusions in FTLD-FUS.” *Acta neuropathologica communications*, 7 (1), p. 18. doi: 10.1186/s40478-019-0673-y.

Gkanatsiou, E., Sahlin, C., Portelius, E., Johannesson, M., Söderberg, L., Fälting, J., Basun, H., Möller, C., Odergren, T., Zetterberg, H., Blennow, K., Lannfelt, L. and Brinkmalm, G. (2021). “Characterization of monomeric and soluble aggregated Aβ in Down’s syndrome and Alzheimer’s disease brains.” *Neuroscience Letters*, 754, p. 135894. doi: 10.1016/j.neulet.2021.135894.

Goldberg, T. E., Huey, E. D. and Devanand, D. P. (2020). “Associations of APOE e2 genotype with cerebrovascular pathology: a postmortem study of 1275 brains.” *Journal of Neurology, Neurosurgery, and Psychiatry*. doi: 10.1136/jnnp-2020-323746.

Golde, T. E., Schneider, L. S. and Koo, E. H. (2011). “Anti-aβ therapeutics in Alzheimer’s disease: the need for a paradigm shift.” *Neuron*, 69 (2), pp. 203–213. doi: 10.1016/j.neuron.2011.01.002.

Gomes, E. and Shorter, J. (2019). “The molecular language of membraneless organelles.” *The Journal of Biological Chemistry*, 294 (18), pp. 7115–7127. doi: 10.1074/jbc.TM118.001192.

Gorno-Tempini, M. L., Hillis, A. E., Weintraub, S., Kertesz, A., Mendez, M., Cappa, S. F., Ogar, J. M., Rohrer, J. D., Black, S., Boeve, B. F., Manes, F., Dronkers, N. F., Vandenberghe, R., Rascovsky, K., Patterson, K., Miller, B. L., Knopman, D. S., Hodges, J. R., Mesulam, M. M. and Grossman, M. (2011). “Classification of primary progressive aphasia and its variants.” *Neurology*, 76 (11), pp. 1006–1014. doi: 10.1212/WNL.0b013e31821103e6.

Goutman, S. A., Hardiman, O., Al-Chalabi, A., Chió, A., Savelieff, M. G., Kiernan, M. C. and Feldman, E. L. (2022). “Emerging insights into the complex genetics and pathophysiology of amyotrophic lateral sclerosis.” *Lancet Neurology*, 21 (5), pp. 465–479. doi: 10.1016/S1474-4422(21)00414-2.

Grad, L. I., Rouleau, G. A., Ravits, J. and Cashman, N. R. (2017). “Clinical spectrum of amyotrophic lateral sclerosis (ALS).” *Cold Spring Harbor perspectives in medicine*, 7 (8). doi: 10.1101/cshperspect.a024117.

Greenberg, S. M., Bacskai, B. J., Hernandez-Guillamon, M., Pruzin, J., Sperling, R. and van Veluw, S. J. (2020). “Cerebral amyloid angiopathy and Alzheimer disease - one peptide, two pathways.” *Nature Reviews. Neurology*, 16 (1), pp. 30–42. doi: 10.1038/s41582-019-0281-2.

Grover, A., DeTure, M., Yen, S. H. and Hutton, M. (2002). “Effects on splicing and protein function of three mutations in codon N296 of tau in vitro.”

Neuroscience Letters, 323 (1), pp. 33–36. doi: 10.1016/s0304-3940(02)00124-6.

Gruijs da Silva, L. A., Simonetti, F., Hutten, S., Riemenschneider, H., Sternburg, E. L., Pietrek, L. M., Gebel, J., Dötsch, V., Edbauer, D., Hummer, G., Stelzl, L. S. and Dormann, D. (2022). "Disease-linked TDP-43 hyperphosphorylation suppresses TDP-43 condensation and aggregation." *The EMBO Journal*, 41 (8), p. e108443. doi: 10.15252/embj.2021108443.

Gulisano, W., Maugeri, D., Baltrons, M. A., Fà, M., Amato, A., Palmeri, A., D'Adamio, L., Grassi, C., Devanand, D. P., Honig, L. S., Puzzo, D. and Arancio, O. (2018). "Role of Amyloid-β and Tau Proteins in Alzheimer's Disease: Confuting the Amyloid Cascade." *Journal of Alzheimer's Disease*, 64 (s1), pp. S611–S631. doi: 10.3233/JAD-179935.

Haeusler, A. R., Donnelly, C. J., Periz, G., Simko, E. A. J., Shaw, P. G., Kim, M.-S., Maragakis, N. J., Troncoso, J. C., Pandey, A., Sattler, R., Rothstein, J. D. and Wang, J. (2014). "C9orf72 nucleotide repeat structures initiate molecular cascades of disease." *Nature*, 507 (7491), pp. 195–200. doi: 10.1038/nature13124.

Haley, B., Paunesku, T., Protić, M. and Woloschak, G. E. (2009). "Response of heterogeneous ribonuclear proteins (hnRNP) to ionising radiation and their involvement in DNA damage repair." *International journal of radiation biology*, 85 (8), pp. 643–655. doi: 10.1080/09553000903009548.

Halliday, G. (2017). "Pathology and hippocampal atrophy in Alzheimer's disease." *Lancet Neurology*, 16 (11), pp. 862–864. doi: 10.1016/S1474-4422(17)30343-5.

Hall, T. C., Miller, A. K. H. and Corsellis, J. A. N. (1975). "Variations in the human purkinje cell population according to age and sex." *Neuropathology and Applied Neurobiology*, 1 (3), pp. 267–292. doi: 10.1111/j.1365-2990.1975.tb00652.x.

Hammond, S. M., Bernstein, E., Beach, D. and Hannon, G. J. (2000). "An RNA-directed nuclease mediates post-transcriptional gene silencing in Drosophila cells." *Nature*, 404 (6775), pp. 293–296. doi: 10.1038/35005107.

Hampel, H., Mesulam, M. M., Cuello, A. C., Khachaturian, A. S., Vergallo, A., Farlow, M. R., Snyder, P. J., Giacobini, E. and Khachaturian, Z. S. (2019). "Revisiting the Cholinergic Hypothesis in Alzheimer's Disease: Emerging Evidence from Translational and Clinical Research." *The journal of prevention of Alzheimer's disease*, 6 (1), pp. 2–15. doi: 10.14283/jpad.2018.43.

Hanahan, D. and Weinberg, R. A. (2011). "Hallmarks of cancer: the next generation." *Cell*, 144 (5), pp. 646–674. doi: 10.1016/j.cell.2011.02.013.

Handley, E. E., Pitman, K. A., Dawkins, E., Young, K. M., Clark, R. M., Jiang, T. C., Turner, B. J., Dickson, T. C. and Blizzard, C. A. (2017). “Synapse Dysfunction of Layer V Pyramidal Neurons Precedes Neurodegeneration in a Mouse Model of TDP-43 Proteinopathies.” *Cerebral Cortex*, 27 (7), pp. 3630–3647. doi: 10.1093/cercor/bhw185.

Hansen, D. V., Hanson, J. E. and Sheng, M. (2018). “Microglia in Alzheimer’s disease.” *The Journal of Cell Biology*, 217 (2), pp. 459–472. doi: 10.1083/jcb.201709069.

Hanson, K. A., Kim, S. H. and Tibbetts, R. S. (2012). “RNA-binding proteins in neurodegenerative disease: TDP-43 and beyond.” *Wiley interdisciplinary reviews. RNA*, 3 (2), pp. 265–285. doi: 10.1002/wrna.111.

Han, R., Liang, J. and Zhou, B. (2021). “Glucose Metabolic Dysfunction in Neurodegenerative Diseases-New Mechanistic Insights and the Potential of Hypoxia as a Prospective Therapy Targeting Metabolic Reprogramming.” *International Journal of Molecular Sciences*, 22 (11). doi: 10.3390/ijms22115887.

Harada, C. N., Natelson Love, M. C. and Triebel, K. L. (2013). “Normal cognitive aging.” *Clinics in geriatric medicine*, 29 (4), pp. 737–752. doi: 10.1016/j.cger.2013.07.002.

Hardy, J. and Allsop, D. (1991). “Amyloid deposition as the central event in the aetiology of Alzheimer’s disease.” *Trends in Pharmacological Sciences*, 12 (10), pp. 383–388. doi: 10.1016/0165-6147(91)90609-V.

Hardy, J. A. and Higgins, G. A. (1992). “Alzheimer’s disease: the amyloid cascade hypothesis.” *Science*, 256 (5054), pp. 184–185. doi: 10.1126/science.1566067.

Harley, J. and Patani, R. (2020). “Stress-Specific Spatiotemporal Responses of RNA-Binding Proteins in Human Stem-Cell-Derived Motor Neurons.” *International Journal of Molecular Sciences*, 21 (21). doi: 10.3390/ijms21218346.

Harris, K. D. and Shepherd, G. M. G. (2015). “The neocortical circuit: themes and variations.” *Nature Neuroscience*, 18 (2), pp. 170–181. doi: 10.1038/nn.3917.

Hickman, S., Izzy, S., Sen, P., Morsett, L. and El Khoury, J. (2018). “Microglia in neurodegeneration.” *Nature Neuroscience*, 21 (10), pp. 1359–1369. doi: 10.1038/s41593-018-0242-x.

Hinz, J. M., Laughery, M. F. and Wyrick, J. J. (2015). “Nucleosomes inhibit cas9 endonuclease activity in vitro.” *Biochemistry*, 54 (48), pp. 7063–7066. doi: 10.1021/acs.biochem.5b01108.

Hoche, F., Guell, X., Vangel, M. G., Sherman, J. C. and Schmahmann, J. D. (2018). “The cerebellar cognitive affective/Schmahmann syndrome scale.” *Brain: A Journal of Neurology*, 141 (1), pp. 248–270. doi: 10.1093/brain/awx317.

Hodge, R. D., Miller, J. A., Novotny, M., Kalmbach, B. E., Ting, J. T., Bakken, T. E., Aevermann, B. D., Barkan, E. R., Berkowitz-Cerasano, M. L., Cobbs, C., Diez-Fuertes, F., Ding, S.-L., McCorrison, J., Schork, N. J., Shehata, S. I., Smith, K. A., Sunkin, S. M., Tran, D. N., Venepally, P., Yanny, A. M. and Lein, E. S. (2020). “Transcriptomic evidence that von Economo neurons are regionally specialized extratelencephalic-projecting excitatory neurons.” *Nature Communications*, 11 (1), p. 1172. doi: 10.1038/s41467-020-14952-3.

Hofmann, Y. and Wirth, B. (2002). “hnRNP-G promotes exon 7 inclusion of survival motor neuron (SMN) via direct interaction with Htra2-beta1.” *Human Molecular Genetics*, 11 (17), pp. 2037–2049. doi: 10.1093/hmg/11.17.2037.

Hof, P. R., Bouras, C., Perl, D. P., Sparks, D. L., Mehta, N. and Morrison, J. H. (1995). “Age-related distribution of neuropathologic changes in the cerebral cortex of patients with Down’s syndrome. Quantitative regional analysis and comparison with Alzheimer’s disease.” *Archives of Neurology*, 52 (4), pp. 379–391. doi: 10.1001/archneur.1995.00540280065020.

Hof, P. R., Cox, K. and Morrison, J. H. (1990). “Quantitative analysis of a vulnerable subset of pyramidal neurons in Alzheimer’s disease: I. Superior frontal and inferior temporal cortex.” *The Journal of Comparative Neurology*, 301 (1), pp. 44–54. doi: 10.1002/cne.903010105.

Horlbeck, M. A., Gilbert, L. A., Villalta, J. E., Adamson, B., Pak, R. A., Chen, Y., Fields, A. P., Park, C. Y., Corn, J. E., Kampmann, M. and Weissman, J. S. (2016). “Compact and highly active next-generation libraries for CRISPR-mediated gene repression and activation.” *eLife*, 5. doi: 10.7554/eLife.19760.

Hornbaker, M. J., Gallardo, M., Zhang, X., Ma, H., Hu, P., Khoury, J. D., Kornblau, S. M., Bueso-Ramos, C. E. and Post, S. M. (2016). “hnRNP K Overexpression Drives AML Progression By Altering Pathways Critical for Myeloid Proliferation and Differentiation.” *Blood*, 128 (22), pp. 744–744. doi: 10.1182/blood.V128.22.744.744.

Hou, Y., Dan, X., Babbar, M., Wei, Y., Hasselbalch, S. G., Croteau, D. L. and Bohr, V. A. (2019). “Ageing as a risk factor for neurodegenerative disease.” *Nature Reviews. Neurology*, 15 (10), pp. 565–581. doi: 10.1038/s41582-019-0244-7.

Huelga, S. C., Vu, A. Q., Arnold, J. D., Liang, T. Y., Liu, P. P., Yan, B. Y., Donohue, J. P., Shiue, L., Hoon, S., Brenner, S., Ares, M. and Yeo, G. W. (2012). “Integrative genome-wide analysis reveals cooperative regulation of alternative splicing by hnRNP proteins.” *Cell reports*, 1 (2), pp. 167–178. doi: 10.1016/j.celrep.2012.02.001.

Hug, N., Longman, D. and Cáceres, J. F. (2016). “Mechanism and regulation of the nonsense-mediated decay pathway.” *Nucleic Acids Research*, 44 (4), pp. 1483–1495. doi: 10.1093/nar/gkw010.

Hulme, A. J., Maksour, S., St-Clair Glover, M., Miellet, S. and Dottori, M. (2022). “Making neurons, made easy: The use of Neurogenin-2 in neuronal differentiation.” *Stem cell reports*, 17 (1), pp. 14–34. doi: 10.1016/j.stemcr.2021.11.015.

Humphrey, J., Birsa, N., Milioto, C., McLaughlin, M., Ule, A. M., Robaldo, D., Eberle, A. B., Kräuchi, R., Bentham, M., Brown, A.-L., Jarvis, S., Bodo, C., Garone, M. G., Devoy, A., Soraru, G., Rosa, A., Bozzoni, I., Fisher, E. M. C., Mühlemann, O., Schiavo, G. and Fratta, P. (2020). “FUS ALS-causative mutations impair FUS autoregulation and splicing factor networks through intron retention.” *Nucleic Acids Research*, 48 (12), pp. 6889–6905. doi: 10.1093/nar/gkaa410.

Humphrey, J., Emmett, W., Fratta, P., Isaacs, A. M. and Plagnol, V. (2017). “Quantitative analysis of cryptic splicing associated with TDP-43 depletion.” *BMC Medical Genomics*, 10 (1), p. 38. doi: 10.1186/s12920-017-0274-1.

Hu, W., Lei, L., Xie, X., Huang, L., Cui, Q., Dang, T., Liu, G. L., Li, Y., Sun, X. and Zhou, Z. (2019). “Heterogeneous nuclear ribonucleoprotein L facilitates recruitment of 53BP1 and BRCA1 at the DNA break sites induced by oxaliplatin in colorectal cancer.” *Cell death & disease*, 10 (8), p. 550. doi: 10.1038/s41419-019-1784-x.

Hwang, J.-Y., Aromolaran, K. A. and Zukin, R. S. (2017). “The emerging field of epigenetics in neurodegeneration and neuroprotection.” *Nature Reviews. Neuroscience*, 18 (6), pp. 347–361. doi: 10.1038/nrn.2017.46.

Ince, P. G., Tomkins, J., Slade, J. Y., Thatcher, N. M. and Shaw, P. J. (1998). “Amyotrophic lateral sclerosis associated with genetic abnormalities in the gene encoding Cu/Zn superoxide dismutase: molecular pathology of five new cases, and comparison with previous reports and 73 sporadic cases of ALS.” *Journal of Neuropathology and Experimental Neurology*, 57 (10), pp. 895–904. doi: 10.1097/00005072-199810000-00002.

Irwin, D. J., Cairns, N. J., Grossman, M., McMillan, C. T., Lee, E. B., Van Deerlin, V. M., Lee, V. M.-Y. and Trojanowski, J. Q. (2015). “Frontotemporal lobar degeneration: defining phenotypic diversity through personalized medicine.” *Acta Neuropathologica*, 129 (4), pp. 469–491. doi: 10.1007/s00401-014-1380-1.

Isaac, R. S., Jiang, F., Doudna, J. A., Lim, W. A., Narlikar, G. J. and Almeida, R. (2016). “Nucleosome breathing and remodeling constrain CRISPR-Cas9 function.” *eLife*, 5. doi: 10.7554/eLife.13450.

Iwamoto, M., Björklund, T., Lundberg, C., Kirik, D. and Wandless, T. J. (2010). “A general chemical method to regulate protein stability in the mammalian central nervous system.” *Chemistry & Biology*, 17 (9), pp. 981–988. doi: 10.1016/j.chembiol.2010.07.009.

Jackson, S. P. and Bartek, J. (2009). “The DNA-damage response in human biology and disease.” *Nature*, 461 (7267), pp. 1071–1078. doi: 10.1038/nature08467.

Jaitin, D. A., Weiner, A., Yofe, I., Lara-Astiaso, D., Keren-Shaul, H., David, E., Salame, T. M., Tanay, A., van Oudenaarden, A. and Amit, I. (2016). “Dissecting Immune Circuits by Linking CRISPR-Pooled Screens with Single-Cell RNA-Seq.” *Cell*, 167 (7), pp. 1883-1896.e15. doi: 10.1016/j.cell.2016.11.039.

Jansen, R., Embden, J. D. A. van, Gaastra, W. and Schouls, L. M. (2002). “Identification of genes that are associated with DNA repeats in prokaryotes.” *Molecular Microbiology*, 43 (6), pp. 1565–1575. doi: 10.1046/j.1365-2958.2002.02839.x.

Jeong, Y. H., Ling, J. P., Lin, S. Z., Donde, A. N., Braunstein, K. E., Majounie, E., Traynor, B. J., LaClair, K. D., Lloyd, T. E. and Wong, P. C. (2017). “Tdp-43 cryptic exons are highly variable between cell types.” *Molecular Neurodegeneration*, 12 (1), p. 13. doi: 10.1186/s13024-016-0144-x.

Jeppesen, D. K., Bohr, V. A. and Stevnsner, T. (2011). “DNA repair deficiency in neurodegeneration.” *Progress in Neurobiology*, 94 (2), pp. 166–200. doi: 10.1016/j.pneurobio.2011.04.013.

Jiang, Y. X., Cao, Q., Sawaya, M. R., Abskharon, R., Ge, P., DeTure, M., Dickson, D. W., Fu, J. Y., Ogorzalek Loo, R. R., Loo, J. A. and Eisenberg, D. S. (2022). “Amyloid fibrils in FTLD-TDP are composed of TMEM106B and not TDP-43.” *Nature*, 605 (7909), pp. 304–309. doi: 10.1038/s41586-022-04670-9.

Jinek, M., Chylinski, K., Fonfara, I., Hauer, M., Doudna, J. A. and Charpentier, E. (2012). “A programmable dual-RNA-guided DNA endonuclease in adaptive bacterial immunity.” *Science*, 337 (6096), pp. 816–821. doi: 10.1126/science.1225829.

Jinek, M., East, A., Cheng, A., Lin, S., Ma, E. and Doudna, J. (2013). “RNA-programmed genome editing in human cells.” *eLife*, 2, p. e00471. doi: 10.7554/eLife.00471.

Josephs, K. A., Mackenzie, I., Frosch, M. P., Bigio, E. H., Neumann, M., Arai, T., Dugger, B. N., Ghetti, B., Grossman, M., Hasegawa, M., Herrup, K., Holton, J., Jellinger, K., Lashley, T., McAleese, K. E., Parisi, J. E., Revesz, T., Saito, Y., Vonsattel, J. P., Whitwell, J. L. and Hu, W. (2019). “LATE to the

PART-y.” *Brain: A Journal of Neurology*, 142 (9), p. e47. doi: 10.1093/brain/awz224.

Jo, M., Lee, S., Jeon, Y.-M., Kim, S., Kwon, Y. and Kim, H.-J. (2020). “The role of TDP-43 propagation in neurodegenerative diseases: integrating insights from clinical and experimental studies.” *Experimental & Molecular Medicine*, 52 (10), pp. 1652–1662. doi: 10.1038/s12276-020-00513-7.

Jovičić, A., Paul, J. W. and Gitler, A. D. (2016). “Nuclear transport dysfunction: a common theme in amyotrophic lateral sclerosis and frontotemporal dementia.” *Journal of Neurochemistry*, 138 Suppl 1, pp. 134–144. doi: 10.1111/jnc.13642.

Kabashi, E., Valdmanis, P. N., Dion, P., Spiegelman, D., McConkey, B. J., Vande Velde, C., Bouchard, J.-P., Lacomblez, L., Pochigaeva, K., Salachas, F., Pradat, P.-F., Camu, W., Meininger, V., Dupre, N. and Rouleau, G. A. (2008). “TARDBP mutations in individuals with sporadic and familial amyotrophic lateral sclerosis.” *Nature Genetics*, 40 (5), pp. 572–574. doi: 10.1038/ng.132.

van der Kall, L. M., Truong, T., Burnham, S. C., Doré, V., Mulligan, R. S., Bozinovski, S., Lamb, F., Bourgeat, P., Fripp, J., Schultz, S., Lim, Y. Y., Laws, S. M., Ames, D., Fowler, C., Rainey-Smith, S. R., Martins, R. N., Salvado, O., Robertson, J., Maruff, P., Masters, C. L. and Rowe, C. C. (2021). “Association of β-Amyloid Level, Clinical Progression, and Longitudinal Cognitive Change in Normal Older Individuals.” *Neurology*, 96 (5), pp. e662–e670. doi: 10.1212/WNL.0000000000011222.

Kampmann, M. (2017). “A CRISPR approach to neurodegenerative diseases.” *Trends in Molecular Medicine*, 23 (6), pp. 483–485. doi: 10.1016/j.molmed.2017.04.003.

Kattuah, W., Rogelj, B., King, A., Shaw, C. E., Hortobágyi, T. and Troakes, C. (2019). “Heterogeneous Nuclear Ribonucleoprotein E2 (hnRNP E2) Is a Component of TDP-43 Aggregates Specifically in the A and C Pathological Subtypes of Frontotemporal Lobar Degeneration.” *Frontiers in Neuroscience*, 13, p. 551. doi: 10.3389/fnins.2019.00551.

Kawakami, I., Arai, T. and Hasegawa, M. (2019). “The basis of clinicopathological heterogeneity in TDP-43 proteinopathy.” *Acta Neuropathologica*, 138 (5), pp. 751–770. doi: 10.1007/s00401-019-02077-x.

Kawas, C. H., Greenia, D. E., Bullain, S. S., Clark, C. M., Pontecorvo, M. J., Joshi, A. D. and Corrada, M. M. (2013). “Amyloid imaging and cognitive decline in nondemented oldest-old: the 90+ Study.” *Alzheimer’s & Dementia*, 9 (2), pp. 199–203. doi: 10.1016/j.jalz.2012.06.005.

Kemmerer, K., Fischer, S. and Weigand, J. E. (2018). “Auto- and cross-regulation of the hnRNPs D and DL.” *RNA (New York)*, 24 (3), pp. 324–331. doi: 10.1261/rna.063420.117.

Khalil, B., El Fissi, N., Aouane, A., Cabirol-Pol, M. J., Rival, T. and Liévens, J. C. (2015). “PINK1-induced mitophagy promotes neuroprotection in Huntington’s disease.” *Cell death & disease*, 6, p. e1617. doi: 10.1038/cddis.2014.581.

Khan, A. A., Betel, D., Miller, M. L., Sander, C., Leslie, C. S. and Marks, D. S. (2009). “Transfection of small RNAs globally perturbs gene regulation by endogenous microRNAs.” *Nature Biotechnology*, 27 (6), pp. 549–555. doi: 10.1038/nbt.1543.

Kimura, T., Jiang, H., Konno, T., Seto, M., Iwanaga, K., Tsujihata, M., Satoh, A., Onodera, O., Kakita, A. and Takahashi, H. (2014). “Bunina bodies in motor and non-motor neurons revisited: a pathological study of an ALS patient after long-term survival on a respirator.” *Neuropathology*, 34 (4), pp. 392–397. doi: 10.1111/neup.12105.

Kim, B. W., Jeong, Y. E., Wong, M. and Martin, L. J. (2020). “DNA damage accumulates and responses are engaged in human ALS brain and spinal motor neurons and DNA repair is activatable in iPSC-derived motor neurons with SOD1 mutations.” *Acta neuropathologica communications*, 8 (1), p. 7. doi: 10.1186/s40478-019-0874-4.

Kim, H. J., Kim, N. C., Wang, Y.-D., Scarborough, E. A., Moore, J., Diaz, Z., MacLea, K. S., Freibaum, B., Li, S., Molliex, A., Kanagaraj, A. P., Carter, R., Boylan, K. B., Wojtas, A. M., Rademakers, R., Pinkus, J. L., Greenberg, S. A., Trojanowski, J. Q., Traynor, B. J., Smith, B. N. and Taylor, J. P. (2013). “Mutations in prion-like domains in hnRNPA2B1 and hnRNPA1 cause multisystem proteinopathy and ALS.” *Nature*, 495 (7442), pp. 467–473. doi: 10.1038/nature11922.

Kim, W. K., Liu, X., Sandner, J., Pasmantier, M., Andrews, J., Rowland, L. P. and Mitsumoto, H. (2009). “Study of 962 patients indicates progressive muscular atrophy is a form of ALS.” *Neurology*, 73 (20), pp. 1686–1692. doi: 10.1212/WNL.0b013e3181c1dea3.

Klim, J. R., Williams, L. A., Limone, F., Guerra San Juan, I., Davis-Dusenbery, B. N., Mordes, D. A., Burberry, A., Steinbaugh, M. J., Gamage, K. K., Kirchner, R., Moccia, R., Cassel, S. H., Chen, K., Wainger, B. J., Woolf, C. J. and Eggan, K. (2019). “ALS-implicated protein TDP-43 sustains levels of STMN2, a mediator of motor neuron growth and repair.” *Nature Neuroscience*, 22 (2), pp. 167–179. doi: 10.1038/s41593-018-0300-4.

Knopman, D. S. and Petersen, R. C. (2014). “Mild cognitive impairment and mild dementia: a clinical perspective.” *Mayo Clinic Proceedings*, 89 (10), pp. 1452–1459. doi: 10.1016/j.mayocp.2014.06.019.

Koike, Y., Sugai, A., Hara, N., Ito, J., Yokoseki, A., Ishihara, T., Yamagishi, T., Tsuboguchi, S., Tada, M., Ikeuchi, T., Kakita, A. and Onodera, O. (2021). “Age-related demethylation of the TDP-43 autoregulatory region in the human motor cortex.” *Communications Biology*, 4 (1), p. 1107. doi: 10.1038/s42003-021-02621-0.

Kolberg, L., Raudvere, U., Kuzmin, I., Vilo, J. and Peterson, H. (2020). “gprofiler2 -- an R package for gene list functional enrichment analysis and namespace conversion toolset g:Profiler.” *F1000Research*, 9. doi: 10.12688/f1000research.24956.2.

Koyama, A., Sugai, A., Kato, T., Ishihara, T., Shiga, A., Toyoshima, Y., Koyama, M., Konno, T., Hirokawa, S., Yokoseki, A., Nishizawa, M., Kakita, A., Takahashi, H. and Onodera, O. (2016). “Increased cytoplasmic TARDBP mRNA in affected spinal motor neurons in ALS caused by abnormal autoregulation of TDP-43.” *Nucleic Acids Research*, 44 (12), pp. 5820–5836. doi: 10.1093/nar/gkw499.

Krecic, A. M. and Swanson, M. S. (1999). “hnRNP complexes: composition, structure, and function.” *Current Opinion in Cell Biology*, 11 (3), pp. 363–371. doi: 10.1016/S0955-0674(99)80051-9.

Krus, K. L., Strickland, A., Yamada, Y., Devault, L., Schmidt, R. E., Bloom, A. J., Milbrandt, J. and DiAntonio, A. (2022). “Loss of Stathmin-2, a hallmark of TDP-43-associated ALS, causes motor neuropathy.” *BioRxiv*. doi: 10.1101/2022.03.13.484188.

Lai, S.-L., Abramzon, Y., Schymick, J. C., Stephan, D. A., Dunckley, T., Dillman, A., Cookson, M., Calvo, A., Battistini, S., Giannini, F., Caponnetto, C., Mancardi, G. L., Spataro, R., Monsurro, M. R., Tedeschi, G., Marinou, K., Sabatelli, M., Conte, A., Mandrioli, J., Sola, P. and Traynor, B. J. (2011). “FUS mutations in sporadic amyotrophic lateral sclerosis.” *Neurobiology of Aging*, 32 (3), p. 550.e1–4. doi: 10.1016/j.neurobiolaging.2009.12.020.

Lanata, S. C. and Miller, B. L. (2016). “The behavioural variant frontotemporal dementia (bvFTD) syndrome in psychiatry.” *Journal of Neurology, Neurosurgery, and Psychiatry*, 87 (5), pp. 501–511. doi: 10.1136/jnnp-2015-310697.

Lane, C. A., Hardy, J. and Schott, J. M. (2018). “Alzheimer’s disease.” *European Journal of Neurology*, 25 (1), pp. 59–70. doi: 10.1111/ene.13439.

Larson, M. H., Gilbert, L. A., Wang, X., Lim, W. A., Weissman, J. S. and Qi, L. S. (2013). “CRISPR interference (CRISPRi) for sequence-specific control of gene expression.” *Nature Protocols*, 8 (11), pp. 2180–2196. doi: 10.1038/nprot.2013.132.

Lashley, T., Rohrer, J. D., Bandopadhyay, R., Fry, C., Ahmed, Z., Isaacs, A. M., Brelstaff, J. H., Borroni, B., Warren, J. D., Troakes, C., King, A., Al-Saraj,

S., Newcombe, J., Quinn, N., Ostergaard, K., Schrøder, H. D., Bojsen-Møller, M., Braendgaard, H., Fox, N. C., Rossor, M. N. and Revesz, T. (2011). “A comparative clinical, pathological, biochemical and genetic study of fused in sarcoma proteinopathies.” *Brain: A Journal of Neurology*, 134 (Pt 9), pp. 2548–2564. doi: 10.1093/brain/awr160.

Lashley, T., Rohrer, J. D., Mead, S. and Revesz, T. (2015). “Review: an update on clinical, genetic and pathological aspects of frontotemporal lobar degenerations.” *Neuropathology and Applied Neurobiology*, 41 (7), pp. 858–881. doi: 10.1111/nan.12250.

Laursen, L. S., Chan, C. W. and Ffrench-Constant, C. (2011). “Translation of myelin basic protein mRNA in oligodendrocytes is regulated by integrin activation and hnRNP-K.” *The Journal of Cell Biology*, 192 (5), pp. 797–811. doi: 10.1083/jcb.201007014.

Le Rhun, A., Escalera-Maurer, A., Bratovič, M. and Charpentier, E. (2019). “CRISPR-Cas in Streptococcus pyogenes.” *RNA Biology*, 16 (4), pp. 380–389. doi: 10.1080/15476286.2019.1582974.

Leal, G., Comprido, D., de Luca, P., Morais, E., Rodrigues, L., Mele, M., Santos, A. R., Costa, R. O., Pinto, M. J., Patil, S., Berentsen, B., Afonso, P., Carreto, L., Li, K. W., Pinheiro, P., Almeida, R. D., Santos, M. A. S., Bramham, C. R. and Duarte, C. B. (2017). “The RNA-Binding Protein hnRNP K Mediates the Effect of BDNF on Dendritic mRNA Metabolism and Regulates Synaptic NMDA Receptors in Hippocampal Neurons.” *eNeuro*, 4 (6). doi: 10.1523/ENEURO.0268-17.2017.

Lee, E. B., Porta, S., Michael Baer, G., Xu, Y., Suh, E., Kwong, L. K., Elman, L., Grossman, M., Lee, V. M.-Y., Irwin, D. J., Van Deerlin, V. M. and Trojanowski, J. Q. (2017). “Expansion of the classification of FTLD-TDP: distinct pathology associated with rapidly progressive frontotemporal degeneration.” *Acta Neuropathologica*, 134 (1), pp. 65–78. doi: 10.1007/s00401-017-1679-9.

Lee, Y.-B., Chen, H.-J., Peres, J. N., Gomez-Deza, J., Attig, J., Stalekar, M., Troakes, C., Nishimura, A. L., Scotter, E. L., Vance, C., Adachi, Y., Sardone, V., Miller, J. W., Smith, B. N., Gallo, J.-M., Ule, J., Hirth, F., Rogelj, B., Houart, C. and Shaw, C. E. (2013). “Hexanucleotide repeats in ALS/FTD form length-dependent RNA foci, sequester RNA binding proteins, and are neurotoxic.” *Cell reports*, 5 (5), pp. 1178–1186. doi: 10.1016/j.celrep.2013.10.049.

de Leon, A. S. and M Das, J. (2022). “Neuroanatomy, Dentate Nucleus.” in *StatPearls*. Treasure Island (FL): StatPearls Publishing.

Leung, C. L., He, C. Z., Kaufmann, P., Chin, S. S., Naini, A., Liem, R. K. H., Mitsumoto, H. and Hays, A. P. (2004). “A pathogenic peripherin gene

mutation in a patient with amyotrophic lateral sclerosis." *Brain Pathology*, 14 (3), pp. 290–296. doi: 10.1111/j.1750-3639.2004.tb00066.x.

Lin, H.-C., He, Z., Ebert, S., Schörnig, M., Santel, M., Nikolova, M. T., Weigert, A., Hevers, W., Kasri, N. N., Taverna, E., Camp, J. G. and Treutlein, B. (2021). "NGN2 induces diverse neuron types from human pluripotency." *Stem cell reports*, 16 (9), pp. 2118–2127. doi: 10.1016/j.stemcr.2021.07.006.

Lindeboom, R. G. H., Supek, F. and Lehner, B. (2016). "The rules and impact of nonsense-mediated mRNA decay in human cancers." *Nature Genetics*, 48 (10), pp. 1112–1118. doi: 10.1038/ng.3664.

Ling, J. P., Chhabra, R., Merran, J. D., Schaughency, P. M., Wheelan, S. J., Corden, J. L. and Wong, P. C. (2016). "PTBP1 and PTBP2 repress nonconserved cryptic exons." *Cell reports*, 17 (1), pp. 104–113. doi: 10.1016/j.celrep.2016.08.071.

Ling, J. P., Pletnikova, O., Troncoso, J. C. and Wong, P. C. (2015). "TDP-43 repression of nonconserved cryptic exons is compromised in ALS-FTD." *Science*, 349 (6248), pp. 650–655. doi: 10.1126/science.aab0983.

Lin, X., Ruan, X., Anderson, M. G., McDowell, J. A., Kroeger, P. E., Fesik, S. W. and Shen, Y. (2005). "siRNA-mediated off-target gene silencing triggered by a 7 nt complementation." *Nucleic Acids Research*, 33 (14), pp. 4527–4535. doi: 10.1093/nar/gki762.

Liu, E. Y., Russ, J., Cali, C. P., Phan, J. M., Amlie-Wolf, A. and Lee, E. B. (2019). "Loss of Nuclear TDP-43 Is Associated with Decondensation of LINE Retrotransposons." *Cell reports*, 27 (5), pp. 1409-1421.e6. doi: 10.1016/j.celrep.2019.04.003.

Liu, X., Gallay, C., Kjos, M., Domenech, A., Slager, J., van Kessel, S. P., Knoops, K., Sorg, R. A., Zhang, J.-R. and Veening, J.-W. (2017). "High-throughput CRISPRi phenotyping identifies new essential genes in Streptococcus pneumoniae." *Molecular Systems Biology*, 13 (5), p. 931. doi: 10.15252/msb.20167449.

Liu, Y. and Szaro, B. G. (2011). "hnRNP K post-transcriptionally co-regulates multiple cytoskeletal genes needed for axonogenesis." *Development*, 138 (14), pp. 3079–3090. doi: 10.1242/dev.066993.

Li, B. and Dewey, C. N. (2011). "RSEM: accurate transcript quantification from RNA-Seq data with or without a reference genome." *BMC Bioinformatics*, 12, p. 323. doi: 10.1186/1471-2105-12-323.

Li, M., Zhang, W., Yang, X., Liu, H., Cao, L., Li, W., Wang, L., Zhang, G. and Gao, R. (2019). "Downregulation of HNRNPK in human cancer cells inhibits lung metastasis." *Animal Models and Experimental Medicine*, 2 (4), pp. 291–296. doi: 10.1002/ame2.12090.

Li, Y. I., Knowles, D. A., Humphrey, J., Barbeira, A. N., Dickinson, S. P., Im, H. K. and Pritchard, J. K. (2018). “Annotation-free quantification of RNA splicing using LeafCutter.” *Nature Genetics*, 50 (1), pp. 151–158. doi: 10.1038/s41588-017-0004-9.

Li, Z., Liu, X., Ma, J., Zhang, T., Gao, X. and Liu, L. (2018). “hnRNPK modulates selective quality-control autophagy by downregulating the expression of HDAC6 in 293 cells.” *International Journal of Oncology*, 53 (5), pp. 2200–2212. doi: 10.3892/ijo.2018.4517.

Lobo, A., Launer, L. J., Fratiglioni, L., Andersen, K., Di Carlo, A., Breteler, M. M., Copeland, J. R., Dartigues, J. F., Jagger, C., Martinez-Lage, J., Soininen, H. and Hofman, A. (2000). “Prevalence of dementia and major subtypes in Europe: A collaborative study of population-based cohorts. Neurologic Diseases in the Elderly Research Group.” *Neurology*, 54 (11 Suppl 5), pp. S4-9.

Lopez-Gonzalez, R., Lu, Y., Gendron, T. F., Karydas, A., Tran, H., Yang, D., Petrucelli, L., Miller, B. L., Almeida, S. and Gao, F.-B. (2016). “Poly(GR) in C9ORF72-Related ALS/FTD Compromises Mitochondrial Function and Increases Oxidative Stress and DNA Damage in iPSC-Derived Motor Neurons.” *Neuron*, 92 (2), pp. 383–391. doi: 10.1016/j.neuron.2016.09.015.

López-Otín, C., Blasco, M. A., Partridge, L., Serrano, M. and Kroemer, G. (2013). “The hallmarks of aging.” *Cell*, 153 (6), pp. 1194–1217. doi: 10.1016/j.cell.2013.05.039.

Love, M. I., Huber, W. and Anders, S. (2014). “Moderated estimation of fold change and dispersion for RNA-seq data with DESeq2.” *Genome Biology*, 15 (12), p. 550. doi: 10.1186/s13059-014-0550-8.

Low, Y.-H., Asi, Y., Foti, S. C. and Lashley, T. (2021). “Heterogeneous nuclear ribonucleoproteins: implications in neurological diseases.” *Molecular Neurobiology*, 58 (2), pp. 631–646. doi: 10.1007/s12035-020-02137-4.

Mackenzie, I. R. A., Neumann, M., Bigio, E. H., Cairns, N. J., Alafuzoff, I., Kril, J., Kovacs, G. G., Ghetti, B., Halliday, G., Holm, I. E., Ince, P. G., Kamphorst, W., Revesz, T., Rozemuller, A. J. M., Kumar-Singh, S., Akiyama, H., Baborie, A., Spina, S., Dickson, D. W., Trojanowski, J. Q. and Mann, D. M. A. (2009). “Nomenclature for neuropathologic subtypes of frontotemporal lobar degeneration: consensus recommendations.” *Acta Neuropathologica*, 117 (1), pp. 15–18. doi: 10.1007/s00401-008-0460-5.

Mackenzie, I. R. A., Neumann, M., Bigio, E. H., Cairns, N. J., Alafuzoff, I., Kril, J., Kovacs, G. G., Ghetti, B., Halliday, G., Holm, I. E., Ince, P. G., Kamphorst, W., Revesz, T., Rozemuller, A. J. M., Kumar-Singh, S., Akiyama, H., Baborie, A., Spina, S., Dickson, D. W., Trojanowski, J. Q. and Mann, D. M. A. (2010). “Nomenclature and nosology for neuropathologic subtypes of

frontotemporal lobar degeneration: an update.” *Acta Neuropathologica*, 119 (1), pp. 1–4. doi: 10.1007/s00401-009-0612-2.

Mackenzie, I. R. A. and Neumann, M. (2016). “Molecular neuropathology of frontotemporal dementia: insights into disease mechanisms from postmortem studies.” *Journal of Neurochemistry*, 138 Suppl 1, pp. 54–70. doi: 10.1111/jnc.13588.

Maekawa, S., Al-Sarraj, S., Kibble, M., Landau, S., Parnavelas, J., Cotter, D., Everall, I. and Leigh, P. N. (2004). “Cortical selective vulnerability in motor neuron disease: a morphometric study.” *Brain: A Journal of Neurology*, 127 (Pt 6), pp. 1237–1251. doi: 10.1093/brain/awh132.

Makeyev, A. V., Chkheidze, A. N. and Liebhaber, S. A. (1999). “A set of highly conserved RNA-binding proteins, alphaCP-1 and alphaCP-2, implicated in mRNA stabilization, are coexpressed from an intronless gene and its intron-containing paralog.” *The Journal of Biological Chemistry*, 274 (35), pp. 24849–24857. doi: 10.1074/jbc.274.35.24849.

Mali, P., Yang, L., Esvelt, K. M., Aach, J., Guell, M., DiCarlo, J. E., Norville, J. E. and Church, G. M. (2013). “RNA-guided human genome engineering via Cas9.” *Science*, 339 (6121), pp. 823–826. doi: 10.1126/science.1232033.

Malpartida, A. B., Williamson, M., Narendra, D. P., Wade-Martins, R. and Ryan, B. J. (2021). “Mitochondrial dysfunction and mitophagy in parkinson’s disease: from mechanism to therapy.” *Trends in Biochemical Sciences*, 46 (4), pp. 329–343. doi: 10.1016/j.tibs.2020.11.007.

Mann, D. M. (1996). “Pyramidal nerve cell loss in Alzheimer’s disease.” *Neurodegeneration : a journal for neurodegenerative disorders, neuroprotection, and neuroregeneration*, 5 (4), pp. 423–427. doi: 10.1006/neur.1996.0057.

Maphis, N., Xu, G., Kokiko-Cochran, O. N., Jiang, S., Cardona, A., Ransohoff, R. M., Lamb, B. T. and Bhaskar, K. (2015). “Reactive microglia drive tau pathology and contribute to the spreading of pathological tau in the brain.” *Brain: A Journal of Neurology*, 138 (Pt 6), pp. 1738–1755. doi: 10.1093/brain/awv081.

Marrone, L., Drexler, H. C. A., Wang, J., Tripathi, P., Distler, T., Heisterkamp, P., Anderson, E. N., Kour, S., Moraiti, A., Maharana, S., Bhatnagar, R., Belgard, T. G., Tripathy, V., Kalmbach, N., Hosseinzadeh, Z., Crippa, V., Abo-Rady, M., Wegner, F., Poletti, A., Troost, D. and Sterneckert, J. (2019). “FUS pathology in ALS is linked to alterations in multiple ALS-associated proteins and rescued by drugs stimulating autophagy.” *Acta Neuropathologica*, 138 (1), pp. 67–84. doi: 10.1007/s00401-019-01998-x.

Matano, S. (2001). “Brief communication: Proportions of the ventral half of the cerebellar dentate nucleus in humans and great apes.” *American Journal*

of Physical Anthropology, 114 (2), pp. 163–165. doi: 10.1002/1096-8644(200102)114:2<163::AID-AJPA1016>3.0.CO;2-F.

Matej, R., Tesar, A. and Rusina, R. (2019). “Alzheimer’s disease and other neurodegenerative dementias in comorbidity: A clinical and neuropathological overview.” *Clinical Biochemistry*, 73, pp. 26–31. doi: 10.1016/j.clinbiochem.2019.08.005.

Mattson, M. P. and Arumugam, T. V. (2018). “Hallmarks of brain aging: adaptive and pathological modification by metabolic states.” *Cell Metabolism*, 27 (6), pp. 1176–1199. doi: 10.1016/j.cmet.2018.05.011.

Matunis, M. J., Michael, W. M. and Dreyfuss, G. (1992). “Characterization and primary structure of the poly(C)-binding heterogeneous nuclear ribonucleoprotein complex K protein.” *Molecular and Cellular Biology*, 12 (1), pp. 164–171. doi: 10.1128/mcb.12.1.164-171.1992.

Ma, X. R., Prudencio, M., Koike, Y., Vatsavayai, S. C., Kim, G., Harbinski, F., Briner, A., Rodriguez, C. M., Guo, C., Akiyama, T., Schmidt, H. B., Cummings, B. B., Wyatt, D. W., Kurylo, K., Miller, G., Mekhoubad, S., Sallee, N., Mekonnen, G., Ganser, L., Rubien, J. D. and Gitler, A. D. (2022). “TDP-43 represses cryptic exon inclusion in the FTD-ALS gene UNC13A.” *Nature*, 603 (7899), pp. 124–130. doi: 10.1038/s41586-022-04424-7.

McClory, S. P., Lynch, K. W. and Ling, J. P. (2018). “HnRNP L represses cryptic exons.” *RNA (New York)*, 24 (6), pp. 761–768. doi: 10.1261/rna.065508.117.

McGlincy, N. J. and Ingolia, N. T. (2017). “Transcriptome-wide measurement of translation by ribosome profiling.” *Methods*, 126, pp. 112–129. doi: 10.1016/j.ymeth.2017.05.028.

Mehta, P. R., Lashley, T., Fratta, P. and Bampton, A. (2022). “Markers of cognitive resilience and a framework for investigating clinical heterogeneity in ALS.” *The Journal of Pathology*. doi: 10.1002/path.5897.

Mejzini, R., Flynn, L. L., Pitout, I. L., Fletcher, S., Wilton, S. D. and Akkari, P. A. (2019). “ALS genetics, mechanisms, and therapeutics: where are we now?” *Frontiers in Neuroscience*, 13, p. 1310. doi: 10.3389/fnins.2019.01310.

Melamed, Z., López-Erauskin, J., Baughn, M. W., Zhang, O., Drenner, K., Sun, Y., Freyermuth, F., McMahon, M. A., Beccari, M. S., Artates, J. W., Ohkubo, T., Rodriguez, M., Lin, N., Wu, D., Bennett, C. F., Rigo, F., Da Cruz, S., Ravits, J., Lagier-Tourenne, C. and Cleveland, D. W. (2019). “Premature polyadenylation-mediated loss of stathmin-2 is a hallmark of TDP-43-dependent neurodegeneration.” *Nature Neuroscience*, 22 (2), pp. 180–190. doi: 10.1038/s41593-018-0293-z.

Meyer, T., Funke, A., Münch, C., Kettemann, D., Maier, A., Walter, B., Thomas, A. and Spittel, S. (2019). “Real world experience of patients with amyotrophic lateral sclerosis (ALS) in the treatment of spasticity using tetrahydrocannabinol:cannabidiol (THC:CBD).” *BMC Neurology*, 19 (1), p. 222. doi: 10.1186/s12883-019-1443-y.

Michael, W. M., Choi, M. and Dreyfuss, G. (1995). “A nuclear export signal in hnRNP A1: a signal-mediated, temperature-dependent nuclear protein export pathway.” *Cell*, 83 (3), pp. 415–422. doi: 10.1016/0092-8674(95)90119-1.

Michael, W. M., Eder, P. S. and Dreyfuss, G. (1997). “The K nuclear shuttling domain: a novel signal for nuclear import and nuclear export in the hnRNP K protein.” *The EMBO Journal*, 16 (12), pp. 3587–3598. doi: 10.1093/emboj/16.12.3587.

Mijalkov, M., Volpe, G., Fernaud-Espinosa, I., DeFelipe, J., Pereira, J. B. and Merino-Serrais, P. (2021). “Dendritic spines are lost in clusters in Alzheimer’s disease.” *Scientific Reports*, 11 (1), p. 12350. doi: 10.1038/s41598-021-91726-x.

Mitra, J., Guerrero, E. N., Hegde, P. M., Liachko, N. F., Wang, H., Vasquez, V., Gao, J., Pandey, A., Taylor, J. P., Kraemer, B. C., Wu, P., Boldogh, I., Garruto, R. M., Mitra, S., Rao, K. S. and Hegde, M. L. (2019). “Motor neuron disease-associated loss of nuclear TDP-43 is linked to DNA double-strand break repair defects.” *Proceedings of the National Academy of Sciences of the United States of America*, 116 (10), pp. 4696–4705. doi: 10.1073/pnas.1818415116.

Mitra, J. and Hegde, M. L. (2019). “A Commentary on TDP-43 and DNA Damage Response in Amyotrophic Lateral Sclerosis.” *Journal of experimental neuroscience*, 13, p. 1179069519880166. doi: 10.1177/1179069519880166.

Molliex, A., Temirov, J., Lee, J., Coughlin, M., Kanagaraj, A. P., Kim, H. J., Mittag, T. and Taylor, J. P. (2015). “Phase separation by low complexity domains promotes stress granule assembly and drives pathological fibrillization.” *Cell*, 163 (1), pp. 123–133. doi: 10.1016/j.cell.2015.09.015.

Molnár, Z. and Cheung, A. F. P. (2006). “Towards the classification of subpopulations of layer V pyramidal projection neurons.” *Neuroscience Research*, 55 (2), pp. 105–115. doi: 10.1016/j.neures.2006.02.008.

Moodley, K. K. and Chan, D. (2014). “The hippocampus in neurodegenerative disease.” *Frontiers of neurology and neuroscience*, 34, pp. 95–108. doi: 10.1159/000356430.

Mori, K., Nihei, Y., Arzberger, T., Zhou, Q., Mackenzie, I. R., Hermann, A., Hanisch, F., German Consortium for Frontotemporal Lobar Degeneration, Bavarian Brain Banking Alliance, Kamp, F., Nuscher, B., Orozco, D.,

Edbauer, D. and Haass, C. (2016). “Reduced hnRNPA3 increases C9orf72 repeat RNA levels and dipeptide-repeat protein deposition.” *EMBO Reports*, 17 (9), pp. 1314–1325. doi: 10.15252/embr.201541724.

Mori, K., Weng, S.-M., Arzberger, T., May, S., Rentzsch, K., Kremmer, E., Schmid, B., Kretzschmar, H. A., Cruts, M., Van Broeckhoven, C., Haass, C. and Edbauer, D. (2013). “The C9orf72 GGGGCC repeat is translated into aggregating dipeptide-repeat proteins in FTLD/ALS.” *Science*, 339 (6125), pp. 1335–1338. doi: 10.1126/science.1232927.

Mormino, E. C. and Papp, K. V. (2018). “Amyloid accumulation and cognitive decline in clinically normal older individuals: implications for aging and early alzheimer’s disease.” *Journal of Alzheimer’s Disease*, 64 (s1), pp. S633–S646. doi: 10.3233/JAD-179928.

Moujalled, D., Grubman, A., Acevedo, K., Yang, S., Ke, Y. D., Moujalled, D. M., Duncan, C., Caragounis, A., Perera, N. D., Turner, B. J., Prudencio, M., Petrucelli, L., Blair, I., Ittner, L. M., Crouch, P. J., Liddell, J. R. and White, A. R. (2017). “TDP-43 mutations causing amyotrophic lateral sclerosis are associated with altered expression of RNA-binding protein hnRNP K and affect the Nrf2 antioxidant pathway.” *Human Molecular Genetics*, 26 (9), pp. 1732–1746. doi: 10.1093/hmg/ddx093.

Moujalled, D., James, J. L., Yang, S., Zhang, K., Duncan, C., Moujalled, D. M., Parker, S. J., Caragounis, A., Lidgerwood, G., Turner, B. J., Atkin, J. D., Grubman, A., Liddell, J. R., Proepper, C., Boeckers, T. M., Kanninen, K. M., Blair, I., Crouch, P. J. and White, A. R. (2015). “Phosphorylation of hnRNP K by cyclin-dependent kinase 2 controls cytosolic accumulation of TDP-43.” *Human Molecular Genetics*, 24 (6), pp. 1655–1669. doi: 10.1093/hmg/ddu578.

Mou, H., Smith, J. L., Peng, L., Yin, H., Moore, J., Zhang, X.-O., Song, C.-Q., Sheel, A., Wu, Q., Ozata, D. M., Li, Y., Anderson, D. G., Emerson, C. P., Sontheimer, E. J., Moore, M. J., Weng, Z. and Xue, W. (2017). “CRISPR/Cas9-mediated genome editing induces exon skipping by alternative splicing or exon deletion.” *Genome Biology*, 18 (1), p. 108. doi: 10.1186/s13059-017-1237-8.

Munoz, D. G., Neumann, M., Kusaka, H., Yokota, O., Ishihara, K., Terada, S., Kuroda, S. and Mackenzie, I. R. (2009). “FUS pathology in basophilic inclusion body disease.” *Acta Neuropathologica*, 118 (5), pp. 617–627. doi: 10.1007/s00401-009-0598-9.

Mu, Y. and Gage, F. H. (2011). “Adult hippocampal neurogenesis and its role in Alzheimer’s disease.” *Molecular Neurodegeneration*, 6, p. 85. doi: 10.1186/1750-1326-6-85.

Naro, C., Bielli, P., Pagliarini, V. and Sette, C. (2015). “The interplay between DNA damage response and RNA processing: the unexpected role of splicing

factors as gatekeepers of genome stability.” *Frontiers in genetics*, 6, p. 142. doi: 10.3389/fgene.2015.00142.

Nelson, P. T., Dickson, D. W., Trojanowski, J. Q., Jack, C. R., Boyle, P. A., Arfanakis, K., Rademakers, R., Alafuzoff, I., Attems, J., Brayne, C., Coyle-Gilchrist, I. T. S., Chui, H. C., Fardo, D. W., Flanagan, M. E., Halliday, G., Hokkanen, S. R. K., Hunter, S., Jicha, G. A., Katsumata, Y., Kawas, C. H. and Schneider, J. A. (2019). “Limbic-predominant age-related TDP-43 encephalopathy (LATE): consensus working group report.” *Brain: A Journal of Neurology*, 142 (6), pp. 1503–1527. doi: 10.1093/brain/awz099.

Nelson, S. B., Hempel, C. and Sugino, K. (2006). “Probing the transcriptome of neuronal cell types.” *Current Opinion in Neurobiology*, 16 (5), pp. 571–576. doi: 10.1016/j.conb.2006.08.006.

Neumann, M., Bentmann, E., Dormann, D., Jawaid, A., DeJesus-Hernandez, M., Ansorge, O., Roeber, S., Kretzschmar, H. A., Munoz, D. G., Kusaka, H., Yokota, O., Ang, L.-C., Bilbao, J., Rademakers, R., Haass, C. and Mackenzie, I. R. A. (2011). “FET proteins TAF15 and EWS are selective markers that distinguish FTLD with FUS pathology from amyotrophic lateral sclerosis with FUS mutations.” *Brain: A Journal of Neurology*, 134 (Pt 9), pp. 2595–2609. doi: 10.1093/brain/awr201.

Neumann, M., Rademakers, R., Roeber, S., Baker, M., Kretzschmar, H. A. and Mackenzie, I. R. A. (2009). “A new subtype of frontotemporal lobar degeneration with FUS pathology.” *Brain: A Journal of Neurology*, 132 (Pt 11), pp. 2922–2931. doi: 10.1093/brain/awp214.

Neumann, M., Sampathu, D. M., Kwong, L. K., Truax, A. C., Micsenyi, M. C., Chou, T. T., Bruce, J., Schuck, T., Grossman, M., Clark, C. M., McCluskey, L. F., Miller, B. L., Masliah, E., Mackenzie, I. R., Feldman, H., Feiden, W., Kretzschmar, H. A., Trojanowski, J. Q. and Lee, V. M.-Y. (2006). “Ubiquitinated TDP-43 in frontotemporal lobar degeneration and amyotrophic lateral sclerosis.” *Science*, 314 (5796), pp. 130–133. doi: 10.1126/science.1134108.

Nguyen, H. P., Van Broeckhoven, C. and van der Zee, J. (2018). “ALS Genes in the Genomic Era and their Implications for FTD.” *Trends in Genetics*, 34 (6), pp. 404–423. doi: 10.1016/j.tig.2018.03.001.

Nguyen, T. M., Kabotyanski, E. B., Reineke, L. C., Shao, J., Xiong, F., Lee, J.-H., Dubrulle, J., Johnson, H., Stossi, F., Tsoi, P. S., Choi, K.-J., Ellis, A. G., Zhao, N., Cao, J., Adewunmi, O., Ferreon, J. C., Ferreon, A. C. M., Neilson, J. R., Mancini, M. A., Chen, X. and Rosen, J. M. (2020). “The SINEB1 element in the long non-coding RNA Malat1 is necessary for TDP-43 proteostasis.” *Nucleic Acids Research*, 48 (5), pp. 2621–2642. doi: 10.1093/nar/gkz1176.

Niccoli, T. and Partridge, L. (2012). “Ageing as a risk factor for disease.” *Current Biology*, 22 (17), pp. R741-52. doi: 10.1016/j.cub.2012.07.024.

Nicolas, A., Kenna, K. P., Renton, A. E., Ticozzi, N., Faghri, F., Chia, R., Dominov, J. A., Kenna, B. J., Nalls, M. A., Keagle, P., Rivera, A. M., van Rheenen, W., Murphy, N. A., van Vugt, J., Geiger, J. T., Van der Spek, R. A., Pliner, H. A., Shankaracharya, Smith, B. N., Marangi, G. and et al. (2018). “Genome-wide analyses identify *KIF5A* as a novel ALS gene.” *Neuron*, 97 (6), pp. 1268-1283.e6. doi: 10.1016/j.neuron.2018.02.027.

Niedermeyer, S., Murn, M. and Choi, P. J. (2019). “Respiratory failure in amyotrophic lateral sclerosis.” *Chest*, 155 (2), pp. 401–408. doi: 10.1016/j.chest.2018.06.035.

O’Brien, R. J. and Wong, P. C. (2011). “Amyloid precursor protein processing and Alzheimer’s disease.” *Annual Review of Neuroscience*, 34, pp. 185–204. doi: 10.1146/annurev-neuro-061010-113613.

Okamoto, K., Mizuno, Y. and Fujita, Y. (2008). “Bunina bodies in amyotrophic lateral sclerosis.” *Neuropathology*, 28 (2), pp. 109–115. doi: 10.1111/j.1440-1789.2007.00873.x.

Okamoto, N. (2019). “Okamoto syndrome has features overlapping with Au-Kline syndrome and is caused by HNRNPK mutation.” *American Journal of Medical Genetics. Part A*, 179 (5), pp. 822–826. doi: 10.1002/ajmg.a.61079.

Okunola, H. L. and Krainer, A. R. (2009). “Cooperative-binding and splicing-repressive properties of hnRNP A1.” *Molecular and Cellular Biology*, 29 (20), pp. 5620–5631. doi: 10.1128/MCB.01678-08.

Olivito, G., Serra, L., Marra, C., Di Domenico, C., Caltagirone, C., Toniolo, S., Cercignani, M., Leggio, M. and Bozzali, M. (2020). “Cerebellar dentate nucleus functional connectivity with cerebral cortex in Alzheimer’s disease and memory: a seed-based approach.” *Neurobiology of Aging*, 89, pp. 32–40. doi: 10.1016/j.neurobiolaging.2019.10.026.

Otoshi, T., Tanaka, T., Morimoto, K. and Nakatani, T. (2015). “Cytoplasmic accumulation of heterogeneous nuclear ribonucleoprotein K strongly promotes tumor invasion in renal cell carcinoma cells.” *Plos One*, 10 (12), p. e0145769. doi: 10.1371/journal.pone.0145769.

Palmos, A. B., Duarte, R. R. R., Smeeth, D. M., Hedges, E. C., Nixon, D. F., Thuret, S. and Powell, T. R. (2020). “Telomere length and human hippocampal neurogenesis.” *Neuropsychopharmacology*, 45 (13), pp. 2239–2247. doi: 10.1038/s41386-020-00863-w.

Paré, B., Lehmann, M., Beaudin, M., Nordström, U., Saikali, S., Julien, J.-P., Gilthorpe, J. D., Marklund, S. L., Cashman, N. R., Andersen, P. M., Forsberg, K., Dupré, N., Gould, P., Brännström, T. and Gros-Louis, F. (2018).

"Misfolded SOD1 pathology in sporadic Amyotrophic Lateral Sclerosis." *Scientific Reports*, 8 (1), p. 14223. doi: 10.1038/s41598-018-31773-z.

Pattanayak, V., Lin, S., Guilinger, J. P., Ma, E., Doudna, J. A. and Liu, D. R. (2013). "High-throughput profiling of off-target DNA cleavage reveals RNA-programmed Cas9 nuclease specificity." *Nature Biotechnology*, 31 (9), pp. 839–843. doi: 10.1038/nbt.2673.

Perl, D. P. (2010). "Neuropathology of Alzheimer's disease." *The Mount Sinai Journal of Medicine, New York*, 77 (1), pp. 32–42. doi: 10.1002/msj.20157.

Persson, J., Nyberg, L., Lind, J., Larsson, A., Nilsson, L.-G., Ingvar, M. and Buckner, R. L. (2006). "Structure-function correlates of cognitive decline in aging." *Cerebral Cortex*, 16 (7), pp. 907–915. doi: 10.1093/cercor/bhj036.

Polymenidou, M., Lagier-Tourenne, C., Hutt, K. R., Huelga, S. C., Moran, J., Liang, T. Y., Ling, S.-C., Sun, E., Wancewicz, E., Mazur, C., Kordasiewicz, H., Sedaghat, Y., Donohue, J. P., Shiue, L., Bennett, C. F., Yeo, G. W. and Cleveland, D. W. (2011). "Long pre-mRNA depletion and RNA missplicing contribute to neuronal vulnerability from loss of TDP-43." *Nature Neuroscience*, 14 (4), pp. 459–468. doi: 10.1038/nn.2779.

Pottier, C., Ravenscroft, T. A., Sanchez-Contreras, M. and Rademakers, R. (2016). "Genetics of FTLD: overview and what else we can expect from genetic studies." *Journal of Neurochemistry*, 138 Suppl 1, pp. 32–53. doi: 10.1111/jnc.13622.

Pottier, C., Ren, Y., Perkerson, R. B., Baker, M., Jenkins, G. D., van Blitterswijk, M., DeJesus-Hernandez, M., van Rooij, J. G. J., Murray, M. E., Christopher, E., McDonnell, S. K., Fogarty, Z., Batzler, A., Tian, S., Vicente, C. T., Matchett, B., Karydas, A. M., Hsiung, G.-Y. R., Seelaar, H., Mol, M. O. and Rademakers, R. (2019). "Genome-wide analyses as part of the international FTLD-TDP whole-genome sequencing consortium reveals novel disease risk factors and increases support for immune dysfunction in FTLD." *Acta Neuropathologica*, 137 (6), pp. 879–899. doi: 10.1007/s00401-019-01962-9.

Preussner, M., Schreiner, S., Hung, L.-H., Porstner, M., Jäck, H.-M., Benes, V., Rätsch, G. and Bindereif, A. (2012). "HnRNP L and L-like cooperate in multiple-exon regulation of CD45 alternative splicing." *Nucleic Acids Research*, 40 (12), pp. 5666–5678. doi: 10.1093/nar/gks221.

Prudencio, M., Humphrey, J., Pickles, S., Brown, A.-L., Hill, S. E., Kachergus, J. M., Shi, J., Heckman, M. G., Spiegel, M. R., Cook, C., Song, Y., Yue, M., Daughrity, L. M., Carlomagno, Y., Jansen-West, K., de Castro, C. F., DeTure, M., Koga, S., Wang, Y.-C., Sivakumar, P. and Petrucelli, L. (2020). "Truncated stathmin-2 is a marker of TDP-43 pathology in frontotemporal dementia." *The Journal of Clinical Investigation*, 130 (11), pp. 6080–6092. doi: 10.1172/JCI139741.

Pulecio, J., Verma, N., Mejía-Ramírez, E., Huangfu, D. and Raya, A. (2017). “CRISPR/Cas9-Based Engineering of the Epigenome.” *Cell Stem Cell*, 21 (4), pp. 431–447. doi: 10.1016/j.stem.2017.09.006.

Purice, M. D. and Taylor, J. P. (2018). “Linking hnRNP Function to ALS and FTD Pathology.” *Frontiers in Neuroscience*, 12, p. 326. doi: 10.3389/fnins.2018.00326.

Qi, L. S., Larson, M. H., Gilbert, L. A., Doudna, J. A., Weissman, J. S., Arkin, A. P. and Lim, W. A. (2013). “Repurposing CRISPR as an RNA-guided platform for sequence-specific control of gene expression.” *Cell*, 152 (5), pp. 1173–1183. doi: 10.1016/j.cell.2013.02.022.

Rademakers, R., Neumann, M. and Mackenzie, I. R. (2012). “Advances in understanding the molecular basis of frontotemporal dementia.” *Nature Reviews. Neurology*, 8 (8), pp. 423–434. doi: 10.1038/nrneurol.2012.117.

Rafii, M. S., Lukic, A. S., Andrews, R. D., Brewer, J., Rissman, R. A., Strother, S. C., Wernick, M. N., Pennington, C., Mobley, W. C., Ness, S., Matthews, D. C. and Down Syndrome Biomarker Initiative and the Alzheimer’s Disease Neuroimaging Initiative. (2017). “PET Imaging of Tau Pathology and Relationship to Amyloid, Longitudinal MRI, and Cognitive Change in Down Syndrome: Results from the Down Syndrome Biomarker Initiative (DSBI).” *Journal of Alzheimer’s Disease*, 60 (2), pp. 439–450. doi: 10.3233/JAD-170390.

Rainero, I., Rubino, E., Michelerio, A., D’Agata, F., Gentile, S. and Pinessi, L. (2017). “Recent advances in the molecular genetics of frontotemporal lobar degeneration.” *Functional neurology*, 32 (1), pp. 7–16. doi: 10.11138/fneur/2017.32.1.007.

Ran, F. A., Hsu, P. D., Wright, J., Agarwala, V., Scott, D. A. and Zhang, F. (2013). “Genome engineering using the CRISPR-Cas9 system.” *Nature Protocols*, 8 (11), pp. 2281–2308. doi: 10.1038/nprot.2013.143.

Ravits, J., Appel, S., Baloh, R. H., Barohn, R., Brooks, B. R., Elman, L., Floeter, M. K., Henderson, C., Lomen-Hoerth, C., Macklis, J. D., McCluskey, L., Mitsumoto, H., Przedborski, S., Rothstein, J., Trojanowski, J. Q., van den Berg, L. H. and Ringel, S. (2013). “Deciphering amyotrophic lateral sclerosis: what phenotype, neuropathology and genetics are telling us about pathogenesis.” *Amyotrophic lateral sclerosis & frontotemporal degeneration*, 14 Suppl 1, pp. 5–18. doi: 10.3109/21678421.2013.778548.

Ravits, J. M. and La Spada, A. R. (2009). “ALS motor phenotype heterogeneity, focality, and spread: deconstructing motor neuron degeneration.” *Neurology*, 73 (10), pp. 805–811. doi: 10.1212/WNL.0b013e3181b6bbbd.

Renton, A. E., Chiò, A. and Traynor, B. J. (2014). “State of play in amyotrophic lateral sclerosis genetics.” *Nature Neuroscience*, 17 (1), pp. 17–23. doi: 10.1038/nn.3584.

Renton, A. E., Majounie, E., Waite, A., Simón-Sánchez, J., Rollinson, S., Gibbs, J. R., Schymick, J. C., Laaksovirta, H., van Swieten, J. C., Myllykangas, L., Kalimo, H., Paetau, A., Abramzon, Y., Remes, A. M., Kaganovich, A., Scholz, S. W., Duckworth, J., Ding, J., Harmer, D. W., Hernandez, D. G. and Traynor, B. J. (2011). “A hexanucleotide repeat expansion in C9ORF72 is the cause of chromosome 9p21-linked ALS-FTD.” *Neuron*, 72 (2), pp. 257–268. doi: 10.1016/j.neuron.2011.09.010.

Rezak, M. and de Carvalho, M. (2020). “Disease modification in neurodegenerative diseases: Not quite there yet.” *Neurology*, 94 (1), pp. 12–13. doi: 10.1212/WNL.0000000000008690.

van Rheenen, W., van der Spek, R. A. A., Bakker, M. K., van Vugt, J. J. F. A., Hop, P. J., Zwamborn, R. A. J., de Klein, N., Westra, H.-J., Bakker, O. B., Deelen, P., Shireby, G., Hannon, E., Moisse, M., Baird, D., Restuadi, R., Dolzhenko, E., Dekker, A. M., Gawor, K., Westeneng, H.-J., Tazelaar, G. H. P. and Veldink, J. H. (2021). “Common and rare variant association analyses in amyotrophic lateral sclerosis identify 15 risk loci with distinct genetic architectures and neuron-specific biology.” *Nature Genetics*, 53 (12), pp. 1636–1648. doi: 10.1038/s41588-021-00973-1.

van der Rijt, S., Molenaars, M., McIntyre, R. L., Janssens, G. E. and Houtkooper, R. H. (2020). “Integrating the hallmarks of aging throughout the tree of life: A focus on mitochondrial dysfunction.” *Frontiers in cell and developmental biology*, 8, p. 594416. doi: 10.3389/fcell.2020.594416.

Rogalski, E., Stebbins, G. T., Barnes, C. A., Murphy, C. M., Stoub, T. R., George, S., Ferrari, C., Shah, R. C. and deToledo-Morrell, L. (2012). “Age-related changes in parahippocampal white matter integrity: a diffusion tensor imaging study.” *Neuropsychologia*, 50 (8), pp. 1759–1765. doi: 10.1016/j.neuropsychologia.2012.03.033.

Rohrer, J. D. and Warren, J. D. (2011). “Phenotypic signatures of genetic frontotemporal dementia.” *Current Opinion in Neurology*, 24 (6), pp. 542–549. doi: 10.1097/WCO.0b013e32834cd442.

Rosa, F., Dhingra, A., Uysal, B., Mendis, G. D. C., Loeffler, H., Elsen, G., Mueller, S., Schwarz, N., Castillo-Lizardo, M., Cuddy, C., Becker, F., Heutink, P., Reid, C. A., Petrou, S., Lerche, H. and Maljevic, S. (2020). “In Vitro Differentiated Human Stem Cell-Derived Neurons Reproduce Synaptic Synchronicity Arising during Neurodevelopment.” *Stem cell reports*, 15 (1), pp. 22–37. doi: 10.1016/j.stemcr.2020.05.015.

Rosen, H. J., Allison, S. C., Ogar, J. M., Amici, S., Rose, K., Dronkers, N., Miller, B. L. and Gorno-Tempini, M. L. (2006). “Behavioral features in

semantic dementia vs other forms of progressive aphasias.” *Neurology*, 67 (10), pp. 1752–1756. doi: 10.1212/01.wnl.0000247630.29222.34.

Rossbach, O., Hung, L.-H., Schreiner, S., Grishina, I., Heiner, M., Hui, J. and Bindereif, A. (2009). “Auto- and cross-regulation of the hnRNP L proteins by alternative splicing.” *Molecular and Cellular Biology*, 29 (6), pp. 1442–1451. doi: 10.1128/MCB.01689-08.

Rossi, S., Serrano, A., Gerbino, V., Giorgi, A., Di Francesco, L., Nencini, M., Bozzo, F., Schininà, M. E., Bagni, C., Cestra, G., Carrì, M. T., Achsel, T. and Cozzolino, M. (2015). “Nuclear accumulation of mRNAs underlies G4C2-repeat-induced translational repression in a cellular model of C9orf72 ALS.” *Journal of Cell Science*, 128 (9), pp. 1787–1799. doi: 10.1242/jcs.165332.

Rosso, S. M., Donker Kaat, L., Baks, T., Joosse, M., de Koning, I., Pijnenburg, Y., de Jong, D., Dooijes, D., Kamphorst, W., Ravid, R., Niermeijer, M. F., Verheij, F., Kremer, H. P., Scheltens, P., van Duijn, C. M., Heutink, P. and van Swieten, J. C. (2003). “Frontotemporal dementia in The Netherlands: patient characteristics and prevalence estimates from a population-based study.” *Brain: A Journal of Neurology*, 126 (Pt 9), pp. 2016–2022. doi: 10.1093/brain/awg204.

Saxon, J. A., Thompson, J. C., Jones, M., Harris, J. M., Richardson, A. M., Langheinrich, T., Neary, D., Mann, D. M. and Snowden, J. S. (2017). “Examining the language and behavioural profile in FTD and ALS-FTD.” *Journal of Neurology, Neurosurgery, and Psychiatry*, 88 (8), pp. 675–680. doi: 10.1136/jnnp-2017-315667.

Schmahmann, J. D. and Sherman, J. C. (1998). “The cerebellar cognitive affective syndrome.” *Brain: A Journal of Neurology*, 121 (Pt 4), pp. 561–579. doi: 10.1093/brain/121.4.561.

Schubert, M., Gautam, D., Surjo, D., Ueki, K., Baudler, S., Schubert, D., Kondo, T., Alber, J., Galldiks, N., Küstermann, E., Arndt, S., Jacobs, A. H., Krone, W., Kahn, C. R. and Brüning, J. C. (2004). “Role for neuronal insulin resistance in neurodegenerative diseases.” *Proceedings of the National Academy of Sciences of the United States of America*, 101 (9), pp. 3100–3105. doi: 10.1073/pnas.0308724101.

Schweighauser, M., Arseni, D., Bacioglu, M., Huang, M., Lövestam, S., Shi, Y., Yang, Y., Zhang, W., Kotecha, A., Garringer, H. J., Vidal, R., Hallinan, G. I., Newell, K. L., Tarutani, A., Murayama, S., Miyazaki, M., Saito, Y., Yoshida, M., Hasegawa, K., Lashley, T. and Scheres, S. H. W. (2022). “Age-dependent formation of TMEM106B amyloid filaments in human brains.” *Nature*. doi: 10.1038/s41586-022-04650-z.

Seelaar, H., Klijnsma, K. Y., de Koning, I., van der Lugt, A., Chiu, W. Z., Azmani, A., Rozemuller, A. J. M. and van Swieten, J. C. (2010). “Frequency of ubiquitin and FUS-positive, TDP-43-negative frontotemporal lobar

degeneration.” *Journal of Neurology*, 257 (5), pp. 747–753. doi: 10.1007/s00415-009-5404-z.

Seelaar, H., Rohrer, J. D., Pijnenburg, Y. A. L., Fox, N. C. and van Swieten, J. C. (2011). “Clinical, genetic and pathological heterogeneity of frontotemporal dementia: a review.” *Journal of Neurology, Neurosurgery, and Psychiatry*, 82 (5), pp. 476–486. doi: 10.1136/jnnp.2010.212225.

Semizarov, D., Frost, L., Sarthy, A., Kroeger, P., Halbert, D. N. and Fesik, S. W. (2003). “Specificity of short interfering RNA determined through gene expression signatures.” *Proceedings of the National Academy of Sciences of the United States of America*, 100 (11), pp. 6347–6352. doi: 10.1073/pnas.1131959100.

Seo, S., Lim, J.-W., Yellajoshyula, D., Chang, L.-W. and Kroll, K. L. (2007). “Neurogenin and NeuroD direct transcriptional targets and their regulatory enhancers.” *The EMBO Journal*, 26 (24), pp. 5093–5108. doi: 10.1038/sj.emboj.7601923.

Sephton, C. F., Good, S. K., Atkin, S., Dewey, C. M., Mayer, P., Herz, J. and Yu, G. (2010). “TDP-43 is a developmentally regulated protein essential for early embryonic development.” *The Journal of Biological Chemistry*, 285 (9), pp. 6826–6834. doi: 10.1074/jbc.M109.061846.

Shen, J. and Kelleher, R. J. (2007). “The presenilin hypothesis of Alzheimer’s disease: evidence for a loss-of-function pathogenic mechanism.” *Proceedings of the National Academy of Sciences of the United States of America*, 104 (2), pp. 403–409. doi: 10.1073/pnas.0608332104.

Sidhu, R., Gatt, A., Fratta, P., Lashley, T. and Bampton, A. (2022). “HnRNP K mislocalisation in neurons of the dentate nucleus is a novel neuropathological feature of neurodegenerative disease and ageing.” *Neuropathology and Applied Neurobiology*. doi: 10.1111/nan.12793.

Sigoillot, F. D. and King, R. W. (2011). “Vigilance and validation: Keys to success in RNAi screening.” *ACS Chemical Biology*, 6 (1), pp. 47–60. doi: 10.1021/cb100358f.

Sims, R., Hill, M. and Williams, J. (2020). “The multiplex model of the genetics of Alzheimer’s disease.” *Nature Neuroscience*, 23 (3), pp. 311–322. doi: 10.1038/s41593-020-0599-5.

Sleegers, K., Brouwers, N., Gijselinck, I., Theuns, J., Goossens, D., Wauters, J., Del-Favero, J., Cruts, M., van Duijn, C. M. and Van Broeckhoven, C. (2006). “APP duplication is sufficient to cause early onset Alzheimer’s dementia with cerebral amyloid angiopathy.” *Brain: A Journal of Neurology*, 129 (Pt 11), pp. 2977–2983. doi: 10.1093/brain/awl203.

Snider, B. J., Fagan, A. M., Roe, C., Shah, A. R., Grant, E. A., Xiong, C., Morris, J. C. and Holtzman, D. M. (2009). “Cerebrospinal fluid biomarkers and rate of cognitive decline in very mild dementia of the Alzheimer type.” *Archives of Neurology*, 66 (5), pp. 638–645. doi: 10.1001/archneurol.2009.55.

Snowden, J. S., Pickering-Brown, S. M., Mackenzie, I. R., Richardson, A. M. T., Varma, A., Neary, D. and Mann, D. M. A. (2006). “Progranulin gene mutations associated with frontotemporal dementia and progressive non-fluent aphasia.” *Brain: A Journal of Neurology*, 129 (Pt 11), pp. 3091–3102. doi: 10.1093/brain/awl267.

Sternburg, E. L., Gruijs da Silva, L. A. and Dormann, D. (2022). “Post-translational modifications on RNA-binding proteins: accelerators, brakes, or passengers in neurodegeneration?” *Trends in Biochemical Sciences*, 47 (1), pp. 6–22. doi: 10.1016/j.tibs.2021.07.004.

Stojic, L., Lun, A. T. L., Mangei, J., Mascalchi, P., Quarantotti, V., Barr, A. R., Bakal, C., Marioni, J. C., Gergely, F. and Odom, D. T. (2018). “Specificity of RNAi, LNA and CRISPRi as loss-of-function methods in transcriptional analysis.” *Nucleic Acids Research*, 46 (12), pp. 5950–5966. doi: 10.1093/nar/gky437.

Strang, K. H., Golde, T. E. and Giasson, B. I. (2019). “MAPT mutations, tauopathy, and mechanisms of neurodegeneration.” *Laboratory Investigation*, 99 (7), pp. 912–928. doi: 10.1038/s41374-019-0197-x.

Subhramanyam, C. S., Wang, C., Hu, Q. and Dheen, S. T. (2019). “Microglia-mediated neuroinflammation in neurodegenerative diseases.” *Seminars in Cell & Developmental Biology*, 94, pp. 112–120. doi: 10.1016/j.semcdb.2019.05.004.

Suk, T. R. and Rousseaux, M. W. C. (2020). “The role of TDP-43 mislocalization in amyotrophic lateral sclerosis.” *Molecular Neurodegeneration*, 15 (1), p. 45. doi: 10.1186/s13024-020-00397-1.

Sun, M., Bell, W., LaClair, K. D., Ling, J. P., Han, H., Kageyama, Y., Pletnikova, O., Troncoso, J. C., Wong, P. C. and Chen, L. L. (2017). “Cryptic exon incorporation occurs in Alzheimer’s brain lacking TDP-43 inclusion but exhibiting nuclear clearance of TDP-43.” *Acta Neuropathologica*, 133 (6), pp. 923–931. doi: 10.1007/s00401-017-1701-2.

Sun, Y., Nadal-Vicens, M., Misono, S., Lin, M. Z., Zubiaga, A., Hua, X., Fan, G. and Greenberg, M. E. (2001). “Neurogenin promotes neurogenesis and inhibits glial differentiation by independent mechanisms.” *Cell*, 104 (3), pp. 365–376. doi: 10.1016/s0092-8674(01)00224-0.

Suzuki, H., Shibagaki, Y., Hattori, S. and Matsuoka, M. (2019). “C9-ALS/FTD-linked proline-arginine dipeptide repeat protein associates with

paraspeckle components and increases paraspeckle formation." *Cell death & disease*, 10 (10), p. 746. doi: 10.1038/s41419-019-1983-5.

Swinnen, B. and Robberecht, W. (2014). "The phenotypic variability of amyotrophic lateral sclerosis." *Nature Reviews. Neurology*, 10 (11), pp. 661–670. doi: 10.1038/nrneurol.2014.184.

Takahama, K., Takada, A., Tada, S., Shimizu, M., Sayama, K., Kurokawa, R. and Oyoshi, T. (2013). "Regulation of telomere length by G-quadruplex telomere DNA- and TERRA-binding protein TLS/FUS." *Chemistry & Biology*, 20 (3), pp. 341–350. doi: 10.1016/j.chembiol.2013.02.013.

Tan, F. C. C., Hutchison, E. R., Eitan, E. and Mattson, M. P. (2014). "Are there roles for brain cell senescence in aging and neurodegenerative disorders?" *Biogerontology*, 15 (6), pp. 643–660. doi: 10.1007/s10522-014-9532-1.

Tan, Q., Yalamanchili, H. K., Park, J., De Maio, A., Lu, H.-C., Wan, Y.-W., White, J. J., Bondar, V. V., Sayegh, L. S., Liu, X., Gao, Y., Sillitoe, R. V., Orr, H. T., Liu, Z. and Zoghbi, H. Y. (2016). "Extensive cryptic splicing upon loss of RBM17 and TDP43 in neurodegeneration models." *Human Molecular Genetics*, 25 (23), pp. 5083–5093. doi: 10.1093/hmg/ddw337.

Tapiola, T., Alafuzoff, I., Herukka, S.-K., Parkkinen, L., Hartikainen, P., Soininen, H. and Pirttilä, T. (2009). "Cerebrospinal fluid {beta}-amyloid 42 and tau proteins as biomarkers of Alzheimer-type pathologic changes in the brain." *Archives of Neurology*, 66 (3), pp. 382–389. doi: 10.1001/archneurol.2008.596.

Tartaglia, M. C., Rowe, A., Findlater, K., Orange, J. B., Grace, G. and Strong, M. J. (2007). "Differentiation between primary lateral sclerosis and amyotrophic lateral sclerosis: examination of symptoms and signs at disease onset and during follow-up." *Archives of Neurology*, 64 (2), pp. 232–236. doi: 10.1001/archneur.64.2.232.

Taylor, J. P., Brown, R. H. and Cleveland, D. W. (2016). "Decoding ALS: from genes to mechanism." *Nature*, 539 (7628), pp. 197–206. doi: 10.1038/nature20413.

Tcw, J. and Goate, A. M. (2017). "Genetics of β-Amyloid Precursor Protein in Alzheimer's Disease." *Cold Spring Harbor perspectives in medicine*, 7 (6). doi: 10.1101/cshperspect.a024539.

Thanan, R., Oikawa, S., Hiraku, Y., Ohnishi, S., Ma, N., Pinlaor, S., Yongvanit, P., Kawanishi, S. and Murata, M. (2014). "Oxidative stress and its significant roles in neurodegenerative diseases and cancer." *International Journal of Molecular Sciences*, 16 (1), pp. 193–217. doi: 10.3390/ijms16010193.

Tian, R., Gachechiladze, M. A., Ludwig, C. H., Laurie, M. T., Hong, J. Y., Nathaniel, D., Prabhu, A. V., Fernandopulle, M. S., Patel, R., Abshari, M., Ward, M. E. and Kampmann, M. (2019). “CRISPR Interference-Based Platform for Multimodal Genetic Screens in Human iPSC-Derived Neurons.” *Neuron*, 104 (2), pp. 239-255.e12. doi: 10.1016/j.neuron.2019.07.014.

Timmers, M., Tesseur, I., Bogert, J., Zetterberg, H., Blennow, K., Börjesson-Hanson, A., Baquero, M., Boada, M., Randolph, C., Tritsmans, L., Van Nueten, L., Engelborghs, S. and Streffer, J. R. (2019). “Relevance of the interplay between amyloid and tau for cognitive impairment in early Alzheimer’s disease.” *Neurobiology of Aging*, 79, pp. 131–141. doi: 10.1016/j.neurobiolaging.2019.03.016.

Tollervey, J. R., Wang, Z., Hortobágyi, T., Witten, J. T., Zarnack, K., Kayikci, M., Clark, T. A., Schweitzer, A. C., Rot, G., Curk, T., Zupan, B., Rogelj, B., Shaw, C. E. and Ule, J. (2011). “Analysis of alternative splicing associated with aging and neurodegeneration in the human brain.” *Genome Research*, 21 (10), pp. 1572–1582. doi: 10.1101/gr.122226.111.

Torres, P., Andrés-Benito, P., Fernàndez-Bernal, A., Ricart, M., Ayala, V., Pamplona, R., Ferrer, I. and Portero-Otin, M. (2020). “Selected cryptic exons accumulate in hippocampal cell nuclei in Alzheimer’s disease with and without associated TDP-43 proteinopathy.” *Brain: A Journal of Neurology*, 143 (3), p. e20. doi: 10.1093/brain/awaa013.

Trabzuni, D., Ryten, M., Walker, R., Smith, C., Imran, S., Ramasamy, A., Weale, M. E. and Hardy, J. (2011). “Quality control parameters on a large dataset of regionally dissected human control brains for whole genome expression studies.” *Journal of Neurochemistry*, 119 (2), pp. 275–282. doi: 10.1111/j.1471-4159.2011.07432.x.

Turner, M. R., Barnwell, J., Al-Chalabi, A. and Eisen, A. (2012). “Young-onset amyotrophic lateral sclerosis: historical and other observations.” *Brain: A Journal of Neurology*, 135 (Pt 9), pp. 2883–2891. doi: 10.1093/brain/aws144.

Turner, M. R., Barohn, R. J., Corcia, P., Fink, J. K., Harms, M. B., Kiernan, M. C., Ravits, J., Silani, V., Simmons, Z., Statland, J., van den Berg, L. H., Delegates of the 2nd International PLS Conference and Mitsumoto, H. (2020). “Primary lateral sclerosis: consensus diagnostic criteria.” *Journal of Neurology, Neurosurgery, and Psychiatry*, 91 (4), pp. 373–377. doi: 10.1136/jnnp-2019-322541.

Turner, M. R. and Talbot, K. (2013). “Mimics and chameleons in motor neurone disease.” *Practical Neurology*, 13 (3), pp. 153–164. doi: 10.1136/practneurol-2013-000557.

Tziortzouda, P., Van Den Bosch, L. and Hirth, F. (2021). “Triad of TDP43 control in neurodegeneration: autoregulation, localization and aggregation.”

Nature Reviews. Neuroscience, 22 (4), pp. 197–208. doi: 10.1038/s41583-021-00431-1.

Unniyampurath, U., Pilankatta, R. and Krishnan, M. N. (2016). “RNA Interference in the Age of CRISPR: Will CRISPR Interfere with RNAi?” *International Journal of Molecular Sciences*, 17 (3), p. 291. doi: 10.3390/ijms17030291.

Van Damme, P., Robberecht, W. and Van Den Bosch, L. (2017). “Modelling amyotrophic lateral sclerosis: progress and possibilities.” *Disease Models & Mechanisms*, 10 (5), pp. 537–549. doi: 10.1242/dmm.029058.

Van Deerlin, V. M., Leverenz, J. B., Bekris, L. M., Bird, T. D., Yuan, W., Elman, L. B., Clay, D., Wood, E. M., Chen-Plotkin, A. S., Martinez-Lage, M., Steinbart, E., McCluskey, L., Grossman, M., Neumann, M., Wu, I.-L., Yang, W.-S., Kalb, R., Galasko, D. R., Montine, T. J., Trojanowski, J. Q. and Yu, C.-E. (2008). “TARDBP mutations in amyotrophic lateral sclerosis with TDP-43 neuropathology: a genetic and histopathological analysis.” *Lancet Neurology*, 7 (5), pp. 409–416. doi: 10.1016/S1474-4422(08)70071-1.

Van Deerlin, V. M., Sleiman, P. M. A., Martinez-Lage, M., Chen-Plotkin, A., Wang, L.-S., Graff-Radford, N. R., Dickson, D. W., Rademakers, R., Boeve, B. F., Grossman, M., Arnold, S. E., Mann, D. M. A., Pickering-Brown, S. M., Seelaar, H., Heutink, P., van Swieten, J. C., Murrell, J. R., Ghetti, B., Spina, S., Grafman, J. and Lee, V. M.-Y. (2010). “Common variants at 7p21 are associated with frontotemporal lobar degeneration with TDP-43 inclusions.” *Nature Genetics*, 42 (3), pp. 234–239. doi: 10.1038/ng.536.

Vance, C., Rogelj, B., Hortobágyi, T., De Vos, K. J., Nishimura, A. L., Sreedharan, J., Hu, X., Smith, B., Ruddy, D., Wright, P., Ganesalingam, J., Williams, K. L., Tripathi, V., Al-Saraj, S., Al-Chalabi, A., Leigh, P. N., Blair, I. P., Nicholson, G., de Belleroche, J., Gallo, J.-M. and Shaw, C. E. (2009). “Mutations in FUS, an RNA processing protein, cause familial amyotrophic lateral sclerosis type 6.” *Science*, 323 (5918), pp. 1208–1211. doi: 10.1126/science.1165942.

Vaquero-Garcia, J., Barrera, A., Gazzara, M. R., González-Vallinas, J., Lahens, N. F., Hogenesch, J. B., Lynch, K. W. and Barash, Y. (2016). “A new view of transcriptome complexity and regulation through the lens of local splicing variations.” *eLife*, 5, p. e11752. doi: 10.7554/eLife.11752.

Verberk, I. M. W., Thijssen, E., Koelewijn, J., Mauroo, K., Vanbrabant, J., de Wilde, A., Zwan, M. D., Verfaillie, S. C. J., Ossenkoppele, R., Barkhof, F., van Berckel, B. N. M., Scheltens, P., van der Flier, W. M., Stoops, E., Vanderstichele, H. M. and Teunissen, C. E. (2020). “Combination of plasma amyloid beta(1-42/1-40) and glial fibrillary acidic protein strongly associates with cerebral amyloid pathology.” *Alzheimer’s research & therapy*, 12 (1), p. 118. doi: 10.1186/s13195-020-00682-7.

Verghese, P. B., Castellano, J. M. and Holtzman, D. M. (2011). “Apolipoprotein E in Alzheimer’s disease and other neurological disorders.” *Lancet Neurology*, 10 (3), pp. 241–252. doi: 10.1016/S1474-4422(10)70325-2.

Visser, J., van den Berg-Vos, R. M., Franssen, H., van den Berg, L. H., Wokke, J. H., de Jong, J. M. V., Holman, R., de Haan, R. J. and de Visser, M. (2007). “Disease course and prognostic factors of progressive muscular atrophy.” *Archives of Neurology*, 64 (4), pp. 522–528. doi: 10.1001/archneur.64.4.522.

Viswanathan, A. and Greenberg, S. M. (2011). “Cerebral amyloid angiopathy in the elderly.” *Annals of Neurology*, 70 (6), pp. 871–880. doi: 10.1002/ana.22516.

Wallings, R. L., Humble, S. W., Ward, M. E. and Wade-Martins, R. (2019). “Lysosomal dysfunction at the centre of parkinson’s disease and frontotemporal dementia/amyotrophic lateral sclerosis.” *Trends in Neurosciences*, 42 (12), pp. 899–912. doi: 10.1016/j.tins.2019.10.002.

Wang, C., Ward, M. E., Chen, R., Liu, K., Tracy, T. E., Chen, X., Xie, M., Sohn, P. D., Ludwig, C., Meyer-Franke, A., Karch, C. M., Ding, S. and Gan, L. (2017). “Scalable Production of iPSC-Derived Human Neurons to Identify Tau-Lowering Compounds by High-Content Screening.” *Stem cell reports*, 9 (4), pp. 1221–1233. doi: 10.1016/j.stemcr.2017.08.019.

Wang, F., Li, J., Fan, S., Jin, Z. and Huang, C. (2020). “Targeting stress granules: A novel therapeutic strategy for human diseases.” *Pharmacological Research*, 161, p. 105143. doi: 10.1016/j.phrs.2020.105143.

Wang, H. and Hegde, M. L. (2019). “New Mechanisms of DNA Repair Defects in Fused in Sarcoma-Associated Neurodegeneration: Stage Set for DNA Repair-Based Therapeutics?” *Journal of experimental neuroscience*, 13, p. 1179069519856358. doi: 10.1177/1179069519856358.

Wang, J., Gao, Q.-S., Wang, Y., Lafyatis, R., Stamm, S. and Andreadis, A. (2004). “Tau exon 10, whose missplicing causes frontotemporal dementia, is regulated by an intricate interplay of cis elements and trans factors.” *Journal of Neurochemistry*, 88 (5), pp. 1078–1090. doi: 10.1046/j.1471-4159.2003.02232.x.

Wang, T., Wei, J. J., Sabatini, D. M. and Lander, E. S. (2014). “Genetic screens in human cells using the CRISPR-Cas9 system.” *Science*, 343 (6166), pp. 80–84. doi: 10.1126/science.1246981.

Wang, Y., Gao, L., Tse, S.-W. and Andreadis, A. (2010). “Heterogeneous nuclear ribonucleoprotein E3 modestly activates splicing of tau exon 10 via its proximal downstream intron, a hotspot for frontotemporal dementia mutations.” *Gene*, 451 (1–2), pp. 23–31. doi: 10.1016/j.gene.2009.11.006.

Warren, J. D., Rohrer, J. D. and Rossor, M. N. (2013). “Clinical review. Frontotemporal dementia.” *BMJ (Clinical Research Ed.)*, 347, p. f4827. doi: 10.1136/bmj.f4827.

West, K. O., Scott, H. M., Torres-Odio, S., West, A. P., Patrick, K. L. and Watson, R. O. (2019). “The Splicing Factor hnRNP M Is a Critical Regulator of Innate Immune Gene Expression in Macrophages.” *Cell reports*, 29 (6), pp. 1594-1609.e5. doi: 10.1016/j.celrep.2019.09.078.

White, A., Moujalled, D., James, J., Grubman, A., Kanninen, K. and Crouch, P. (2013). “Phosphorylation of hnRNP K controls cytosolic accumulation of TDP-43.” *Molecular Neurodegeneration*, 8 (Suppl 1), p. P46. doi: 10.1186/1750-1326-8-S1-P46.

White, M. A., Kim, E., Duffy, A., Adalbert, R., Phillips, B. U., Peters, O. M., Stephenson, J., Yang, S., Massenzio, F., Lin, Z., Andrews, S., Segonds-Pichon, A., Metterville, J., Saksida, L. M., Mead, R., Ribchester, R. R., Barhomi, Y., Serre, T., Coleman, M. P., Fallon, J. R. and Sreedharan, J. (2018). “TDP-43 gains function due to perturbed autoregulation in a Tardbp knock-in mouse model of ALS-FTD.” *Nature Neuroscience*, 21 (4), pp. 552–563. doi: 10.1038/s41593-018-0113-5.

Wilson, R. C. and Doudna, J. A. (2013). “Molecular mechanisms of RNA interference.” *Annual review of biophysics*, 42, pp. 217–239. doi: 10.1146/annurev-biophys-083012-130404.

Wisdom, N. M., Mignogna, J. and Collins, R. L. (2012). “Variability in Wechsler Adult Intelligence Scale-IV subtest performance across age.” *Archives of Clinical Neuropsychology*, 27 (4), pp. 389–397. doi: 10.1093/arclin/acs041.

Wollerton, M. C., Gooding, C., Wagner, E. J., Garcia-Blanco, M. A. and Smith, C. W. J. (2004). “Autoregulation of polypyrimidine tract binding protein by alternative splicing leading to nonsense-mediated decay.” *Molecular Cell*, 13 (1), pp. 91–100. doi: 10.1016/s1097-2765(03)00502-1.

Wolozin, B. and Ivanov, P. (2019). “Stress granules and neurodegeneration.” *Nature Reviews. Neuroscience*, 20 (11), pp. 649–666. doi: 10.1038/s41583-019-0222-5.

Wood, A., Gurfinkel, Y., Polain, N., Lamont, W. and Lyn Rea, S. (2021). “Molecular Mechanisms Underlying TDP-43 Pathology in Cellular and Animal Models of ALS and FTLD.” *International Journal of Molecular Sciences*, 22 (9). doi: 10.3390/ijms22094705.

Woollacott, I. O. C. and Rohrer, J. D. (2016). “The clinical spectrum of sporadic and familial forms of frontotemporal dementia.” *Journal of Neurochemistry*, 138 Suppl 1, pp. 6–31. doi: 10.1111/jnc.13654.

Wyss-Coray, T. (2016). “Ageing, neurodegeneration and brain rejuvenation.” *Nature*, 539 (7628), pp. 180–186. doi: 10.1038/nature20411.

Xie, S., Duan, J., Li, B., Zhou, P. and Hon, G. C. (2017). “Multiplexed engineering and analysis of combinatorial enhancer activity in single cells.” *Molecular Cell*, 66 (2), pp. 285-299.e5. doi: 10.1016/j.molcel.2017.03.007.

Xu, X. and Qi, L. S. (2019). “A CRISPR-dCas Toolbox for Genetic Engineering and Synthetic Biology.” *Journal of Molecular Biology*, 431 (1), pp. 34–47. doi: 10.1016/j.jmb.2018.06.037.

Yano, M., Okano, H. J. and Okano, H. (2005). “Involvement of Hu and heterogeneous nuclear ribonucleoprotein K in neuronal differentiation through p21 mRNA post-transcriptional regulation.” *The Journal of Biological Chemistry*, 280 (13), pp. 12690–12699. doi: 10.1074/jbc.M411119200.

Yedavalli, V. S., Patil, A. and Shah, P. (2018). “Amyotrophic lateral sclerosis and its mimics/variants: A comprehensive review.” *Journal of clinical imaging science*, 8, p. 53. doi: 10.4103/jcis.JCIS_40_18.

Yoshino, H. (2019). “Edaravone for the treatment of amyotrophic lateral sclerosis.” *Expert Review of Neurotherapeutics*, 19 (3), pp. 185–193. doi: 10.1080/14737175.2019.1581610.

Zabolocki, M., McCormack, K., van den Hurk, M., Milky, B., Shoubridge, A. P., Adams, R., Tran, J., Mahadevan-Jansen, A., Reineck, P., Thomas, J., Hutchinson, M. R., Mak, C. K. H., Añonuevo, A., Chew, L. H., Hirst, A. J., Lee, V. M., Knock, E. and Bardy, C. (2020). “BrainPhys neuronal medium optimized for imaging and optogenetics in vitro.” *Nature Communications*, 11 (1), p. 5550. doi: 10.1038/s41467-020-19275-x.

Zarnack, K., König, J., Tajnik, M., Martincorena, I., Eustermann, S., Stévant, I., Reyes, A., Anders, S., Luscombe, N. M. and Ule, J. (2013). “Direct competition between hnRNP C and U2AF65 protects the transcriptome from the exonization of Alu elements.” *Cell*, 152 (3), pp. 453–466. doi: 10.1016/j.cell.2012.12.023.

van der Zee, J., Urwin, H., Engelborghs, S., Bruyland, M., Vandenberghe, R., Dermaut, B., De Pooter, T., Peeters, K., Santens, P., De Deyn, P. P., Fisher, E. M., Collinge, J., Isaacs, A. M. and Van Broeckhoven, C. (2008). “CHMP2B C-truncating mutations in frontotemporal lobar degeneration are associated with an aberrant endosomal phenotype in vitro.” *Human Molecular Genetics*, 17 (2), pp. 313–322. doi: 10.1093/hmg/ddm309.

Zhang, H., Ma, Q., Zhang, Y.-W. and Xu, H. (2012). “Proteolytic processing of Alzheimer’s β-amyloid precursor protein.” *Journal of Neurochemistry*, 120 Suppl 1, pp. 9–21. doi: 10.1111/j.1471-4159.2011.07519.x.

Zhang, Q.-S., Manche, L., Xu, R.-M. and Krainer, A. R. (2006). “hnRNP A1 associates with telomere ends and stimulates telomerase activity.” *RNA (New York)*, 12 (6), pp. 1116–1128. doi: 10.1261/rna.58806.

Zhang, Y., Pak, C., Han, Y., Ahlenius, H., Zhang, Z., Chanda, S., Marro, S., Patzke, C., Acuna, C., Covy, J., Xu, W., Yang, N., Danko, T., Chen, L., Wernig, M. and Südhof, T. C. (2013). “Rapid single-step induction of functional neurons from human pluripotent stem cells.” *Neuron*, 78 (5), pp. 785–798. doi: 10.1016/j.neuron.2013.05.029.

Zhou, R., Shanas, R., Nelson, M. A., Bhattacharyya, A. and Shi, J. (2010). “Increased expression of the heterogeneous nuclear ribonucleoprotein K in pancreatic cancer and its association with the mutant p53.” *International Journal of Cancer*, 126 (2), pp. 395–404. doi: 10.1002/ijc.24744.

Zhou, Y., Liu, S., Liu, G., Oztürk, A. and Hicks, G. G. (2013). “ALS-associated FUS mutations result in compromised FUS alternative splicing and autoregulation.” *PLoS Genetics*, 9 (10), p. e1003895. doi: 10.1371/journal.pgen.1003895.

Zhu, A., Ibrahim, J. G. and Love, M. I. (2019). “Heavy-tailed prior distributions for sequence count data: removing the noise and preserving large differences.” *Bioinformatics*, 35 (12), pp. 2084–2092. doi: 10.1093/bioinformatics/bty895.

Ziegler, L. H. (1930). “Psychotic and emotional phenomena associated with amyotrophic lateral sclerosis.” *Archives of Neurology & Psychiatry*, 24 (5), p. 930. doi: 10.1001/archneurpsyc.1930.02220170050006.

Appendices

Appendix 1. Ethical approval of the study.

Copy of ethical approval confirmation excerpted from signed material transfer agreement (MTA): UCLMTA11/19 (**Expiry date:** 30/04/2024).

IN WITNESS WHEREOF this Agreement has been signed by the duly authorised representatives of the RECIPIENT and the PROVIDER.

For and on behalf of the RECIPIENT

Title: Principal Researcher.

Signature: [redacted for purpose of publishing open access]

Name in capitals: TAMMARYN LASHLEY

Date: 16/4/2019

For and on behalf of the PROVIDER

Confirmation by the Director of Neuropathology in the Queen Square Brain Bank for Neurological Disorders at the 1, Wakefield Street Satellite Site under the UCL Institute of Neurology HTA Licence number 12198 (Research Sector) that the RESEARCH PROJECT detailed in Appendix A has been approved by this tissue bank's MTA Approval Committee, and has also been given Research Tissue Bank generic ethical approval or NHS Research Ethics Committee approval:

Signature: [redacted for purpose of publishing open access]

Name in capitals: DR ZANE JAUNMUKTANE

Date: 11/9/2019

Title: HTA Designated Individual for the UCL Institute of Neurology HTA Licence number 12198.

Signature: [redacted for purpose of publishing open access]

Name in capitals: PROFESSOR MARIA THOM

Date: 6/9/19

Appendix 2. List of all (*n* = 209) differentially expressed genes found in CRISPRi-i^3 hnRNP K KD neurons.

Gene	baseMean	LFC	LFC SE	*p* value	*p* adj
AATBC	250.0254	0.511457	0.145837	2.65E-05	0.003734
ABR	462.0184	0.309976	0.113004	5.93E-04	0.030202
AC004158.1	110.3786	-0.64789	0.251217	4.01E-04	0.023778
AC004528.2	289.3192	0.362546	0.131359	4.42E-04	0.025426
AC005606.2	305.3005	0.370193	0.130227	3.43E-04	0.022131
AC005785.1	667.5532	0.40466	0.115668	3.45E-05	0.004318
AC006128.1	921.5185	0.319825	0.124121	8.86E-04	0.040743
AC006487.1	181.898	0.549576	0.188633	1.83E-04	0.016122
AC008708.2	124.8416	-0.62746	0.225857	2.39E-04	0.01779
AC009955.4	152.3559	-0.49479	0.177308	2.81E-04	0.019104
AC010157.2	203.8326	-0.51687	0.147999	2.81E-05	0.003851
AC010247.2	92.73839	0.964576	0.208152	1.80E-07	6.38E-05
AC010980.1	324.3303	-0.38297	0.134938	3.26E-04	0.021349
AC011446.2	658.5964	0.464302	0.112036	2.34E-06	5.53E-04
AC011611.3	349.4621	0.534738	0.151638	2.40E-05	0.0036
AC011755.1	68.07169	-0.77806	0.223922	2.38E-05	0.0036
AC018688.1	97.2321	-0.88128	0.212973	1.62E-06	3.94E-04
AC040162.1	416.5703	0.40007	0.141781	3.24E-04	0.021349
AC067863.1	66.48161	1.25716	0.275053	2.12E-07	7.21E-05
AC079385.1	148.5378	-0.43653	0.182506	9.12E-04	0.041138
AC079385.3	214.2242	-0.46264	0.155469	1.76E-04	0.015948
AC097654.1	164.5272	-0.43312	0.164908	5.07E-04	0.027459
AC105233.5	195.3769	-0.40765	0.173361	0.001094	0.046902
AC106886.4	3193.576	0.32757	0.105182	1.69E-04	0.015598
AC125611.4	327.6659	1.043637	0.205619	1.81E-08	1.10E-05
AC127164.1	156.5988	-0.50205	0.178176	2.53E-04	0.018237
AC145207.2	1353.571	0.341516	0.1282	6.33E-04	0.031512
AC148477.2	149.8198	0.729101	0.21506	3.13E-05	0.004033
AC234582.1	362.8763	0.507949	0.136189	1.16E-05	0.002155
AC245100.4	185.3583	-0.72938	0.155522	1.45E-07	5.35E-05
ADA	116.3536	1.320578	0.18867	1.27E-13	1.54E-10
ADCYAP1	111.9959	0.550085	0.190446	1.98E-04	0.016617
AF106564.1	18823.16	0.726819	0.096157	1.94E-15	8.27E-12
AFAP1	299.8235	0.352866	0.14537	0.001121	0.047409
AL021937.1	97.27309	0.87409	0.224325	4.44E-06	9.45E-04
AL049557.1	366.8567	0.519071	0.159611	6.45E-05	0.007042
AL132633.1	449.0859	-0.93737	0.127048	8.59E-15	2.44E-11
AL133284.1	99.85276	-0.53851	0.201897	3.75E-04	0.023271
AL354733.3	402.8117	-0.41559	0.154005	4.33E-04	0.02527
AL359396.1	538.8694	-0.65917	0.155399	1.17E-06	2.94E-04
AL929472.3	903.2739	0.435643	0.122452	2.60E-05	0.003734
ANK2	1269.801	0.281895	0.111036	0.001225	0.049975

ANKRD36BP1	150.3249	-0.49646	0.213181	9.30E-04	0.041674
AP000894.2	596.8327	0.702075	0.132721	6.73E-09	4.51E-06
AP000942.2	229.0522	-0.48762	0.14606	4.88E-05	0.005691
AP001172.1	83.43037	-0.60224	0.229305	3.73E-04	0.023271
AP001972.1	279.4378	0.338682	0.137626	0.0011	0.046902
AP002893.1	508.3711	0.48006	0.117362	2.85E-06	6.22E-04
AP003396.5	541.5671	0.493919	0.112002	6.94E-07	2.04E-04
APP	1318.959	0.306734	0.1013	2.57E-04	0.018255
ARF3	157.3391	0.459406	0.17028	4.00E-04	0.023778
ARHGAP31	63.70427	0.550101	0.241808	9.96E-04	0.043942
ARHGEF26	70.90549	-0.80543	0.238358	3.18E-05	0.004035
ARHGEF4	104.4291	0.503051	0.197686	5.47E-04	0.029266
ATP1A3	1277.38	0.396226	0.12282	9.36E-05	0.009594
ATP6V1G2	92.83063	0.707486	0.197235	1.63E-05	0.002719
AURKAIP1	96.15228	0.484666	0.208049	9.67E-04	0.043095
B3GALT2	74.16191	-0.70009	0.246942	1.99E-04	0.016617
BASP1	6078.634	0.332882	0.09966	8.04E-05	0.008452
BCL2L14	62.71721	-0.6514	0.257156	4.60E-04	0.026077
BRAT1	320.0148	-0.48028	0.135139	2.38E-05	0.0036
BSCL2	1899.532	0.525182	0.103023	2.31E-08	1.31E-05
C12orf65	1187.128	-0.42532	0.1099	8.01E-06	0.001624
C14orf93	156.4537	-0.79908	0.161944	4.17E-08	2.09E-05
C16orf92	1108.462	0.363545	0.121626	2.24E-04	0.017364
CAPS	219.9029	1.294139	0.143844	1.16E-20	9.91E-17
CARHSP1	401.9396	0.344629	0.119329	3.31E-04	0.021509
CDK5R2	176.4381	0.462843	0.161256	2.42E-04	0.01779
CELF3	305.5159	0.337965	0.127643	6.75E-04	0.033228
CEMIP	120.9065	0.643953	0.188439	3.08E-05	0.004033
CFAP44	1122.52	-0.30561	0.103408	3.15E-04	0.021087
CNTN2	290.3894	0.629332	0.130992	8.87E-08	3.59E-05
COL7A1	94.46578	-0.57507	0.197605	1.77E-04	0.015948
COTL1	294.1598	0.553309	0.196427	2.39E-04	0.01779
CPLX2	578.5105	0.442786	0.119415	1.38E-05	0.002394
CRABP2	170.1967	0.727049	0.199628	1.26E-05	0.002291
CRELD2	151.3574	0.412414	0.162636	7.01E-04	0.034085
CSPG4	185.5435	0.486131	0.158096	1.22E-04	0.012045
CYB561D2	274.783	0.392364	0.14621	4.90E-04	0.027268
DDB2	211.8884	0.72163	0.14503	3.55E-08	1.89E-05
DDX18P1	62.42584	-0.83782	0.257667	4.99E-05	0.005742
DUX4L50	435.6824	0.495426	0.130208	8.81E-06	0.00174
EEF1A2	320.6685	0.442486	0.131644	5.20E-05	0.005901
EID2	80.05049	0.53178	0.211725	5.75E-04	0.029828
ELAVL3	987.3829	0.375702	0.113411	7.46E-05	0.007934
ELP4	315.4265	-0.44414	0.193481	0.001137	0.047409
ERVFRD-1	228.7339	-0.41091	0.157934	5.77E-04	0.029828
FJX1	324.2983	0.362121	0.131927	4.63E-04	0.026103
FP700111.1	97.9061	-0.72178	0.251925	1.78E-04	0.015948
G6PD	87.9992	0.864078	0.246458	2.00E-05	0.003274

GAP43	822.2203	0.381146	0.131072	2.80E-04	0.019104
GATAD2B	455.2969	-0.36833	0.121897	1.94E-04	0.016617
GLB1L2	697.9419	-0.46043	0.129536	2.44E-05	0.0036
GLB1L3	432.0771	0.363655	0.129456	3.86E-04	0.023271
GLYCTK	501.2874	0.87473	0.166143	6.89E-09	4.51E-06
GMPPA	84.49618	0.508106	0.217093	9.14E-04	0.041138
GRSF1	85.20747	-0.58972	0.210394	2.35E-04	0.01779
HACD4	348.0451	-0.43193	0.167027	5.71E-04	0.029828
HEXB	678.8067	0.353346	0.137839	8.19E-04	0.038308
HMGA2-AS1	112.119	-0.65056	0.229644	1.98E-04	0.016617
HSPA1A	531.667	0.367137	0.138048	5.77E-04	0.029828
HSPA1B	365.0649	0.367894	0.131104	3.82E-04	0.023271
IL21R	63.21437	-0.8169	0.294502	2.03E-04	0.016624
IMP4	110.8316	0.45454	0.190541	9.04E-04	0.041134
INSM1	200.7157	1.195138	0.167727	5.37E-14	9.14E-11
IPO5	143.0015	-0.48502	0.201484	8.11E-04	0.038142
IQSEC1	191.8939	0.371335	0.157289	0.001227	0.049975
JAM2	109.0046	-0.58902	0.190597	9.99E-05	0.010123
KAT7	103.0428	-0.5696	0.208467	2.98E-04	0.020149
KDM8	104.5945	0.898338	0.186943	7.95E-08	3.41E-05
KIAA1614	776.6063	0.386245	0.128901	2.01E-04	0.016624
KLHL35	364.3586	0.393742	0.142139	3.85E-04	0.023271
KMO	599.6237	0.451483	0.147801	1.41E-04	0.013492
KRTAP5-2	807.8167	0.461726	0.130681	2.68E-05	0.003734
L1CAM	960.6734	0.33752	0.114189	2.76E-04	0.019096
LETM2	288.005	-0.57238	0.131149	7.59E-07	2.08E-04
LHFPL2	132.4873	-0.49651	0.201085	6.63E-04	0.032804
LINC00404	117.8562	-0.52891	0.215195	6.32E-04	0.031512
LINC01159	135.8056	-0.59936	0.195497	1.04E-04	0.010384
LINC01268	81.53173	-0.60302	0.238144	4.99E-04	0.027297
LINC01772	354.5513	-0.5646	0.161133	2.45E-05	0.0036
LRBA	2974.854	0.343508	0.140007	0.001102	0.046902
MAPK4	56.07312	0.660532	0.280564	7.06E-04	0.034125
MCRIP2	297.8664	0.452378	0.148475	1.42E-04	0.013492
MISP3	172.655	0.56269	0.16751	4.25E-05	0.005023
MOB2	58.88421	0.814851	0.254313	5.84E-05	0.006536
MPDZ	129.2643	-0.50196	0.200143	6.14E-04	0.031103
MRPS18C	195.6856	-0.64538	0.17461	1.09E-05	0.002065
MYL9	65.17267	-0.54259	0.240655	0.001023	0.044671
MYLK	481.5758	-0.39868	0.114697	3.88E-05	0.004721
MYO1F	152.1401	-0.40089	0.168973	0.001066	0.046274
NCAPH2	351.1702	0.352059	0.141926	9.83E-04	0.043576
NECAP2	183.1759	-0.69418	0.156489	4.81E-07	1.52E-04
NEFL	3235.036	0.567199	0.101356	1.45E-09	1.12E-06
NEFM	6990.344	0.600973	0.087636	4.53E-13	4.82E-10
NEXN	72.8889	-0.60535	0.225142	3.24E-04	0.021349
NGFR	378.7951	0.445012	0.173088	5.78E-04	0.029828
NHLH2	391.5434	0.615655	0.151015	2.52E-06	5.79E-04

NODAL	101.8538	0.668397	0.190661	2.27E-05	0.0036
NPTX2	54.08732	0.840337	0.27126	8.19E-05	0.008496
NR1I3	412.799	0.384851	0.122283	1.25E-04	0.012243
NSUN5P1	267.723	-0.43984	0.151896	2.34E-04	0.01779
NTMT1	322.7211	0.364699	0.152857	0.001173	0.048471
NUDCD2	246.6576	-0.42097	0.184013	0.001221	0.049975
OMG	132.8311	-0.55284	0.193259	2.08E-04	0.016687
PDE6B	103.0424	0.496785	0.196423	5.83E-04	0.029905
PGAM1P9	210.8043	-0.47272	0.144375	6.14E-05	0.006789
PLAC4	222.8255	-0.53113	0.140321	9.00E-06	0.00174
PLCH2	243.0357	0.371978	0.14963	8.90E-04	0.040747
PLEKHG4B	147.5435	-0.56955	0.199822	2.07E-04	0.016687
POLR2J	171.0012	0.45863	0.17254	4.46E-04	0.025449
POU3F1	92.44385	0.597989	0.208425	1.94E-04	0.016617
PPT2-EGFL8	1798.745	0.353361	0.100541	3.95E-05	0.004739
PRKCE	115.9073	0.533842	0.177652	1.43E-04	0.013492
PRPH	59.99678	1.06413	0.344574	7.38E-05	0.007934
PRR26	878.5032	-0.43983	0.118011	1.35E-05	0.002394
R3HDM2P1	55.97376	-0.75542	0.269695	2.11E-04	0.016755
RFX4	147.7108	-0.50872	0.192331	4.16E-04	0.024399
RGMB-AS1	811.4971	0.530094	0.12048	6.81E-07	2.04E-04
RGPD2	140.4054	-0.51319	0.19184	3.82E-04	0.023271
ROBO3	131.23	0.898299	0.185541	6.36E-08	3.01E-05
RTN4	532.3197	0.334704	0.116632	3.65E-04	0.023014
SCRT1	342.7859	0.608543	0.149405	2.59E-06	5.81E-04
SEMA5A	96.95771	-0.53769	0.228306	8.28E-04	0.038495
SEMA5A-AS1	62.23078	-1.11321	0.260855	9.28E-07	2.47E-04
SIAH1	233.8227	-0.44808	0.165793	4.02E-04	0.023778
SLC12A4	229.7453	0.524061	0.151398	3.10E-05	0.004033
SLC13A4	606.5734	-0.32622	0.130924	0.001098	0.046902
SLC48A1	111.3499	-0.46542	0.190754	7.68E-04	0.036737
SLIT1	342.8349	0.383622	0.131379	2.57E-04	0.018255
SNCG	332.9478	0.444983	0.17518	6.20E-04	0.03123
SPAG8	221.5751	0.433055	0.150173	2.47E-04	0.017985
SPATA6L	81.99011	0.81062	0.282844	1.68E-04	0.015598
SRGAP3-AS3	101.9572	-0.56162	0.197867	2.21E-04	0.017364
STARD13-AS	72.07758	-0.91424	0.27528	3.52E-05	0.004336
STKLD1	97.54299	0.556109	0.221864	5.60E-04	0.029777
STMN4	340.1637	0.435129	0.15231	2.67E-04	0.01866
STXBP5L	57.62507	-1.03752	0.240371	7.19E-07	2.04E-04
TAGLN3	255.5311	0.462613	0.17651	4.83E-04	0.027051
TBC1D10C	139.1859	-0.63112	0.164623	6.69E-06	0.001388
TEX10	559.6833	-0.42687	0.173947	8.09E-04	0.038142
THUMPD3	405.7819	-0.42052	0.181037	0.001127	0.047409
TMCC2	103.8404	0.621842	0.247144	5.00E-04	0.027297
TMED8	229.0379	-0.75708	0.177889	1.03E-06	2.66E-04
TMEM243	89.98825	-0.59302	0.233996	4.99E-04	0.027297
TMEM51-AS1	1542.355	0.818097	0.114965	6.72E-14	9.53E-11

TMEM63A	208.5795	0.444367	0.154041	2.42E-04	0.01779
TNFSF13	122.8892	0.458857	0.201015	0.001142	0.047409
TUBB2A	591.8093	0.354623	0.138484	7.91E-04	0.037596
TUBB3	2580.795	0.422061	0.141138	1.84E-04	0.016122
U2AF2	495.0032	0.51071	0.147042	3.03E-05	0.004033
UBE2QL1	123.9956	-0.48735	0.189473	5.30E-04	0.028562
UBXN6	566.627	-0.62534	0.132144	1.22E-07	4.71E-05
UNC5C	683.8491	-0.56066	0.122763	2.99E-07	9.79E-05
UNCX	491.6227	0.348419	0.132531	6.80E-04	0.033281
URM1	1132.481	-0.85013	0.117886	2.95E-14	6.28E-11
VARS	195.0817	0.405604	0.169461	0.001012	0.044411
VGF	287.0044	0.88668	0.147574	9.95E-11	9.41E-08
VMAC	76.64591	1.057351	0.220632	8.00E-08	3.41E-05
VRK2	84.93054	-0.70088	0.267538	3.53E-04	0.022442
VWA3B	85.41934	-1.19519	0.20314	1.89E-10	1.61E-07
WNK2	410.2257	0.362914	0.127628	3.49E-04	0.022333
XYLT2	383.4785	0.337804	0.128658	7.13E-04	0.034269
YRDC	287.7891	0.351856	0.138195	8.35E-04	0.038605
Z82217.1	256.5097	-0.425	0.148215	2.62E-04	0.018407
ZNF550	262.9372	0.527392	0.143589	1.41E-05	0.002405
ZNF654	87.31734	-0.6763	0.26731	4.39E-04	0.025426
ZNF710	1300.797	-0.2961	0.117294	0.001136	0.047409
ZNF829	108.6645	-0.65287	0.233158	2.22E-04	0.017364

baseMean, mean of normalised counts of all samples; LFC, Log_2FoldChange in expression; LFC SE Standard error value returned by DeSeq2; *p* adj, Adjusted *p* value for multiple comparisons.

Appendix 3. List of all (*n* = 364) differentially spliced cassette exons found in CRISPRi-i^3 hnRNP K KD neurons.

Exon co-ordinates	Gene	PSI_{Con}	PSI_{KD}	dPSI	FDR	Novel ?
chr1:103025799-103025952	*COL11A1*	0.085286	0.029754	-0.05553	0.0319	No
chr1:10655648-10655813	*CASZ1*	0.994039	0.919123	-0.07492	0.019	Yes
chr1:114737470-114737563	*CSDE1*	0.143589	0.185215	0.041626	0.0274	No
chr1:11523365-11523442	*DISP3*	0.072927	0.01481	-0.05812	0.0137	Yes
chr1:1337017-1337055	*DVL1*	0.387638	0.467998	0.08036	0.0133	No
chr1:1388625-1388743	*CCNL2*	0.045019	0.017969	-0.02705	0.0151	No
chr1:145394977-145395141	*NBPF20*	0.96013	0.915682	-0.04445	0.0276	No
chr1:149977425-149977576	*OTUD7B*	0.957147	0.856045	-0.1011	0.0344	Yes
chr1:150327556-150327652	*PRPF3*	0.259289	0.472676	0.213387	1.32E-04	No
chr1:153953265-153953369	*CRTC2*	0.90437	0.978812	0.074442	0.044	Yes
chr1:154212319-154212378	*C1orf43*	0.985843	0.967017	-0.01883	0.0186	No
chr1:154249238-154249437	*UBAP2L*	0.96913	0.923254	-0.04588	0.0439	Yes
chr1:155415743-155415923	*ASH1L*	0.927193	0.976638	0.049445	0.0244	Yes
chr1:156266540-156266678	*SMG5*	0.896652	0.850766	-0.04589	0.044	Yes
chr1:160283529-160283639	*PEX19*	0.840489	0.907491	0.067002	0.0469	No
chr1:16441165-16441298	*NECAP2*	0.166797	0.426372	0.259575	0.0175	Yes
chr1:173864483-173864506	*GAS5*	0.956242	0.928151	-0.02809	0.0104	No
chr1:200900936-200901159	*INAVA*	0.845043	0.633332	-0.21171	0.0137	Yes
chr1:201788467-201788638	*NAV1*	0.840034	0.921393	0.081359	0.0151	No
chr1:204146641-204146764	*ETNK2*	0.924747	0.9527	0.027953	0.0186	No
chr1:205305430-205305614	*NUAK2*	0.020612	0.073529	0.052917	0.0179	Yes
chr1:213000785-213000912	*ANGEL2*	0.9042	0.77879	-0.12541	0.0246	Yes
chr1:222623306-222623351	*MIA3*	0.023821	0.058447	0.034626	0.0105	Yes
chr1:227149086-227149106	*CDC42BPA*	0.007194	0.033331	0.026136	0.0325	Yes
chr1:234463836-234463934	*TARBP1*	0.589762	0.754641	0.164879	0.0156	Yes
chr1:27330984-27331137	*TMEM222*	0.14932	0.259571	0.11025	0.0104	No
chr1:27334666-27334754	*TMEM222*	0.029749	0.071815	0.042066	0.0237	No
chr1:32095659-32095762	*TMEM39B*	0.098385	0.236431	0.138046	0.0246	No
chr1:32217436-32217577	*TMEM234*	0.136256	0.035721	-0.10053	0.0369	No
chr1:32329067-32329160	*HDAC1*	0.973153	0.895018	-0.07813	0.0476	Yes
chr1:44926627-44926739	*EIF2B3*	0.992066	0.925776	-0.06629	0.00877	Yes
chr1:45568484-45568684	*AKR1A1*	0.794892	0.660895	-0.134	0.0304	No
chr1:55151911-55151975	*USP24*	0.055675	0.095434	0.039759	0.0417	No
chr1:62017855-62017947	*PATJ*	0.886417	0.879975	-0.00644	0.0396	Yes
chr1:66695433-66695493	*SGIP1*	0.97653	0.911918	-0.06461	0.024	Yes
chr1:81952986-81953025	*ADGRL2*	0.196882	0.250399	0.053517	0.023	No
chr1:86868052-86868102	*SELENOF*	0.91078	0.795378	-0.1154	0.0011	No
chr10:100380982-100381109	*OLMALINC*	0.220228	0.321581	0.101352	0.0184	No
chr10:101667885-101667980	*FBXW4*	0.895172	0.757728	-0.13744	0.03	Yes
chr10:119825951-119826018	*INPP5F*	0.016555	0.07853	0.061975	0.00742	No

chr10:120890715-120890887	*WDR11*	0.924023	0.810729	-0.11329	0.0486	No
chr10:124767223-124767347	*EEF1AKMT2*	0.425296	0.801361	0.376065	0.0199	Yes
chr10:15130141-15130312	*NMT2*	0.903539	0.989995	0.086456	0.034	Yes
chr10:37856434-37856532	*ZNF248*	0.64815	0.489789	-0.15836	0.0474	No
chr10:5735303-5735546	*TASOR2*	0.792445	0.894316	0.101871	0.0388	No
chr10:73791323-73791499	*ZSWIM8*	0.972826	0.838528	-0.1343	0.0178	Yes
chr10:98429790-98429889	*HPS1*	0.656966	0.365374	-0.29159	0.029	No
chr11:111674323-111674384	*SIK2*	0.02529	0.141734	0.116444	0.0217	Yes
chr11:119026602-119026688	*SLC37A4*	0.758473	0.545619	-0.21285	0.0313	No
chr11:119049017-119049203	*HYOU1*	0.961118	0.984475	0.023357	0.04	No
chr11:121036504-121036612	*TBCEL*	0.167301	0.072945	-0.09436	0.0246	No
chr11:121570156-121570270	*SORL1*	0.977295	0.816937	-0.16036	0.0111	Yes
chr11:125627606-125627830	*CHEK1*	0.845576	0.705631	-0.13994	0.00121	No
chr11:130137255-130137291	*APLP2*	0.374001	0.489034	0.115033	1.90E-05	No
chr11:27506316-27506455	*LIN7C*	0.016358	0.025435	0.009077	0.0313	Yes
chr11:33348165-33348228	*HIPK3*	0.160953	0.285384	0.124431	0.0382	No
chr11:47725736-47725836	*FNBP4*	0.196358	0.385334	0.188977	0.0153	No
chr11:62141499-62141511	*INCENP*	0.226059	0.360329	0.134271	0.00513	No
chr11:62789600-62789679	*TMEM179B*	0.918626	0.980345	0.061718	0.0301	No
chr11:62854887-62854938	*SNHG1*	0.867978	0.802825	-0.06515	0.0413	No
chr11:63903985-63904147	*MARK2*	0.848426	0.681277	-0.16715	0.00142	No
chr11:6401976-6401982	*APBB1*	0.797149	0.857428	0.060279	0.0344	No
chr11:67289828-67289965	*ANKRD13D*	0.121085	0.234243	0.113158	0.0339	No
chr11:78720369-78720390	*TENM4*	0.753439	0.878241	0.124802	0.0148	Yes
chr11:810233-810357	*RPLP2*	0.980837	0.955635	-0.0252	0.0089	Yes
chr11:92765506-92765575	*FAT3*	0.543846	0.645054	0.101208	0.0325	Yes
chr12:109523977-109524115	*UBE3B*	0.971399	0.877518	-0.09388	0.00627	Yes
chr12:111217889-111217937	*CUX2*	0.892552	0.815186	-0.07737	0.0399	Yes
chr12:1112214-1112298	*ERC1*	0.145203	0.060718	-0.08448	0.017	No
chr12:111554865-111555074	*ATXN2*	0.029459	0.069941	0.040482	0.0458	Yes
chr12:117010322-117010450	*FBXW8*	0.931477	0.918003	-0.01347	0.0254	Yes
chr12:120098810-120098935	*RAB35*	0.961918	0.906238	-0.05568	0.0376	No
chr12:120351343-120351400	*MSI1*	0.780596	0.859299	0.078704	2.89E-05	No
chr12:120351343-120351400	*MSI1*	0.527638	0.951814	0.424176	0.0111	No
chr12:124385744-124385887	*NCOR2*	0.991921	0.962374	-0.02955	0.0348	Yes
chr12:124457105-124457162	*NCOR2*	0.954063	0.914954	-0.03911	0.0361	No
chr12:125136661-125136864	*AACS*	0.692975	0.476393	-0.21658	0.0329	No
chr12:15883540-15883676	*STRAP*	0.950221	0.918634	-0.03159	0.0186	No
chr12:16357604-16357699	*MGST1*	0.963386	0.903573	-0.05981	0.0117	No
chr12:3863835-3863957	*PARP11*	0.435949	0.27377	-0.16218	0.0127	No
chr12:47802223-47802274	*HDAC7*	0.804764	0.602546	-0.20222	0.0201	No
chr12:50671185-50671398	*DIP2B*	0.901799	0.833392	-0.06841	0.0207	Yes
chr12:51191595-51191764	*AC139768.1*	0.963107	0.900425	-0.06268	0.0488	Yes
chr12:54283078-54283234	*HNRNPA1*	0.099654	0.083574	-0.01608	0.0338	No
chr12:56160625-56160670	*MYL6*	0.368113	0.459337	0.091224	0.00968	No
chr12:56164302-56164368	*SMARCC2*	0.197388	0.110789	-0.0866	0.0178	No
chr12:56243784-56243876	*ANKRD52*	0.995711	0.950234	-0.04548	0.0408	Yes

chr12:56670274-56670364	*PTGES3*	0.95063	0.903103	-0.04753	0.00622	No
chr12:57720098-57720263	*OS9*	0.442479	0.5275	0.085021	0.0321	No
chr12:7157488-7157691	*CLSTN3*	0.994332	0.964555	-0.02978	0.0348	Yes
chr12:98703370-98703499	*APAF1*	0.814327	0.731967	-0.08236	0.0408	No
chr13:111292117-111292294	*ARHGEF7*	0.795869	0.878584	0.082715	0.0339	No
chr13:37021447-37021602	*SUPT20H*	0.996675	0.938983	-0.05769	0.00683	Yes
chr13:52183975-52184114	*MRPS31P5*	0.872627	0.590208	-0.28242	0.00367	No
chr14:100137739-100137802	*EVL*	0.783154	0.822013	0.038859	0.0202	No
chr14:100540495-100540579	*BEGAIN*	0.931581	0.718786	-0.21279	0.0398	Yes
chr14:49813987-49814050	*NEMF*	0.944706	0.964451	0.019745	0.0429	No
chr14:55026710-55026803	*WDHD1*	0.975189	0.890359	-0.08483	0.0123	No
chr14:55673171-55673255	*KTN1*	0.062394	0.017655	-0.04474	0.0334	No
chr14:67557268-67557418	*PLEKHH1*	0.973375	0.862058	-0.11132	0.0241	Yes
chr14:70328165-70328283	*SYNJ2BP-COX16*	0.049181	0.028056	-0.02112	0.0441	Yes
chr14:74290026-74290118	*ABCD4*	0.681867	0.85297	0.171103	0.00861	No
chr15:22947002-22947092	*CYFIP1*	0.994793	0.942759	-0.05203	0.0167	Yes
chr15:29719776-29720016	*TJP1*	0.021079	0.028908	0.007829	0.0481	No
chr15:40414888-40414982	*IVD*	0.969721	0.883143	-0.08658	0.0344	No
chr15:43421024-43421174	*TP53BP1*	0.988126	0.962883	-0.02524	0.0241	No
chr15:59668102-59668138	*BNIP2*	0.099275	0.030696	-0.06858	0.0329	No
chr15:60382341-60382441	*ANXA2*	0.993555	0.951096	-0.04246	0.00382	No
chr15:65248116-65248228	*PARP16*	0.849397	0.412643	-0.43675	0.00139	Yes
chr15:65334727-65334865	*IGDCC3*	0.96564	0.933838	-0.0318	0.028	Yes
chr15:69453646-69453721	*RPLP1*	0.970242	0.952687	-0.01756	0.00765	No
chr15:70052373-70052524	*TLE3*	0.996398	0.976497	-0.0199	0.0243	Yes
chr15:72362375-72362466	*HEXA*	0.056962	0.068644	0.011681	0.026	No
chr15:73274691-73274724	*NEO1*	0.662189	0.736145	0.073956	0.0121	No
chr15:75016592-75016749	*SCAMP5*	0.985203	0.931617	-0.05359	0.00489	No
chr15:79463694-79463760	*MINAR1*	0.182194	0.236164	0.05397	0.0479	No
chr15:89268398-89268525	*FANCI*	0.962319	0.878438	-0.08388	0.0198	Yes
chr15:92956458-92956649	*CHD2*	0.958134	0.985386	0.027252	0.0117	Yes
chr16:14927018-14927084	*AC138932.1*	0.029948	0.105916	0.075969	3.25E-05	Yes
chr16:15132995-15133061	*PKD1P6*	0.198565	0.505283	0.306718	0.0334	Yes
chr16:16325669-16325735	*AC138969.1*	0.029992	0.112772	0.082779	2.56E-05	Yes
chr16:18342931-18342997	*AC126755.1*	0.023693	0.130208	0.106515	1.82E-05	Yes
chr16:18382157-18382223	*PKD1P5*	0.022774	0.113455	0.090681	4.81E-05	Yes
chr16:22257642-22257770	*EEF2K*	0.858126	0.759874	-0.09825	0.0366	Yes
chr16:23082437-23082557	*USP31*	0.982269	0.901689	-0.08058	0.0338	Yes
chr16:23566986-23567069	*UBFD1*	0.909437	0.841486	-0.06795	0.0137	Yes
chr16:2768504-2768599	*SRRM2*	0.090665	0.033392	-0.05727	4.81E-05	No
chr16:29809539-29809764	*MAZ*	0.261397	0.433121	0.171724	2.98E-07	No
chr16:29996807-29996860	*INO80E*	0.969872	0.914888	-0.05498	0.0231	Yes
chr16:3791980-3792094	*CREBBP*	0.93578	0.886402	-0.04938	0.00581	No
chr16:4680031-4680097	*MGRN1*	0.427484	0.533418	0.105934	0.00829	No
chr16:50025650-50025701	*CNEP1R1*	0.075481	0.265712	0.190232	0.0217	No
chr16:655028-655147	*WDR90*	0.982798	0.62408	-0.35872	0.0253	Yes
chr16:70131301-70131419	*PDPR*	0.548953	0.767677	0.218724	0.0251	No

chr16:74349741-74349859	*AC009053.1*	0.315338	0.451191	0.135853	0.0351	No
chr16:84590104-84590262	*COTL1*	0.986063	0.945223	-0.04084	0.00672	Yes
chr16:85665014-85665128	*GSE1*	0.842455	0.719817	-0.12264	0.00152	No
chr16:85780378-85780473	*EMC8*	0.996259	0.955473	-0.04079	0.0291	No
chr17:1586948-1586960	*SLC43A2*	0.543614	0.818151	0.274537	0.00206	No
chr17:16151589-16151616	*NCOR1*	0.423726	0.552053	0.128327	0.0155	No
chr17:17175292-17175412	*MPRIP*	0.91855	0.830698	-0.08785	0.00891	No
chr17:29096760-29096915	*MYO18A*	0.994538	0.94841	-0.04613	0.0226	Yes
chr17:3824059-3824092	*NCBP3*	0.025842	0.086531	0.060689	0.0325	No
chr17:39440385-39440518	*MED1*	0.902293	0.814154	-0.08814	0.00701	No
chr17:41896619-41896649	*ACLY*	0.476369	0.573466	0.097096	0.00371	No
chr17:42218722-42218878	*STAT5B*	0.996459	0.925744	-0.07072	0.0145	Yes
chr17:44157832-44157941	*C17orf53*	0.989878	0.726793	-0.26309	0.00419	No
chr17:44210791-44210947	*UBTF*	0.982593	0.955884	-0.02671	0.0193	Yes
chr17:46039026-46039215	*KANSL1*	0.574118	0.658962	0.084844	0.0492	No
chr17:48057031-48057121	*NFE2L1*	0.114525	0.062714	-0.05181	0.00152	No
chr17:50975862-50975901	*SPAG9*	0.233381	0.309899	0.076519	0.00427	No
chr17:57259976-57260054	*MSI2*	0.048468	0.0218	-0.02667	0.00108	No
chr17:57985253-57985465	*VEZF1*	0.037658	0.09017	0.052513	0.0477	Yes
chr17:59687000-59687021	*CLTC*	0.138511	0.092404	-0.04611	0.00103	No
chr17:63049722-63049787	*TANC2*	0.033208	0.016503	-0.0167	0.0468	Yes
chr17:73242243-73242351	*C17orf80*	0.636272	0.521494	-0.11478	0.0301	No
chr17:76558944-76559043	*SNHG16*	0.343347	0.243611	-0.09974	0.0125	No
chr17:76743397-76743456	*MFSD11*	0.820384	0.95049	0.130106	0.00469	No
chr17:81036862-81036961	*BAIAP2*	0.09281	0.045663	-0.04715	5.53E-04	No
chr17:9437796-9437887	*STX8*	0.095995	0.011492	-0.0845	0.0319	Yes
chr18:7001535-7001551	*LAMA1*	0.039844	0.119187	0.079343	0.0235	Yes
chr18:79949518-79949655	*PQLC1*	0.132253	0.044783	-0.08747	0.0338	No
chr18:9563916-9563951	*PPP4R1*	0.022173	0.00218	-0.01999	0.0133	Yes
chr19:10680345-10680443	*ILF3*	0.867955	0.810663	-0.05729	0.00918	No
chr19:12155624-12155794	*ZNF625*	0.043485	0.010453	-0.03303	0.0365	Yes
chr19:1253953-1254082	*MIDN*	0.141429	0.224954	0.083525	0.0367	No
chr19:17327437-17327569	*ANO8*	0.931096	0.746943	-0.18415	0.0109	Yes
chr19:18431352-18431418	*SSBP4*	0.211718	0.398519	0.186801	5.95E-04	No
chr19:18906959-18907112	*COPE*	0.978857	0.910524	-0.06833	2.94E-04	No
chr19:19003495-19003608	*SUGP2*	0.024992	0.091066	0.066074	1.82E-05	No
chr19:2013546-2013718	*BTBD2*	0.031718	0.118317	0.086599	0.00742	Yes
chr19:2191011-2191240	*DOT1L*	0.965229	0.840692	-0.12454	0.00325	Yes
chr19:29610408-29610632	*POP4*	0.97911	0.847557	-0.13155	0.0241	No
chr19:3546254-3546425	*MFSD12*	0.823302	0.706945	-0.11636	0.0428	No
chr19:3619349-3619546	*CACTIN*	0.006154	0.140287	0.134133	0.00261	Yes
chr19:36313807-36313912	*LINC00665*	0.018683	0.191636	0.172953	0.023	Yes
chr19:37470303-37470387	*ZNF570*	0.711881	0.804888	0.093007	0.0338	No
chr19:38632600-38632678	*EIF3K*	0.887995	0.799485	-0.08851	0.001	No
chr19:39458293-39458305	*SUPT5H*	0.882581	0.759542	-0.12304	7.28E-05	No
chr19:45143520-45143633	*PPP1R37*	0.994726	0.930455	-0.06427	0.00823	Yes
chr19:45616460-45616558	*EML2*	0.972747	0.814643	-0.1581	0.0151	No
chr19:47205103-47205129	*SAE1*	0.098149	0.072806	-0.02534	0.0457	Yes

chr19:5273441-5273583	*PTPRS*	0.985944	0.973725	-0.01222	0.00616	Yes
chr19:55658861-55658981	*U2AF2*	0.029292	0.05047	0.021178	0.0292	No
chr19:57575803-57575930	*ZNF416*	0.94257	0.73511	-0.20746	0.00367	Yes
chr19:871925-872118	*MED16*	0.993259	0.940358	-0.0529	0.0202	No
chr19:876973-877180	*MED16*	0.872008	0.713607	-0.1584	0.0109	No
chr2:135622653-135622732	*R3HDM1*	0.99112	0.92122	-0.0699	0.0308	No
chr2:181896029-181896079	*ITPRID2*	0.947673	0.987348	0.039675	0.0353	No
chr2:201640260-201640265	*TMEM237*	0.973004	0.953303	-0.0197	0.0307	No
chr2:218217462-218217544	*ARPC2*	0.977766	0.939082	-0.03868	0.0327	No
chr2:219215996-219216180	*ABCB6*	0.969734	0.628946	-0.34079	5.53E-04	No
chr2:221501016-221501172	*EPHA4*	0.985397	0.9559	-0.0295	0.036	Yes
chr2:231801139-231801207	*COPS7B*	0.005984	0.01636	0.010376	0.0388	No
chr2:25247298-25247338	*DNMT3A*	0.015493	0.05429	0.038798	0.00429	Yes
chr2:25455404-25455494	*DTNB*	0.239591	0.061282	-0.17831	0.0133	No
chr2:272036-272065	*ACP1*	0.75931	0.815561	0.056251	0.0145	No
chr2:27312493-27312589	*MPV17*	0.990691	0.920876	-0.06982	3.11E-04	No
chr2:38989269-38989314	*SOS1*	0.121902	0.184248	0.062346	0.0182	No
chr2:47172413-47172459	*CALM2*	0.023475	0.012191	-0.01128	0.00648	No
chr2:53895006-53895076	*PSME4*	0.996474	0.954473	-0.042	0.0313	Yes
chr2:55528877-55528992	*CFAP36*	0.953762	0.92629	-0.02747	0.0498	Yes
chr2:65077867-65077964	*CEP68*	0.95846	0.865358	-0.0931	0.0177	Yes
chr2:65242048-65242063	*ACTR2*	0.021302	0.046267	0.024965	0.0263	No
chr2:66512148-66512294	*MEIS1*	0.970506	0.928986	-0.04152	0.0418	No
chr2:74363613-74363628	*DCTN1*	0.766672	0.83566	0.068988	0.00323	No
chr2:86119543-86119614	*PTCD3*	0.051945	0.020442	-0.0315	0.0191	No
chr2:86125794-86125880	*PTCD3*	0.836936	0.761577	-0.07536	0.0304	No
chr2:9336035-9336044	*ASAP2*	0.393725	0.536258	0.142534	0.0441	No
chr2:96737136-96737217	*LMAN2L*	0.106918	0.018612	-0.08831	0.0493	No
chr20:11919085-11919176	*BTBD3*	0.982947	0.919695	-0.06325	0.00277	No
chr20:18452614-18452682	*DZANK1*	0.846137	0.98784	0.141704	0.00323	No
chr20:35280653-35280829	*EIF6*	0.846005	0.764077	-0.08193	0.0171	No
chr20:35554371-35554386	*ERGIC3*	0.341223	0.413549	0.072326	0.0109	No
chr20:35630740-35630795	*CPNE1*	0.955044	0.974867	0.019823	0.0394	Yes
chr20:35734185-35734257	*RBM39*	0.031198	0.018636	-0.01256	0.0271	No
chr20:36898439-36898544	*SAMHD1*	0.785578	0.987429	0.201851	0.019	No
chr20:37347117-37347236	*SRC*	0.099144	0.03616	-0.06298	0.0325	Yes
chr20:3800742-3800865	*CDC25B*	0.889327	0.793564	-0.09576	0.0215	No
chr20:45421382-45421583	*PIGT*	0.979597	0.888296	-0.0913	0.00772	No
chr20:48747808-48747880	*PREX1*	0.964324	0.891735	-0.07259	0.0335	Yes
chr20:49231022-49231115	*DDX27*	0.015249	0.093528	0.078279	0.0274	No
chr20:58669290-58669453	*STX16*	0.692282	0.542944	-0.14934	0.00854	No
chr20:62161435-62161580	*SS18L1*	0.99188	0.966237	-0.02564	0.0281	Yes
chr20:63242538-63242623	*NKAIN4*	0.280756	0.175254	-0.1055	3.70E-04	No
chr20:63875815-63875875	*TPD52L2*	0.352442	0.284433	-0.06801	0.0104	No
chr20:63961308-63961407	*ZNF512B*	0.994023	0.951331	-0.04269	0.03	Yes
chr21:37157160-37157214	*TTC3*	0.063782	0.033206	-0.03058	0.0321	No
chr21:46291333-46291462	*YBEY*	0.800841	0.402966	-0.39787	0.0157	No
chr22:21476643-21476764	*PI4KAP2*	0.838287	0.67445	-0.16384	0.0225	No

chr22:29339753-29339774	*AP1B1*	0.722594	0.60871	-0.11388	0.00741	No
chr22:29580098-29580155	*NIPSNAP1*	0.013977	0.058826	0.044848	0.00676	No
chr22:30022028-30022139	*MTMR3*	0.686096	0.481845	-0.20425	0.00972	No
chr22:36766137-36766197	*IFT27*	0.996976	0.919424	-0.07755	3.07E-04	Yes
chr22:38671069-38671188	*CBY1*	0.94156	0.861127	-0.08043	0.0428	Yes
chr22:40364879-40365056	*ADSL*	0.828033	0.729937	-0.0981	0.00277	No
chr22:43255487-43255577	*SCUBE1*	0.358984	0.290313	-0.06867	0.00742	No
chr22:44889759-44889782	*PHF21B*	0.790758	0.866554	0.075796	0.0351	Yes
chr22:46353766-46353867	*TRMU*	0.984518	0.913721	-0.0708	0.0312	Yes
chr22:50247691-50247776	*HDAC10*	0.591991	0.763816	0.171825	0.0104	No
chr22:50260828-50260956	*MAPK12*	0.045424	0.139227	0.093803	0.0178	Yes
chr22:50436987-50437068	*PPP6R2*	0.645054	0.474877	-0.17018	0.0105	No
chr3:113010642-113010704	*NEPRO*	0.958007	0.905104	-0.0529	0.0427	No
chr3:113409105-113409322	*CFAP44*	0.539941	0.655919	0.115978	0.0225	No
chr3:114056998-114057106	*QTRT2*	0.492385	0.675478	0.183093	0.0444	No
chr3:123931307-123931526	*CCDC14*	0.973025	0.881617	-0.09141	0.0468	Yes
chr3:142313135-142313174	*XRN1*	0.192236	0.122641	-0.06959	0.0229	No
chr3:15082366-15082608	*RBSN*	0.950805	0.862753	-0.08805	0.0304	No
chr3:160564520-160564640	*KPNA4*	0.004385	0.028803	0.024418	5.46E-04	Yes
chr3:16264154-16264229	*DPH3*	0.546968	0.393184	-0.15378	0.00147	No
chr3:169774030-169774097	*MYNN*	0.220953	0.385265	0.164312	0.0491	No
chr3:25604759-25604870	*TOP2B*	0.987456	0.967166	-0.02029	0.0252	Yes
chr3:33577201-33577264	*CLASP2*	0.584928	0.65175	0.066822	0.0155	No
chr3:38131595-38131638	*ACAA1*	0.690193	0.528708	-0.16149	0.0118	No
chr3:48406567-48406740	*PLXNB1*	0.097772	0.172322	0.07455	0.00742	Yes
chr3:49025994-49026066	*IMPDH2*	0.010042	0.035515	0.025473	0.0017	No
chr3:51959894-51960023	*PCBP4*	0.899501	0.848178	-0.05132	0.024	No
chr3:62481722-62481869	*CADPS*	0.361254	0.499077	0.137823	0.00139	No
chr3:62530653-62530812	*CADPS*	0.134303	0.084571	-0.04973	0.0124	No
chr3:62544847-62544859	*CADPS*	0.217383	0.268795	0.051412	0.0393	No
chr3:9468518-9468575	*SETD5*	0.143654	0.264554	0.1209	1.90E-04	No
chr3:9816073-9816202	*TTLL3*	0.515231	0.630615	0.115384	0.0237	No
chr3:98825314-98825366	*DCBLD2*	0.897248	0.814404	-0.08284	0.0493	Yes
chr4:139695196-139695267	*MGST2*	0.97652	0.824486	-0.15203	0.0297	No
chr4:151144219-151144288	*SH3D19*	0.581437	0.371168	-0.21027	0.0444	No
chr4:2744696-2744945	*TNIP2*	0.987452	0.842538	-0.14491	0.0398	No
chr4:53414614-53414722	*FIP1L1*	0.622234	0.53555	-0.08668	0.044	No
chr4:55481208-55481267	*CLOCK*	0.181738	0.381721	0.199983	0.0177	Yes
chr4:55866871-55866892	*EXOC1*	0.523739	0.670269	0.14653	0.0348	Yes
chr4:55899684-55899884	*EXOC1*	0.959156	0.997005	0.037849	0.0449	Yes
chr4:61912718-61912757	*ADGRL3*	0.716931	0.797396	0.080464	0.048	No
chr4:68332793-68332847	*YTHDC1*	0.901147	0.776285	-0.12486	0.039	No
chr4:86103185-86103244	*MAPK10*	0.902605	0.951504	0.0489	0.0425	No
chr4:99893954-99894000	*LAMTOR3*	0.770466	0.703242	-0.06722	0.0339	No
chr5:109729341-109729513	*MAN2A1*	0.987743	0.954232	-0.03351	0.013	Yes
chr5:111755769-111755830	*NREP*	0.9869	0.972307	-0.01459	0.0386	No
chr5:115809621-115809697	*CDO1*	0.032652	0.040186	0.007535	0.0483	No
chr5:135339427-135339575	*H2AFY*	0.009283	0.020354	0.011071	0.0146	Yes

chr5:138168469-138168688	*BRD8*	0.605862	0.729579	0.123717	0.0264	No
chr5:141662042-141662255	*ARAP3*	0.940495	0.722696	-0.2178	0.0249	No
chr5:148411079-148411238	*FBXO38*	0.058829	0.093266	0.034438	0.0206	Yes
chr5:154011240-154011320	*FAM114A2*	0.918226	0.85417	-0.06406	0.0291	Yes
chr5:179867444-179867495	*TBC1D9B*	0.400648	0.470046	0.069398	0.0398	No
chr5:34813573-34813660	*RAI14*	0.557089	0.744215	0.187126	0.00596	No
chr5:37516513-37516590	*WDR70*	0.953941	0.989836	0.035895	0.0318	Yes
chr5:95736888-95737075	*RHOBTB3*	0.969013	0.933162	-0.03585	0.048	No
chr6:125298713-125298816	*HDDC2*	0.438779	0.336904	-0.10188	0.00511	No
chr6:157150724-157150853	*ARID1B*	0.147589	0.197215	0.049626	0.0475	No
chr6:157174846-157175005	*ARID1B*	0.390108	0.526159	0.136051	0.00589	No
chr6:20548592-20548705	*CDKAL1*	0.998242	0.969494	-0.02875	0.0427	Yes
chr6:30895403-30895514	*DDR1*	0.494405	0.634755	0.140351	2.23E-05	No
chr6:31639499-31639646	*BAG6*	0.520421	0.589101	0.068679	0.018	No
chr6:31644306-31644414	*BAG6*	0.129794	0.173553	0.043758	0.0199	No
chr6:31758547-31758620	*MSH5*	0.850157	0.968901	0.118744	0.0244	No
chr6:34879966-34880063	*TAF11*	0.980794	0.928605	-0.05219	0.0403	No
chr6:35293750-35293915	*ZNF76*	0.556401	0.731073	0.174672	0.00684	No
chr6:43675201-43675271	*MRPS18A*	0.725358	0.854207	0.128849	0.0294	No
chr6:56598475-56598709	*DST*	0.944479	0.898245	-0.04623	0.0241	Yes
chr6:75911671-75911698	*MYO6*	0.081894	0.020013	-0.06188	0.0304	No
chr7:107459670-107459788	*COG5*	0.092226	0.025699	-0.06653	0.00303	Yes
chr7:108191253-108191283	*NRCAM*	0.638551	0.753758	0.115206	2.90E-04	No
chr7:140785688-140785808	*BRAF*	0.022622	0.105325	0.082703	0.00583	No
chr7:143293146-143293270	*CASP2*	0.031075	0.004213	-0.02686	0.0492	Yes
chr7:151241163-151241394	*SMARCD3*	0.020978	0.076473	0.055494	0.00987	Yes
chr7:158662193-158662367	*NCAPG2*	0.827475	0.571193	-0.25628	0.0481	No
chr7:20381726-20381885	*ITGB8*	0.978608	0.897563	-0.08104	0.00105	Yes
chr7:26197830-26197866	*HNRNPA2B1*	0.17261	0.147335	-0.02527	0.0479	No
chr7:2659939-2660040	*TTYH3*	0.028889	0.072428	0.043538	5.71E-05	No
chr7:45710527-45710652	*ADCY1*	0.921547	0.848954	-0.07259	0.0483	Yes
chr7:73204562-73204604	*GTF2IP4*	0.969975	0.956624	-0.01335	0.037	Yes
chr7:74190246-74190306	*EIF4H*	0.052398	0.078122	0.025724	0.0212	No
chr7:74757958-74758000	*GTF2I*	0.981077	0.972056	-0.00902	0.0468	Yes
chr7:8084896-8085017	*GLCCI1*	0.682934	0.577095	-0.10584	0.00367	No
chr7:98203943-98204186	*LMTK2*	0.994182	0.945369	-0.04881	0.0454	Yes
chr7:99050914-99050992	*SMURF1*	0.069721	0.145726	0.076004	0.0246	No
chr7:99459146-99459263	*ATP5MF*	0.912263	0.821105	-0.09116	0.00103	No
chr8:102849998-102850144	*AZIN1*	0.135706	0.078783	-0.05692	0.0105	No
chr8:130160784-130160793	*ASAP1*	0.589704	0.715966	0.126262	8.21E-04	No
chr8:143586218-143586290	*EEF1D*	0.865113	0.76091	-0.1042	1.69E-04	No
chr8:143793256-143793340	*SCRIB*	0.034964	0.095929	0.060965	0.0339	Yes
chr8:143937748-143937784	*PLEC*	0.369812	0.472962	0.10315	0.0235	No
chr8:144537720-144537813	*ARHGAP39*	0.433619	0.269398	-0.16422	0.0434	No
chr8:22067084-22067159	*DMTN*	0.206633	0.330181	0.123548	0.0154	No
chr8:22101975-22102062	*FAM160B2*	0.032289	0.231958	0.199669	0.0178	Yes
chr8:23293302-23293373	*R3HCC1*	0.994317	0.940265	-0.05405	0.011	Yes

chr8:28859435-28859563	*INTS9*	0.977385	0.926379	-0.05101	0.0428	No
chr8:29046191-29046416	*HMBOX1*	0.05982	0.209372	0.149553	0.00262	Yes
chr8:32763217-32763359	*NRG1*	0.111834	0.223638	0.111803	0.044	No
chr8:38417305-38417416	*FGFR1*	0.993789	0.936771	-0.05702	0.00113	Yes
chr8:41303460-41303538	*SFRP1*	0.99299	0.965101	-0.02789	0.00303	Yes
chr8:86435632-86435704	*WWP1*	0.980232	0.904565	-0.07567	0.046	Yes
chr8:94868691-94868813	*INTS8*	0.077882	0.029031	-0.04885	0.0157	No
chr8:96231378-96231515	*UQCRB*	0.005757	0.043891	0.038134	1.98E-06	No
chr9:105461519-105461615	*FSD1L*	0.093584	0.067674	-0.02591	0.0224	No
chr9:114269240-114269294	*COL27A1*	0.974174	0.823654	-0.15052	0.0125	Yes
chr9:128162003-128162115	*C9orf16*	0.032032	0.061696	0.029664	0.037	No
chr9:128609650-128609665	*SPTAN1*	0.957735	0.979915	0.02218	0.00144	No
chr9:129086138-129086267	*DOLPP1*	0.624069	0.519573	-0.1045	0.0408	No
chr9:130698161-130698251	*EXOSC2*	0.9067	0.807744	-0.09896	0.0468	No
chr9:13115247-13115334	*MPDZ*	0.76849	0.882624	0.114134	0.0232	No
chr9:132269402-132269489	*SETX*	0.066195	0.096283	0.030088	0.0141	No
chr9:133787245-133787260	*VAV2*	0.529766	0.645042	0.115276	0.0355	No
chr9:137752330-137752408	*EHMT1*	0.909776	0.843166	-0.06661	0.0382	No
chr9:34616029-34616113	*DCTN3*	0.983468	0.959808	-0.02366	0.02	No
chr9:35102685-35102823	*STOML2*	0.9898	0.960076	-0.02972	0.0201	No
chr9:36642996-36643083	*MELK*	0.929449	0.760488	-0.16896	0.0319	Yes
chr9:37857240-37857351	*DCAF10*	0.872575	0.534538	-0.33804	0.0145	No
chr9:5753535-5753646	*RIC1*	0.889531	0.586404	-0.30313	0.0304	No
chr9:79706746-79706899	*TLE4*	0.933724	0.974637	0.040913	0.0412	No
chr9:83666349-83666433	*UBQLN1*	0.7429	0.839559	0.096659	0.00309	No
chr9:97912872-97912975	*TRMO*	0.218186	0.061438	-0.15675	0.00343	No
chr9:98394174-98394255	*GABBR2*	0.987055	0.907481	-0.07957	0.0178	Yes
chrX:111744667-111744904	*ALG13*	0.686229	0.343366	-0.34286	0.0101	No
chrX:120285624-120285696	*TMEM255A*	0.391044	0.679393	0.288348	0.0133	No
chrX:136209242-136209442	*FHL1*	0.441069	0.59872	0.157651	0.0124	No
chrX:14026139-14026221	*GEMIN8*	0.77364	0.849681	0.076041	0.0339	No
chrX:153863367-153863379	*L1CAM*	0.845663	0.894599	0.048936	0.00823	No
chrX:153873227-153873242	*L1CAM*	0.800464	0.859617	0.059153	0.00963	No
chrX:154357250-154357274	*FLNA*	0.071942	0.113207	0.041265	0.00329	No
chrX:154400463-154400626	*RPL10*	0.954721	0.937168	-0.01755	0.0104	No
chrX:18951103-18951272	*PHKA2*	0.964461	0.786181	-0.17828	0.0408	Yes
chrX:47171027-47171258	*RBM10*	0.95553	0.849619	-0.10591	0.0304	No
chrX:47175018-47175092	*RBM10*	0.974535	0.922641	-0.05189	0.0249	Yes
chrX:81202436-81202576	*SH3BGRL*	0.020613	0.005619	-0.01499	0.00482	No

PSI_{con}, mean percent spliced in within controls; PSI_{hnRNPK} mean percent spliced in within CRISPRi-i^3 hnRNP K KDs; dPSI, delta PSI (PSI_{hnRNPK} - PSI_{con}) which must be > |10 %| to have been classified as significant (*n* = 126); FDR, False discovery rate applied by LeafCutter to each cluster; Novelty defined by prior annotation of junction in GENCODE (v30) (No) or not (Yes).